TRANSACTIONS
OF THE ASME
Series A

Journal of ENGINEERING FOR POWER

July 1960

Divisions: POWER • GAS TURBINE POWER • NUCLEAR ENGINEERING • FUELS OIL AND GAS POWER • HYDRAULIC • **Research Committees:** FURNACE PERFORMANCE FACTORS • CORROSION AND DEPOSITS FROM COMBUSTION GASES • BOILER FEEDWATER STUDIES • HIGH TEMPERATURE STEAM GENERATION • CONDENSER TUBES • PROPERTIES OF STEAM • **Committees on:** AIR POLLUTION CONTROLS SOLAR ENERGY APPLICATION • **And:** POWER TEST CODES COMMITTEES

Published Quarterly by
THE AMERICAN SOCIETY OF MECHANICAL ENGINEERS

TRANSACTIONS OF THE ASME
Series A

EDITORIAL DEPARTMENT

Editor, J. J. JAKLITSCH, JR.
Consulting Editor, LEO BLODGETT
Production, JEAN NORTH
Art Editor, HENRY BALFOUR

OFFICERS OF THE ASME

President, W. L. CISLER
Secretary, O. B. SCHIER, II
Treasurer, E. J. KATES
Assistant Treasurer, H. J. BAUER

PUBLICATIONS COMMITTEE

Chairman, B. G. A. SKROTZKI
HENDLEY N. BLACKMON
R. D. MINDLIN
MARTIN GOLAND
VITO L. SALERNO

Junior Representatives
A. S. GOLDSTEIN
J. W. FOLLANSBEE

REGIONAL ADVISORY BOARD

Region I, H. M. ROGERS, JR.
Region II, GLENN R. FRYLING
Region III, F. J. HEINZE
Region IV, FRANCIS C. SMITH
Region V, H. M. CATHER
Region VI, C. R. EARLE
Region VII, M. S. UMBENHAUER
Region VIII, CARL J. ECKHARDT

Published quarterly by The American Society of Mechanical Engineers. Publication office at 20th and Northampton Streets, Easton, Pa. The editorial department is located at the headquarters of the Society, 29 West Thirty-Ninth Street, New York 18, N. Y. Cable address, "Mechaneer," New York. Price $3.00 a copy, $10.00 annually; to members, $1.50 a copy, $5.00 annually. Add 50 cents for postage to all countries outside the United States and Canada. Changes of address must be received at Society headquarters seven weeks before they are to be effective on the mailing list. Please send old as well as new address. . . . By-Law: The Society shall not be responsible for statements or opinions advanced in papers or . . . printed in its publications (B13, Par. 4). . . . Second-class mail privileges authorized at Easton, Penna. . . . This publication is authorized to be mailed at the special rates of postage prescribed by Section 132.122 . . . © Copyright, 1960, by The American Society of Mechanical Engineers. Reprints from this publication may be made on condition that full credit be given the TRANSACTIONS OF THE ASME, Series A—Journal of Engineering for Power, and the author, and the date of publication be stated.

TRANSACTIONS OF THE ASME is indexed by the Engineering Index, Inc.

Journal of
ENGINEERING FOR POWER

VOLUME 82 • SERIES A • NUMBER 3

July 1960

CONTENTS

169 **An Experimental Investigation of Fuel Additives in a Supercharged Boiler**
R. J. Zoschak and R. W. Bryers

181 **External Corrosion of Superheaters in Boilers Firing High-Alkali Coals**
P. Sedor, E. K. Diehl, and D. H. Barnhart

194 **Corrosion of Superheaters and Reheaters of Pulverized-Coal-Fired Boilers**
Wharton Nelson and Carl Cain, Jr.

205 **Considerations for the Reduction of Noise in Ship Installations of Gas Turbines**
E. M. Herrmann

215 **A Torsional Vibration Problem as Associated With Synchronous Motor Driven Machines**
R. N. Brown

221 **Design Control of Overcompression in Rotary-Vane Compressors**
E. O. Bransford and R. A. Stein

227 **Operation of Steam Turbines to Minimize Shell Cracking**
S. B. Coulter and R. L. Jackson

TRANSACTIONS
Series D

Journal of
BASIC ENGINEERING

Vol. 82 • Series D • No. 2

CONTENTS FOR JUNE, 1960

251 The Fluids Engineering Laboratory at the University of Michigan, by G. V. Edmonson. (59—Hyd-16)

257 Flow Parameters in Hydrostatic Lubrication for Several Bearing Shapes, by S. Raynor and A. Charnes. (59—SA-61)

265 A General Method for Correlating Labyrinth-Seal Leak-Rate Data, by F. E. Heffner. (59—Lub-7)

276 Hydrostatic Gas Bearings, by J. H. Laub. (59—Lub-1)

287 Effect of Hardness, Surface Finish, and Grain Size on Rolling-Contact Fatigue Life of M-50 Bearing Steel, by R. A. Baughman. (59—Lub-11)

295 The Importance of Spinning Friction in Thrust-Carrying Ball Bearings, by G. S. Reichenbach. (59—Lub-9)

302 The Effect of Ball Bearing Steel Structure on Rolling Friction and Contact Plastic Deformation, by R. C. Drutowski and E. B. Mikus. (59—Lub-2)

309 A General Theory for Elastically Constrained Ball and Radial Roller Bearings Under Arbitrary Load and Speed Conditions, by A. B. Jones. (59—Lub-10)

321 A Sommerfeld Solution for Finite Bearings With Circumferential Grooves, by J. V. Fedor. (59—Lub-4)

327 Bearing Oil-Ring Performance, by D. C. Lemmon and E. R. Booser. (59—Lub-5)

335 Torque Produced by Misalignment of Hydrodynamic Gas-Lubricated Journal Bearings, by J. S. Ausman. (59—Lub-3)

342 Friction Characteristics of Sliding Surfaces Undergoing Subsurface Plastic Flow, by M. C. Shaw, A. Ber, and P. A. Mamin.

347 Machining Characteristics of Leaded Steel, by F. L. Bagley, Jr., and R. Mennell.

360 A General Flow Graph Technique for the Solution of Multiloop Sampled Systems, by R. Ash, W. H. Kim, and G. M. Kranc. (59—NAC-1)

371 Control System Analysis and Design Via the "Second Method" of Lyapunov, Part I, by R. E. Kalman and J. E. Bertram. (59—NAC-2)

394 Control System Analysis and Design Via the "Second Method" of Lyapunov, Part II, by R. E. Kalman and J. E. Bertram. (59—NAC-3)

401 Relations Between the Notch Tensile Strength of Cylindrical and Prismatic Specimens of Titanium Alloys and Heat-Treated Steels, by G. Sachs, J. G. Sessler, R. F. Pray, and T. H. Yeh. (59—Met-2)

411 Nonmetallic Inclusions and Fracture Behavior of Steels, by S. Yukawa. (59—Met-10)

417 Fracture Mode Transition for a Crack Traversing a Plate, by G. R. Irwin.

426 Use of the Moire Effect to Measure Plastic Strains, by A. Vinckier and R. Dechaene. (59—Met-7)

435 A Generalization of Cumulative Damage, by R. M. Mains. (59—Met-1)

441 Effect of Relaxation on the Behavior of Materials Under Combined Alternating and Static Stress, by F. H. Vitovec. (59—Met-3)

447 Cyclic Operation of Pressure Piping With γ Heating, by K. R. Merckx. (59—Met-4)

453 Creep Rupture Tests for Design of High-Pressure Steam Equipment, by E. A. Davis. (59—Met-14)

462 Steady Creep of a Tube Under Combined Bending and Internal Pressure, by Iain Finnie. (59—Met-5)

465 Effect of Wall Thickness on Stress-Rupture Life of Tubular Specimens, by J. T. Tucker, Jr., E. E. Coulter, and L. F. Kooistra. (59—Met-11)

477 Design of Pressurized Cylinders for High-Temperature Applications, by J. F. Traexler. (59—Met-8)

482 The Response of a Pressure-Sensing System, by R. P. Benedict. (59—A-289)

489 Dynamics of Heat Exchangers and Their Models, by Herman Thal-Larsen. (59—A-117)

TRANSACTIONS
Series C

Journal of
HEAT TRANSFER

Vol. 82 • Series C • No. 2

CONTENTS FOR MAY, 1960

77 Heat Transfer From Transverse and Yawed Cylinders in Continuum, Slip, and Free Molecule Air Flows, by L. V. Baldwin, V. A. Sandborn, and J. C. Laurence. (58—A-202 and 59—HT-5)

87 Magnetohydrodynamic Effects Upon Heat Transfer for Laminar Flow Across a Flat Plate, by R. D. Cess. (59—HT-14)

94 Conical Turbulent Boundary Layer Experiments and a Correlation With Flat Plate Data, by W. S. Bradfield. (59—HT-6)

101 The Influence of Free Stream Turbulence on the Local Heat Transfer From Cylinders, by R. A. Seban. (59—HT-3)

108 Heat Transfer to Fully Developed Laminar Flow in a Circular Tube With Arbitrary Circumferential Heat Flux, by W. C. Reynolds. (59—HT-13)

113 Steam Slip—Theoretical Prediction From Momentum Model, by S. Levy. (59—HT-15)

125 Pressure Drop and Heat Transfer in a Duct With Triangular Cross Section, by E. R. G. Eckert and T. F. Irvine, Jr. (59—HT-10)

139 Heat Transfer in Flow Through Rotating Ducts, by C. Y. Kuo, H. T. Iida, J. H. Taylor, and F. Kreith. (59—HT-12)

TECHNICAL BRIEF

152 Comparison of Turbulent Heat-Transfer Results for Uniform Wall Heat Flux and Uniform Wall Temperature, by R. Siegel and E. M. Sparrow.

TRANSACTIONS OF THE ASME Series E

Journal of
APPLIED MECHANICS

Volume 82 • Series E • No. 2

CONTENTS FOR JUNE, 1960

TECHNICAL PAPERS

223 Note on the Assessment of Flow Disturbances at a Blunt Body Traveling at Supersonic Speeds Owing to Flow Disturbances in Free Stream, M. V. Morkovin. (60—APM-10)

230 Possible Similarity Solutions for Laminar Free Convection on Vertical Plates and Cylinders, Kwang-Tzu Yang. (59—A-86)

237 On the Annular Damper for a Freely Precessing Gyroscope, G. F. Carrier and J. W. Miles. (59—A-44)

241 Heat Transfer for Laminar Flow in Ducts With Arbitrary Time Variations in Wall Temperature, Robert Siegel. (59—APMW-21)

250 A Study of the Stability of Externally Pressurized Gas Bearings, Lazar Licht and Harold Elrod. (60—APM-5)

259 On the Theoretical Analysis of a Dynamic Thermocouple: 2—The Continuous Area Interface, W. F. Hughes and E. W. Gaylord. (60—APM-19)

263 Normal Modes of Nonlinear Dual-Mode Systems, R. M. Rosenberg. (59—A-93)

269 Classical Normal Modes in Damped Linear Dynamic Systems, T. K. Caughey. (59—A-62)

272 The Vibration Response of a Linear Undamped System Resting on a Nonlinear Spring, P. R. Paslay and M. E. Gurtin. (60—APM-6)

275 The Approximate Analysis of Certain Boundary-Value Problems, H. D. Conway. (59—A-80)

278 Stresses in a Slab Having a Spherical Cavity Under Circular Bending, Chih-Bing Ling and Chen-Peng Tsai. (59—A-64)

283 Elastic Equilibrium of a Plate With a Reinforced Ellipitical Hole, Eugene Levin. (59—A-45)

289 A Method of Solution for the Elastic Quarter-Plane, M. Hetényi. (59—A-92)

297 Thermal Stress in a Viscoelastic-Plastic Plate With Temperature-Dependent Yield Stress, H. G. Landau, J. H. Weiner, and E. E. Zwicky, Jr. (59—A-33)

303 Prediction of Creep Failure Time for Pressure Vessels, F. P. J. Rimrott, E. J. Mills, and Joseph Marin. (60—APM-7)

309 On the Plastic Behavior of Rotating Cylinders, F. P. J. Rimrott. (59—A-65)

316 On the Optimum Design of Shells, R. T. Shield. (59—A-47)

323 Yield Conditions for Rotationally Symmetric Shells Under Axisymmetric Loading, P. G. Hodge, Jr. (59—A-129)

332 An Approximate Analysis of the Influence of Aerodynamic Heating and Initial Twist on the Torsional Stiffness of Thin Wings, L. S. Han. (60—APM-13)

335 Postbuckling Behavior of Rectangular Plates With Small Initial Curvature Loaded in Edge Compression—(continued), Noboru Yamaki. (59—APMW-22)

343 The Junction Problem of Solid-Slotted Cylindrical Shells, D. H. Cheng and N. A. Weil. (60—APM-2)

BRIEF NOTES

350 Method of Numerical Evaluation of a Large Determinant, F. R. E. Crossley and U. Germen. **352** On the Griffith-Irwin Theory, J. L. Sanders, Jr. **353** On the Flexure of Plastic Plates, S. Lerner and W. Prager. **355** Induced Velocities in Two-Dimensional Cascade Theory, J. Polasek. **356** Relation Between Stress Concentration and Boundary Displacement, J. S. Brock. **357** Bending of an Isotropic Triangular Plate, B. D. Aggarwala. **358** Simplified Analysis of a Thrust-Augmentation System, K. L. Bergman. **359** Stress Concentration in a Rotating Disk, Ta-Cheng Ku.

DISCUSSION

361 Discussion of previously published papers by M. K. Newman; M. V. Morkovin; P. G. Hodge, Jr., and R. Sankaranarayanan; Joseph Marin; R. R. Berlot; Norman Davids; T. Gillespie and A. W. Gunter; J. W. Dally, W. F. Riley, and A. J. Durelli; T. K. Caughey; H. H. Bleich and O. W. Dillon, Jr.; H. D. Conway; P. S. Theocaris; D. S. Johnson; R. P. Kanwal; Yi-Yuan Yu; C. W. Nelson; A. E. Bryson

377 BOOK REVIEWS

TRANSACTIONS OF THE ASME Series B

Journal of
ENGINEERING FOR INDUSTRY

Volume 82 • Series B • Number 2

CONTENTS FOR MAY, 1960

87 Simplified Approach to Understanding the Suction Problems for Reciprocating Mud Pumps, by W. E. Liljestrand. (59—Pet-23)

93 Prevention of Sulfide-Stress Cracking in Sour-Condensate Well Equipment, by W. J. McGuire and L. W. Vollmer. (59—Pet-36)

103 Overstrain Tests on Thick-Walled Cylinders, by S. M. Jorgensen. (59—Pet-1)

122 An Analytical Study of Drill-String Vibration, by J. J. Bailey and I. Finnie. (59—Pet-15)

129 An Experimental Study of Drill-String Vibration, by I. Finnie and J. J. Bailey. (59—Pet-16)

136 The Theory of the Ideal Design of a Compound Vessel, by S. J. Becker and L. Mollick. (59—A-125)

143 The Strength of Thick Cylinders Subjected to Repeated Internal Pressure, by J. L. M. Morrison, B. Crossland, and J. S. C. Parry. (59—A-167)

154 The Interaction of Textile Structures and High-Speed Textile Processes, by H. M. Morgan. (59—A-115)

159 Effect of Transient Loads on the Refrigerated-Space Temperature of a Cooling Complex, by C. F. Kayan. (59—A-181)

167 Uniform Two-Way Orientation of Plastic Films by M. O. Longstreth and Turner Alfrey, Jr. (59—A-113)

R. J. ZOSCHAK
Project Supervisor, Research Division
Mem. ASME

R. W. BRYERS
Development Engineer, Research Division
Assoc. Mem. ASME

Foster Wheeler Corporation,
New York, N. Y.

An Experimental Investigation of Fuel Additives in a Supercharged Boiler

To permit the use of high-vanadium residual oil as fuel for combined super-charged-boiler gas-turbine power plants, it is necessary to determine the treatment required to prevent the high-temperature corrosion and deposit problems associated with this fuel. A test program has been undertaken wherein a number of magnesium and aluminum-bearing additives have been injected into washed residual oil when firing a laboratory-scale, simulated supercharged boiler. Different tube arrangements within the boiler have been tried. Ash collected on the tubes at various locations has been analyzed and its corrosive effect at high temperatures on some types of stainless steel has been evaluated. The results thus far obtained are presented together with some hypotheses regarding the formation of deposits.

EARLY IN 1955 the authors' company began active sales promotion of supercharged boilers for use in combined supercharged-boiler gas-turbine cycles. Although no unusual problems were foreseen in firing natural gas or distillate oil in a cycle of this type, it was evident that the use of raw residual oil would most likely cause serious trouble in the form of high-temperature corrosion and deposits in both boiler and gas turbine.

These problems were by no means new to operators of conventional boilers. However, the gas-turbine manufacturers had been faced with the same problems in even more serious form and had made some progress in overcoming the difficulties through special treatment of the oil.

Since it was obvious that the application of this cycle would be extremely restricted unless residual oil, and ultimately coal, could be used as fuel, it was decided to begin a test and development program which would evaluate fuel-oil treatment methods used by the gas-turbine manufacturers and indicate means of alleviating deposit and corrosion problems through modifications of the treatment method or the boiler design. Work began on this program late in 1955. This paper covers the results to date.

Design of Test Unit

At the time this test program was started, the design concept of a stationary oil or gas-fired supercharged boiler was identical with that of a supercharged boiler which had recently been built for the Navy. It was reasoned that the compact size and possibility of shop assembly of complete units would be points in favor of this design.

In view of this reasoning, the test unit was initially arranged to simulate the conditions existing in the Navy boiler as far as possible within the limitations of cost and existing laboratory facilities. Since duplication of the pressure and heat release existing in the furnace of the Navy boiler was judged to be very important, the test unit was sized to use 250 scfm (1150 lb/hr) of air, which is about the maximum that can be obtained from the plant air system in the laboratory while satisfying the condition of 65-psia furnace pressure. At this air rate about 77 lb of Bunker-C oil can be fired per hour with 10 per cent excess air. By way of comparison, air flow in the Navy boiler at full load is 154,000 lb/hr.

In scaling down to this extent it is difficult to obtain complete dynamic, geometric, and thermal similarity between the model and the full-scale unit. In effecting a compromise, it was reasoned that the most important variables affecting deposit formation and corrosion in the boiler were:

1 Gas temperature at furnace exit and in superheater
2 Metal temperature
3 Geometry of tube banks
4 Gas-side Reynolds number in tube banks
5 Furnace heat release per unit volume.

Table 1 compares the test unit with the Navy boiler with respect to the listed variables. This comparison shows that similarity has been reasonably well maintained except for the temperature of the furnace-exit screen tubes. Exact duplication of screen-tube temperature would have resulted in disproportionately high cost of either installation or operation. This lack of duplication of screen-tube temperature is not considered a serious drawback since it has subsequently been shown that deposits accumulate very rapidly on the relatively cool test-unit screen-tube surfaces which might be expected to have a reduced tendency to accumulate deposits. Regarding corrosion, screen tubes of all boilers can be kept well below the temperature level at which vanadium corrosion becomes a problem.

Description of Unit

The test unit, shown schematically in Fig. 1, is a small boiler complete with water-cooled furnace and furnace-exit screen, and steam-cooled superheater. The furnace walls and screen tubes comprise the heating surface of a small natural-circulation boiler, complete with drum, risers, and downcomers.

A horizontal cross section through the furnace, screen, and superheater is shown in Fig. 2. The water-cooled furnace consists of concentric 10-in. and 12-in. Sch. 40 pipes with horizontal axis. The space between the 10 and 12-in. pipes forms the water jacket. Three 3-in. Sch. 40 feeders admit circulating water to the bottom of the water jacket and four 4-in. Sch. 40 risers carry the steam-water mixture from the top of the jacket to the 12-in. diameter drum which is located 8 ft above the furnace. Circular openings formed from short pieces of 5-in. Sch. 40 pipe are located at each end of the furnace. The burner projects into

Contributed by the Research Committee on Corrosion and Deposits from Combustion Gases and presented at the Annual Meeting, Atlantic City, N. J., November 29–December 4, 1959, of THE AMERICAN SOCIETY OF MECHANICAL ENGINEERS.

NOTE: Statements and opinions advanced in papers are to be understood as individual expressions of their authors and not those of the Society. Manuscript received at ASME Headquarters, August 13, 1959. Paper No. 59—A-160.

Table 1 Comparison of performance figures at full load

	Test boiler		Supercharged Navy boiler
Fuel flow, lb/hr	77		9,230
Air flow, lb/hr	1150		154,000
Excess air, per cent	10		15
Furnace net heat release per ft³ of volume, Btu/hr-ft³	1,460,000		1,550,000
Furnace net heat release per ft² proj., Btu/hr-ft²	365,000		1,390,000
Furnace net heat absorption per ft² proj., Btu/hr-ft²	110,000		208,000
Furnace exit temperature, deg F	2,850		2,980
	Staggered	In-line	
Furnace-screen heat absorption, Btu/hr-ft²	146,000	124,500	125,000
Furnace-screen gas mass flow, lb/hr-ft²	36,200	41,500	30,800
Furnace-screen gas velocity, ft/sec[a]	157	210	195
Furnace-screen gas Reynolds number[b]	23,800	35,100	29,700
Furnace-screen exit temperature, deg F	2,700	2,540	2,700
Approximate tube temperature, deg F	350	350	750
	Closely spaced	Widely spaced	
Superheater heat absorption, Btu/hr-ft².	117,000	87,000	95,900
Superheater gas mass flow, lb/hr-ft²	23,500	18,600	30,400
Superheater gas velocity, ft/sec[a]	84	75	165
Superheater gas Reynolds number[b]	10,200	7,750	21,600
Superheater exit temperature, deg F	2,030	2,000	2,035
Approximate tube temperature, deg F	1,000	1,000	1,140

[a] Average gas velocity through minimum-free-flow area

[b] Reynolds number—DG/μ

where:

D = tube OD, ft

G = gas mass flow, lb/hr-ft²

μ = gas viscosity at t_m, lb/ft-hr

t_m = ½ (average gas temperature + average tube temperature)

the furnace through one of these openings and the combustion gases leave through the other. Refractory lining is provided on the inner surface of the caps forming the ends of the furnace to prevent high heat absorption at locations where water-side flow may be stagnant. The lining at the burner end is also an aid in stabilizing combustion.

Directly after leaving the furnace the combustion gases pass through a water-cooled furnace-exit screen. Details of the two screen arrangements which have been used are given in Table 2. The screen tubes are fitted within a short length of 16-in. Sch. 40 pipe which is flanged on both ends and bolted to a mating flange on the rear of the furnace section. The 16-in. pipe is completely lined with high-alumina refractory except for the centrally located gas passage which is approximately 5 in. square in cross section. The screen tubes pass vertically through this gas passage. A separate downcomer-and-riser system connects the screen section with the drum. These risers and downcomers contain flanged connections so that the entire screen section can be removed for cleaning.

Bolted to the downstream side of the screen section is a similar 16-in. pipe section housing the superheater. This section is

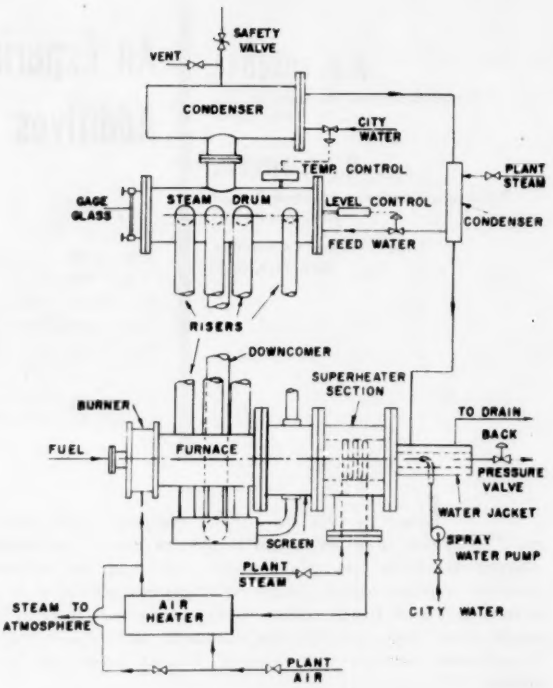

Fig. 1 Schematic diagram of test unit

Table 2 Supercharged test boiler physical constants

Furnace			
Volume, ft³	1.0	Length, ft	2.0
Surface (proj.), ft²	4.0	Diameter, in.	10.0

Screen	Staggered	In-line
Surface, ft²	0.43	0.70
Gas-side free area (min), in²	4.9	4.9
Tube arrangement	Staggered	In-line
Transverse pitch, in.	1.5	1.5
Longitudinal pitch, in.	1	2
Number of rows deep	2	3
Tubes per row	3 in 1st 2 in 2nd	3
Tube outside diameter, in.	1	1
Tube wall thickness, in.	0.120	0.120
Tube material	Carbon steel	Carbon steel

Superheater	Closely spaced	Widely spaced
Surface, ft²	2.2	2.1
Gas-side free area (min), in²	7.5	9.5
Tube arrangement	In-line	In-line
Transverse pitch, in.	11/16	7/8
Longitudinal pitch, in.	1	1
Number of rows deep	6	8
Tubes per row	7	6
Tubes to carry steam	7	6
Tube outside diameter, in.	1/2	1/2
Tube wall thickness, in.	0.047	0.047
Tube material	SA 213 TP 347	SA-213 TP 347

also lined with high-alumina refractory having a 5-in. square passage through the center. The superheater is inserted horizontally through a 10-in. pipe-side connection which forms a tee with the 16-in. pipe. Details of the two superheater arrangements which have been used are given in Table 2 and a photograph of the closely spaced superheater is shown in Fig. 3. Although steam flow through the tubes is in parallel with the flow of combustion gas, the connections may be interchanged to

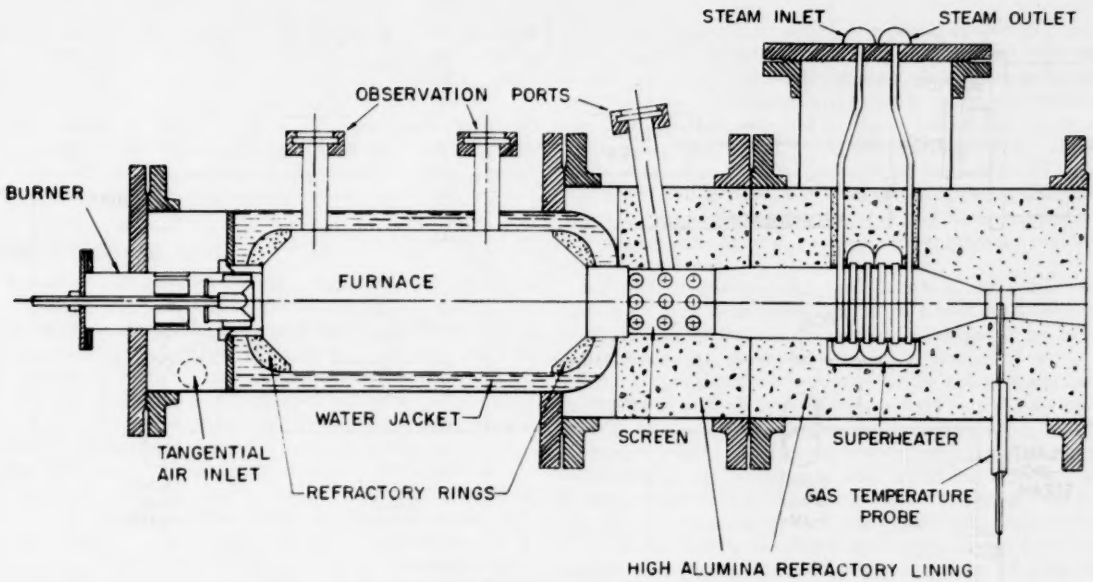

Fig. 2 Plan section through furnace, screen, and superheater

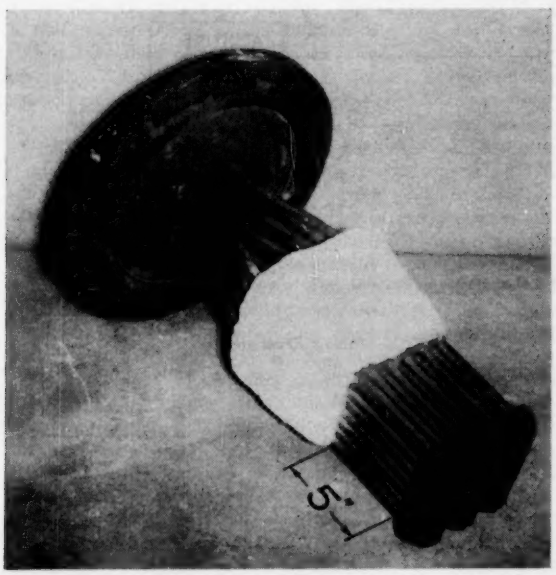

Fig. 3 Photograph of superheater. Dimension shown is width of gas flow path.

make a counterflow arrangement if desired. Saturated steam for cooling the superheater is taken from the 150-psig plant steam system since the quantity and pressure of steam generated in the unit are not adequate for cooling. Thermometers, pressure gages, and a flowmeter are provided to measure the flow rate and the steam conditions entering and leaving the superheater so that superheater duty can be calculated.

Immediately downstream of the superheater the gas pass necks down to a 2-in-diameter cross section to provide a high gas velocity which is necessary for proper functioning of a self-aspirating, double-shielded, chromel-alumel thermocouple used to measure gas temperature leaving the superheater. This couple is in the form of a probe which is inserted in the gas stream only at the time that a temperature reading is desired.

Pressure taps located in the furnace, in the gas pass between screen and superheater, and in the gas pass after the superheater provide a means for measuring draft loss across the tube banks.

After leaving the superheater casing the combustion gas is cooled by a water spray using city water raised to the required pressure by means of a centrifugal pump. After cooling, the gas passes through a back-pressure valve to the atmosphere.

Steam generated in the unit is condensed in a condenser located directly above the steam drum and the condensate is returned to the drum by gravity. The flow of cooling water for this condenser is controlled to maintain a constant preset temperature (250 F) and consequently pressure (15 psig) in the steam drum by means of a temperature-control valve. After leaving the condenser, the cooling water also serves to cool, in series, a feedwater condenser which condenses plant steam for use as feedwater, and a jacket around the exhaust line in the vicinity of the water spray. Provision is made for measuring the flow and temperature change of the cooling water through the condenser to determine the combined duty of the furnace and screen.

Fig. 4 shows a simplified schematic diagram of the fuel-and-additive system. The desired atomizing pressure of 300 psig is obtained by using three gear pumps arranged in series. Each pump has a capacity considerably in excess of the required fuel flow so that pressure rise across each stage can be regulated by pressure-control valves which bypass a portion of the oil back to the suction side of their respective stages. Additive in liquid form is injected into the oil by a small proportioning pump at a point between the first and second-stage oil pumps and is thoroughly mixed with the oil by means of a small, high-speed centrifugal pump rotating backward. A fuel-oil heater using plant steam as the heating medium is located between the final-stage pump and the burner. Fuel-oil flow is measured by a rotameter in the fuel line close to the burner and controlled by a bypass valve which permits recirculation of a portion of the oil back to the suction of the second-stage pump.

The burner is a mechanical atomizing type using tips designed for domestic oil burners. The burner is complete with spark-ignited propane ignitor and flame-failure protection system.

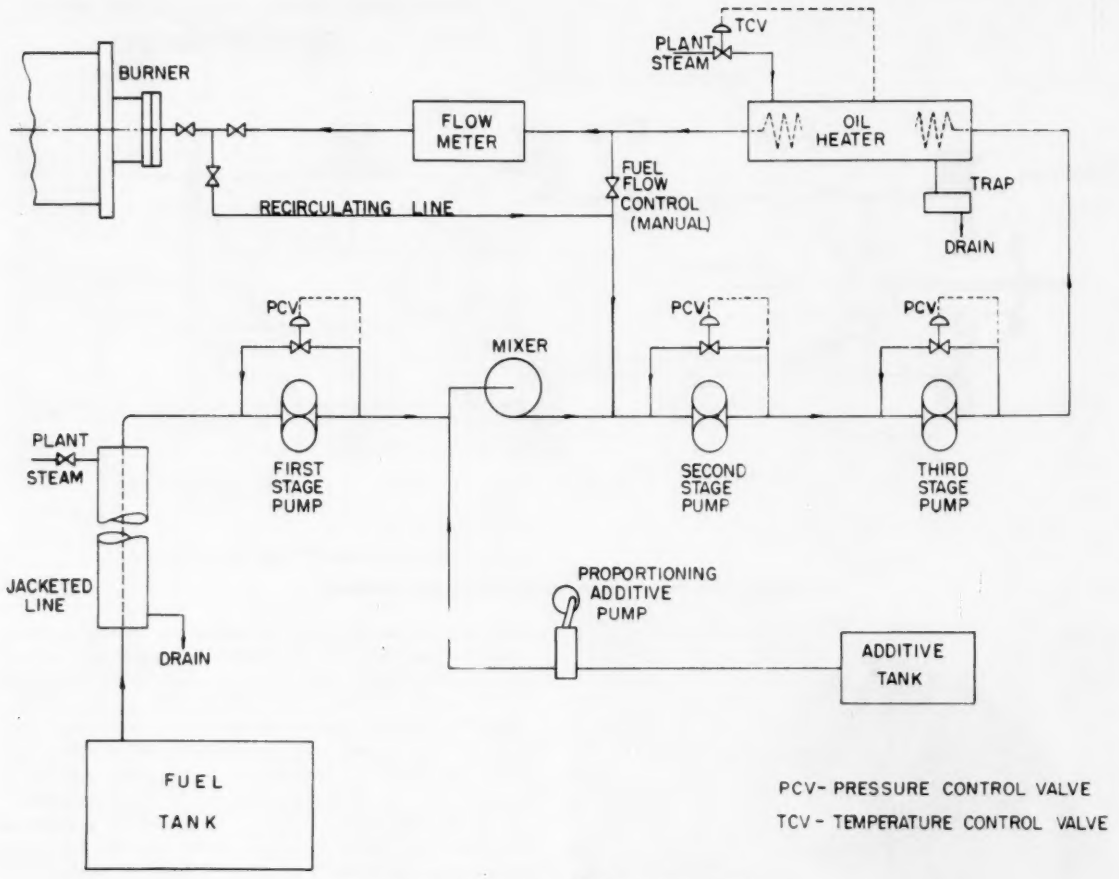

Fig. 4 Schematic diagram of fuel and additive system

Air for combustion is supplied from the plant air system and preheated to 485 F, to simulate heat of compression, in a double-pipe heat exchanger by exchange of heat with the steam leaving the superheater. An orifice is installed in the air line to measure the flow of air. Air flow is controlled by adjusting both the air-inlet valve and the back-pressure valve so that furnace pressure and air flow are at their required values.

Other safety features in addition to the flame-failure protection system are safety valves, a water-level control and cutout which adds feedwater if drum level falls below a set point and trips out fuel supply in case water level falls to a still lower level, and temperature cutouts which trip out fuel in case of either high superheater-outlet steam temperature or high exhaust-gas temperature downstream of the water spray.

Operation

The fuel used in the test boiler to date is Bunker-C oil which has been washed relatively free of sodium. Table 3 lists the analyses of the two batches of this type of oil which have been used. It will be noted that the two batches are nearly alike with respect to total ash, sulfur, and metals content.

The test boiler has been operated at the full design firing rate of 77 lb oil per hr for all tests to date except for one test at lower firing rate and another test at higher excess air. Some calculated full-load performance figures for the test unit are shown in Table 1.

Table 3 Fuel analyses

Washed Bunker-C fuel oil	Batch 1	Batch 2
A.P.I. gravity at 60 F	12.9	13.7
Viscosity SSF/122 F	280	260
SSU/210 F	230	225
Water by distillation, per cent	0.35	0.30
Ash weight, per cent	0.09	0.106
Sulfur, per cent	2.6	2.4
Metals, parts per million		
Na	6	16
V	385	345
Mg	47	44
Ca	3	4
Fe	4	9
Ni	42	46
Al	8	38
SiO_2	16	27

Control of all flow rates on the unit is manual with the exception of the condenser-water flow. Comparatively little adjustment of valve settings is necessary once the system has reached equilibrium, provided that main plant air and steam pressure remain constant.

A complete set of readings of all pertinent pressures, temperatures, and flow rates is taken once each hour during all test runs. In addition, fuel samples are taken periodically during the run from a point immediately upstream of the burner so that the additive-vanadium ratio may be checked.

At the completion of a run, screen and superheater are re-

moved, photographs taken, and the ash deposits are removed in separate batches from each transverse row of tubes. Batches from individual rows are sometimes combined to form a sample representative of a larger zone to minimize analytical work.

Any remaining ash is removed and collected to determine total weight of ash deposit. Samples from other locations such as refractory surfaces or furnace wall are taken when desired. All samples are analyzed by wet chemical analysis.

Additive Evaluation Tests

Numerous tests have been made using additives whose prime constituents have been magnesium or aluminum or both. The selection of the magnesium and aluminum cations, and the ratios of magnesium and aluminum to vanadium have been based on the results of extensive tests made by previous investigators. Certain of these tests [1, 2][1] indicated that three parts magnesium to one part vanadium by weight provides the best corrosion protection for the least amount of magnesium additive.

The initial series of tests was made with the staggered screen arrangement and the closely spaced superheater installed. The first run was made using washed Bunker-C oil treated with a water solution of magnesium sulfate[2] to provide a ratio of 3Mg:1V by weight. (All additive ratios in the present paper are reported by weight.) After 14 hr operating time the run was terminated since the maximum increase in draft loss, arbitrarily set at 5 in. Hg, had been reached. The operating time of 14 hr was tentatively set as the duration of future runs so that comparative data could be obtained. Inspection of the unit revealed a heavy accumulation of yellow-white, flaky ash in the superheater and considerable black, hard ash in the screen section. It appeared that the former would have been easily removed by a soot blower as evidenced by the fact that some ash had been dislodged while removing the superheater for inspection. The ash in the screen section, although not firmly bound to the tubes, would undoubtedly accumulate in large heavy pieces downstream if broken loose. Analysis of the ash indicated large quantities of magnesium and an appreciable amount of vanadium in the screen section and superheater. Hypothetical analysis of the ash, based on its water solubility and percentage of the various constituents present, indicated that magnesium was deposited in the screen section as an oxide. The magnesium in the superheater was deposited primarily as an oxide with considerable quantities of the sulfate present, the former decreasing and the latter increasing in quantity as the colder end of the superheater was approached. The superheater over-all heat-transfer coefficient, an indication of superheater ash accumulation, decreased approximately 25 per cent in the course of the test.

A second test was run under identical conditions except that the excess air was increased from 10 to 40 per cent to see if a shorter flame length and lower furnace-exit gas temperature would remedy the difficulty. There was no significant difference in the results. The reproducibility of the results on the test unit was verified on completion of a third run in which all known or controllable influencing factors were kept the same as in the first run.

Up to this point in the testing program, all runs had been made with a water-soluble additive. To challenge the possibility of the deposit being a result of mixing a water-soluble additive with the fuel, a run was made with oil-soluble magnesium naphthenate. The resulting draft loss and deposit inspection and analysis resembled the results of the magnesium-sulfate runs sufficiently to eliminate this factor as a cause for the screen-deposit problem.

At this time other investigators reported encouraging results with magnesium hydroxide. It was discovered that when magnesium sulfate was replaced with magnesium oxide as an additive, the proportion of magnesium sulfate in the ash was diminished and the magnesium oxide was increased—the over-all ash deposit decreasing. On the basis of the previous suggestion, a run was made with a magnesium-hydroxide oil dispersion. The test was terminated at the end of 10 hr due to operating difficulties. However, the results for that period of time were comparable to the magnesium-sulfate and magnesium-naphthenate runs over the same time span.

Although magnesium had been found to be a successful inhibitor of high-temperature vanadium corrosion, it presented a serious deposit problem. Aluminum, as suggested by Young and Hershey [3], should be a satisfactory additive as far as the deposit problem was concerned since the sulfate of aluminum dissociates to form an oxide at temperatures only slightly below 1650 F at the pressure existing in the supercharged furnace. Aluminum oxide has a melting temperature exceeding any predicted screen-inlet temperature and should aid in raising the melting temperature of the ash deposited. Results of corrosion tests by other investigators indicated that aluminum had little effect as an inhibitor but had a tendency to create a powdery deposit when mixed with magnesium in ratios of 3Mg:2Al. In view of this, a run of 14-hr duration was made using magnesium aluminum citrate as the additive. Inspection revealed reduced quantities of ash in the superheater and only a small quantity of ash deposited in the screen section. A repeat run verified the encouraging results. Fuel samples indicated that the actual ratio of magnesium to aluminum as-fired was 3Mg:1.9Al. Ash that was deposited in the screen section with the addition of aluminum was white and powdery as compared to the hard, black, fused ash of the runs with magnesium additive only. Analysis indicated the percentage of magnesium in the screen-section deposits was reduced by approximately 50 per cent. The total weight of superheater deposits was reduced somewhat.

Since the use of magnesium aluminum citrate in a full-size installation would be economically prohibitive, another additive containing magnesium and aluminum, a mixture of magnesium HBC[3] and aluminum HBC, was tried. After operation with this additive, inspection of the unit revealed a wedge-shaped deposit built up in the second row of the screen section. The ash was white in color, similar to chalk in consistency, and lightly bound to the tubes. The ash deposited in the superheater was identical to that from the magnesium aluminum citrate run in appearance and quantity—white powder with a yellow base built up on the front and rear surface of the tube. Variation of the over-all superheater heat-transfer coefficient was considerably less with the addition of aluminum. The cyclic nature of this variation suggested a periodic sloughing of the deposit. A second run under identical conditions verified the previous results.

The firing rate was reduced in a third run to see if lowering of furnace-exit temperature had any marked effect on the screen-tube deposit. Although the temperature, as calculated, dropped approximately from 2800 to 2500 F, there was no change in the characteristic or quantity of the deposits.

An additive consisting of aluminum hydroxide and magnesium hydroxide dispersed in oil was tried with a ratio of 3Mg:2Al:1V under standard operating conditions. Although the operating time during which the additive was being mixed with the oil was somewhat shorter than previous runs due to operational difficulties, the results were comparable for the same period of time. The pattern of increase in draft loss was identical

[1] Numbers in brackets designate References at end of paper.

[2] Descriptive data and analyses of all additives are given in the Appendix.

[3] HBC is a designation for a specific proprietary additive. See Appendix.

to previous runs using magnesium and aluminum oil dispersions in 3Mg:2Al ratios. The ratio of Mg:Al was slightly higher than 3:2 and the results resembled those from the pure magnesium runs—the ash was white, fused, and considerably harder than from runs having 3Mg:2Al. The quantity of ash was comparable to other runs also using magnesium and aluminum jointly. The superheater heat-transfer coefficient followed the same pattern as other runs using magnesium and aluminum.

Three tests were made firing washed Bunker-C without additive. The first was of short duration to be used as a basis of comparison for runs with an additive. There was no change in heat transfer after the first hour and no increase in draft loss. The resulting deposit on the superheater was a shiny, black scale, $^1/_{32}$ in. thick, completely encircling the tube. Upon breaking this scale loose, a thin film or layer of yellow-orange material was revealed. Analysis of this deposit revealed about 30 to 60 per cent vanadium pentoxide or about 4 to 7 times the percentage deposited when using an additive. The screen section had a small deposit of black, porous substance on the front of the first and second-row tubes. Two long runs of 80 hr each were made to determine what the deposit would be over a longer period of time. Although each test was hampered by numerous shutdowns due to operational difficulties, there was no apparent effect on the deposit since there was no cycling of over-all heat-transfer coefficient and draft loss. The ash appeared to be intact at the end of each run and showed no signs of flaking off. The results of the 80-hr runs did not differ from those of the shorter run.

Corrosion Tests

A corrosion test program was initiated to complement the data already obtained in the study of ash deposits. The ratio of inhibiting magnesium oxide to the vanadium pentoxide in the deposits appeared to be in excess of that required for adequate corrosion protection established by others working on this problem. Reduction in the quantity of MgO fired would reduce the quantity of ash available for deposit and possibly alleviate the deposit problem.

Considering the quantity of ash available, a testing program was selected whereby $^5/_8 \times ^5/_8 \times ^3/_{16}$-in. steel specimens were placed in Coors No. 0 crucibles containing approximately 4 grams of ash each and soaked in a muffle furnace at 1600 F ± 20 F for 100 hr. The milled steel specimens had a surface roughness of approximately 200 microns and $^1/_{32}$-in. tolerance on all dimensions. Under these circumstances the worst conditions would allow for a 0.8 per cent error in specimen surface. Considering the other variables entering the control of the test, such as temperature variation, ash swelling, and similar factors, this limit was felt to be satisfactory. All samples were partially submerged to an equal depth in ash. The weight loss was established as the index of corrosion rate.

There were 63 specimens used, representing five different types of steel soaked in 10 different ash samples collected from tubes at various locations in the test rig. The types of steel used were 310, 316, 321, Croloy 20–2 (20Cr–2Al), and Croloy 12–7 (12Cr–7Al). Additional Croloy 20–2 and Croloy 12–7 specimens were heat-treated by air quenching after soaking for 1 hr at 1600 F, thus giving essentially 7 different steel specimens.

In addition, one specimen of each type was exposed to the atmosphere only, at 1600 F, providing a scaling index for the test. Upon completing the test, the samples were inspected, descaled according to the procedure given in the Appendix, and weighed. Also, one clean specimen of each type was run through the descaling process to determine any weight loss that might result. The maximum descaling weight loss for any specimen was 0.0025 gram.

Upon completion of the 100-hr soaking, the 63 specimens were removed and inspected. There was no evidence of liquefaction of the ash. Samples of 316, 321, and 310 were black with an oxide coating covering the specimen uniformly. There was no visual difference between the specimens soaked in the inhibited ash and the specimens subject to atmospheric oxidation. Samples of 310, 316, and 321 soaked in untreated Bunker-C ash appeared as a flowerlike display of porous scale approximately two to three times the original size. When these three scaled samples were broken open no evidence of the original sample was seen. The Croloy steels were somewhat corroded and were covered with a tight thin scale as compared to the voluminous porous scales on the other three steels. All specimens were descaled and weighed.

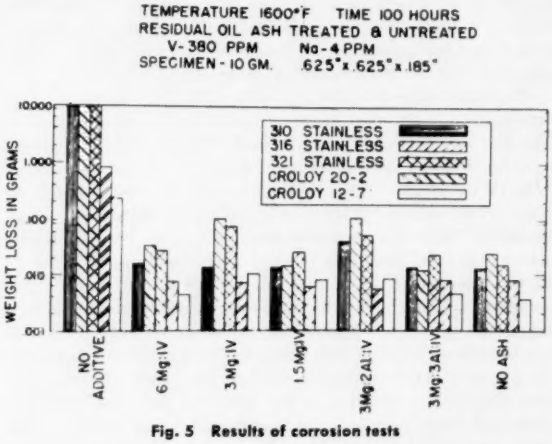

Fig. 5 Results of corrosion tests

The results of these weight-loss determinations are plotted in condensed form in Fig. 5. Since there was little variation in weight loss with ash samples from the same additive taken from different locations, only data representative of different additives and varying additive-to-vanadium ratios have been plotted for the various steels tested. Table 4 shows the additive used and the corresponding ash analysis for each test reported in Fig. 5.

The results indicated that both Croloy specimens revealed considerably more resistance to vanadium corrosion at 1600 F than the high alloy steels, with the Croloy 12–7 somewhat better than Croloy 20–2. None of the materials, however, could be considered satisfactory for use with uninhibited oils. All specimens soaked in inhibited ash evidenced corrosion at a rate not exceeding their oxidation rate when subject to atmospheric oxidation with the exception of some of the 316 and 321 specimens. These particular specimens had been used previously in a similar, less comprehensive test at 1400 F. Metallographic inspection of a 316-stainless sample showed evidence of carbide precipitation and intergranular attack, suggesting that the piece may have been sensitized while being cooled slowly from 1400 F in the first test. The second sample, 321, which is a titanium-stabilized steel, was checked to verify identification and was given a metallographic examination. There was evidence of discontinuous carbide precipitation and sparse intergranular attack. No explanation can be given for the discrepancies in the results of the 321 specimen.

The results of the tests at 1400 F were the same as those at 1600 F except that all corrosion rates were proportionately reduced and type-310 stainless steel was somewhat superior to the two Croloys in uninhibited ash.

As a result of the two tests, it appears that the inhibited

Table 4 Coupon corrosion test ash samples and their analysis

Ratio	Additive	Ash analysis								
		$MgSO_4$	$NaSO_4$	$CaSO_4$	V_2O_5	MgO	Al_2O_3	NiO	Fe_2O_3	SiO_2
...	None	5.46	6.14	0.19	75.00	2.17	3.65	5.61	2.86	1.57
6Mg:1V	$MgSO_4$	...	...	...	7.71	89.94	Trace	1.61	0.39	0.10
3Mg:1V	$Mg(OH)_2$	...	...	...	16.85	71.53	4.73	1.68	2.15	0.58
1.5Mg:1V	$MgSO_4$	0.53	...	...	15.57	70.69	4.01	3.93	1.03	0.21
3Mg:2Al:1V	MgHBC & AlHBC	14.33	0.26	0.36	12.37	37.87	30.74	0.97	0.44	0.46
3Mg:3Al:1V	MgHBC & AlHBC	...	...	...	8.79	43.08	47.35	1.03	0.21	0.10

ash is safe up to and including 1600 F when the additive ratio is as low as 1.5Mg:1V. This is somewhat to be expected, as ash-fusion temperatures revealed a dry ash up to the range of 1900 to 2400 F for all ashes tested. However, these results should not be considered conclusive since the ash samples used were a composite taken from each location and cannot represent the difference in layers as it was deposited. The accumulated deposit cannot take into consideration that minute layer which may be molten and initiating the deposit on the cool tubes.

Correlation of the results with data obtained by other investigators is difficult due to variations in testing conditions and methods of defining the corrosion rate. In comparison with results of other investigators the corrosion rates appear to be lower for the inhibited ash.

Further Work on Deposits

Speculation as to the cause of the heavy deposits in the screen section in the previous tests presented two hypotheses for future consideration in the test program:

1 The large accumulation of ash deposited in the screen section was a result of the flow pattern created by the geometry of the tube arrangement.

2 The severe tube deposits in the high gas-temperature zones were due to a low melting constituent in the ash varying in quantity with the quantity of magnesium in the ash.

With the previous hypotheses as a guide for further testing, a new in-line screen section was designed as described in Table 2. As an added feature, an inspection port (see Fig. 2) was installed so that the second-row screen tubes could be viewed periodically in the course of testing.

Several short tests of 14-hr duration were made using $MgSO_4$ solution as an additive in the ratio of 3Mg:1V. The results were very encouraging as there was no increase in draft loss and only a slight build-up of deposit on the leading edge of the second and third-row tubes of the screen section which broke loose upon shutting down. There was no evidence of a change in the quantity of ash deposited in the superheater section as a result of the alteration of the screen section. The deposits with the new screen section were not excessive and indicated that an extended test would be desirable to obtain more conclusive results.

An extended test of approximately 70-hr duration was therefore made with $MgSO_4$ as the additive. Due to a test error, a proportion of 6Mg:1V was used which is greater than proportions used in any prior test. However, since it was intended eventually to vary the ratio of Mg to V, the outcome of the test did provide some useful data. The test was terminated short of the intended 100 hr due to an extremely high draft loss caused by a $^1/_2$-in-thick coating of fused ash on the first row of the superheater which reduced the gas pass to a small opening approximately $^1/_2 \times 3$ in.

The ash accumulated in the screen section was greater than in previous tests but gave no indication of restriction of flow with the exception of the narrow lane adjacent to the refractory. The ash was completely fused and similar to ash collected in this zone in previous tests.

A second test run with a lower magnesium-to-vanadium ratio, 3Mg:1V, to see if the excess magnesium caused the heavy deposits, showed that there was no significant benefit gained by decreasing the quantity of magnesium added to the fuel.

It was apparent that the deposit problem had shifted from the screen section to the superheater. Since the lateral pitch of the superheater was extremely small, increasing it to a value approximately equal to the pitch of the screen section seemed reasonable. This change was accomplished by building a new wide-spaced superheater, as described in Table 2.

A third extended run was made with the new screen and superheater sections installed. The duration of the test was approximately 70 hr before the draft loss increase made it necessary to shut down. Ash deposited on the front of the superheater was fused and the accumulation was somewhat less than in previous tests. A considerable amount of fused ash had accumulated in the screen section apparently causing a high draft loss. The ash had the appearance of drifted snow growing from the intersection of the tube and the refractory.

No increase in draft loss was noticed until after 14 hr operating time. Since it is also known from the previous tests that the ash remains powdery through the first 14 hr, it may be assumed that the ash begins to fuse shortly after this period of time.

This suggested that periodic soot blowing while the ash was in a dry state might be beneficial. Accordingly, a small steam soot blower was installed in front of the superheater. After operating the supercharged boiler for 14 hr, the soot blower was tried, and the ash was effectively removed from the tubes in the vicinity of the blower. However, the ash removed fused upon entering the hot gas stream, and large agglomerates of fused ash collected in the tube bundle down stream, making conditions worse.

Finally, a short test of 14-hr duration was made at a reduced additive ratio of 1.5Mg:1V to determine the effect of the reduced rate on the type and quantity of ash deposited. There was no change in the appearance of the ash. However, the quantity deposited was reduced somewhat.

During the course of the testing program, a periodic inspection of the screen ash deposits was made through the observation port. While firing untreated, washed, Bunker C, the atmosphere appeared to be slightly contaminated with small glowing particles which were deposited on the tubes as molten globules of ash. The same particles were moved along the tube by the gas stream and eventually blew free of the tube at a tangent 90 deg from the stagnation point.

With the addition of $MgSO_4$ to the oil, the atmosphere was completely clear to the naked eye. After a period of immunity of several hours, small particles began to grow at a point on the tube at the 45-deg upstream tangent line. The number of ash particles increased and individual particles began to grow until one large wedge-shaped accumulation of ash formed on the front of the tube. After 7 hr of operating time, the leading edge of the ash began to glow, suggesting that it might be molten. There was no indication that the ash was running.

Fusion tests were run on 12 different ash samples using a stereo microscope and fusion apparatus similar to that described by Hershey and Young and also by heating test cones which were prepared in accordance with ASTM standard procedure D271-58.

The fusion point of the test cones was determined by inspection of the ash after progressive heating to higher temperatures as the cones remained rigid even though they indicated a fused state upon cooling.

Results of tests with the stereo microscope and fusion apparatus showed a fusion temperature exceeding 2360 F for MgO-V_2O_5 ashes containing little or no sulfur. Contraction and liquefaction began at progressively lower temperatures as the sulfur content increased. All fused samples appeared as a black, crystalline, or glasslike material upon cooling.

Heating of test cones indicated that all ashes containing MgO-V_2O_5, and MgO-V_2O_5-Al_2O_3 fused in the vicinity of 2400 F and appeared to be glass or marblelike in structure on cooling—black in the case of MgO-V_2O_5 and grey-white in the case of MgO-V_2O_5-Al_2O_3. When sulfur was present, liquefaction began at some lower temperature. Untreated, washed, Bunker-C ash began to melt at 1200 F and fused at 1600 F.

In all cases the ratio of MgO to V_2O_5 was equal to or greater than 1:1. The higher ratios had no apparent effect on the fusion point as ashes containing 89 per cent MgO and 7.7 per cent V_2O_5 fused at 2400 F also.

Stereo microscopic observations of screen ash deposits from the first series of tests indicated there was a small layer adjacent to the tube common to ashes containing MgO and MgO-Al_2O_3. It was felt that this small layer might be the cause of the deposit problem and an analysis by x-ray spectrographic methods might be beneficial. Results of these analyses of the inner and outer layers of two ash deposits laid down while firing oil containing: (*a*) $Mg(OH)_2$, and (*b*) $Mg(OH)_2$ and $Al(OH)_3$ as additives indicated an unidentified crystalline substance common to the tube side layer of both samples and apparently containing a preponderance of vanadium. About 60 to 70 per cent of the ash deposited consisted of MgO in the first case and MgO and $MgAl_2O_4$ in the second case. Nickel was found to be distributed uniformly throughout the ash samples, and silica and iron were found to be more prevalent on the inner layers

Several samples deposited in the screen section resulting from the use of four different additives all in the ratios of 3Mg:2Al:1V or 3Mg:1V were also analyzed. The x-ray patterns indicate the presence of MgO, $MgAl_2O_4$, $Mg_3(VO_4)_2$ and some unknown in the ash when using $Mg(OH)_2$ and $Al(OH)_3$ or MgHBC and AlHBC as additives. MgO and $Mg_3(VO_4)_2$ were also found in the ash when $Mg(OH)_2$ was used as the sole additive. No $Mg_3(VO_4)_2$ was detected in the ash accumulated while using MgAl citrate as an additive. However, the presence of excess water and sulfur in the ash may have prevented the detection of the $Mg_3(VO_4)_2$.

Some Comments on Deposit Formation

Accumulation of ash on the superheater tubes appears to begin with an initial layer, usually distinguished by a yellow or orange color in the unsintered state, which completely encircles the tube and is deposited when firing both treated and untreated washed fuel. This layer is highly water soluble, with 13 per cent constituting a water-soluble magnesium-vanadium compound. This could indicate that either one of two vanadium compounds might be present, magnesium metavanadate or vanadium pentoxide, whose melting temperatures are between 1200 and 1400 F. Vanadium pentoxide has been considered more likely since the magnesium in the metavanadate represents a small percentage of the total ash and could be considered in the realm of analytical error. Since wet analysis also reveals several constituents that are volatile at gas-stream temperature, the pattern of deposit would seem to indicate that the initial layer was being formed by molecular diffusion of a gas, or of liquid or solid particles of molecular size.

Deposits in the screen section can be divided into three groups depending on their location: (*a*) A minute layer of powdery ash deposited on the rear side of the tubes; (*b*) a heavy, fused, multilayer, wedge-shaped deposit on the front of all tubes internal to the bundle and apparently growing forward from a point 45 deg from the stagnation point; (*c*) an occasional small, multilayer, powdery deposit located on an arc ± 10 deg from the stagnation point of the first-row tubes.

Ash deposited on the rear side of all screen tubes appears to be limited in growth to a minute layer similar to the ash deposited in the furnace. By nature of its location and quantity, the ash appears to have been deposited by molecular diffusion.

Visual observation while operating disclosed that deposits on the front side of the tubes in the interior of the screen section were apparently initiated by submacroscopic particles deposited on the tube at a tangent 45 deg from the stagnation point. The particles grew until a thin layer of powdered ash was formed. The initial layer of powdered ash was somewhat greater on tubes in the in-line arrangement than on tubes of the staggered arrangement. The two subsequent layers in both arrangements were fused. The inner fused layer was found to be common to all ashes deposited in this location while using an additive. Growth beyond the initial fused layer apparently originated at the center of the tube as indicated by subsequent "growth rings" in the deposit. This is clearly shown in Fig. 6.

X-ray analysis of the fused inner layer indicated the presence of magnesium oxide, magnesium orthovanadate, magnesium aluminate, and an unidentified phase. Since the unidentified phase, peculiar to the inner layer, was found in ashes resulting from additives containing the magnesium cation as well as additives containing both magnesium and aluminum cations, it would seem reasonable to believe aluminum was not a component of the unidentified phase. It would then appear that the unidentified phase was part of a two-component system of magnesium oxide and vanadium pentoxide. However, this would violate Gibbs' phase rule and therefore a third component must be present.

Comparison of the analyses of the inner and outer layers indicates the unidentified phase contains a preponderance of vanadium and thus a small percentage of a third component. Since iron and silica, occurring in the deposits in small percentages, were found to be more prevalent in the inner layer, and the other minor constituents were reported to be uniformly spread throughout the deposit, it would seem probable that either iron or silica constitutes the third component. The presence of the iron in the ash in the percentage reported is unexplainable as very little iron is present in the oil compared to other minor impurities and there is no evidence of tube corrosion. Silica, however, could be depositing by condensation of silica volatilized in the high-temperature zone.

Several investigators have postulated that volatile SiS, SiS_2, and SiO formed in the fuel bed and flame condense on cool surfaces in high-temperature zones where they are oxidized to form SiO_2. This will hold true if the residence time in the gas stream is short prior to deposit or there is insufficient oxygen for oxidation. It has also been established rather conclusively by numerous investigators that humidification of the flue gas reduces these silica deposits [4].

Analysis of the ash resulting from the use of magnesium aluminum citrate, a water-soluble additive, indicates the deposit contains $MgAl_2O_4$, MgO, and some unknown. In addition, it was observed that the water and sulfur contents were high compared to other samples taken from this location. The ash deposit was also powdery and very small in quantity. It was felt since magnesium aluminum citrate was a very dilute solution, there may have been a sufficient quantity of water present to humidify the flue gas and reduce deposits that might

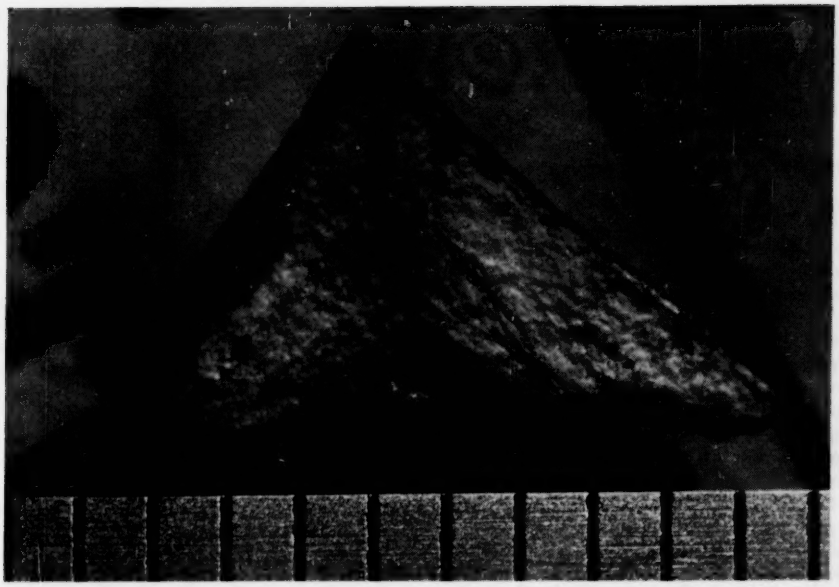

Fig. 6 Photomicrograph of MgO-Al_2O_3-V_2O_5 ash deposited in the second row of the screen section (graductions along bottom of picture are at 1/16-in. intervals)

have been initiated by volatile silicates. This would further substantiate the hypothesis that silica may be initiating deposits in the screen section.

Stereo microscopic investigation of various deposits taken from tubes internal to the in-line and staggered-screen-section bundles have revealed several layers of powdery and fused ash of uniform thickness ± 45 deg from the stagnation point with sharp lines of demarcation. These layers have the same pattern as the gas-stream temperature profile [5] and suggest a change in equilibrium conditions with temperature for the gas contaminants condensing and depositing on the tube. The outside layer of fused ash takes on the shape of the deposit with no further indication of stratification other than that which may be attributed to density. A similar phenomenon was observed during the fusion tests as there was no visual change in ash heated to temperatures between 2400 and 3000 F.

Wet analyses indicate the magnesium-to-vanadium ratio of the unsintered ash is always the same as the ratio fired once the magnesium necessary to form the aluminate has been accounted for. In the fused ash the ratio of magnesium to vanadium increases as the quantity of fused ash increases. Photomicrographs of ash deposit reveal a thin black layer on the outer periphery of the ash containing a sparse deposit of yellow particles. The latter are similar in appearance to the particles found on the tube-side surface.

Since the dissociation pressure of vanadium pentoxide increases rapidly with an increase in temperature [6], it would appear that dry magnesium oxide particles react with a thin film of molten vanadium pentoxide that has been deposited or condensed on the tubes or ash surface. Furthermore, it would appear that all the aluminum deposits as magnesium aluminate formed during the process of combustion. The latter has been verified by x-ray analysis.

A similar explanation would then account for the difference in distribution of silica in the deposit. The inner layer apparently contains volatile and nonvolatile silica contaminants while the outer layer contains nonvolatile silica contaminants only.

Magnesium sulfate has been reported in unsintered ash at the lower gas-stream temperature. Since there is no evidence of sulfur in the fused ash and the magnesium-to-vanadium ratio is constant for unsintered ash regardless of the sulfur present, it would seem reasonable to expect the formation of sulfur trioxide from sulfur dioxide at the tube surface with vanadium pentoxide apparently acting as the catalyst.

Conclusions

Based on the test results obtained thus far on the test rig, the following conclusions can be drawn:

1 When magnesium is the sole cation in the additive, the amount and nature of deposits are essentially unchanged regardless of whether the additive is oil-soluble, a water solution, or a suspension of solid particles.

2 The highest ash-fusion temperature attainable using magnesium as an additive is in the vicinity of 2400 F.

3 Soot blowing is relatively ineffective at the elevated gas temperatures existing in the test unit.

4 The composite, inhibited ash from any given location is not corrosive to the alloy steels tested at temperatures up to 1600 F when the additive ratio is as low as 1.5Mg:1V.

In addition, although not supported by sufficient experimental data from these tests to be conclusive, the following hypotheses are based on evidence from these tests together with data of other investigators:

1 Ash deposits are being initiated by the diffusion and condensation of volatile vanadium pentoxide in the high and low-temperature gas zones and silica sulfide in the high-temperature zones.

2 Vanadium pentoxide is reacting with magnesium oxide and other minor constituents in the vicinity of the tubes. This may apply to the high temperature (1900 F +) gas stream only.

3 Sulfur trioxide is formed in the vicinity of the tubes and reacts with the ash constituents upon deposit.

4 When alumina and magnesia are present, magnesium aluminate is formed in the vicinity of the flame. No evidence of an alumina vanadate has been observed. The condition of sufficient magnesium to react with the aluminum may have a

considerable effect on the role aluminum plays in the ash-deposition problem.

5 A solid solution of magnesium orthovanadate and magnesium oxide is formed when magnesium is added to the oil in the ratio of 1.5 magnesium to 1 vanadium or higher.

Acknowledgments

The authors appreciate the co-operation of Mr. Bruce Buckland of General Electric Company, Mr. J. O. Collins of Esso Research and Engineering Company, and Dr. W. E. Young of the Westinghouse Research Laboratories, who, together with their associates, offered valuable technical assistance as well as many helpful suggestions.

Acknowledgment is also due Peabody Engineering Corporation for designing and fabricating the miniature burner, Esso Research and Engineering Company for furnishing the residual fuel to close specifications, Bangor Hydroelectric Company for washing the oil at their facilities, and Dow Chemical Company for making x-ray analyses of ash samples.

References

1 Bruce O. Buckland and Donald G. Sanders, "Modified Residual Fuel for Gas Turbines," ASME Paper No. 54—A-246.

2 Bruce O. Buckland, C. M. Gardiner, and D. G. Sanders, "Residual Fuel-Oil Ash Corrosion," ASME Paper No. 52—A-161.

3 W. E. Young and A. E. Hershey, "A Thermochemical Study of Some Additives to Reduce Residual-Fuel Ash Corrosion," Westinghouse Scientific Paper 8-0524-P11, presented at the 13th Annual Conference, National Association of Corrosion Engineers, St. Louis Mo., March 11–15, 1957.

4 Battelle Memorial Institute (H. W. Nelson, H. H. Krause, E. W. Unger, A. A. Putnam, C. J. Slunder, P. D. Miller, J. D. Hummel, and B. A. Landry), "A Review of Available Information on Corrosion and Deposits in Boilers and Gas Turbines," report of ASME Research Committee on Corrosion and Deposits From Combustion Gases, The American Society of Mechanical Engineers, New York, N. Y., 1959, pp. 22–24, 127–128.

5 E. R. G. Eckert, "Introduction to the Transfer of Heat and Mass," McGraw-Hill Book Company, Inc., New York, N. Y., first edition, p. 139.

6 C. T. Evans, Jr., "Oil Ash Corrosion of Materials at Elevated Temperatures," 53rd Annual Meeting ASTM, Atlantic City, N. J., 1950, p. 69.

APPENDIX

Additive Data

$MgSO_4$ solution

Water-soluble salts—$MgSO_4 \cdot 7H_2O$
Mg by weight in solution— 5 per cent

$Mg(OH)_2$

Manufacturer—Dow Chemical Company
Oil dispersion of $Mg(OH)_2$
Particle size—average 0.48 microns,
99 per cent of all particles less than 1.05 microns
$Mg(OH)_2$ by weight 57 per cent
Viscosity at 25 C 3850 centipoise
100 C 450 centipoise
Density at 25 C 1.372 gm/cc
100 C 1.321 gm/cc

MgAl citrate

Laboratory sample
Water-soluble solution of magnesium oxide and aluminum nitrate with citric acid as a sequestering agent
Mg by weight 2.4 per cent
Al by weight 1.6 per cent

Mg HBC

Manufacturer—Continental Oil Company
Colloidally dispersed $Mg(OH)_2$ and $MgCO_3$
Mg by weight 7.62 per cent
Sulfonate 16 per cent
CO_2 9.3 per cent
Oil 58 per cent
H_2O 0.2 per cent
Viscosity at 100 F 203 centistokes
210 F 20.8 centistokes
Specific gravity 1.068

Al HBC

Manufacturer—Continental Oil Company
Colloidally dispersed $Al(OH)_3$
Al by weight 4.36 per cent
Sulfonate ca. 35 per cent
CO_2
Oil ca. 50 per cent
H_2O 0.8 per cent
Viscosity at 100 F 4821 centistokes
210 F 157 centistokes
Specific gravity 0.994

$Al(OH)_3$

Manufacturer—Dow Chemical Company
Oil dispersion of $Al(OH)_3$ inversion products
Particle size—average agglomerate 0.50 microns,
95 per cent of agglomerates less than 1.50 microns
$Al(OH)_3$ by weight 51.0 per cent
H_2O 7.8 per cent
Viscosity at 25 C 5500 centipoise
Density at 25 C 1.51 gm/cc

$Mg(OH)_2$

Manufacturer—Dow Chemical Company
Oil dispersion of $Mg(OH)_2$
Particle size—average agglomerate 0.28 microns,
95 per cent of particles less than 1.20 microns
$Mg(OH)_2$ by weight 43.2 per cent
H_2O 18.3 per cent
Viscosity at 25 C 9500 centipoise

Descaling Process

The descaling process consisted of 5-min immersion in molten salt (Virgo) at 475 C (887 F), quenching in cold water, 30-sec immersion in hot water, 30-sec immersion in six-normal hydrochloric acid at 64 C (148 F), water washing, and scrubbing.

DISCUSSION

J. O. Collins[4]

To those of us who are interested in the problems of oil ash corrosion and deposits in boilers and gas turbines, this meeting has been a fruitful one in this field. Both the present excellent paper and the one presented earlier this week by Messrs. Phillips and Wagoner not only have enhanced our knowledge of what can be expected from the use of additives but serve to emphasize the complexity of the mechanisms involved and the need for more fundamental studies.

The authors of the present paper are to be commended for venturing forward into an area of severe operating conditions which has not been investigated before to my knowledge. There is no question in my mind that the supercharged boiler with its combined high gas and metal temperatures together with physical

[4] Esso Research & Engineering Co., Process Research Division, Linden, N. J. Assoc. Mem. ASME.

compactness represents a new high in severity for heavy fuel oil or coal application. If a satisfactory solution can be found in this area, I am sure the same answer will apply to more conventional boilers and probably gas turbines as well. It is hoped that these studies will be pursued further.

Taking a look at the paper as a whole, it appears that magnesium in almost any form is a good high temperature corrosion inhibitor for vanadium even under these most severe conditions, when used in amounts which have been applied elsewhere for this purpose. The authors based this conclusion on static crucible tests in which the metal specimens were imbedded in what I choose to call "equilibrium" ash deposits removed from the operating unit. While I could find no direct statement in the report, I wonder if the authors can assure me that the same low degree of corrosion was found on the superheater elements in the operating unit during the formative stage of the deposits.

The hypotheses advanced by the authors regarding possible mechanisms by which corrosion and deposits occur are certainly thought-provoking and deserve close consideration. The inhibiting properties of magnesium compounds seem to stem from the formation of noncorrosive magnesium vanadates, usually associated with excess magnesium oxide or sulfate. Just where the reaction occurs is a matter of much speculation but of vital importance. If the major reaction occurs on the surface of the metal, then it is quite clear that deposit formation is almost inevitable. We cannot assume that the corrodent and the inhibitor arrive at the tube surface in the proper proportions simultaneously and therefore the reaction must proceed through initial stages in which the sintering and initial melting points of the reaction products are quite low. Under these conditions, adherent deposits which later attain considerable strength at the tube surface can occur.

To avoid such a condition, it would seem that we must look for some additive or operating condition by which the desired reaction can be obtained rapidly in the gas phase in the hope that the final higher fusion point reaction products will be formed before they reach the metal. In this way, more of the solids may be carried past the heat exchange surfaces and, in addition, those which do strike the surfaces by some physical or aerodynamical means may not develop such a strong bond. This leads to a question I would like to ask the authors, namely, whether any flue gas samples were withdrawn from in front of the screen or superheater section and the solids contained therein analyzed for comparison with the actual tube deposits? From such data, some idea of the amount of gas phase reaction occurring between additives and corrodents could be obtained.

Other investigators have indicated that deposits formed on hot metal surfaces, except in cases where severe corrosion has occurred, are not too far different in character than the ash found in the oil by the conventional oil ash test method. Since quantitative data were obtained on total ash deposits in the present study, we wonder whether an attempt was made to correlate the amount of these deposits with total ash fed to the unit from the fuel oil. The establishment of this so-called "collection efficiency" of the unit might provide a better basis for comparing the effect on deposits of various ratios of a given additive or different additives than just a comparison of the total deposits, per se.

I was particularly interested in the observations made through the observation ports of the unit describing the way in which deposits tend to form.

To me, this means of studying the mechanism of deposit build-up, possibly supplemented by time elapsed movies to obtain a permanent record, deserves more consideration by all investigators in this field.

Finally, I would like to say that we in Esso Research are very much concerned with the problems of deposits and corrosion from oil ash and are actively engaged in laboratory and field studies of them. These studies include unit operations under isothermal conditions similar to those encountered in gas turbines, current construction of a simulated boiler unit for deposit investigations, and bench scale studies aimed at learning more about high temperature corrosion and deposits and their inhibition.

W. E. Young[5] and A. E. Hershey[6]

The authors are to be congratulated on an excellent piece of experimental work, the results of which are another step toward the eventual understanding and solution of the high temperature corrosion and deposition problem. Furthermore, they should be commended for their fortitude in attacking this problem at a temperature level of 2500 to 3000 F. We in the gas turbine industry have found a formidable challenge even at a 1500 F level.

It is gratifying to see a test program of this nature carried out at pressures characteristic of operating pressures in supercharged boilers and gas turbines. For some time we have felt that deposits and corrosion occurring in atmospheric test rigs do not reproduce those occurring in gas turbines because of the effect of pressure on the chemical reactions which are taking place. We would suggest that pressure be added to the list of five variables affecting deposit formation and corrosion if only to emphasize its importance.

Our interest in aluminum-magnesium mixtures as additives stemmed from an examination of the periodic table and some elementary chemical reasoning. Metals of group two such as beryllium, magnesium, calcium, zinc, strontium, and barium, are very active, and in fact are second only to the alkali group in basic strength. They should tend to form metal vanadates with the vanadium in the fuel. Metals of the higher groups such as aluminum and boron of group three, silicon of group four, chromium, iron, and many others, are amphoteric and may react in either an acid or basic manner. (Vanadium itself has this property.) In the presence of sufficient excess active metal of the groups one or two, they should form acid radicals and a compound such as magnesium aluminate would result. Essentially these may still be considered mixtures of metal oxides or spinels of high melting point. It is only necessary that the acid radical be more active than the SO_3 radical formed in the combustion gas stream. Otherwise the active metal sulfate would result. This hypothesis is at least partially verified in the present case where $Mg_3(VO_4)_2$, $MgAl_2O_4$, and MgO were identified in a deposit. Excess magnesium in the form of an oxide would be expected from the initial ratio in the fuel of 3 Mg: 2Al: 1V. On the expectation of possible sulfate formation in the lower temperature regions, it would be preferable to have excess aluminum but one would have to assure himself that the vanadate radical was more active than the aluminate, otherwise all the vanadium might not be combined with the available magnesium and free V_2O_5 rather than Al_2O_3 would result.

The hypothesis may also explain why it has been found necessary to remove sodium compounds from residual oil before combustion. Sodium is such an active element that it tends to disrupt the reactions just outlined and produces the relatively low melting point sodium vanadates and sulfates. These can be counteracted only physically by large amounts of high melting point material and even then a small amount of low melting point eutectic may remain to cause the mixture to become deposit forming. But once more, referring to activities of the acid radicals, it is possible that for a low vanadium, high sodium oil, an aluminum addition might result in the formation of sodium aluminate $NaAlO_2$, a stable compound, with a melting point of 3000

[5] Research Engineer, Research Laboratory, Westinghouse Electric Corporation, East Pittsburgh, Pa. Mem. ASME.

[6] Manager, Development Engineering, Steam Division, Westinghouse Electric Corporation, Lester, Pa. Mem. ASME.

F, rather than sodium sulfate. Thus the necessity of washing a low vanadium fuel might be eliminated but would still be required when sodium and vanadium are both present to prevent the formation of the more stable sodium vanadate. The reaction just outlined will take place only at high temperatures. We have found that furnace heating of a stoichiometric mixture of sodium sulfate and aluminum oxide at 2000 F results in little if any sodium aluminate but that if the mixture is heated with a torch, the reaction proceeds readily. This suggests that, although the gas turbine combustion system might not be depended upon to reach the necessary temperature for reaction, the presently described high temperature furnace may be adequate. Perhaps the authors would consider runs on unwashed low vanadium fuel with and without an aluminum addition for comparative purposes. It should be pointed out that all of the foregoing is based on simple chemical reactions. In practice there are many factors to be considered such as time and the conditions under which the reactions are taking place. The net effect may be that equilibrium is never reached, and the reactions, if they occur at all, may be only partially complete, resulting in a hopelessly complicated mixture of compounds.

One final comment on additive economics is perhaps in order. It was stated, and correctly so, that the use of magnesium aluminum citrate in a full-size installation would be economically prohibitive. This applies to other oil soluble and proprietary additives whose high cost per pound of contained metal makes their use unattractive with highly corrosive fuels where rather large amounts of additive are necessary. However, in some of our newer gas turbine installations, the vanadium content of the fuel has been consistently lower than 100 ppm rather than the 400 ppm figure on which earlier economic studies were based. We are also considering applications where vanadium contents will be in the order of 20 to 50 ppm. And, finally, where machines are sometimes operated at part load it may be possible to cut back on the amount of additive if not to eliminate it entirely during these lower temperature intervals. Thus there appears to be an area, in the case of gas turbine operation at least, where oil soluble additives such as the metallic soaps with their inherent advantages may be economically feasible.

Authors' Closure

The authors appreciate these thoughtful and informative discussions both of which contain excellent suggestions for future experimental work.

In answer to the questions asked by Mr. Collins, the superheater elements are always kept at a temperature low enough to avoid corrosion since replacement of the superheater involves considerable expense. Recently, controlled-temperature test probes were inserted in the gas pass behind the superheater to obtain corrosion data. Initial results have been inconsistent and additional tests and refinement of technique appear to be necessary.

No sampling and analysis of solids contained in the flue gas has been attempted.

The so-called "collection efficiency" of the unit does provide a convenient basis for comparing the relative merits of different additives with regard to deposits. However, its use alone can be misleading if its variation with time is not taken into account along with the selective collection efficiency of the different surfaces in the unit.

P. SEDOR
Test Engineer
Assoc. Mem. ASME

E. K. DIEHL
Senior Chemist

D. H. BARNHART
Research Engineer,
The Babcock & Wilcox Company,
Research Center, Alliance, Ohio

External Corrosion of Superheaters in Boilers Firing High-Alkali Coals

In the past few years, corrosion of high-temperature superheaters and reheaters has become an increasingly serious problem on coal-fired boilers. A type of corrosion that has occurred on several boilers in the Chicago area which burn high-alkali coal is described. The results obtained from an experimental study of the factors influencing the rate of attack and the control measures applied are described.

In striving to reduce the cost of producing electricity, the utilities and manufacturers have designed and built more efficient generating equipment. Today, less than 1 lb of coal is used to produce 1 kw of electrical energy, as compared to 3 lb in 1920. This remarkable progress has been due to many developments including regenerative feedwater heating, steam reheat, and improved fuel-burning methods, to mention but a few. The incorporation of increased operating pressures and temperatures in the design of central stations, however, has been the most important single factor in recent years.

In the Commonwealth Edison Company, as in other systems, a rapid increase in design steam temperatures was made in the late 1940's, as shown in Fig. 1. In a short span of three years, steam temperature rose from 935 F to 1050 F, and steam reheat came into general use. As might be expected, this had a marked effect on boiler design. The amount of heat absorbed in the superheater and reheater increased from 28 to 45 per cent, while the heat absorbed in the furnace walls and economizer decreased proportionally. The additional heat for the higher steam temperatures and reheat was obtained, for the most part, by placing part of the superheater or reheater in the higher gas-temperature zones of the secondary furnace. The increased metal temperatures have required the more extensive use of austenitic materials.

In general, boiler installations designed by the authors' company for these conditions have been free from corrosion. The four cyclone-furnace boilers (1050-F main steam, 1000-F reheat steam) that burned high-alkali coals at Will County and Ridgeland Stations of the Commonwealth Edison Company, Chicago, Ill., have been exceptions.

The high-duty surfaces of these units, i.e., the secondary superheater platens in the upper secondary furnace, as shown in Fig. 2, presented two problems. First, slag and sintered-ash deposits gradually accumulated on both the long and short platens over a period of several months, Fig. 3, despite regular and frequent operation of the soot blowers. Because of the wide spacing of platens, these deposits did not appreciably restrict the flow of gases, nor did they adversely affect the thermal performance of the boiler. Large accumulations falling from the bottom of the platens, however, were a menace to the furnace screen below and had to be removed during outages before personnel could safely enter the furnace.

The second and far more serious of the two problems was the accelerated corrosion of the 18-8, Type 321, tubes in the short

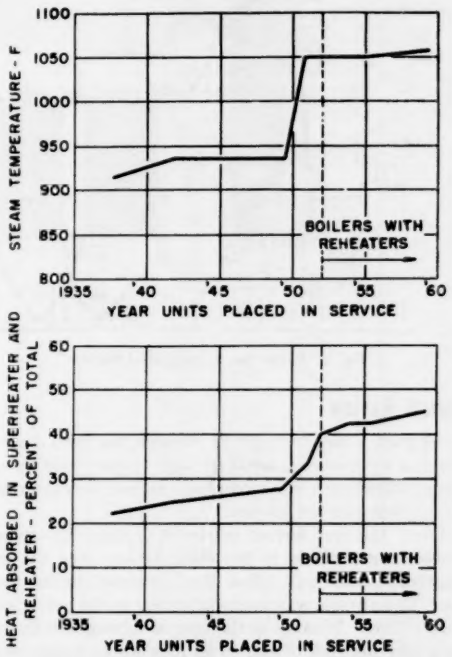

Fig. 1 Trend in boiler-design requirements for units burning Central Illinois coals

superheater platens caused by the components in the ash deposits. The severity of this corrosion is illustrated in Fig. 4, where a cross section of a corroded tube is compared to that of a noncorroded one. While metal was lost all around the periphery of the tube, the metal loss was greatest on the side subjected to the blast of the soot-blower nozzles. After only 18 months of service, one tube failed because of thinning of the wall, and many other tubes were also badly corroded. Most of the tubes in the corroded area were replaced to prevent a series of service interruptions from similar failures.

This paper describes the nature and occurrence of corrosion observed on these superheaters, presents some of the results obtained from an experimental study of the factors involved, and outlines the control measures applied to prevent further serious loss of tube metal. Since ash fouling and corrosion of the platens seem to be closely related, some aspects of the ash-deposit problems are also included.

While most of this information was obtained from the Ridgeland units, it applies in general to the Will County units too.

Contributed by the Research Committee on Corrosion and Deposits from Combustion Gases and presented at the Annual Meeting, Atlantic City, N. J., November 29–December 4, 1959, of The American Society of Mechanical Engineers.

Note: Statements and opinions advanced in papers are to be understood as individual expressions of their authors and not those of the Society. Manuscript received at ASME Headquarters, August 3, 1959. Paper No. 59—A-76.

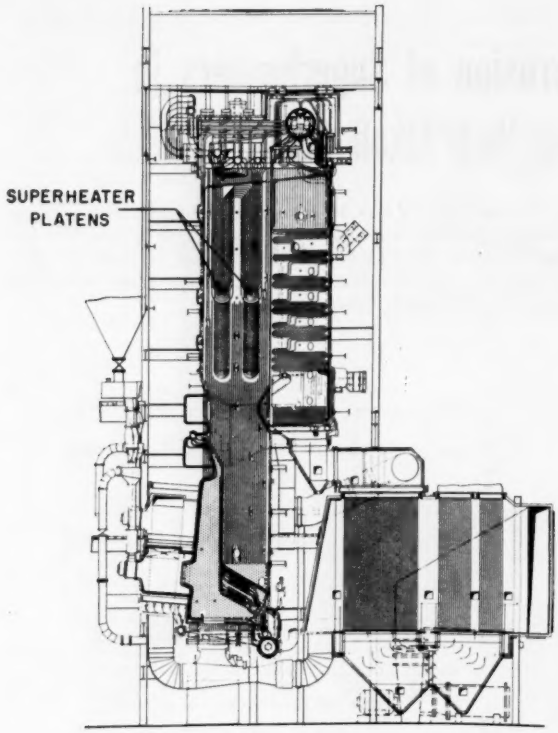

Fig. 2 Boiler No. 5, Ridgeland Station

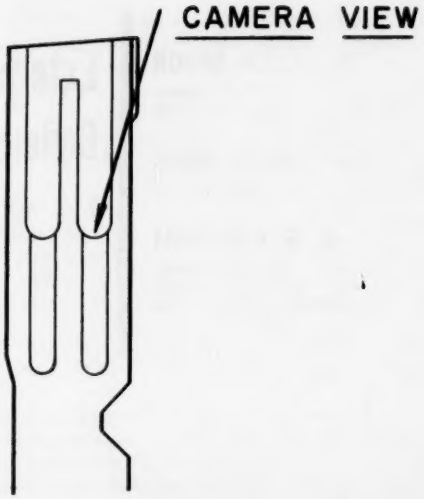

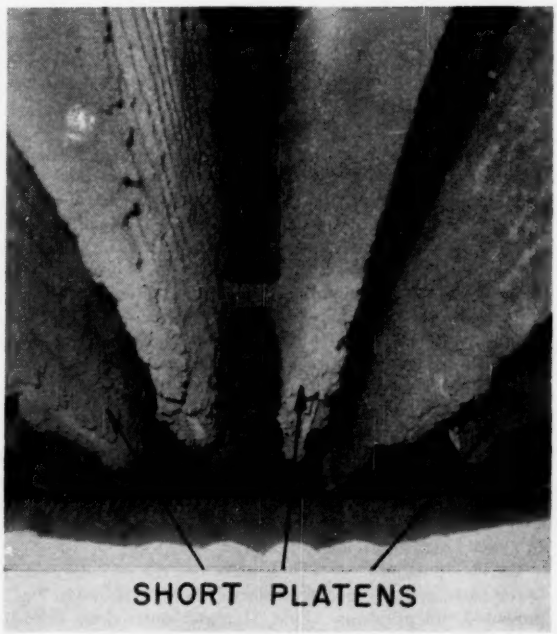

Fig. 3 Ash deposits on platens

Historical Review

In the past, a large amount of research has been done on the accelerated oxidation of metal at high temperature by oil ash, but very little on corrosion by coal ash; at least very few references have been found on the subject.

Probably the first serious corrosion of the high-temperature heat-absorbing surfaces in coal-fired boilers was the external wastage of furnace-wall tubes that occurred during the early 1940's. This trouble was confined largely to the pulverized-coal, slag-tap boilers. Wastage or thinning of tubes generally occurred under a lacy network of slag in an area where flames swept the walls and carbon monoxide was present in the flue gases. Gas temperatures ranged between 2500 and 3200 F and metal temperatures between 550 and 800 F.

Reid, Corey, and others [1, 2, 3][1] attributed the wastage of furnace-wall tubes to an enamel-like deposit consisting of alkali sulfates and/or pyrosulfates that destroy the protective oxide on the tube by the following reactions:

$$3(Na, K)_2 SO_4 + Fe_2O_3 + 3SO_3 \rightarrow 2(Na, K)_3 Fe(SO_4)_3$$

$$3(Na, K)_2 S_2O_7 + Fe_2O_3 \rightarrow 2(Na, K)_3 Fe(SO_4)_3$$

This wastage has been largely overcome by properly positioning burners to avoid flame impingement and uniformly proportioning the coal and air to the burners. In some cases, the use of tertiary air or air belting has been used successfully.

Blank, Hall, and Jackson [4] tested uncooled specimens of superheater alloys in several oil-fired and coal-fired boilers. The corrosion rates of the alloys, held at a nominal temperature of 1350 F, were very low in the coal-fired boilers. As part of the same program, Slunder and Jackson [5] tested the alloys in contact with a mixture of alkali salts in an atmosphere of synthetic boiler-flue gases containing varying amounts of carbon monoxide and sulfur dioxide. Again, the results of these tests did not show an alarming rate of corrosion.

Crossley [6] noted that superheater wastage, caused by the alkali pyrosulfates, occurred in several British power stations with design steam temperatures less than 1000 F but with local overheating of parts of the superheater.

Recently, Koopman, et al. [7], reported corrosion of 18-8, Type 321, superheater and reheater tubes on several dry-ash boilers at the Joppa Station of Electric Energy, Inc., that burn a mixture of Southern Illinois and Western Kentucky coals. These investigators describe the corrosion as a chemical attack resulting from low-melting alkali-sulfate deposits. From probe tests in the

[1] Numbers in brackets designate References at end of paper.

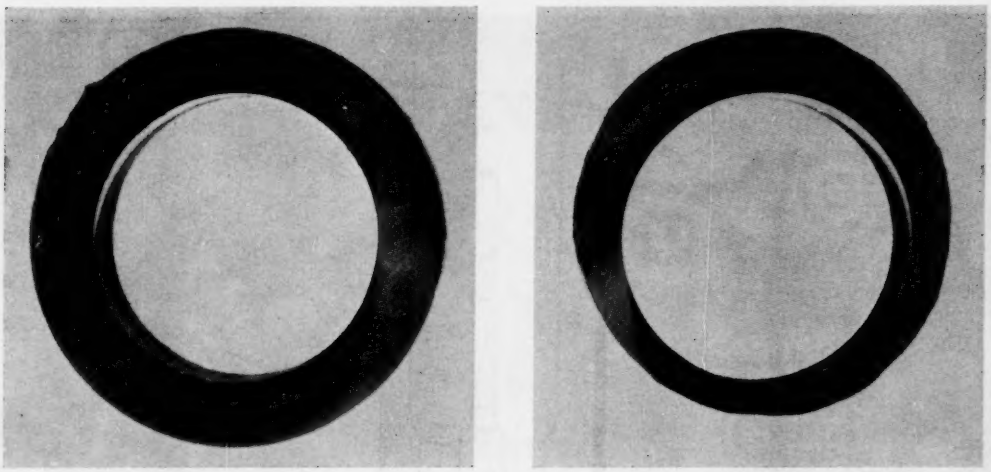

Noncorroded Corroded

Fig. 4 Noncorroded and corroded 18-8, Type 321, tubes from short superheater platen

boilers, they concluded that the corrective measures indicated are to select a more suitable coal and to pulverize it to a finer size consist.

In most boilers, there is a layer of ash next to the superheater tubes that is rich in alkali sulfates, irrespective of the alkali content of coal burned [8, 9]. The amount of this material may vary from mere flecks to a $^1/_4$-in-thick layer. Corrosion has not occurred on these surfaces of boilers designed for steam temperatures less than 1050 F, nor on those designed for 1050-F steam, but without reheaters. As mentioned before, it was the 1050 to 1000 F reheat units, in the Chicago area, burning high-alkali coals, that experienced this difficulty.

To understand the reason for this behavior and the corrective measures that have been applied, a discussion of the nature of coal-ash corrosion and a review of what has been learned concerning its severity and occurrence may be helpful.

Description of Corrosion

General. It is important to trace the steam flow through the secondary superheater platens to understand why corrosion occurred where it did. On Boiler No. 5 at Ridgeland, there are three headers above the platens, Fig. 2. The one at the front of the boiler is the superheater-inlet header. Steam flows from it through the long platens in the front of the furnace and then through the long platens in the rear of the furnace to the intermediate header directly above. From the intermediate header, the steam flows through the short platens in the rear of the furnace and then through the short platens in the front of the furnace to the superheater-outlet header, located between the inlet and intermediate headers.

Owing to this arrangement of surface, the temperatures of the tubes in the long platens are low, while those of the tubes in the short platens are comparatively high. The maximum metal temperature occurs at the bottom of the short platens in the front of the furnace and has been measured as high as 1225 F, although it is usually around 1175 F. The true gas-temperature range in this zone is 2100 to 2300 F with the boiler operating at rated capacity.

Extent of Metal Loss. The pattern of metal loss on the 18-8, Type 321, platens after 18 months of service is shown in Fig. 5. Contours of constant metal loss were derived from the numerous OD measurements made on the tubes in the short platens. The metal loss shown represents the maximum, without regard to where it occurred around the tube.

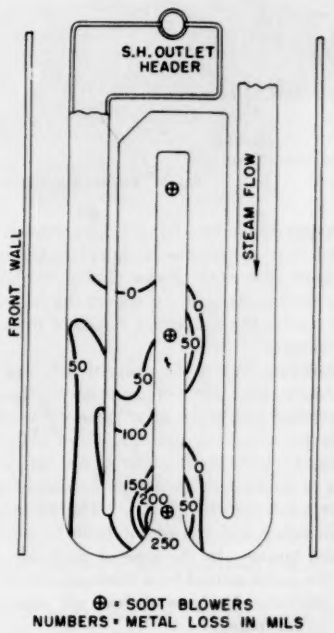

Fig. 5 Pattern of corrosion on 18-8, Type 321, tubes in short superheater platens

Several features of corrosion are shown by the contour plot in Fig. 5. For example, the maximum metal loss occurred on the outside tube in the front platen directly opposite the lower soot blowers. Approximately 0.250 in. of the original 0.380-in. wall was gone; 75 per cent of this loss was on the tube walls nearest the soot blowers and 25 per cent on the walls away from the blowers. Metal loss was still quite severe several feet away from the blower. Although the maximum loss in this area occurred on the sides of the tubes in the platens, a substantial amount of corrosion had taken place around the entire tube, even on those portions not directly exposed to the blast of the soot blowers.

Metal loss was found to diminish rapidly about half-way up the platen in the front of the furnace. Very little metal loss was found on the platens in the rear of the furnace, probably because

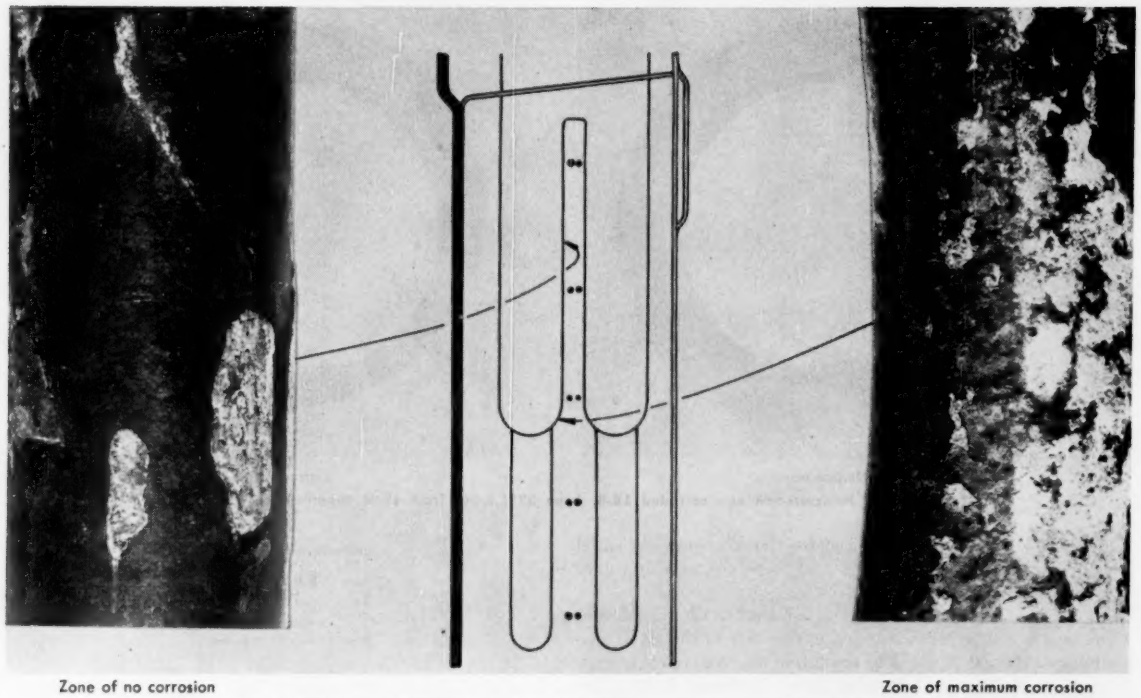

Fig. 6 Surface conditions on 18-8, Type 321, tubes in secondary superheater platens

the metal temperatures were too low for corrosion to proceed at an appreciable rate. There was no sign of attack or a measurable amount of metal loss in the cooler Croloy 3M and Croloy 2¼ tubes on the short platens in the rear of the furnace, nor on the long platens, nor in the convection banks of the primary superheater and reheater.

Surface Conditions. When the sintered ash and slag were removed, a white-to-gray layer of material on the surface of the tubes was exposed and some of it came off with the ash. In general, there was about the same amount of white-layer material along the length of the short platens, but more of it remained on the tubes in the zone of maximum corrosion than in the zone where no corrosion occurred, Fig. 6. This material was tightly bonded to the tubes, and was very difficult to remove completely by mechanical means. In the zone of maximum corrosion, the white layer was accompanied by a black glassy scale, presumably a corrosion product. Analyses of these ash deposits will be discussed later in this paper.

When the white layer and black scale were removed from the corroded tubes (by Virgo salt at 900 F) an undulated and pitted surface was revealed. Although this surface condition prevailed throughout the corroded platens, oddly enough, it was most pronounced on the tubes where metal loss was light to moderate.

Metallurgical Examination. Several corroded 18-8, Type 321, tubes were obtained from the superheater platens of Boiler No. 5 at Ridgeland for a complete metallurgical and chemical study of the corroded metal and its external deposits. Numerous samples through the corroded surface of these tubes were removed for metallographic examination which showed that:

1 The corrosion was a general type of attack that proceeded irregularly across the individual grains of metal. Intergranular corrosion was completely absent from all specimens examined.

2 The tube-metal surface was carburized in varying degrees up to a depth of a few mils. It was most pronounced in the zones of greatest metal loss and diminished in areas where corrosion was less severe, until it was not detected at all where corrosion was absent. A comparison of the extremes is shown in Fig. 7.

Carburization was confirmed by determining the carbon content of the external surface of the tube and the center of the tube wall. The external surface (2 to 5 mils deep) showed a carbon content of 0.66 per cent as compared to 0.063 per cent for the center.

Some sections of the tube showed alternate carburization and decarburization. The white tracery above the blackened carburized zone in Fig. 7 indicates decarburization.

3 There were subscale sulfide penetrations at many locations along the tube (see Fig. 8), but like carburization they were most prevalent in the zone of heavy corrosion.

4 There was some indication from the thickness of the internal scale (steam side) that the lower extremities of the short platens in the front of the furnace had been operating between 1250 and 1300 F.

In summary, metallographic examination of the tubes indicated that the corrosion at the Ridgeland and Will County Stations was the pitting type, accompanied by surface carburization and subsurface sulfide formation. The evidence indicates that alternate reducing and oxidizing conditions prevailed on the surfaces of the tubes with a possibility that some, but not all, of the corroded surfaces had been operating between 1250 and 1300 F.

Chemical Studies. During the 18-month period prior to the platen-tube failure, several coals from Central Illinois were burned at Ridgeland Station, of which more than 75 per cent were from Christian County mines. The analysis of the "average" coal is shown in Table 1. Note that it is a high-volatile, high-ash coal having a low-fusing-temperature ash. Perhaps more important to the ash-fouling and corrosion problems, it contains substantial quantities of alkalis and chlorides. When these high-alkali coals are burned in boilers, they invariably result in alkali-rich and sulfur-rich ash deposits on the convection surfaces. These deposits may also lead to corrosion if the tube metal and gas temperatures are high enough.

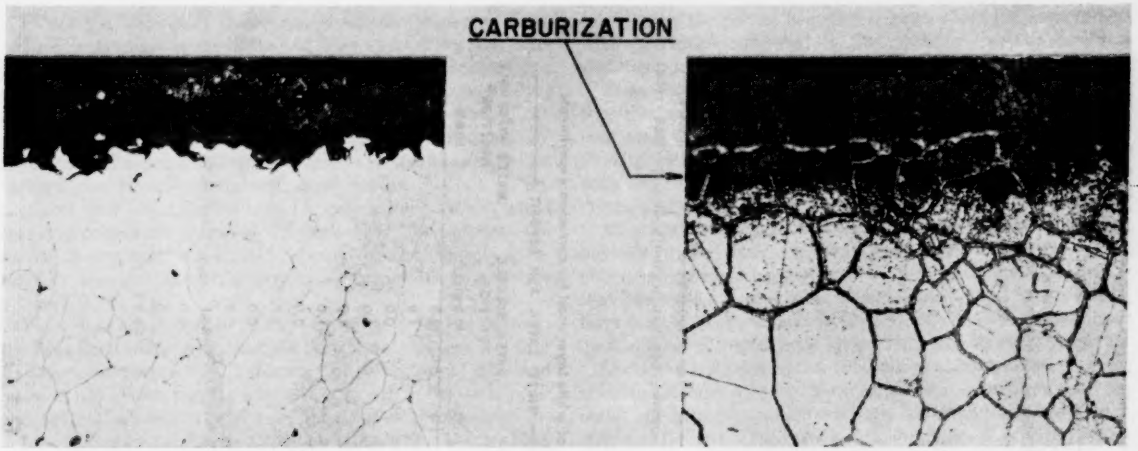

Zone of no corrosion; etched; 500×

Zone of maximum corrosion; etched; 500×

Fig. 7 Polished sections through external surfaces of 18-8, Type 321, superheater tubes

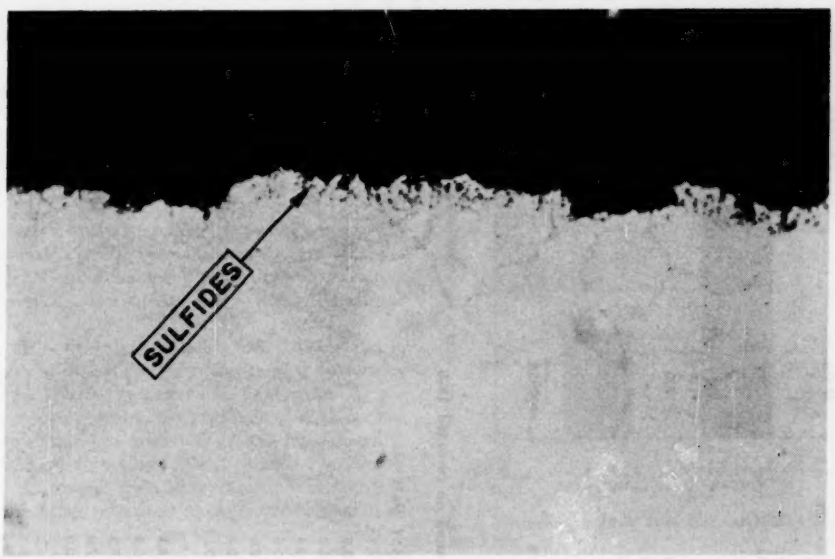

Fig. 8 Polished section through the external surface of corroded 18-8, Type 321, superheater tubes; unetched; 500×

Table 1 Average analysis of Central Illinois coal

PROXIMATE ANALYSIS	
VOLATILE MATTER	40.3 %
FIXED CARBON	44.6
ASH	15.1
TOTAL	100.0 %

ASH FUSION TEMPERATURES	REDUCING	OXIDIZING
I.D.	1940 F	2260 F
S.T.	2000 F	2370 F
F.T.	2560 F	2580 F

SULFUR	4.6 %
TOTAL ALKALI (as Na_2O)	0.63 %
CHLORINE	0.35 %

The white-layer ash deposit on the platens was studied extensively because it was believed that it probably contained the corroding agent and possibly the products of corrosion as well. "Averaged" analyses of white layer from the Ridgeland boilers, of the outer deposit of sintered ash, and the parent coal ash are shown in Table 2. Several characteristics of these ashes are worthy of note. The analysis of the white layer, as one might suspect from its physical appearance, is quite different from that of either the sintered-ash deposit or the coal ash. The white layer is composed mainly of alkali and alkaline-earth sulfates contaminated with small quantities of fly ash and corrosion products. X-ray diffraction analyses show that $NaKSO_4$, $CaSO_4$, $Na_2O \cdot Al_2O_3 \cdot 6SiO_2$, and Fe_3O_4 are present. A 1 per cent water solution of the white layer gives the characteristically strong acid reaction, pH of 3.0, indicating the presence of acid sulfates such as $Na_2S_2O_7$ or $Na_3Fe(SO_4)_3$.

Probably the most important property of the white layer is its low melting point, since it has been demonstrated repeatedly that severe corrosion starts at a certain threshold temperature, which is associated with the melting point of the corrosive mixture. The melting point of the white layer varies at temperatures between 1200 and 1500 F depending upon the amount of contaminating fly ash.

Table 2 Composition of ash deposits from the 18-8, Type 321, superheater tubes

	ASH DEPOSITS		COAL ASH
	WHITE LAYER NEXT TO TUBE	OUTER DEPOSIT (SINTERED ASH)	
SiO_2	9.7%	38.8%	41.7%
Al_2O_3	3.2	17.2	17.0
Fe_2O_3	15.0	16.9	22.0
FeO	5.9	0.0	–
TiO_2	0.3	1.0	0.8
CaO	5.8	6.5	9.7
MgO	1.4	1.3	1.2
Na_2O	3.3	2.2	1.3
K_2O	7.4	3.4	2.0
NiO	2.2	0.0	–
Cr_2O_3	6.5	0.0	–
SO_3	36.9	11.5	4.3
Cl^-	0.0	0.0	0.0
LOI (900 F)	0.4	1.2	–
TOTAL	100.0%	100.0%	100.0%

Table 3 The composition of white layers from corroded 18-8, Type 321, superheater tubes

	WHITE LAYER ASH DEPOSITS		
	NO CORROSION ZONE	MAXIMUM CORROSION ZONE	TYPICAL WHITE LAYER*
SiO_2	10.8%	8.5%	18.2%
Al_2O_3	4.5	1.9	7.5
Fe_2O_3	13.3	16.7	11.1
FeO	6.2	5.5	0.6
TiO_2	0.3	0.3	0.8
CaO	4.5	7.1	5.5
MgO	1.4	1.4	0.8
Na_2O	2.5	4.1	4.9
K_2O	9.2	5.6	7.5
NiO	2.0	2.4	0.0
Cr_2O_3	3.7	9.3	0.0
SO_3	40.5	37.2	41.6
Cl^-	0.0	0.0	0.0
LOI (900 F)	1.1	–	1.5
TOTAL	100.0%	100.0%	100.0%

* FROM SEVERAL BOILERS BURNING CENTRAL ILLINOIS COALS (1950-1956)

Table 4 Composition of corrosion products found on corroded 18-8, Type 321, superheater tubes

	BLACK GLASSY MATERIAL
SiO_2	1.7%
Al_2O_3	0.6
Fe_2O_3	15.2
FeO	12.4
TiO_2	0.6
CaO	0.6
MgO	0.0
Na_2O	0.1
K_2O	–
NiO	6.3
Cr_2O_3	40.9
SO_3	7.9
$S^=$	7.0
Cl^-	0.0
LOI (900 F)	–
TOTAL	93.3%

Table 5 The composition of white layer used for corrosion experiments

	WHITE LAYER ASH DEPOSIT		
	AS RECEIVED	WATER SOLUBLE FRACTION	WATER INSOLUBLE FRACTION*
SiO_2	15.6%	0.0%	15.6%
Al_2O_3	8.8	2.9	5.9
Fe_2O_3	10.3	1.8	8.5
FeO	1.1	0.0	1.1
TiO_2	0.5	0.0	0.5
CaO	7.0	4.0	3.0
MgO	1.0	1.0	0.0
Na_2O	5.1	5.0	0.1
K_2O	7.0	5.7	1.3
NiO	0.1	0.0	0.1
Cr_2O_3	0.2	0.0	0.2
SO_3	40.5	35.1	5.4
Cl^-	0.0	0.0	0.0
LOI (900 F)	2.8	1.0	1.8
TOTAL	100.0%	56.5%	43.5%

* BY DIFFERENCE

It was also important to determine whether there was a difference in the composition of the white layers from the area of no corrosion and those from the area of maximum corrosion. Table 3 shows that the white layers from these zones, though differing in concentration of some elements, mainly the alkalis, are basically the same. The sample from the seriously corroded sections contains a larger amount of corrosion products, as indicated by its higher chromium content. Both deposits contain an appreciable amount of ferrous iron, indicating the possibility that reducing conditions prevailed on the tubes. As has been observed in the past, the chloride content of the deposits is essentially zero and its role, if any, in the corrosion mechanism is a transient one.

There does not appear to be any significant difference between the Ridgeland white layers and the typical white layer except for the amount of ferrous iron, Table 3. The differences in silica and alumina come from varying amounts of fly ash in the white layer and are not believed to be of great importance in corrosion.

In the zone of maximum corrosion, there was a black glassy scale immediately next to the tube metal. This scale, except for sulfur, contained relatively small amounts of ash constituents and was high in chromium, nickel, and iron, showing that it consisted essentially of corrosion products from the tube metal, Table 4. These scales contained significant amounts of sulfates and, of most importance, significant amounts of sulfide. The sulfide was identified by x-ray diffraction as iron sulfide, FeS. Since iron sulfide is known to dissolve protective oxide coatings, thus exposing the metal to the oxygen in the flue gases, it was believed to have played an important part in promoting corrosion.

Experimental

A laboratory program was undertaken at the Babcock & Wilcox Company's Research Center to evaluate the corrosiveness of the white-layer ash deposit on various superheater alloy materials in reducing and oxidizing atmospheres over a range of temperatures.

The tests were made on $1^1/_4$-in-sq specimens, 0.050 in. thick, rolled from actual tube stock, properly heat-treated to remove stress, and lightly sandblasted to remove the light oxide. Triplicate specimens were used for each test, and each of the tests was 100 hr in duration. The white layer was ground fine enough to pass through a 200-mesh screen and was then placed in shallow porcelain dishes. The metal specimens were immersed in the white layer, and the dishes with their contents were placed in an electric furnace and heated to the test temperature. One set of three specimens was used at each temperature—1100, 1200, 1300, and 1400 F. Every 25 hr, the dishes were removed from the furnace and the corrosion agent replenished. At the end of the test, the specimens were descaled and the amount of metal loss was determined by the weight-loss method.

Previous investigations [8, 9] had shown that a large part of the white layer was water soluble. Ridgeland white layers were no exception, as shown in Table 5. Most of the alkalis (except for some of the potassium), all the magnesium, and more than half the calcium were water soluble. The sulfur, except that tied up in the $CaSO_4$, was also water soluble. Most of the iron remained in the insoluble residue. Since its melting temperatures were 1180 to 1220 F in synthetic flue gas, the dried water-soluble fraction would probably exist in the molten state on the corroded parts of the platens during normal operation.

Corrosion tests were then run on 18-8, Type 321, at 1200 F in a synthetic flue gas using the white layer from tubes, the dried water-soluble fraction, and the water-insoluble fraction as corrosive media. The results are shown in Fig. 9. Even though this was a partially spent white layer; i.e., it contained corrosion products, it was still very corrosive. Test specimens indicated that the dried water-soluble fraction was more than twice as corrosive as the parent white layer from which it was obtained, while specimens subjected to the insoluble fraction showed a slight gain in weight due to oxidation.

These tests demonstrated that the white layer is indeed very corrosive, and that a reducing atmosphere is not necessary to obtain accelerated corrosion of the type observed at Ridgeland. Subsequent tests showed corrosion rates at this temperature are truly "catastrophic" when either a reducing or an alternating reducing and oxidizing atmosphere is used.

After it was discovered that the white layer was corrosive under any conditions when the metal temperature was 1200 F or above, efforts were concentrated on finding a superheater alloy that possessed greater resistance than 18-8, Type 321, to white-layer attack. Tests similar to those already described were made on a number of superheater alloys, including 25-20, Type 310.

A series of tests was run on these alloys using synthetic flue gas alone to establish a base. A second series was then run with the metal specimens immersed in white layer and enveloped in a synthetic flue gas. The results of this work are plotted in Fig. 10. It will be noted that 18-8 and 25-20 experience a negligible amount of metal loss in synthetic flue gas. In the presence of the white layer, 18-8 begins to have an appreciable loss of metal at 1100 F, increases gradually to 1200 F, rises rapidly to a maximum at 1300 F, and then falls off rapidly. The corrosion of 25-20 does not take place until the temperature reaches 1200 F. It then behaves similarly to 18-8. Clearly, the critical temperature for accelerated corrosion on 25-20 is approximately 100 deg higher than that for

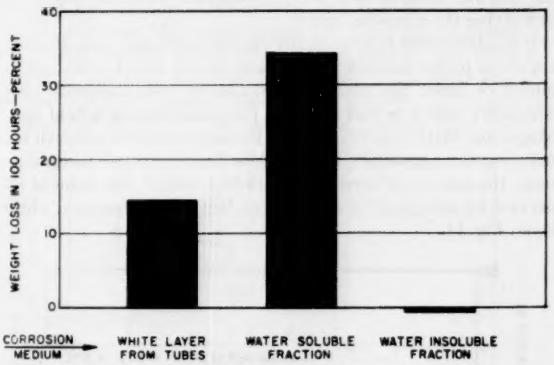

Fig. 9 Corrosion of 18-8, Type 321, at 1200 F in various fractions of white layer

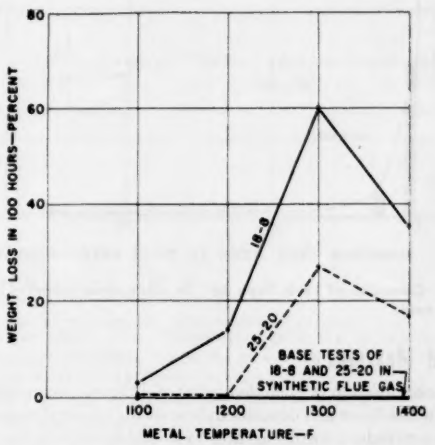

Fig. 10 Corrosion of 18-8, Type 321, and 25-20, Type 310, by white layer in synthetic flue gas

18-8. Moreover, the corrosion resistance of 25-20 is considerably greater than that of 18-8 in the 1150 to 1250-F temperature range of immediate concern. Thus it appears that 25-20 would have a longer service life than 18-8 in boilers where alkali-sulfate deposits are present but, of course, it is not possible from these tests to say how much more life could be expected.

The phenomenon of corrosion rate passing through a maximum around 1300 F was also observed in 24-hr probe tests run on Boiler No. 5 at Ridgeland Station. The corrosion rate on the 18-8 probes was measured by the depth of pits in mils. The pits were from 1 to 2 mils at 1100 F, 2 to 4 mils at 1200 F, 5 to 7 mils at 1300 F, and finally 3 to 4 mils at 1400 F.

Koopman and co-workers [7] observed the same phenomenon while conducting probe tests on a pulverized-coal-fired boiler. They obtained a bell-shaped curve of corrosion versus metal temperature with a maximum occurring over a fairly wide temperature range of 1100 to 1300 F.

The reason for corrosion occurring in this manner is not immediately clear. Temperature usually increases the speed of chemical reactions; uninhibited corrosion of metal is usually linear with respect to temperature. One explanation may be that a temperature is reached at which the corroding agents become unstable in their environment and their concentrations are lowered. If this is so, then we may have a clue as to the identity of the corroding agents. The authors of this paper are presently studying this reaction in various atmospheres over a 500 to 1500 F temperature range using differential thermal analysis and x-ray techniques with the object of identifying the corrosion agents.

If a satisfactory resistant alloy cannot be found, then another approach to the problem of corrosion is the use of additives to inhibit or arrest the attack. A number of basic materials were laboratory tested to find the most promising one for a field test Magnesia (MgO) was found to be the most effective additive for reducing the corrosivity of the white layer. In the laboratory tests, the amount of corrosion on 18-8 at 1200 F was reduced 85 per cent by using as little as 2 per cent MgO with 98 per cent white layer, Fig. 11.

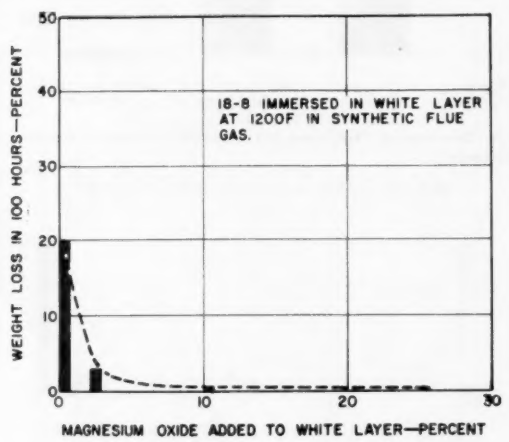

Fig. 11 Corrosion of 18-8, Type 321, in white layer inhibited by magnesium oxide

Control Measures

The examination of corroded tubes and the supplemental work on the white-layer ash deposits indicated that several steps could be taken to reduce corrosion rates to tolerable levels in the Ridgeland and Will County boilers.

Although surveys of the upper-furnace region failed to reveal

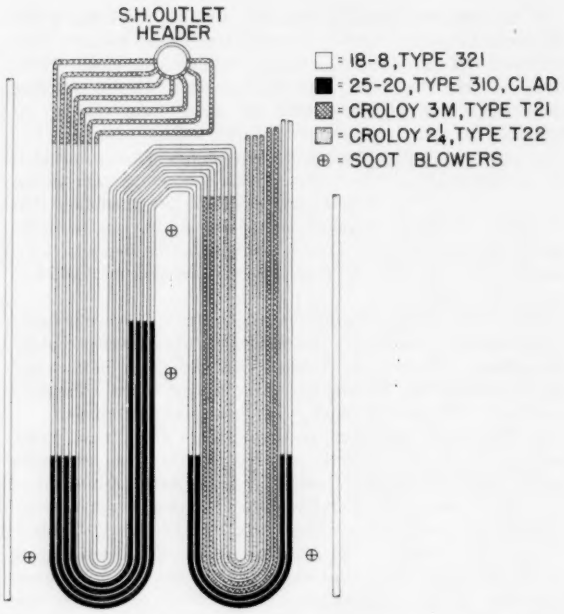

Fig. 12 Arrangement of alloys in short secondary superheater platens

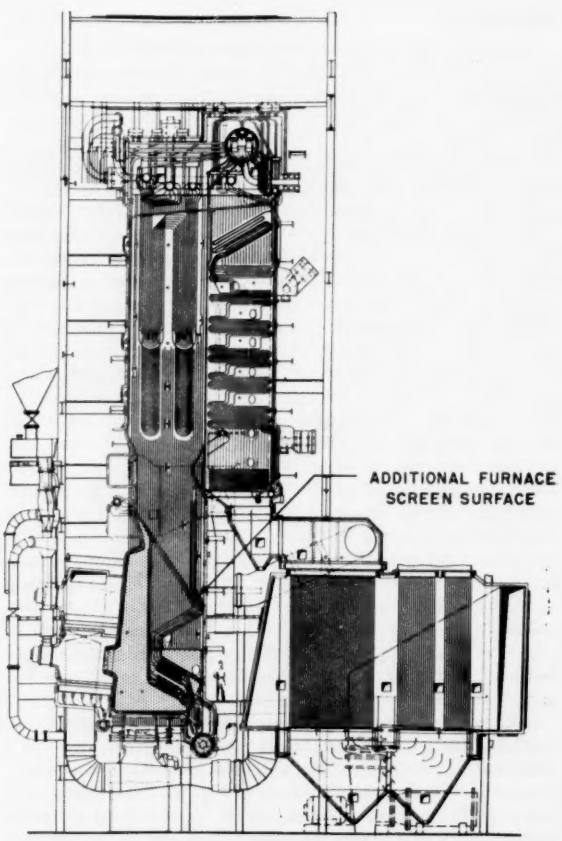

Fig. 13 Boiler No. 5, Ridgeland Station after alterations

any carbon monoxide or gaseous combustibles around the platens, and the carbon content of the fly ash passing through the platens was quite low, the fact still remained that the platen tubes had been carburized and the white-layer ash deposit contained sulfide sulfur and ferrous iron. The excess air on the boiler was, therefore, raised from an average of 8 to 13 per cent, and regular monitoring of excess air and the combustion performance of the individual cyclones was put into practice.

For several months after the platen tube failure on Boiler No. 5 at Ridgeland, the unit was operated at reduced pressure and temperature to prolong the life of the remainder of the badly corroded tubes until they could be replaced. When they were replaced, 18-8, Type 321 tubes, clad with approximately $^1/_8$-in. thickness of 25-20, were installed in their place as shown in Fig. 12.

While the unit was out of service for platen-tube replacement, additional furnace-screen surface was installed, Fig. 13, to ease both the ash-cleaning and the platen-corrosion problems by reducing gas temperature in the superheater. The importance of reducing gas temperature in so far as corrosion is concerned is brought out by the fact that the older boilers in Ridgeland Station, Fig. 14, operate at 1050-F main steam temperature and do not experience corrosion of their 18-8, Type 321, tubes even though superheater metal temperature is approximately 1200 F. These hot surfaces are located in a 1700 to 1900-F gas-temperature zone as compared to 2100 to 2300-F gas temperature in Boilers Nos. 5 and 6 with reheat.

The soot blowers between the lower ends of the short platens were moved out of the critical, high heat-input zone and relocated at the same level in a lower heat-input zone between the front furnace wall and platens. It was felt that here the blowers could do an adequate cleaning job on the platens while permitting a protective layer of oxides to build up on the tubes where corrosion had been most severe.

After the surface changes were made in Boiler No. 5, a $10^1/_2$-month additive test was run using magnesia in a further effort to reduce the corrosion of platens.

There was a substantial change in coals supplying this station at the end of 1957. The Pana mine was closed and low-alkali coals from Southern Illinois and Western Kentucky were substituted.

Present Status

Owing to the seriousness of the corrosion problem, several of the corrective measures discussed were applied to the Ridgeland and Will County boilers at the same time. The effectiveness of these changes is best typified by Boiler No. 5 at Ridgeland Station where corrosion had definitely been a problem and where progress was made in reducing its severity.

A brief history of Boiler No. 5, tracing the progress made in reducing corrosion, is shown in Fig. 15. It is readily apparent that the corrosion rate, as determined by OD tube measurements, was greatly reduced after a number of alterations were made to the boiler and Pana coal was discontinued. The metal loss, expressed as a percentage of tube-wall loss per year, dropped from a maximum of 50 to 6 per cent. This decrease in tube-wall

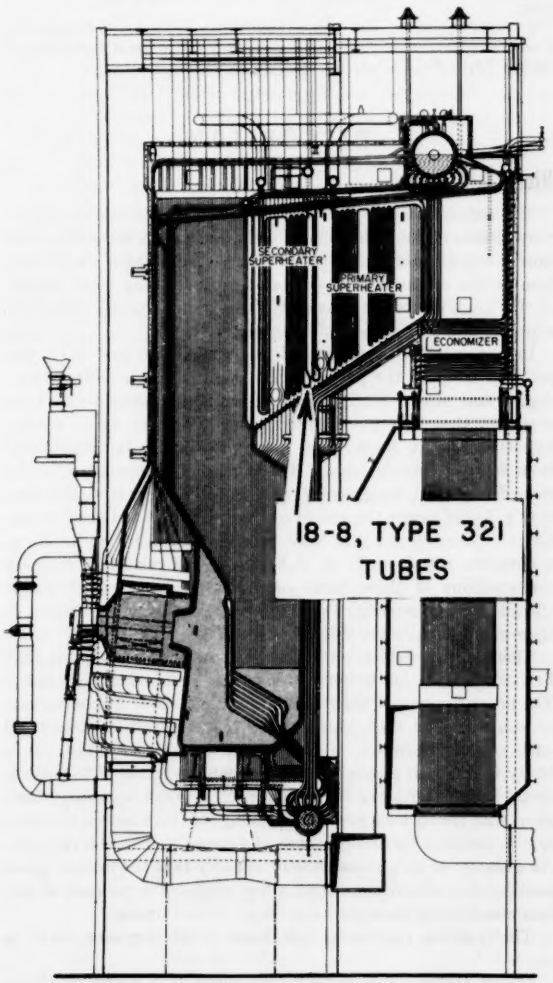

Fig. 14 Boiler Nos. 1, 2, 3, and 4, Ridgeland Station

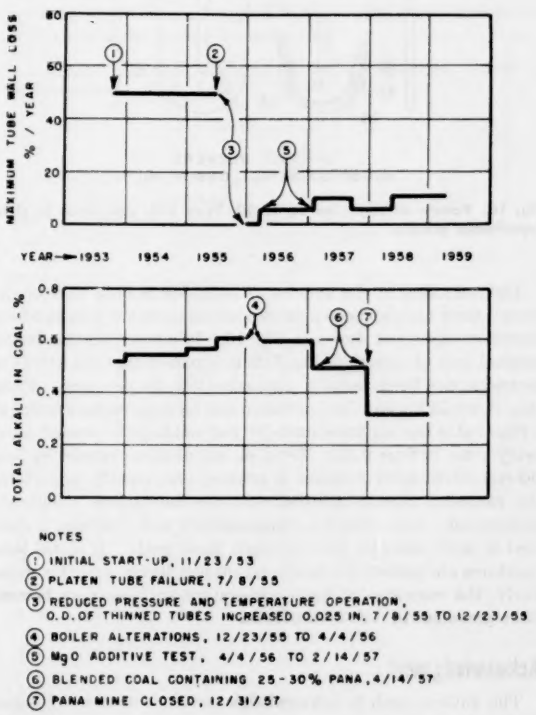
MAXIMUM TUBE WALL LOSS % / YEAR
80
60
40
20
0
YEAR → 1953 1954 1955 1956 1957 1958 1959
TOTAL ALKALI IN COAL - %
0.8
0.6
0.4
0.2
0
NOTES
(1) INITIAL START-UP, 11/23/53
(2) PLATEN TUBE FAILURE, 7/8/55
(3) REDUCED PRESSURE AND TEMPERATURE OPERATION, O.D. OF THINNED TUBES INCREASED 0.025 IN. 7/8/55 TO 12/23/55
(4) BOILER ALTERATIONS, 12/23/55 TO 4/4/56
(5) MgO ADDITIVE TEST, 4/4/56 TO 2/14/57
(6) BLENDED COAL CONTAINING 25-30% PANA, 4/14/57
(7) PANA MINE CLOSED, 12/31/57

Fig. 15 Major events in the history of corrosion on boiler No. 5, Ridgeland Station

wastage is not entirely due to the discontinuance of Pana coal in this boiler. Indeed, it may not even primarily be due to this fact. After burning 25 to 30 per cent Pana coal in 1957 (the same amount as during the first 18 months of operation), the corrosion rate remained low, 5 to 10 per cent, instead of returning to the higher rate of 50 per cent as might be expected if Pana coal were the major factor.

The abrupt reduction in corrosion is more likely to have been due to the reduced metal and gas temperatures in the platens resulting from the installation of furnace-screen surface. Also, the use of higher excess air and the installation of 25-20 clad tubes have undoubtedly been beneficial in reducing corrosion. The use of additive and the shift of soot blowers seem to have been helpful, but the role they played was not decisive in the over-all effort.

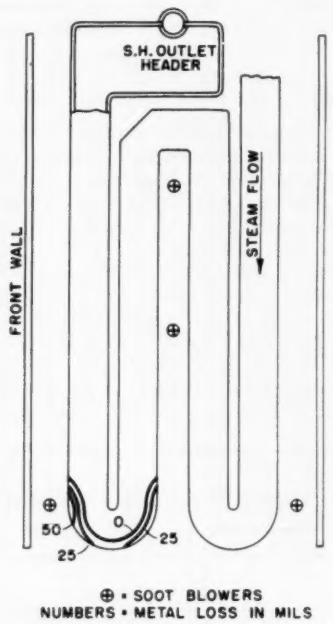

Fig. 16 Pattern of corrosion on 25-20, Type 310, clad tubes in short superheater platens

The reduction in the amount of corrosion is only part of the story; there has also been a drastic reduction in the area in which corrosion occurs, as shown in Fig. 16. In comparing this to the original area of corrosion, Fig. 5, it is apparent that the extent of corrosion has been reduced approximately 90 per cent. From this, it would appear that corrosion can be kept under control at a reasonable cost on these units by pad welding the wasted areas every three or four years. Even so, the problem cannot be considered solved until corrosion is arrested and, equally important, the corrosion agents identified and the mechanism completely understood. Since this is a comparatively new problem, a great deal of work must be done to reach these goals. If metal temperatures are pushed much beyond present levels, and this seems likely, the corrosion of high-temperature surfaces may become more prevalent in coal-fired boilers.

Acknowledgment

The authors wish to acknowledge the work of their colleague, the late F. M. Cook, who conducted the metallurgical phase of this investigation.

References

1 W. T. Reid, R. C. Corey, and B. J. Cross, "External Corrosion of Furnace-Wall Tubes—I, History and Occurrence," TRANS. ASME, vol. 67, 1945, pp. 279–288.

2 R. C. Corey, B. J. Cross, and W. T. Reid, "External Corrosion of Furnace-Wall Tubes—II, Significance of Sulphate Deposits and Sulphur Trioxide in Corrosion Mechanism," TRANS. ASME, vol. 67, 1945, pp. 289–302.

3 R. C. Corey, H. A. Grabowski, and B. J. Cross, "External Corrosion of Furnace-Wall Tubes—III, Further Data on Sulphate Deposits and the Significance of Iron Sulphide Deposits," TRANS. ASME, vol. 71, 1949, pp. 951–963.

4 H. A. Blank, A. M. Hall, and J. H. Jackson, "Behavior of Superheater Tubing Materials in Contact With Combustion Atmospheres at 1350 F," TRANS. ASME, vol. 74, 1952, pp. 813–819.

5 C. J. Slunder, A. M. Hall, and J. H. Jackson, "Laboratory Investigation of Superheater-Tubing Materials in Contact With Synthetic Combustion Atmospheres at 1350 F," TRANS. ASME, vol. 75, 1953, pp. 1015–1019.

6 H. E. Crossley and E. M. Hamilton, "Pulverized Fuel and Boiler Availability Since 1947," Second Conference on Pulverized Fuel, Institute of Fuels, 1957, Preprint B37-B41.

7 J. G. Koopman, E. M. Marselli, J. Jonakin, and R. C. Ulmer, "Development and Use of a Probe for Studying Corrosion in Superheaters and Reheaters," paper presented at the Annual Meeting, Chicago, Ill., March 31–April 2, 1959, of the American Power Conference.

8 J. R. Michel and L. S. Wilcoxson, "Ash Deposits on Boiler Surfaces From Burning Central Illinois Coal," ASME Paper No. 55—A-95.

9 C. H. Anderson and E. K. Diehl, "Bonded Fireside Deposits in Coal-Fired Boilers—A Progress Report on the Manner of Formation," ASME Paper No. 55—A-200.

DISCUSSION

Richard C. Corey[2]

The authors have successfully correlated with laboratory investigations certain phenomena associated with external corrosion of superheater and reheater tubes. Although a clearer picture of the mechanism of corrosion is developing from studies of this kind, the need for more laboratory work under controlled experimental conditions is also becoming clearer.

In general, I believe that if everyone concerned with this problem adopted the premise that there is only a difference of degree and not of kind (compared with the furnace-wall tube corrosion that was investigated some 15 years ago), several hypotheses that have been proposed could be eliminated from further consideration. The common denominator to the corrosion of wall, superheater, and reheater tubes is a corrodent that is liquid under the conditions prevailing at the sites of corrosion. The liquid phase may be an alkali-metal pyrosulfate, a complex sulfate such as $K_3Fe(SO_4)_3$, or relatively complex combinations of these basic compounds. A source of sulfur trioxide also is essential for the formation and the stability of these compounds, other things being equal.

There is little evidence to justify the authors' assumption that FeS plays "... an important part in promoting corrosion." The phase diagram of the iron-sulfur system shows no compounds or eutectics that melt in the range of temperatures associated with external corrosion of superheater or reheater tubes. It is likely that FeS is formed by the reaction of certain of the alkali-metal sulfates with the ferrous alloys. It is not necessary, however, that the furnace gases be reducing for this reaction to occur, nor to account for the presence of ferrous iron in the deposits. As a matter of fact, it seems very unlikely that the furnace gases ever would contain more than a few tenths of a per cent of carbon monoxide in the superheater zone of the furnace.

The question concerning the shape of the corrosion curve in

[2] Chief, Division of Solid Fuels Technology, U. S. Bureau of Mines, Region V, Pittsburgh, Pa. Mem. ASME.

Fig. 10 is an interesting one. We do not know much at present about the phase relationships in the complex sulfate systems, consequently, a rigorous thermodynamic analysis cannot be made. For example, potassium ferric trisulfate might be expected to decompose as follows:

$$2K_3Fe(SO_4)_3 \rightarrow 3K_2SO_4 + Fe_2O_3 + 3SO_3$$

But it may form solid solutions or other compounds with the products. However, if it is assumed for simplicity that this is not the case, the shape of the corrosion curve might be explained as follows:

At about 1150 F the complex sulfate melts, and the corrosion rate increases with temperature until the vapor pressure of SO_3 of the liquid exceeds the partial pressure of SO_3 in the simulated flue gas. The complex then begins to decompose as shown above, solid phase being precipitated from the melt until the mass solidifies. In the absence of liquid phase, the rate of corrosion is comparatively low. This is probably an overly simplified explanation, but it might be verified by conducting the laboratory experiments with specimens immersed in pure $K_3Fe(SO_4)_3$ and varying the temperature from 1100–1500 F, with SO_3 concentrations of 0.2, 0.5, 1.0, and 2.0 per cent by volume in the simulated flue gas. I should expect the peak in the corrosion rate to shift to higher temperatures as the SO_3 concentration increased.

An extensive physical chemical investigation of the alkali metal-iron-sulfur trioxide system clearly is needed. Some work was done along these lines several years ago,[3] which established that only the trisulfates are formed when gaseous SO_3 reacts with alkali-metal sulfates and ferric oxide. But we need to know more about the phases that are formed and their melting characteristics and equilibrium SO_3 vapor pressures. Such studies should be complemented by investigating the effects of adding calcium and magnesium oxides, and other substances that might alter the melting characteristics of pyrosulfates and complex metal-alkali sulfates.

[3] R. C. Corey and S. D. Sidhu, "X-Ray Diffraction Studies of Anhydrous Sodium and Potassium Ferric Sulfates. I. The Disulfates," *Journal, Amer. Chem. Soc.*, vol. 67, 1945, p. 1490.

William T. Reid[4]

This is a precise and informative account of what is evidently proving to be a corrosion problem of increasingly great importance in steam generators. It is a complex problem, difficult to relate to operating conditions, furnace design, or the fuel being burned. Superficially, it appears to be similar in nature to the external corrosion of furnace wall tubes, a problem which caused so much trouble in 1942–1944. It is not a new problem, for some superheater wastage of this type was observed then during inspection of boilers with wall-tube corrosion. Except for the somewhat higher temperature of superheater elements (1175–1225 F) as compared with wall tubes (600–800 F), the pattern of corrosion, the general nature of the deposits present in corrosion areas, and the rate of corrosion are strikingly alike. However, these may be only superficial similarities, and close study may well indicate different mechanisms of corrosion. The authors have done a real service to the industry by providing these data on the composition and nature of deposits on corroded areas.

One technique used with varying success in studying furnace corrosion has been to calculate the possible chemical compounds in the deposits. Such compounds may have contributed to conditions leading to corrosion, or they may indicate the mode of corrosion. Juggling chemical analyses in this manner is open to criticism because, at best, a great many perhaps ill-founded assumptions must be made. Nevertheless, for what they are worth, such calculations have been made for the analyses reported by the authors; they are summarized in the following table. In these calculations, all the iron was calculated as equivalent Fe_2O_3. Only this equivalent Fe_2O_3, the $Na_2O + K_2O$, and the SO_3 were considered significant. The remainder of the deposit was considered to be flyash trapped in the deposit and not to be contributory to the corrosion mechanism.

[4] Assistant Technical Director, Battelle Memorial Institute, Columbus, Ohio. Mem. ASME.

	Table 2		Table 3			Table 5	
Analysis of deposit:	White layer	Outer deposit	No corrosion	Maximum corrosion	Average white layer	White layer	Water soluble
Equivalent Fe_2O_3	21.6	16.9	20.2	22.8	11.8	11.5	1.8
Na_2O	3.3	2.2	2.5	4.1	4.9	5.1	5.0
K_2O	7.4	3.4	9.2	5.6	7.5	7.0	5.7
SO_3	38.9	11.5	40.5	37.2	41.6	40.5	35.1
$Na_3Fe(SO_4)_3$ equiv. to Na_2O	14.7	9.8	11.1	18.2	21.8	22.7	22.2
$K_3Fe(SO_4)_3$ equiv. to K_2O	24.1	11.1	30.0	18.3	24.4	22.8	18.6
Total trisulfates	38.8	20.9	41.1	36.5	46.2	45.5	40.8
Fe_2O_3 equiv. to $Na_3Fe(SO_4)_3$	2.8	1.9	2.1	3.5	4.2	4.4	4.3
Fe_2O_3 equiv. to $K_3Fe(SO_4)_3$	4.2	1.9	5.2	3.2	4.2	3.9	3.2
Total Fe_2O_3 in trisulfates	7.0	3.8	7.3	6.7	8.4	8.3	7.5
Fe_2O_3 from flyash[a]	5.1	20.4	5.7	4.5	9.6	8.2	0.0
Unaccounted for Fe_2O_3	9.5	−7.3	7.2	11.6	−6.2	−5.0	−5.7
SO_3 equiv. to $Na_3Fe(SO_4)_3$	8.5	5.7	6.5	10.6	12.7	13.2	12.9
SO_3 equiv. to $K_3Fe(SO_4)_3$	12.6	5.8	15.6	9.5	12.7	11.9	9.7
Total SO_3 in trisulfates	21.1	11.5	22.1	20.1	25.4	25.1	22.6
SO_3 in excess of trisulfates	17.8	0.0	18.4	17.1	16.2	15.4	12.5
SO_3 equiv. to $FeSO_4$ from unaccounted for Fe_2O_3	5.5	...	4.1	6.7	...	...	...
Total excess SO_3	12.3	0.0	14.3	10.4	16.2	15.4	12.5
Ratio, K_2O/Na_2O[b]	2.24	1.55	3.68	1.37	1.53	1.37	1.14

[a] Based on SiO_2/Fe_2O_3 ratio of 1.9 in coal ash of Table 2.
[b] Ratio in glaserite ($3K_2SO_4 \cdot Na_2SO_4$) = 3.67

On the basis that the alkali ferric trisulfates are intimately connected with corrosion, as was concluded in the earlier work on wall-tube wastage, the quantity was calculated of the $Na_3Fe(SO_4)_3$ equivalent to the Na_2O shown by the analysis, and of the $K_3Fe(SO_4)_3$ equivalent to the K_2O. Then, the amount of Fe_2O_3 and SO_3 equivalent to these amounts of the alkali ferric trisulfates was determined as an indication of how completely the alkali ferric trisulfates accounted for the materials present. In all cases but two, both the Fe_2O_3 and the SO_3 were present in excess.

Some broad generalizations can be drawn from these calculations. First, there is a remarkable similarity between all the analyses. In considering the white layer, the total alkali ferric trisulfate varies only between 36.5 and 46.2 per cent. Even with the outer deposit, which had been exposed to relatively high temperatures, 20.9 per cent was alkali ferric trisulfate. Because somewhat more than one third the deposit may consist of these trisulfates, the authors' conclusion that they were present, based on a low pH, seems to be justified.

Second, excess iron beyond that required to form the trisulfates is present in all the samples except the water-soluble portion in Table 5. A silica balance permits estimation of the quantity of iron expected in the trapped flyash; this Fe_2O_3 ranges from zero in the water-soluble sample of Table 5 to 20.4 per cent for the outer deposit of Table 2. Adding this Fe_2O_3 to that in the trisulfates, and deducting the sum from the Fe_2O_3 shown by analysis, gives the "unaccounted for" Fe_2O_3. In four of the samples this is a negative quantity, indicating that not enough iron was present in the sample to account for the Fe_2O_3 in the flyash and the trisulfates. In the other three samples, more than enough Fe_2O_3 was present, and it may be significant that the largest excess of Fe_2O_3 occurred with the sample taken from the maximum corrosion area.

Third, treating the SO_3 similarly, all but one sample showed an SO_3 content greater than would be necessary to form alkali ferric trisulfates. This one sample, having been heated to a higher temperature because it was the outer layer of the deposit, would be expected not to contain excess SO_3. With the others, the excess SO_3 amounted to about one sixth the weight of the sample. A check to determine how this SO_3 might be combined was inconclusive. For example, with those deposits having Fe_2O_3 in excess of that equivalent to the sum of the trisulfates and flyash, the SO_3 unaccounted for would be sufficient to convert about twice as much Fe_2O_3 to $FeSO_4$ as would be available. Hence, one might deduce that the total SO_3 in the sample would have been sufficient to have converted all the alkalies to the alkali ferric trisulfates, all the excess available Fe_2O_3 to $FeSO_4$, and still leave an appreciable quantity of SO_3 to form pyrosulfates.

Fourth, the ratio of K_2O to Na_2O remains remarkably constant in all these samples. Although somewhat lower than the ratio of 3.67 for glaserite ($3K_2SO_4{\cdot}Na_2SO_4$), a known corroding agent particularly in the presence of excess SO_3, the K_2O/Na_2O ratio nonetheless may be important.

Finally, although such calculations as these may demonstrate only a willingness to try any expedient leading to understanding the incomprehensible, they may point out clues to the corrosion mechanism not otherwise easily spotted. Certainly every available path to such understanding will need exploring.

J. P. Winkin[5]

The authors are to be complimented on their excellent presentation of the field and laboratory work which has been done in connection with coal ash corrosion in boilers burning high-alkali coals. It will be of general interest to note that the Jersey Central Power & Light Company has encountered the same general type of corrosion in the secondary superheater outlet sections in the Nos. 7 and 8 boilers at its Sayreville Station.

The Nos. 7 and 8 boilers at Sayreville are very similar in design to the Nos. 5 and 6 boilers at the Ridgeland Station of the Commonwealth Edison Company. They both have 1050 F radiant platen-type secondary superheaters with 1000 F convection type reheaters. The Nos. 7 and 8 boilers at Sayreville are 900,000 lb per hour units which operate at a design peak load of 990,000 lb per hour for 4 hours a day.

The Nos. 7 and 8 boilers at Sayreville, in general, have been burning low alkali strip mine coals from West Virginia; however, some low alkali strip mine coal from Pennsylvania also has been burned. The total alkali content of coals from this area is generally less then 0.2 per cent by weight compared with the 0.6 per cent total alkali found in many of the Central Illinois coals referred to in the paper.

Most of the corrosion in the Sayreville units has occurred in the lower bend areas of the short secondary superheater outlet platens in the No. 7 boiler, which has been in service about 5 years. The maximum metal loss in this area has amounted to about 0.034 in. per year. Evidence of the same type of corrosion has been found in the secondary superheater of the No. 8 boiler, which has been in service about one year.

An interesting feature of the corrosion in the superheater platens in the Nos. 7 and 8 boilers at Sayreville, is that it also has occurred on the bottom of the inner loops, which are shielded from sootblower action. The wastage at the bottom of the inner loops has been almost as great as the wastage on the bottom of the outer loops. In this connection it should be noted that the superheat sections on the Sayreville unit have remained relatively clean with very little back spacing deposits.

It is interesting to note that the corrosion rate is greater on the sides of the secondary superheater platens which face the wide spaced areas where some of the long platens were omitted. Further evidence of the effect of temperature on wastage rates is found in the localized accelerated wastage which has taken place at the base of the lower support lugs on the short secondary superheater outlet platens. The wastage at the base of the lugs was found under small sintered deposits which adhered to the base of the lugs.

Corrective action to date has consisted of replacing severely corroded sections, pad welding areas where the corrosion is localized, removing some support lugs and raising others to cooler zones. Steps also are being taken to improve the combustion controls on No. 7 boiler and to improve the control of the fineness from the coal crushers.

In looking for other corrective measures, it is encouraging to note that the work done by B & W research, as presented in their paper, indicates that 25-20 tubing is considerably more resistant to this type of corrosion than the 18-8 type 321 material installed in the high temperature sections of the Ridgeland and Sayreville superheaters.

There are many boilers in service today which have not had accelerated coal ash corrosion with 1050 F superheaters. The fact that the Nos. 5 and 6 boilers at Ridgeland and the Nos. 7 and 8 boilers at Sayreville have experienced this difficulty on different types of coal indicates that there is something in the arrangement of these units which makes them susceptible to coal ash corrosion. It is likely that this sensitivity results from the fact that the outlet sections of the 1050 F secondary superheater platens are exposed to high furnace temperatures which, as indicated in the paper, can produce metal temperatures in the 1225 F range.

The effect of metal temperature on coal ash corrosion can be seen by the absence of accelerated corrosion in the 1000 F radiant superheater platens on the cyclone fired boiler in Jersey Central Power & Light Company's South Amboy Station. This boiler

[5] Engineer, Jersey Central Power & Light Company, South Amboy, N. J. Assoc. Mem. ASME.

has been in operation for about 8 years. The radiant platens on the South Amboy unit hang down in the secondary furnace, and are exposed to about the same gas temperatures and radiation conditions as exist in the affected areas of the Nos. 7 and 8 boilers at Sayreville; however, they are about 50 F cooler.

The effect of metal temperatures on coal ash corrosion is brought out in the paper by its disclosure that accelerated corrosion has not occurred on the 1050 F secondary superheater on the Ridgeland Nos. 1 to 4 boilers. This is an important point, since the superheater sections in these boilers are buried in the rear of parallel flow banks, which are located in cooler gas temperature zones. This protected location certainly results in lower outer fiber metal temperatures than exist in the affected areas of the Nos. 5 and 6 boilers at Ridgeland and the Nos. 7 and 8 boilers at Sayreville.

There is much to be learned about coal ash corrosion now that it has been recognized as a major problem in the operation of high temperature units. It is hoped that the experience of those who are now suffering from coal ash corrosion will guide both the designers and the researchers to better methods of coping with this problem.

Authors' Closure

The authors would like to express their appreciation to Messrs. Corey, Reid, and Winkin for their interesting comments and helpful suggestions which have greatly added to the value of this paper.

The authors agree with Messrs. Corey and Reid that the Ridgeland ash deposits probably contain alkali-metal pyrosulfates and complex sulfates such as $K_3Fe(SO_4)_3$. However, positive identification of these substances by x-ray and optical techniques has been made in only a few of the hundreds of white layer ash deposits taken from the Ridgeland boilers and others throughout the country. This may be due to the general complexity and poor crystallinity of the deposits, or these components actually may not be present in very large concentrations.

As a matter of fact, it is not necessary for the white layer to contain pyrosulfates or the complex alkali-iron sulfates for excessive tube wastage to occur. In extending the work of Simons[6] and Shirley,[7] the authors found that the normal sulfates of sodium, potassium, and calcium attack both ferritic and austenitic alloys when only small amounts of chlorides, sulfides, or carbon are present. Moreover, probe and fly-ash sampling surveys in the field have shown that enough of these substances may be present under some operating conditions. Thus, at Ridgeland where the outer ash deposits are frequently removed by soot blowers, the white layer ash deposits are exposed to the flue gases for several hours each day. It is entirely possible that the tube wastage may be caused by the normal sulfates in the white layer which have been contaminated by chlorides from the flue gases or by small amounts of carbon from the fly ash. That carbon was present in the Ridgeland deposits was evidenced by the carburized condition of the corroded superheater tubes. Carbon burn-out in the deposit could also be responsible for causing the highly reducing atmosphere at the tube surface.

There are other possible corrosive agents. For example, sodium silicate and sodium hydroxide are corrosive to superheater alloys operating at 1200 F. While it is considered unlikely that these corrosive substances would survive in the furnace atmosphere long enough to reach the tubes, such a possibility should not be overlooked in a study of mechanisms.

Mr. Winkin describes a type of corrosion that takes place on virtually a clean superheater. The white layer deposit that is usually found under the sintered ash was detected as mere flecks in a few widely scattered areas on the tubes. The metallographic features of the corrosion, i.e., heavy carburization, sulfidization followed by oxidation, etc., were the same as those observed on the Ridgeland tubes. On the basis of present knowledge, it is difficult to visualize how complex alkali sulfates could have been involved, owing to the small amount of white layer present. The authors are led to the tentative conclusion that the mechanism of corrosion occurring on the Sayreville boilers is entirely different from that at work on the Ridgeland boilers. In our opinion, there may be several types of corrosion occurring on boilers, depending upon the composition of the ash and flue gases, and boiler operating conditions.

While we agree with Mr. Corey that additional research work should be done on the alkali-iron-sulfur system, we believe that it should not be limited to this mechanism alone.

[6] Edward L. Simons, George V. Browning, and H. A. Liebhafsky, "Sodium Sulfate in Gas Turbines," *Corrosion*, vol. 11, December, 1955, pp. 17–26.

[7] H. T. Shirley, "Effects of Sulphate-Chloride Mixtures in Fuel-Ash Corrosion of Steels and High-Nickel Alloys," *Journal of The Iron and Steel Institute*, vol. 182, February, 1956, pp. 144–153.

WHARTON NELSON
Chemical Section Leader

CARL CAIN, JR.
Research Engineer,
Kreisinger Development Laboratory,
Combustion Engineering, Inc.,
Chattanooga, Tenn.

Corrosion of Superheaters and Reheaters of Pulverized-Coal-Fired Boilers

Field Inspections

SEVERAL YEARS AGO inspection of the reheater and finishing superheater tubes in a 1055-F, 1005-F boiler firing pulverized midwest coal revealed considerable external corrosion loss of tube metal. Although in operation only two years, some 321 stainless-steel reheater tubes had lost about 50 per cent of the original 0.125 in. thickness, a penetration rate of 0.032 in. per year. Corrosion was spread fairly evenly from left to right and top to bottom in both reheater and finishing superheater. This information initiated inspection of 26 pulverized coal-fired boilers in various parts of the country to determine the nature and extent of the corrosion problem. Advanced corrosion was observed in only a few units. Fig. 1 shows location of the surfaces affected. The inspections revealed a number of points in common to the affected boilers:

1 Corrosion was significant only in units with outlet steam temperature above 950 F.

2 In a few boilers both SA 312 TP 321 stainless steel (18 per cent chromium, 8 per cent nickel, titanium-stabilized) and low-chrome ferritic-alloy tubing corroded at faster rates than one would expect from flue-gas attack at their measured operating skin temperatures. Corrosion of the low-chrome ferritics like SA 213 T22 ($2^1/_4$ per cent chromium and 1 per cent molybdenum) was usually more advanced, as one would expect from their lower oxidation (scaling) resistance.

3 Significant corrosion occurred only on windward surfaces of tubes which accumulated ash deposits. The entire 180-deg leeward surfaces had no pronounced corrosion. Stainless-steel tubes had an appreciable layer of deposits during operation of the boiler, but these spalled off on cooling.

4 Corrosion was severest on lead tubes and sometimes extended to the second row in a bank. On individual tubes, metal loss was often shifted to the left and right of the point of flue-gas impingement. Fig. 2 shows these locations and the appearance of wasted tubes of both alloys. In corroded areas metal was changed into metal-oxide scale (predominantly Fe_3O_4) which, in the case of ferritic alloy, remained on the tube as a hard, adherent, black layer directly above the corroded surface.

5 Corrosion rate depended on both metal temperature and presence of ash deposits. Screen and water-wall tubes often had ash deposits but never had pronounced metal loss.

6 Retractable sootblowers, both air and steam, in some units severely damaged lead tubes, especially those of ferritic alloy, near the impingement area. The extent of damage increased with skin metal temperature. Corrosion losses, however, were observed beyond the reach of the retractables.

Contributed by the Research Committee on Corrosion and Deposits from Combustion Gases and presented at the Annual Meeting, Atlantic City, N. J., November 29–December 4, 1959, of THE AMERICAN SOCIETY OF MECHANICAL ENGINEERS.

NOTE: Statements and opinions advanced in papers are to be understood as individual expressions of their authors and not those of the Society. Manuscript received at ASME Headquarters, August 13, 1959. Paper No. 59—A-89.

These findings led to the establishment of a research program to determine the cause and prevention of accelerated wastage. The corrosion mechanism has been studied extensively and a description of these investigations constitutes the main body of this paper.

Laboratory Work

Initial laboratory experiments sought to find the corrosion rates of T22 and 321 stainless-steel alloys in flue gas and air. For this purpose a series of tubular muffle furnaces equipped with electronic temperature regulators was set up. This apparatus is shown in Fig. 3. Each furnace was equipped with a Vycor glass tube liner and supplied with air or synthetic flue gas of the following typical composition (in per cent by volume): 15 per cent CO_2, 3.6 per cent O_2, 81.15 per cent N_2, and 0.25 per cent SO_2. Electropolished coupons $1^1/_2 \times {}^3/_4 \times {}^1/_8$ in. of each alloy were placed in a furnace and heated in air or flue gas at precise (±5-F) temperature intervals from 1000 to 1400 F for a week. Tests were run at a pressure of 4 in. Hg. These tests, due to the parabolic nature of gas-phase attack and the short exposure compared with boiler use, gave higher average corrosion rates than would be experienced in typical field use of the same alloy in flue gas alone. They did, however, allow the following observations:

1 Flue-gas attack on T22 mounted rapidly with increasing temperature above the normal limit of use, 1100 F.

2 Gas-phase corrosion of T22, which developed a semiprotective scale, followed the parabolic law, $y^2 = kt$, where y = scale thickness and t = time.

3 The T22 scale spalled off upon reaching a critical thickness. This characteristic may account for much of its wastage in sootblower impingement areas. By contrast, the 321 stainless steel in flue gas rapidly built up a type of scale which was fully protective and nonspalling.

4 Flue-gas attack on 321 stainless steel, even at temperatures as high as 1400 F, did not result in the corrosion rates observed in actual boiler operation at the first unit inspected.

Other tests using pure sulfur dioxide and pure sulfur trioxide with T22 and 321 stainless steel at 1200 F showed that neither atmosphere was substantially more corrosive than synthetic flue gas. With carbon steel Corey, et al. [1][1] found little difference in corrosiveness between sulfur dioxide and air up to about 1300 F. It was concluded that gas-phase attack, particularly of stainless steel, could not account for the corrosion rates observed in operating boilers, and that an inherently faster liquid-phase corrosion mechanism was probably involved.

Chemical Analysis of Deposits

The second phase of laboratory work was a detailed wet-chemical analysis of the various layers of deposits collected from field inspections. A diagram of these layers on ferritic tubing is shown in Fig. 4. The layer furthest from the tube surface was usually

[1] Numbers in brackets designate References at end of paper.

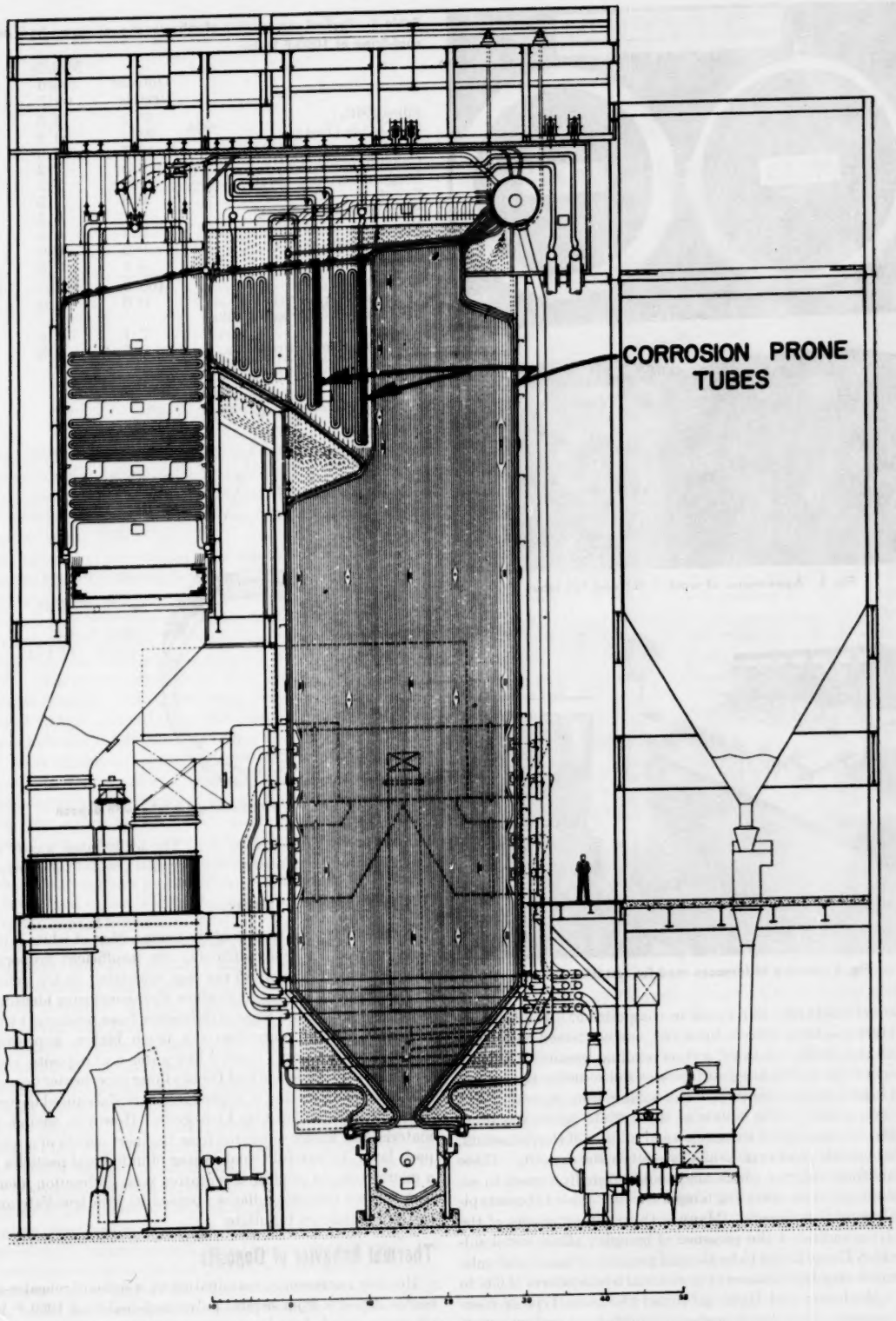

Fig. 1

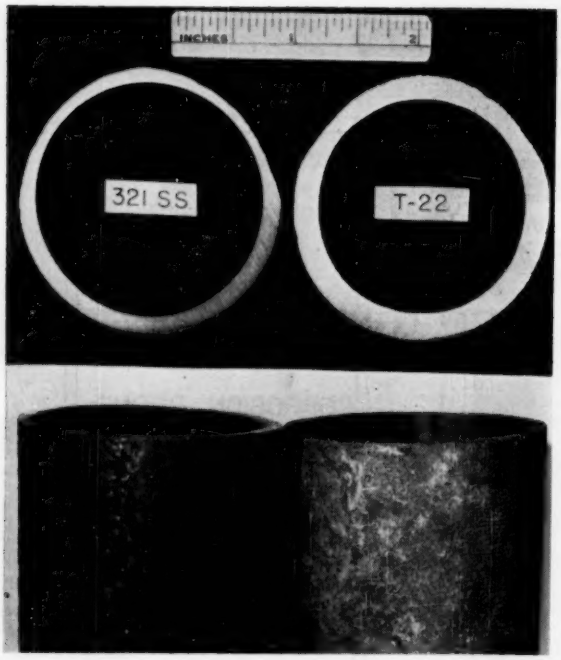

Fig. 2 Appearance of wasted 321 and T22 tubes

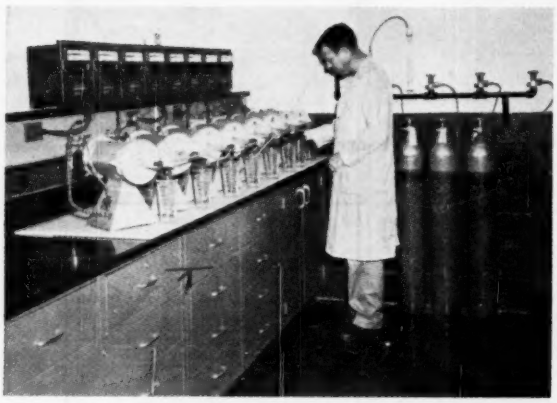

Fig. 3 Battery of furnaces used for corrosion studies

friable and essentially like flyash in composition. The intermediate layer was hard, usually brick red, and contained higher sulfate and iron oxide. A third, soft, crystalline, cream-white layer which occurred on the tube surface was quite unlike the others. It had higher water-solubility, water-soluble iron, potassium, sodium, and sulfate. The sulfate of these white layers was often in excess of that required to form normal sulfates of the potassium, sodium, calcium, and magnesium present in the deposit. These elements form sulfates which one would normally expect to remain stable at boiler operating temperatures. Table 1 shows typical analyses of these layers. Many of these characteristics of the white layer indicated the presence of complex alkali metal sulfates which Corey found to be the end product of water-wall tube corrosion in slag-tap furnaces at skin-metal temperatures of 600 to 750 F. Anderson and Diehl [2] found this same type of compound present in bonded deposits on finishing convection superheater surfaces of a modern boiler furnace. The next efforts were therefore centered on identifying the specific corrosive com-

Table 1 Typical composition of reheater deposit layers from pulverized coal-firing of 1050-F boiler

	Outside (friable)	Middle (hard red)	Inner (white)
Silica (SiO_2)	45.9	15.6	52.4
Iron oxide (Fe_2O_3)	23.1	54.8	8.6
Aluminum oxide (Al_2O_3)	18.7	15.0	7.2
Calcium oxide (CaO)	2.5	3.2	2.4
Magnesium oxide (MgO)	1.9	2.2	2.7
Sulfate (as SO_3)	0.8	7.5	15.6
Sodium oxide (Na_2O)	1.1	0.3	0.6
Potassium oxide (K_2O)	2.2	0.6	2.5
Moisture (H_2O)	0.0	0.0	5.4
Other	3.8	0.8	2.6
Total	100.0	100.0	100.0
"Excess" SO_3, per cent	0.0	0.0	3.9
pH of 1 per cent water solution	7.1	4.4	2.5
Water soluble, per cent	2.5	9.5	25.2

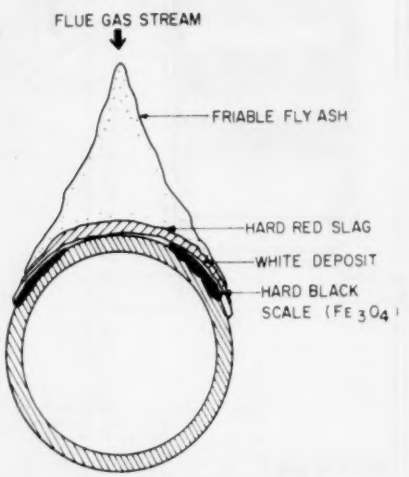

Fig. 4 Ferritic reheater tube with deposit

pounds present in these layers. The white layer was of special interest since it was nearest the corroded areas of tube surface.

X-Ray-Diffraction Studies

X-ray-diffraction studies of the composition of white-layer material proved unusually difficult. An insufficient proportion of complex sulfates, about 15 per cent calculated on the amount of excess sulfate, was present to allow their conclusive identification from the complicated maze of diffraction lines produced by matrix materials. Their proportion ran much higher, approximately 55 per cent, in Corey's enamel-like water-wall deposits, and 30 to 65 per cent in Anderson and Diehl's inner superheater deposit layers. Water extraction of white-layer material caused destruction of its complex sulfates by hydrolysis. However, enough active material was finally separated from the inert matrix of a white deposit layer, by careful visual sorting of individual particles under a microscope, to produce a tentative x-ray-diffraction identification for two complex sulfates—potassium iron trisulfate and potassium aluminum trisulfate.

Thermal Behavior of Deposits

Heating microscopic examination of a series of reheater-superheater deposits from several pulverized-coal-fired 1050-F boilers allowed a detailed study of their fusion characteristics on heating in air. Although the metal temperatures on the tube surfaces from which these deposits were taken would continually run

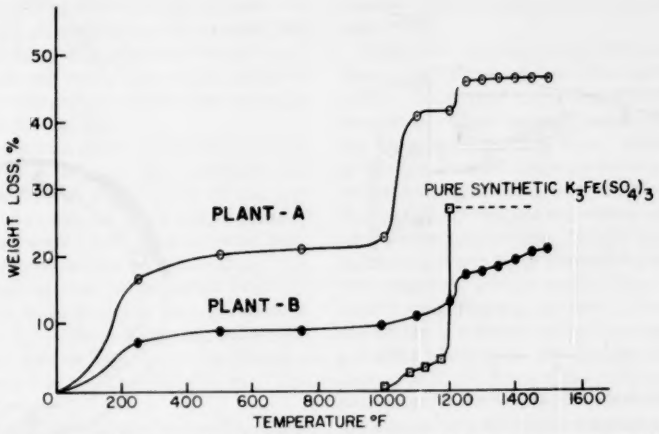

Fig. 5 Thermal decomposition of reheater deposits in air (heating to constant weight)

1100 to 1125 F in service, portions of the deposits became molten and decomposed at 1100 to 1200 F to yield sulfur trioxide and an iron-oxide-rich solid residue. The initial deformation temperatures (reducing atmosphere) of the ash from coal fired in these boilers ran 1900 to 2100 F.

When samples of the original tube deposits were heated in air to constant weight, each displayed one or more decided breaks in a curve relating weight loss to temperatures. Fig. 5 shows this behavior on hard red layers of reheater deposits from two plants. Pure synthetic potassium iron trisulfate, when heated in the same manner, displayed a major weight loss of sulfur trioxide at 1200 F. This point corresponded with decided thermal losses from both deposits. The great sulfur trioxide loss of Plant A sample at 1000 F checked later with that of pure ferric sulfate. The weight losses below 250 F were due to elimination of moisture. Most deposit samples absorbed moisture readily and were changed, i.e., hydrolyzed and formed hydrates, by such contact. Thermal-decomposition curves of this kind were run on corrosive deposits from several boilers. While not in themselves conclusive for identifying component complex sulfates, these calibrated curves did provide the clues necessary for firm proof of existence of such complex sulfates as $K_3Fe(SO_4)_3$, $KFe(SO_4)_2$, $Na_3Fe(SO_4)_3$, $K_3Al(SO_4)_3$, and others in the complicated x-ray-diffractometer scans of the deposit layers.

The fact that sulfur trioxide was given off when the deposits were heated to only 1100 to 1200 F implied that some condition of boiler operation or some condition within deposits themselves permitted formation of these molten complex sulfates *in situ*. Corey showed that their stability depends on temperature and concentration of sulfur trioxide in the surrounding atmosphere. He found that about 0.025 per cent sulfur trioxide by volume was necessary to form potassium iron trisulfate at 1000 F. Flue gas in a boiler normally contains only about 0.005 per cent of sulfur trioxide. Anderson and Diehl showed that iron oxide (Fe_2O_3) in a deposit is a good catalyst for the conversion of sulfur dioxide and oxygen of flue gas to sulfur trioxide. The temperature for most efficient reaction was between 1000 and 1300 F which probably occurs in ash deposits on most reheaters and finishing superheaters of modern units. Thus, although the average concentration of sulfur trioxide in well mixed flue gas is very small, the localized high concentration in a deposit is sufficient to keep complex sulfates molten and stable. The catalytic effect of iron oxide (Fe_2O_3) and flyash was noted in the small muffle furnaces where liquid sulfuric acid invariably condensed in the cooler ends of the tubular furnace liner when synthetic-flue-gas atmosphere was employed. Formation of complex sulfates takes place in a superheater tube deposit when catalytically formed sulfur trioxide combines with potassium sulfate and iron oxide *from the coal ash*, according to Corey's equation

$$3K_2SO_4 + Fe_2O_3 + 3SO_3 \rightleftarrows 2K_3Fe(SO_4)_3 \qquad (1)$$

The complex sulfate can thermally decompose into the reactants if: (*a*) Temperature exceeds its thermal stability limits, and/or (*b*) concentration of sulfur trioxide becomes too low. Thus a reheater or superheater deposit can act as a "chemical factory" in manufacturing molten sulfur-rich complex sulfates within the deposit itself. Therefore the longer a deposit remains on a tube in service in the proper environment the more complex sulfates it will tend to contain.

Migration of Complex Sulfates

Each investigator in this field has sought to explain the high concentration of low-melting-point sulfated materials in the deposit layer closest to the tube surface. Some attributed this occurrence to initial condensation of alkali oxides on cooler tube surface and their subsequent sulfation. Others noted that the white layer was not present initially under a new deposit but appeared and increased only after the deposit was exposed to flue gases in a boiler for long periods of time. Others have also noted that the striated appearance of a deposit occurs only when a thermal gradient exists in the deposit. This layered appearance is evidence of the segregation of components according to melting point. Deposits on noncooled supports, in the same area of a boiler as the striated ones on a tube, are not separated into layers.

This migration process was conveniently demonstrated by the following laboratory experiment. A sample of flyash collected from a superheater zone was ground and intimately mixed with pure potassium iron trisulfate. This mixture was placed in a horizontal cylindrical glass tube and spread out evenly along $5\frac{1}{2}$ in. of tube length. The tube and sample were then placed in a tubular furnace with one end of the deposit at the hot center of the furnace and the other end extending beyond the heating elements at an opposite cool end. The portion of the mixture at the center of the furnace was at 1150 F, and about a 275-F temperature gradient existed between hot and cool ends along the length of the deposit. After one week under a moving synthetic-flue-gas atmosphere, the mixture was removed, sectioned, and analyzed. Results in Fig. 6 show that the molten complex sulfate migrated from the hot toward the cool end so that a difference of 5.5 per cent in concentration of complex sulfate existed between hot and cool ends after heating in flue gas although none

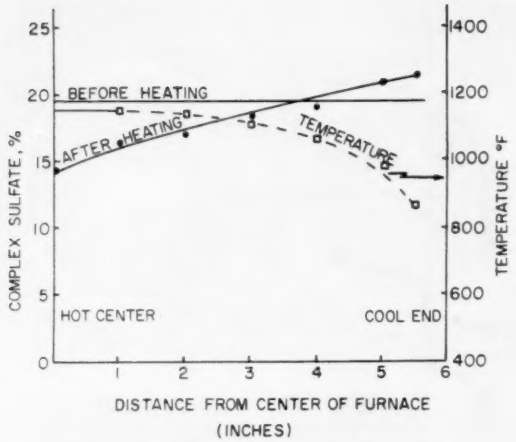

Fig. 6 Migration of complex sulfate in flyash

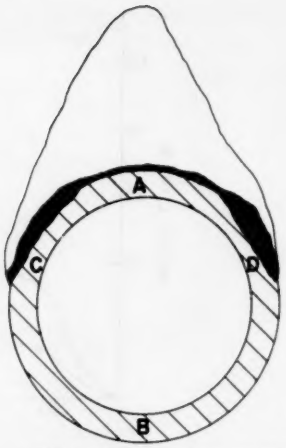

Fig. 8 Sulfide location on a cross section of corroded tube and deposit

Fig. 7 Sulfide print of corroded T22 tube

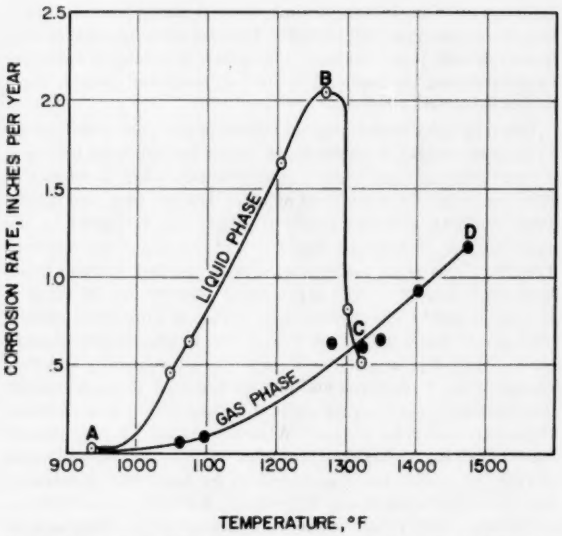

Fig. 9 Comparison of liquid and gas-phase corrosion rates on T22 alloy

had existed before application of a thermal gradient. This experiment offers evidence that molten complex sulfates formed in a field superheater deposit can migrate by a natural convection process to the cooler tube surface due to the thermal gradient which exists in the deposit.

Nature of Corrosion by Complex Sulfates

Most of the literature on corrosion by ash deposits containing complex sulfates has dealt with that on water-wall tubes at 600 to 750-F skin temperatures in slag-tap boilers. Previous investigators concluded that complex sulfates were the innocuous end product of the corrosion process under these conditions. Anderson and Diehl treated of their role in the formation of bonded superheater deposits. The present authors believe that, in the case of modern high-temperature superheaters and reheaters, molten complex sulfates themselves, in certain temperature ranges, are corrosive to most alloys, including 18-8 stainless steels.

On all samples of corroded ferritic tubes peened free of deposits, sulfide compounds have been detected principally at the sites of metal loss. Presence of considerable amounts of this reduced form of sulfur compound on metal surface was surprising in view of the sulfates and plentiful amounts of oxidizing sulfur trioxide in the deposit layers directly above during operation of the boiler. The "sulfur print" technique was used to map the location and relative concentration of sulfides on corroded and uncorroded tube surface. In this test photographic print paper was moistened with 2 per cent sulfuric acid and placed on the area to be tested. Presence of sulfide is shown by shadings of brown and black on the paper due to reaction of silver salts with hydrogen sulfide. Fig. 7 shows the sulfide print of a typical corroded T22 alloy reheater-tube sample. This print made of the outside area of the tube peened free of deposit and scale shows the coincidence of sulfide with the chief sites of corrosion. Layers of magnetic iron-oxide scale were present only above the corroded metal areas of ferritic tube surface. It was interesting to note that sulfide was not detected on the outside of this oxide-scale layer but was in copious supply at the scale-to-tube interface.

Fig. 8 shows a sulfide print of the sawed face of this same corroded tube and deposit. Only the interface of corroded areas and scale showed substantial amounts of sulfide. None was found at any other location in the deposit. Corroded stainless-steel tubes when cool usually had no flyash deposits. In an operating unit,

however, they were observed to be coated with ash deposits. On cooling, these deposits spalled off audibly and left only a thin black scale on pitted-metal surface. This pitted surface gave only a faint test for sulfide. Apparently most of the sulfide spalled off the stainless with the scale or was rapidly oxidized due to lack of a protective deposit layer like that on T22.

Further experiments were run with clean T22 and 321 stainless-steel coupons using pure molten complex sulfates (potassium aluminum trisulfate and potassium iron trisulfate) in air and synthetic-flue-gas atmospheres. In every case both metals were corroded rapidly by the molten complex sulfates and yielded magnetic iron-oxide scale and sulfide as on field-corroded tubes. The sulfide here also existed only at the metal-to-scale interface. Molten pyrosulfates gave the same corrosion products on both T22 and 321 stainless steel. Pyrosulfates were ruled out as field corroding agents due to their greater instability at superheater temperatures and their tendency to react readily with iron oxide to yield complex sulfates.

In an operating boiler it would theoretically be possible to produce sulfides by reduction of sulfates in a deposit with carbon monoxide. With the plentiful supply of oxidizing compounds in the white layer directly above the corroded areas and the thick protective layers of friable ash further above being constantly leached with sulfur trioxide, however, it was difficult to imagine how any external reducing agent such as unburned carbon or carbon monoxide from flue gases could penetrate through these oxidizing layers and produce sulfide only in the corroded areas of tube surface. In any event, measurable carbon monoxide has not been detected in the superheater zones of the boilers inspected and carbon in the flyash of these units is very low. Certainly no external reducing agent had been present in the rapid laboratory corrosion of metals by molten complex sulfates. It was concluded that sulfides and iron-oxide scale must result, both in laboratory and field corrosion, from reaction of metal with molten complex sulfates.

The corrosion process is then essentially an oxidation-reduction reaction in which the iron of tube metal reduces sulfate radical to sulfide and the iron itself is converted to iron-oxide scale. Although the total reaction may be complicated, its essential features can be represented by the following simple equation:

$$\underset{\text{tube metal}}{3\,Fe} + \underset{\substack{\text{molten}\\ \text{complex sulfate}}}{SO_4^{=}} \rightarrow \underset{\text{iron oxide}}{Fe_3O_4} + \underset{\text{sulfide}}{S^{=}} \qquad (2)$$

This reaction was proposed by Simons, et al. [3] to explain the very rapid corrosion of high-alloy gas-turbine blades above 1470 F by normal sodium sulfate resulting from combustion of residual fuel oil. He found that presence of an additional reducing agent or a "triggering" agent like sodium chloride as shown by Shirley [4] was necessary to initiate rapid corrosion of these alloys by normal sodium sulfate.

The present study showed that corrosion by molten complex sulfates at superheater-metal temperatures can proceed essentially in the same manner without the presence of either auxiliary reducing agents or triggering agents. Care was taken in all experiments to use chloride-free chemicals and to avoid fingerprints, which sometimes accelerate corrosion. Although, no external reducing agent or known triggering agent was necessary to effect corrosion in current laboratory experiments, carburization of either type of alloy in boiler service would no doubt greatly increase corrosion rates by flue gas and/or molten complex sulfates.

Corrosion Rates Produced by Complex Sulfates on Metals

The unique bell-shaped temperature versus corrosion curve by Koopman, et al. [5] for 321 stainless steel exposed in the flue-gas stream of Joppa boilers near the outlet reheater tubes prompted a corresponding study of corrosion rates in the laboratory to see if a satisfactory explanation could be provided by controlled experiments.

A series of test coupons of T22 and 321 stainless-steel alloys was covered with a mixture of potassium sulfate, sodium sulfate, and iron oxide (mol ratio 1.5:1.5:1.0) and placed in the tubular furnace at various temperatures under a flowing synthetic-flue-gas atmosphere for five days. Reaction with flue gas in the proper temperature range produced a 1:1 mol mixture of liquid potassium and sodium iron trisulfates contacting the metal. This particular mixture was chosen since: (*a*) It roughly paralleled Joppa alkali ratios, and (*b*) it provided a liquid complex sulfate mixture of fairly low melting point. Temperature ranges were chosen to greatly overlap those which would normally be used on both alloys in the field. For comparison, bare coupons of both alloys were run at the same temperatures in synthetic flue gas alone to establish the gas-phase corrosion-rate curve. Examination of the cooled metal samples after exposure to the complex-sulfate mixture showed each in the 1000 to 1300-F range was encased in a hard shell of solids; each was corroded, and covered with sulfides at the metal-to-metal-oxide interface. Fig. 9 shows results on T22 alloy. It should be noted that liquid-phase penetration values, in inches per year, are much higher here than would be encountered in an operating boiler since laboratory tests were run with almost pure complex sulfates without the great dilution by flyash which characterizes a field deposit from pulverized-coal firing.

Corresponding data for 321 stainless steel including the T22 liquid-phase attack-rate curve dotted on for comparison are shown in Fig. 10. With 321 stainless steel negligible corrosion by flue gas was encountered even at 1450 F. Its resistance to liquid-phase corrosion, however, was much lower than for gas-phase attack. Incipient accelerated attack (liquid phase) occurred at 950 F and rapidly increased with increasing temperature to about 1300 F. Thereafter the rate fell quickly and assumed about the same corrosion rate as that of flue gas alone.

The explanation for these unusually shaped liquid-phase corrosion curves is as follows:

1 Incipient accelerated (liquid-phase) corrosion, which proceeds faster than flue-gas attack at the same temperature, occurs when the melting point of the complex sulfate mixture contacting the metal is reached (point A). This melting point will depend

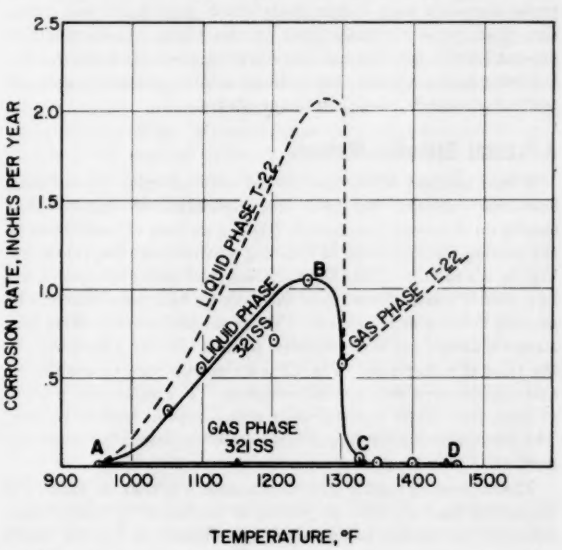

Fig. 10 Comparison of liquid and gas-phase corrosion rates on 321 stainless steel

on the proportion and kind of alkalies, the concentration of sulfur trioxide present in the ash deposit, and the skin-metal temperature.

2 Once liquid complex sulfates are in contact with the metal, corrosion rate accelerates with temperature as in any other chemical reaction (portion AB).

3 The peak corrosion rate (point B) marks the maximum temperature at which complex sulfates are formed faster than they decompose.

4 The descending portion of the curve (portion BC) occurs at temperatures at which complex sulfates are formed at less than the maximum rate due to the shifting equilibrium. Here lowered corrosion rate is due to a decreasing concentration of the corrosive molten material.

5 At about 1350 F on both laboratory liquid-phase curves (point C) the lower corrosion rate characteristic of gas-phase attack of both alloys is again encountered since practically no complex sulfate can form at this temperature.

6 Above this temperature, the much slower gas-phase corrosion again results since metal is only in contact with much less corrosive gases and solids (portion CD).

Future Remedial Measures

Although present studies are not far enough along to solve the liquid-phase corrosion difficulties, a number of approaches do offer promise for its amelioration. Use of more corrosion-resistant alloys would seem the easiest approach. No practical alloy has yet been found, however, which offers consistently better resistance than 321 stainless steel in this service, although many have been tested in field exposure as welded-in tube sections. Corrosion-resistant coatings have not looked promising due to cost and to the fact that they are effective only as long as unperforated. The search for better alloys and coatings has by no means been exhausted by present work and would seem a rewarding field for future effort. Operating conditions such as fineness of coal were found by Koopman to have a decided bearing on corrosion rate of stainless steel. Use of coal ground to 80 per cent through 200 mesh rather than the normal 65 to 68 per cent at Joppa indicated lower metal loss in the 950 to 1250-F metal-temperature range. No doubt the use of better quality coal would ameliorate corrosion trouble. Koopman, for instance, described probe corrosion tests of two coals which gave much less corrosion than those normally used by the plant. Unfortunately, present knowledge does not allow setting adequate limits on the following coal qualities: low sodium, sulfur, potassium, and ash content, and high ash-fusion temperatures.

A Present Remedial Measure

A field method which has proved very effective for reducing lead-tube corrosion has been the application of stainless-steel shields on the front (windward) 180-deg surface of lead tubes in the deposit-forming areas of finishing superheaters and reheaters. Fig. 11 is a picture of lead 321 stainless-steel outlet reheater tubes in a 1050-F unit. New tubes with shields had been installed 10 months before this inspection. These shields were not of current strap-on design but were attached to each tube by a tack weld to the tube at either side. Fig. 12 is a close-up view of unshielded and shielded area with a shield removed. The unshielded portion of tube just below the top weld shows typical surface pitting. The area under the shield was entirely free of pits and as smooth as new.

The interesting part of this examination was that the surface of the shield itself showed no pitting or corrosion. These results, however, can readily be explained by reference to Fig. 10, which relates corrosion rate by complex sulfates to metal temperature, or by reference to the field data of Koopman. The skin temperatures of shields as measured by metallic sheathed thermocouples in the field ranged from 1400 to 1500 F. Although deposits can form on shields in some instances, these deposits do not manufacture complex sulfates because their temperature is too high. Thus liquid-phase corrosion of shields cannot take place because they contact only gaseous and solid products of combustion in this temperature range.

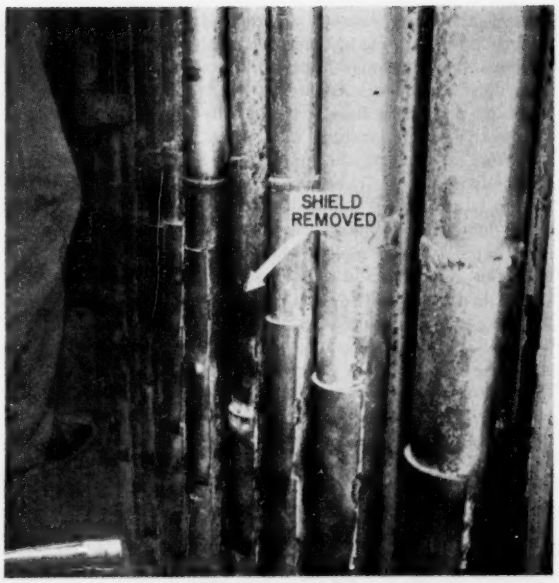

Fig. 11 Shielded lead stainless-steel reheater tubes after 10 months service at 1050-F steam temperature

Fig. 12 Close-up of lead 321 stainless-steel reheater tube with one shield removed (10-months' service)

Type 304 stainless steel has been found satisfactory for this application. Shields about $^1/_8$ in. thick are required to resist mechanical distortion at high temperatures by sootblower action. Shields preferably should be strapped rather than welded on tube surface to avoid localized overheating by fin effect. Straps on the leeward area of the tube are welded to the shield at either side.

These shields have been very effective for periods of longer than two years in units up to 1050-F steam temperature. Shields should be applied to clean, deposit-free metal or preferably to new tubes. A close fit between tube and shield is necessary to keep skin temperature of the shield below that at which excessive oxidation of stainless occurs.

Although use of shields might be thought to occasion some sacrifice of heat-transfer efficiency, this loss is probably considerably less than that due to layers of deposit which normally occur on the windward area of lead tubes, especially those of ferritic alloys. Stainless-steel shields have less tendency to accumulate heavy deposits than the ferritic tubes they shield.

Summary and Conclusions

The present work has shown that molten complex iron and/or aluminum alkali sulfates formed in fireside deposits of boilers having steam temperatures above about 950 F are responsible for corrosion of superheater and reheater tubes. This corrosion is a chemical reaction in which tube metal reacts with molten sulfates to give iron oxide and sulfide. It starts at temperatures below the oxidation (scaling) temperature limit for alloys used in these sections of a boiler. Gas-phase scaling-temperature limits, therefore cannot be used to judge the suitability of a given alloy for service in an area subject to liquid-phase corrosion by complex sulfates of an ash deposit. For instance, the 321 stainless-steel alloy encounters rapid liquid-phase attack at about 1025 F, whereas its resistance to corrosion by flue gas alone is satisfactory at higher than 1450 F. Liquid-phase corrosion is bracketed between melting and maximum synthesis temperatures of the complex sulfates present on tube surface under the deposits. Studies to find more corrosion-resistant alloys or less corrosion-producing coals seem promising fields for future effort.

Shielding lead tubes in the deposit-forming areas of the finishing reheater and superheater where skin-metal temperatures are between 950 and 1300 F is the best practical means to date for preventing accelerated liquid-phase corrosion in pulverized-coal-fired units.

Acknowledgments

The authors wish to express their gratitude for the conscientious efforts of the following men in laboratory work connected with this investigation: E. Clyde Lewis, who operated the tubular muffle furnaces; James R. M. Long, who ran thermal and chemical analyses; Evan Farmer, Jr., who ran and interpreted all x-ray-diffraction analyses.

References

1 R. C. Corey, B. J. Cross, and W. T. Reid, "External Corrosion of Furnace-Wall Tubes—II, Significance of Sulphate Deposits and Sulphur Trioxide in Corrosion Mechanisms," TRANS. ASME, vol. 67, 1945, pp. 289–302.

2 C. H. Anderson and E. K. Diehl, "Bonded Fireside Deposits in Coal-Fired Boilers—A Progress Report on the Manner of Formation," ASME Paper No. 55—A-200.

3 E. L. Simons, George V. Browning, and H. A. Liebhafsky, "Sodium Sulfate in Gas Turbines," *Corrosion*, vol. 11, 1955, pp. 505t–514t.

4 H. T. Shirley, "Effects of Sulphate-Chloride Mixtures in Fuel-Ash Corrosion of Steels and High-Nickel Alloys," *The Journal of the Iron and Steel Institute*, vol. 182, 1956, pp. 144–153.

5 J. G. Koopman, E. M. Marselli, James Jonakin, and R. C. Ulmer, "Development and Use of A Probe for Studying Corrosion in Superheaters and Reheaters," presented at American Power Conference, 21st Annual Meeting, March 31–April 2, 1959.

DISCUSSION

Richard C. Corey[2]

The authors have properly emphasized the most important factor concerning external corrosion of tubes in water-tube boilers, namely, that the comparatively high rates of corrosion experienced are due to a liquid phase in contact with the metal. Corrosion mechanisms based upon contact of the metal with gases such as sulfur dioxide and trioxide, with inorganic solids, or with both gaseous and solid phases, cannot explain the corrosion rates that have been observed in furnaces. The chemical composition of the liquid phase is probably not important, other things being equal. Thus for any given temperature of the metal surface the rate of corrosion will be comparatively high whether the liquid phase is a molten normal sulfate, pyrosulfate, or complex sulfate, such as $(Na,K)_3Fe(SO_4)_3$.

The extent of metal loss will depend (with other things equal) upon the length of time that the metal is in contact with the liquid phase. Accordingly, if the composition of the corrodent changes so that its melting point is raised above the temperature existing at the corroding surface, solid phase will form and the rate of attack will decrease. For example, if the corrodent is a molten alkali-metal pyrosulfate and the source of SO_3 is removed, the pyrosulfate will decompose to the corresponding normal sulfate and solidify, since the normal sulfate melts at a temperature several hundred degrees higher than the pyrosulfate. A similar change would be expected to occur if iron dissolved from the metal, or compounds derived from the coal ash or added to the furnace, combined with the molten pyrosulfate and produced a compound having a higher melting point. The addition of lime or dolomite with the fuel probably is effective in reducing corrosion when circumstances are such that these compounds can react with the liquid phase and raise the melting point of the deposit.

The authors describe an experiment intended to demonstrate "... that molten complex sulfates formed in a field superheater deposit can migrate by a natural convection process to the cooler tube surface due to the thermal gradient which exists in the deposit." Assuming that the authors based their conclusions on differences in the SO_3 content of the charge from the center to the end of the furnace, I wonder if the results of this experiment could not be explained as well by the fact that the vapor pressure of SO_3 in the mixture of fly ash and $K_3Fe(SO_4)_3$ would be higher at the center of the furnace (1150 F), consequently, the cooler section would absorb some of the SO_3 from the gas stream. For a simple analogy, assume the furnace charge was a mixture of normal and pyrosulfate. We would expect the concentration of pyrosulfate in the mixture to decrease in the hottest zone and to increase in the coolest zone, for the same experimental conditions excepting the maximum and minimum temperatures described by the authors.

The comparison of liquid and gas-phase corrosion rates, Fig. 10, is an interesting one. Under certain specified conditions, one can envision a corrosion curve with three distinct peaks. The first peak would occur in the approximate range of 700–900 F, as the result of attack of the metal by molten alkali-metal pyrosulfates. The second peak, as shown by the authors, would be between 1200–1300 F, due to molten complex sulfates. The third would be approximately between 1500–1600 F, corresponding to attack by molten normal alkali-metal sulfate, such as Na_2SO_4. Above 1600 F gas-phase corrosion of the stainless alloys would become significant.

Determination of the melting characteristics of the complex sulfates would be a valuable contribution to these studies. We

[2] Chief, Division of Solid Fuels Technology, Bureau of Mines, U. S. Department of the Interior, Region V, Pittsburgh, Pa.

would suggest including the following compounds: $K_3Fe(SO_4)_3$, $Na_3Fe(SO_4)_3$, $K_3Al(SO_4)_3$, $Na_3Al(SO_4)_3$, and mixtures containing a limited number of mol ratios of these compounds. It would be essential to make these determinations under such conditions that little or no decomposition of the compounds occurred, which might be approximated by using nearly filled, evacuated, sealed tubes.

A. A. Orning[3,4]

Authors Nelson and Cain conclude that molten sulfates are responsible for external corrosion of superheater and reheater tubes at steam temperatures above approximately 950 F. Since they arrive at this conclusion, it is difficult to understand why they report, elsewhere in their paper, that previous investigators asserted that complex sulfates were the innocuous end product of corrosion of water-wall tubes at 600 to 750 F in slag-tap boilers. Corey, Grabowski, and Cross[5] concluded that, under certain conditions, liquid pyrosulfates can attack the oxide on the tube at a much higher rate than in the case of the dry reaction. The evidence is sometimes confusing and often circumstantial, but it clearly shows that direct contact of molten mineral matter is responsible for high rates of corrosion on both superheater and on boiler tubes. Mixed salts of iron, aluminum and alkali metals with sulfur acids may be liquid at temperatures approximating 700 F and again at higher temperatures around 1100 F. The particular salt formed, and hence the fusion temperature, will depend partly upon the concentrations of oxides of sulfur and of catalytic agents at the site of deposit. The presence of liquid is more important than the identity of the particular compound. Liquid electrovalent compounds, sulfates, chlorides, phosphates, and so forth are generally corrosive.

Missing information relates to the manner in which deposits can form with compositions quite different from mineral matter suspended in the gaseous combustion products. It is again largely from circumstantial evidence that various authors have concluded that alkali metals are volatilized and are transported as their oxides. It is possible that, in the presence of water in the combustion products, the oxides would be converted to hydroxides which are also volatile. It appears that the basic compounds can coexist in the gas stream together with acid-forming gases, such as SO_2, SO_3, and HCl, and that reaction to form the corresponding salts may not occur until the basic compounds condense or are absorbed upon a solid surface. A broad and fundamental study is needed of the high-temperature reactions of basic and acidic compounds that may be present in combustion products and of the conditions under which these compounds may be produced from the mineral content of fuels.

William T. Reid[6]

One of the most interesting points of this paper is that it confirms so strongly the importance of the alkali iron trisulfates [$Na_3Fe(SO_4)_3$ and $K_3Fe(SO_4)_3$] in the corrosion mechanism. Perhaps of greatest importance is the new information given here on the mode of formation of these trisulfates, and the ability under laboratory conditions of the trisulfates to migrate from a high-temperature region to a cooler one. The exact mechanism of such migration is not clear; apparently it depends upon the sulfur trioxide equilibrium with the other reactants, which would favor the formation of the trisulfates below their nominal dissociation temperature, in this case about that at the center of the test furnace. It should be noted also in such experiments that the rate of dissociation of trisulfates on heating varies markedly with temperature. The loss of sulfur trioxide is not spontaneous, but occurs gradually over many hours in the range 1000–1100 F. By heating their mixture for one week, the authors were able to observe the results of such dissociation and reformation as a function of specimen temperature.

The sulfide attack described by the authors poses many questions. It is not at all clear how the conventional reducing conditions necessary to form the sulfides could have been present, yet it is clearly shown that sulfides occurred at the scale-tube interface. This point certainly needs further study.

Also, the role of sulfur trioxide in setting up corrosion conditions, although recognized by the authors, seems to have been relegated to a somewhat secondary position. Although it is true that pyrosulfates dissociate at moderately low temperature, it is also reasonable to attribute the formulation of liquid-phase deposits to such materials. Indeed it is difficult to postulate any other compounds with melting points so low. The tubular-furnace tests made by the authors used a "synthetic flue gas," but the sulfur-trioxide level in this atmosphere was not described. It would be interesting to know whether the sulfur trioxide content was measured, how it was controlled, and how it may have varied during the corrosion tests. Until much more information is available, it would seem likely that we must conclude that sulfur trioxide remains as the most important reactant in the corrosion mechanism.

Edward L. Simons[7]

1 The authors report that sulfide compounds were detected in the sulfate deposit-metal interface at the sites of metal loss on corroded ferritic tubes. During our study of residual oil ash corrosion in gas turbines, we also observed a similar condition at the scale-metal interface on austenitic Type 310 first-stage nozzle partitions covered with a sulfate-rich deposit. Corrosion of alloy steels in the presence of sulfates apparently involves the formation of lower-valent sulfur, even when the macroenvironment is of an oxidizing nature.

2 I agree with the authors' conclusion that sulfates are the precursors rather than the end products of the corrosion process. However, the corrosion mechanism that they ascribe to Simons, et al., differs markedly from that proposed by us[8] for the enhanced oxidation of alloy steels in the presence of sodium sulfate.

Nelson and Cain view the corrosion process as "essentially an oxidation-reduction reaction in which the iron of tube metal reduces sulfate radical to sulfide and the iron itself is converted to iron-oxide scale." This mechanism assigns to sulfide the passive role of a reaction by-product.

In our mechanism, on the contrary, the lower-valent sulfur is directly responsible for the increased rate of atmospheric oxidation over that characteristic of a clean metal surface in the absence of sulfur.

It is a moot point whether the alloy itself can reduce some sulfate to sulfide; certainly surface or environmental reducing agents can. In any case, our experimental evidence on Type 310 strongly suggested that enhanced oxidation occurred only after the metal had been penetrated by a liquid metal-metal sulfide eutectic.

Once sulfide has penetrated the alloy, the metal in the eutectic inclusions can subsequently be oxidized either by sodium sulfate or atmospheric oxygen or both. In our crucible tests, where sodium sulfate was undoubtedly the principal oxidizing agent, the

[3] Work on manuscript completed December, 1959.

[4] Chief, Combustion Section, Branch of Bituminous Coal, Division of Solid Fuels Technology, Region V, Bureau of Mines, U. S. Department of the Interior, Pittsburgh, Pa.

[5] R. C. Corey, H. A. Grabowski, and B. J. Cross, "External Corrosion of Furnace Wall Tubes," TRANS. ASME, vol. 71, 1949, pp. 951–963.

[6] Assistant Technical Director, Battelle Memorial Institute, Columbus, Ohio. Mem. ASME.

[7] General Electric Research Laboratory, Schenectady, N. Y.

[8] Edward L. Simons, George V. Browning, and H. A. Liebhafsky, "Sodium Sulfate in Gas Turbines," *Corrosion*, vol. 11, 1955, pp. 505t–514t.

continuing production of lower-valent sulfur, through reduction of sulfate, led to the autocatalytic reaction we observed. In our experiments with thin coatings of sodium sulfate, oxygen gas was the principal oxidizing agent, and the oxidation, though enhanced, was not autocatalytic. The photomicrographs of heavily oxidized specimens showed sulfide inclusions still present in the metal ahead of the advancing front of oxidation.

Thus lower-valent sulfur is more than just a possible reaction product; it is of crucial importance in reducing the normal oxidation resistance of the alloy.

Authors' Closure

The authors appreciate Mr. Corey's detailed comments. The point is well taken that corrosion rates produced by any proportion of the various types of molten sulfates would be expected to exceed those due only to flue gas attack at the same temperatures (within the normal use range of the metal). The relative proportions of pyro, complex, and normal sulfates in the liquid phase are, however, important in regard to magnitude of corrosion rate, as will be explained later. As Mr. Corey and others have shown the partial pressure of sulfur trioxide surrounding the molten phase and also the skin temperature of the metal on which it occurs are both quite important in determining the relative abundance of the various species of molten sulfur compounds. Thus at skin temperatures approaching those of many present day finishing superheater and reheater surfaces (about 1100 F) no reasonable concentration of sulfur trioxide was found adequate to maintain alkali pyrosulfates in a stable, molten condition. As skin temperatures mount in boilers of more advanced design the most abundant types of sulfur compounds would be expected to change successively to those of greater thermal stability, i.e., from alkali pyrosulfates to complex alkali sulfates to normal alkali sulfates. As metal temperatures rise within the liquid phase corrosion range, however, the effect of a smaller equilibrium concentration of molten complex sulfate may be overridden by the effect of temperature increase, and more rapid corrosion may be the net result. For instance, on the 321 ss curve of Fig. 10, a 62 per cent equilibrium concentration of complex sulfate at 1100 F penetrated metal at an average of 0.5 ipy, while 25 per cent at 1275 F corroded metal about twice as fast, 1.0 ipy. Another variable affecting liquid phase corrosion rate was found to be the ratio of sodium-to-potassium in the complex sulfate mixture. The lower this ratio, i.e., the greater the proportion of potassium, the higher the corrosion rate at a given temperature.

The authors also have noted the increase of melting point with decrease of surrounding sulfur trioxide partial pressure. However, not only thermal decomposition, but also the corrosion reaction itself (aside from generation of semiprotective metal scale) tends to limit corrosion rates. Metal exposed to complex sulfates in the liquid phase corrosion range, i.e., between melting and maximum synthesis temperatures, has been found to combine with only the "excess" sulfate portion of the complex sulfate compound. If the formula for potassium iron trisulfate, $K_3Fe(SO_4)_3$, is rewritten in the form of an associated compound, $3K_2SO_4 \cdot Fe_2(SO_4)_3$, the corrosion process may be thought of as one in which only the more loosely bound excess sulfate associated with iron of the molecule is reduced by the corrosive reaction with the tube metal. Thus only half of the sulfate reacts with metal in the corrosion process. The residue from complex sulfate fully reacted with metal would then be a mixture of iron oxide-sulfide and potassium sulfate, which is inert to metal at superheater temperatures due to its high melting point. The proportion of excess sulfate in an ash deposit layer, we believe, provides a good estimate of its potential corrosiveness when molten; other things being equal, the higher the excess sulfate, the more corrosive it is.

The graph of Fig. 6 and the conclusions about thermal migration of complex sulfates were not based on the difference in sulfate concentrations before and after heating, but instead on the potassium analyses of the segments. Analysis of segments along the six-inch length of the deposit mixture of complex sulfate and fly ash before and after heating for a week in moving synthetic flue gas showed conclusively that potassium, iron, and sulfate increased toward the cooler end of the solid mixture while silica and other components decreased proportionally due to the migration of the complex sulfate. To gain a better material balance, seven more experimental runs were made under the same conditions with mixtures of normal potassium sulfate and fly ash from the superheater region of a boiler. In each case complex sulfates were formed *in situ* and migrated to the cooler end of the length of deposit mixture. The result of this transfer of materials was also evident visually after a week-long test, since the white complex sulfate layer was much thicker in the cool end of the glass tube than in the hot end.

The three-peak curve was also envisioned by the authors and corrosion tests were run throughout the temperature range, 700–1600 F. However, the rates of attack by pyrosulfate and normal sulfate in their respective molten temperature ranges proved to be much less than those due to complex sulfates in their own molten region, 1025–1300 F. This result may be due to the following factors: (1) Lower temperature in the pyrosulfate range, hence a slower rate of reaction; (2) a more reactive sulfate radical in the complex compound than in the normal sulfates; hence a higher reaction rate, even though the temperature was lower. With high nickel alloys above about 1200 F the formation of eutectics such as Ni-NiS may tend to enhance metal attack.

Finally, melting point determinations have been made on the various complex sulfates. These data, together with a more detailed discussion of the points presented in the various closures, will be covered in a forthcoming paper by Dr. Cain.

In answer to Dr. Orning's comments, the authors emphasize a distinction among sulfates, pyrosulfates, and complex sulfates, since the physical properties, such as melting point, and chemical properties, such as corrosiveness, vary substantially among these types of alkali sulfates. A great difference exists between water-wall and superheater skin temperatures; hence the nonmolten end product of corrosion at lower wall tube metal temperatures can itself become molten and corrosive at elevated temperatures. Mr. Corey, et al., concluded in reference [1] that the formation of complex sulfates constituted the key reaction in the corrosion of water-wall tubes in slag tap boilers and that complex sulfates were the end product of this reaction. Studies by the present authors on pulverized coal fired boilers, the deposits of which have much less alkalies than those from slag tap boilers, have shown that the higher metal temperatures of some modern finishing superheaters and reheaters are sufficient to maintain complex sulfates in the molten condition in which form they themselves corrode metal by a different reaction. Complex sulfates whose mixtures melt no lower than 1025 F could not be responsible for the liquid phase corrosion of water-wall tubes with skin temperatures of only 600–750 F. Pyrosulfates, on the other hand, would have at best only a fleeting existence at superheater temperatures. They are thermally unstable at these temperatures, and also quite reactive with iron oxide which is a prominent constituent of the ash deposits from pulverized fuel firing.

The following comparison of corrosion-causing reactions in Corey's and the present work may elucidate differences between the two.

Corey's Reaction
at 600–750 F:

$$Fe_2O_3 + 3K_2SO_4 + 3SO_3 \rightleftarrows 2K_3Fe(SO_4)_3$$

Metal Oxide Scale + Potassium Sulfate + Sulfur Trioxide → Potassium Iron Trisulfate

Nelson-Cain Reaction
at 1025–1300 F:

$$3Fe + SO_4^{=} \rightarrow Fe_3O_4 + S^{=}$$

Tube Metal + Excess Sulfate from molten $K_3Fe(SO_4)_3$ → Metal Oxide Scale + Sulfide

Corey's lower temperature corrosion is a *scale destroying* reaction in which complex sulfates are formed. Its progression, according to the authors, depends on periodic tube deslagging and subsequent thermal decomposition of $K_3Fe(SO_4)_3$ and sulfur compounds from melting fiy ash to provide SO_3. Ours is a *scale-creating* irreversible oxidation-reduction reaction occurring at higher temperatures. It does not depend on deslagging for contact between metal and corrosive agent but on thermal migration of complex sulfates formed in the ash deposit to provide a continuous fresh supply of corrosive material on tube surface. The iron oxide necessary for forming complex sulfates probably comes from the ash deposit itself and not from tube metal oxide scale, otherwise the complex sulfate layer would not increase in thickness with exposure time in a fixed deposit.

We do not agree that the presence of a liquid phase *per se* is more important than the identity of the particular compound in accelerated corrosion of superheater tubes. See the discussion of Dr. Simons' remarks for more on this subject. The chlorides and phosphates mentioned as being corrosive have never been found in significant amounts in superheater deposits where rapid corrosion has occurred in this country.

The authors agree with Mr. Reid that sulfur trioxide is indeed an important reactant in the high temperature corrosion process. Sulfur trioxide, which was found by Anderson and Diehl and the current work to be created chiefly by catalytic action of iron oxide in the solid reaction mixtures, would probably be difficult to determine accurately since much is absorbed by the solid laboratory synthesis mixture and converted into complex sulfates. Reasonably high concentrations were obtained as evidenced by the condensation of liquid and solid sulfur trioxide in the cooler portion of the test furnaces during many runs with synthetic flue gas.

An important distinction should be made here between excess sulfate (conveniently reported as sulfur trioxide) and sulfur trioxide itself. The excess sulfate in complex sulfates, although in a labile, more easily reduced form than occurs in normal sulfates, is not present as adsorbed sulfur trioxide, but rather is the constituent sulfate radical in a class of definitely-proportioned, crystalline compounds. Many individual species of these complex sulfates from field deposits and laboratory syntheses have been identified by x-ray diffraction.

The authors recognize several significant differences between the work of Dr. Simons, et al. [3], and the current study. Among others is their use of high nickel alloys; ours were a low chrome ferritic alloy and an 18-8 stainless steel. They used much higher temperatures, above 1470 F; our liquid phase attack extended only to about 1300 F. Their atmospheres were hydrogen, air, and nitrogen, while ours were synthetic flue gas, which aside from lack of moisture and particulate matter, is essentially like that provided by combustion of coal in a boiler. They used sodium sulfate; we used mixtures of complex sulfates which melt lower and hence are corrosive at much lower temperatures. The excess sulfate radical in complex sulfates, as noted in remarks to Mr. Corey, is evidently more labile than the sulfate radical in normal alkali sulfates. The stable, molten (corrosive) ranges of complex alkali sulfates differ widely in both temperature location and range from those of normal alkali sulfates. Our remarks about similarity in mechanism to that of the prior study were hence intended to apply only to equation (2) of the current paper, $3Fe + SO_4^{=} \rightarrow Fe_3O_4 + S^{=}$.

The comment about relegation of sulfide to the role of a passive reaction product discloses an important area of agreement not covered in the paper under discussion. We, too, believe that sulfides greatly accelerate the corrosion of metals in some temperature ranges. Examination of rapidly corroded field 321 stainless-steel superheater tubes showed in every case an abrupt transition between gas-phase and liquid-phase attacked metal structure. Metallographics on tube area under ash deposits showed that base metal has incurred deep intergranular sulfide penetration up to about 0.020 in., while contiguous metal with no ash deposit encountering attack by flue gas only displayed only a slight transgranular attack with no sulfides in the grain boundaries. Intergranular attack was not observed on laboratory complex sulfate corroded specimens, presumably due to a higher corrosion rate which exceeded that of intergranular sulfide penetration. The intergranular attack observed in field exposure is believed to accelerate the rate of corrosion both by exposing a larger surface area to the corroding medium and also by causing grains to separate prematurely from the metal surface. Sulfide generated by the corrosion process evidently plays an active subsequent role in the destruction of metal. The identity of the class of molten corroding compounds, then, is important in accelerated superheater corrosion.

Sulfide analysis of small samples of corroded alloy tubing from the field has proved to be a convenient method of deciding whether the predominant corrosion on ferritic alloys is gas or liquid-phase attack. It was found that the sulfide concentration on field and laboratory metal samples corroded by flue gas alone ranged from 0.2 to 3.0 mg FeS/cm² while that on metal corroded by liquid complex sulfates ranged from 24.3 to 109.0. The per cent by weight of sulfide calculated as ferrous sulfide in these latter scales ran as high as 25 per cent.

There has been no metallographic evidence in our laboratory or field samples to indicate that rapid corrosion in boilers is accompanied by, or due to formation of eutectics. Rapid field wastage of T22 and 321 ss occurred on some first row outlet reheater tubes whose measured skin temperatures were well below 1100 F. Accelerated attack occurred on ferritic alloys which contain no nickel as well as on 18-8 austenitics. The temperature for incipient rapid attack in laboratory tests coincided on both types of alloys with the melting temperature of the complex sulfates, which is far below that of any likely eutectics with which we are familiar. It was learned by corrosion rate studies, however, that the terminal temperature for accelerated attack corresponded to the maximum synthesis temperature of the complex sulfates, about 1300 F, which is within the range in which eutectics would be expected to occur.

EDWARD M. HERRMANN
Head, Applied Mechanics Division,
U. S. Naval Engineering Experiment Station,
Annapolis, Md. Mem. ASME

Considerations for the Reduction of Noise in Ship Installations of Gas Turbines

General noise reduction considerations for shipboard installation of gas turbines are discussed. Specific information relating to sound-absorption materials, duct treatments, structureborne sound isolation, and airborne sound insulation is graphically presented.

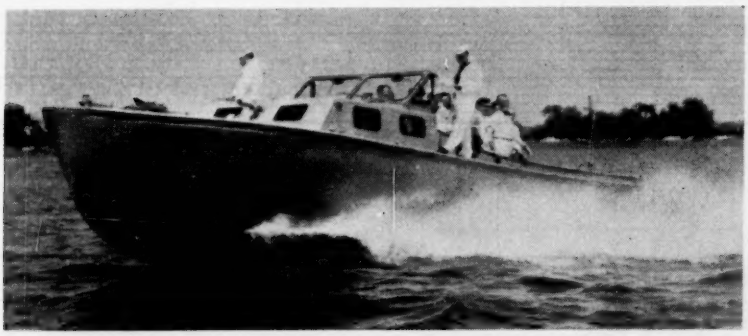

Gas-turbine-powered 40-ft LCP(L)

One of the most serious disadvantages of the increasing use of gas turbines in naval vessels is the noise generated, which is particularly detrimental to the comfort and communication of personnel. Gas-turbine noise reduction differs from the methods used for other naval machinery primarily because of the frequency of the noise generated and the high temperature of the exhaust gases.

Some of the most important acoustical information related to the shipboard installation of gas turbines obtained from other sources and developed by laboratory investigations or in small boats at the U. S. Naval Engineering Experiment Station will be presented. The problems that exist will be stressed and it is hoped will stimulate more interest by manufacturers in reducing the noise generated at the source. Emphasis will be given to the reduction of airborne noise. Although the vibration isolation of the gas turbine from its supporting structure is needed for the ultimate reduction in airborne noise, the use of isolation mountings will not be discussed in detail.

The isolation of gas turbines is no different from the isolation of other machinery and there is much information available that can be used for the shipborne installation of gas turbines. It is important, though, to consider the effects of shock and to provide means of preventing deterioration of the mountings from the effects of heat. The Appendix describes the characteristics of suitable isolation mountings.

Airborne Noise Criteria

The difficulty in the reduction of airborne noise from shipboard installations of gas turbines arises from: (*a*) The frequency of the noise generated, as previously mentioned; (*b*) the unique problems arising from installation of sound-absorption materials, such as shock resistance, fire resistance, and resistance to seawater deterioration; (*c*) the erosion effects of high-velocity air; and, finally (*d*) the high temperatures associated with the operation of gas turbines and their exhaust systems.

The predominant frequency components of a typical airborne sound spectrum of a gas turbine are between 3000 and 9000 cps, Fig. 1. The high-frequency sounds are particularly hazardous to personnel; but, fortunately, are easier to reduce by the use of absorption materials. The human ear is most sensitive to the 500 to 6000-cps range, and, therefore, it becomes necessary to install turbines in such a way as to minimize the sounds at these frequencies. This sound spectrum was made at a distance of 5 ft. To insure satisfactory installation of gas turbines, the U. S. Navy has established criteria of sound pressure levels for various ship compartments [1],[1] Table 1.

These criteria show that a lower sound level is required in the higher frequencies. For the particular turbine whose sound

[1] Numbers in brackets indicate References at end of paper.

Table 1 Limiting sound pressure levels for various ship compartments; sound pressure level (db re: 0.0002 dyne cm^2)

Noise Category	Space Volume cu ft	Frequency Octave Band, cps							
		37 to 75	75 to 150	150 to 300	300 to 600	600 to 1,200	1,200 to 2,400	2,400 to 4,800	4,800 to 9,600
B	500 to 1,999	86	82	78	74	70	66	62	58
	2,000 to 7,999	82	78	74	70	66	62	58	54
	8,000 and larger	78	74	70	66	62	58	54	50
C	500 to 1,999	80	76	72	68	64	60	56	52
	2,000 to 7,999	76	72	68	64	60	56	52	48
	8,000 and larger	72	68	64	60	56	52	48	44
D	Any	110	105	100	95	90	85	85	85

Noise Categories

Category B: Spaces where comfort of personnel in their quarters is normally considered to be an important factor

C: Spaces where it is essential to maintain especially quiet conditions

D: Spaces or areas where a higher noise level is expected and where deafness avoidance is a greater consideration than intelligible speech communication

Contributed by the Gas Turbine Power Division and presented at the Annual Meeting, Atlantic City, N. J., November 29–December 4, 1959, of The American Society of Mechanical Engineers.

Note: Statements and opinions advanced in papers are to be understood as individual expressions of their authors and not those of the Society. Manuscript received at ASME Headquarters, September 3, 1959. Paper No. 59—A-238.

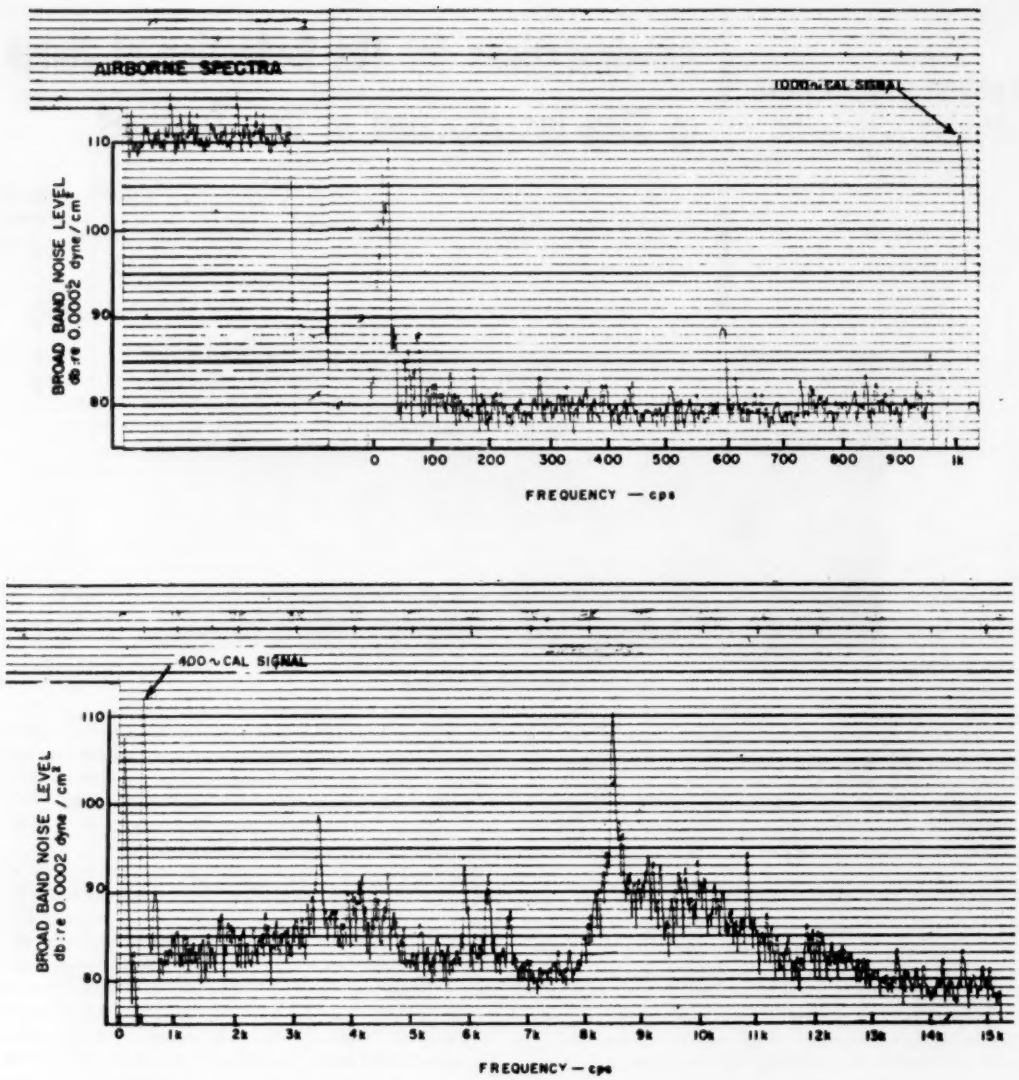

Fig. 1 Typical sound spectrum of a gas turbine

spectrum is shown, it will be necessary to reduce the sound pressure level in the compartment where it is installed approximately 25 decibels, db. The noise reduction effected at any frequency by the addition of sound-absorption materials can be calculated by the equation

$$\text{db reduction} = 10 \log_{10} (A_2/A_1)$$

where

A_2 = total absorption after treatment
A_1 = total absorption before treatment

and

$$A_1 \text{ or } A_2 = \Sigma(S\alpha)$$

where $(S\alpha)$ is the product of the incremental area and the sound-absorption coefficient of that area, and $\Sigma(S\alpha)$ indicates the summation of the incremental area products for total area of the compartment. Absorption coefficients are published in various texts [2].

Noise Absorption

The noise reductions can be obtained only in the reverberant field; that is, if a person is standing in the path of the sound being radiated from a gas turbine, obviously the use of sound-absorption materials behind him will not be effective in reducing the sounds reaching his ears. Fortunately, with increasing sound frequencies, it is possible to obtain higher absorption characteristics with available materials. Fibrous-glass materials have good sound-absorption properties; but their properties change with thickness of fiber, density, method of mounting, and so on. Fig. 2 shows the effect of thickness with frequency for a 1.0 lb/cu ft-density fibrous-glass blanket mounted directly on the floor of the test chamber. The absorption coefficient increases with increasing frequency and thickness to 1000 cps where the absorption tends to become a constant with increasing frequency. Very little information is available on the sound-absorption properties of fibrous-glass materials above 4000 cps. To prevent the de-

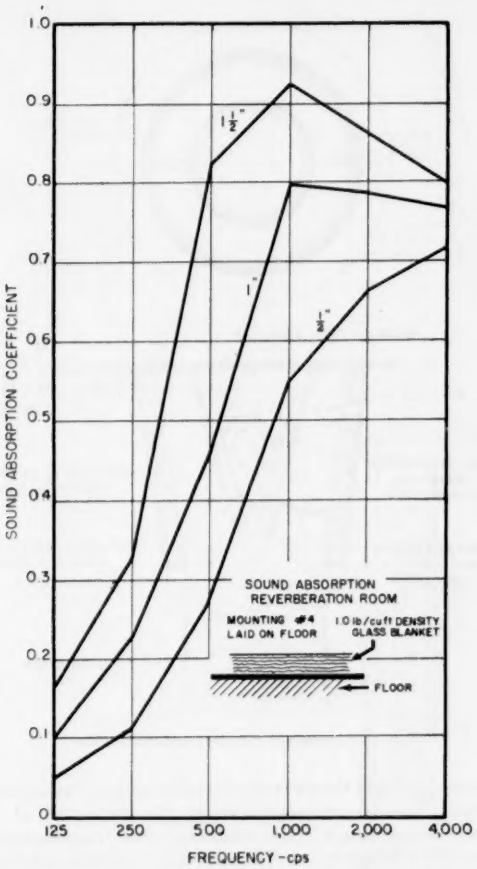

Fig. 2 Plotted data showing increase of sound absorption with thickness

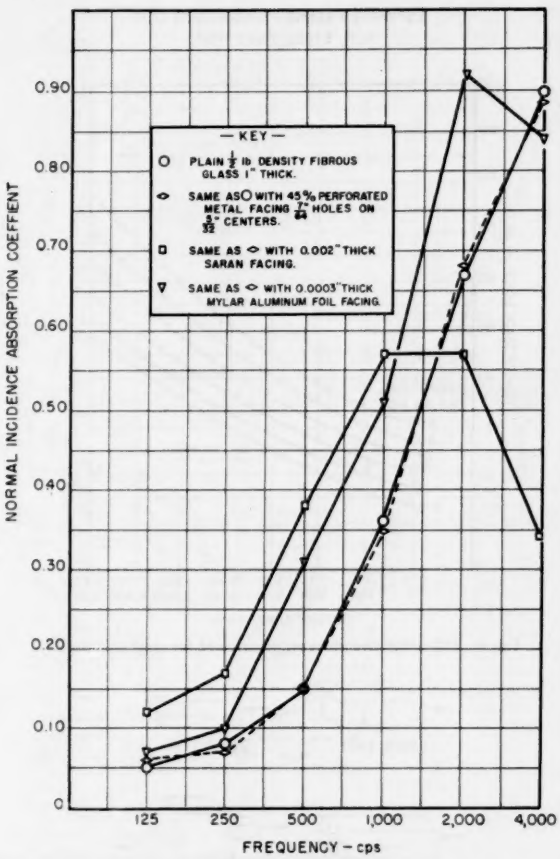
NORMAL INCIDENCE ABSORPTION COEFFIENT
FREQUENCY - cps
— KEY —
PLAIN 1/2 lb. DENSITY FIBROUS GLASS 1" THICK.
SAME AS ○ WITH 45% PERFORATED METAL FACING 7/64" HOLES ON 3/32" CENTERS.
SAME AS ◇ WITH 0.002" THICK SARAN FACING.
SAME AS ◇ WITH 0.0003" THICK MYLAR ALUMINUM FOIL FACING.

Fig. 3 Plotted data showing the effects of perforated and impervious facings on sound absorption of fibrous glass

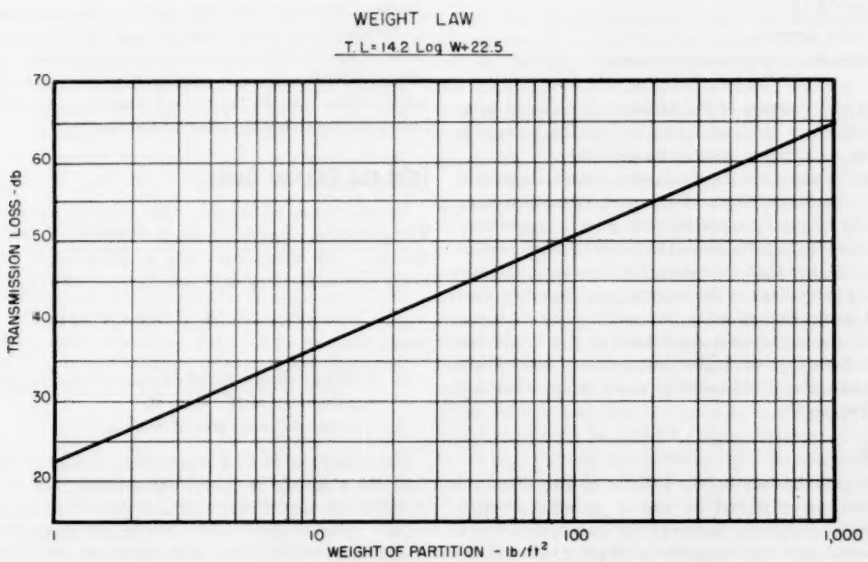

Fig. 4 A plot of the sound-transmission loss versus weight of partition

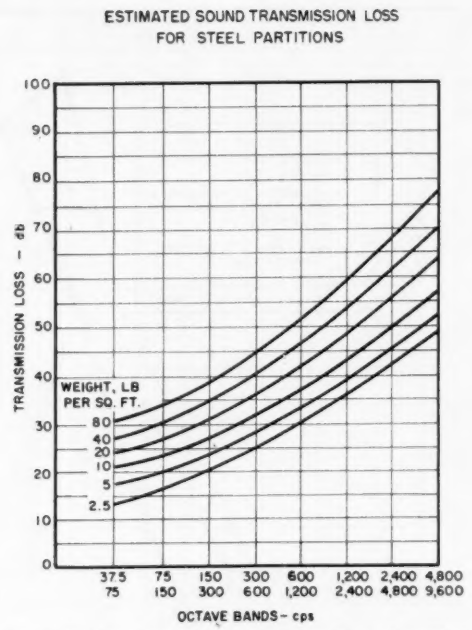

Fig. 5 Estimated sound-transmission loss for steel partitions

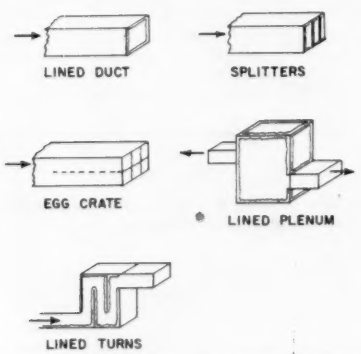

Fig. 6 Various duct configurations for sound attenuation

terioration of the effectiveness of the absorption material from water entrainment, oil or dirt contamination, and to protect it from damage, it is necessary to protect its surface.

Fig. 3 shows the relative results obtained in sound absorption from the use of various coverings. Perforated metal coverings with approximately 50 per cent perforations do not appreciably affect the absorption characteristics in the low-frequency region; but, at frequencies higher than that shown in the figure, the size of the hole and the percentage of the material perforated become more critical. A protective covering of a very thin membrane actually increases the absorption coefficient in the lower frequencies, but decreases it in the higher frequencies. For thicker membrane coverings, the effect becomes more pronounced and occurs at lower frequencies.

Noise Insulation

Methods of reducing the sound pressure levels in compartments where gas turbines are installed by use of sound-absorption materials have been discussed; however, in some cases where sufficient absorption materials cannot be applied, it will be necessary to install the gas turbines in separate compartments.

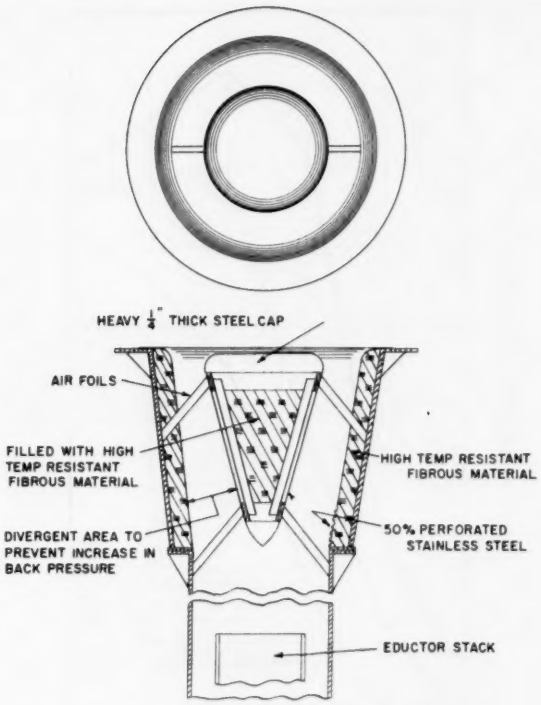
HEAVY ¼" THICK STEEL CAP
AIR FOILS
FILLED WITH HIGH TEMP RESISTANT FIBROUS MATERIAL
HIGH TEMP RESISTANT FIBROUS MATERIAL
DIVERGENT AREA TO PREVENT INCREASE IN BACK PRESSURE
50% PERFORATED STAINLESS STEEL
EDUCTOR STACK

Fig. 7 A design of a turbine-exhaust muffler

The effectiveness of this method of noise reduction is based on the sound-transmission characteristics of the enclosures of the separate compartments. The maximum sound-transmission loss that can be obtained by use of a partition or bulkhead is shown in Fig. 4. The reductions shown cannot usually be obtained because of air leakage around the enclosure, resonance of the structure, and so on. It is necessary when enclosing a gas turbine to make the enclosure as airtight as possible. Where it is necessary to emit ventilation air, suitable ducts should be provided. The effects of resonances can be largely eliminated by use of wood or sandwiched-type steel constructions consisting of two thin sections of steel riveted together so as to sandwich asbestos cloth or other feltlike materials. Fig. 5 is a more realistic plot of the transmission loss that can be obtained by use of steel partitions because it considers the effect of frequency.

Inlet and Exhaust Ducts

Various types of suitable inlet ductings are shown in Fig. 6. The reduction of sound down the duct can be reduced by lining the duct with sound-absorbing materials [3]. The attenuation along a straight-lined duct may be estimated by

$$\text{db/ft} = 12.6\alpha^{1.4}P/A_d$$

where

α = sound-absorption coefficient at the frequency of interest
P = perimeter of the duct, in.
A_d = cross-sectional area of duct, sq in.

Since the ratio of P/A is greater for a narrow rectangular duct than for a square or nearly square duct, the best duct to use would be one that is very wide and thin. Use of splitters or "egg-crate" dividers lined with absorption materials increases the effectiveness of the ducts. The most effective location for lining of ducts is in the bends or turns.

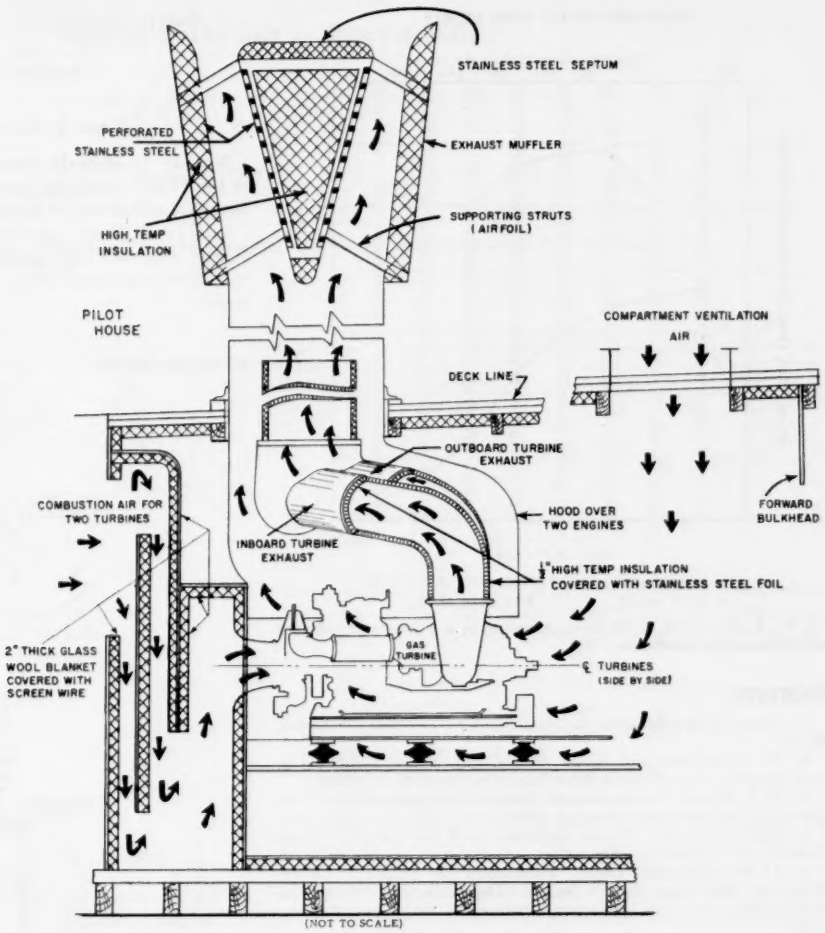

Fig. 8 A typical shipboard installation of a gas turbine for minimum noise output

The same considerations discussed for inlet ducts apply to exhaust ducts except that the gas velocities are much higher and it is necessary to prevent erosion of the absorption materials. Reference [4] lists various constructions of absorption materials and the gas velocities with which they can be used. The materials must also be selected to withstand the gas temperatures. Of course, it is also necessary to consider the flow resistances of the ducts and their effect on the performance of the gas turbine.

Fig. 7 is a general arrangement of an exhaust muffler that is effective for use on gas turbines. The eductor stack [5] is used for compartment ventilation. The length and diameter are dependent on the back-pressure limitations and the diameter of the exhaust ducting. Suitable covering should be provided for long shutdowns to prevent deterioration of the absorption materials resulting from exposure to the weather, or the muffler should be placed in a horizontal position with a permanent covering.

Conclusions

Fig. 8 shows a section of a gas-turbine installation in a small minesweeper [6]. All of the general recommendations discussed in the present paper have been applied to this installation. The problem was to reduce the noise occurring in the pilothouse which was located just above the turbine room. The exhaust stack was attached to the pilothouse and ended just above the roof. The effectiveness of the various treatments is shown in Fig. 9. The criteria established for Category B spaces were exceeded in the lower frequencies in the pilothouse, but the high-frequency criteria were met in the higher frequencies. Further reductions could have been obtained by additional treatments of windows and doors, but the reductions were considered satisfactory.

The extent that the methods discussed in this paper are applied is dependent upon the noise generated by the turbine. By intelligent design, it is possible to employ the methods discussed on the turbine itself by use of inlet and exhaust silencers, housings, and so on. Some turbines have been received with the air inlets so far down in the structures that it is impossible to attach silencers without elaborate designs of inlet ducting and rebuilding of some of the supporting structures. On the other hand, if considerations for noise reductions were made during initial design, the inlet silencer would have been an integral part of the turbine structure or suitable ducting to the compressor would have been installed for easy attachment of the silencer. This is only one example of designing to minimize noise; there are many more, such as in-place balancing, prevention of rattles, use of damped housings, and so forth. If the gas turbine supplied represents the quietest that can be obtained for the horsepower generated, then the installation costs for noise reduction will be minimized.

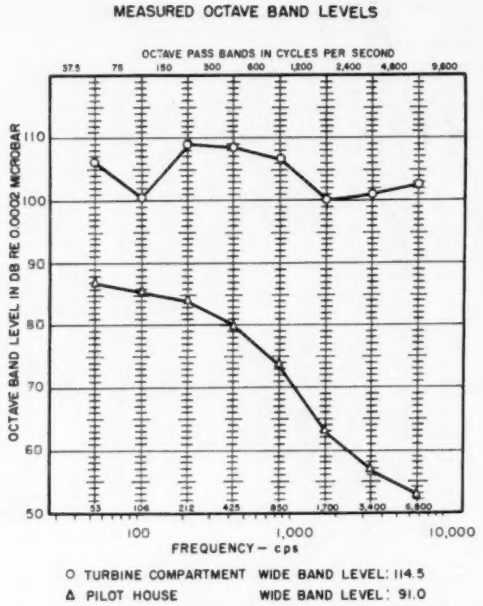

Fig. 9 A plot of the sound levels occurring in a turbine compartment and an overhead pilothouse

References

1 "General Specifications for Ships of the U. S. Navy," Section S1-10.

2 V. O. Knudsen and C. M. Harris, "Acoustical Designing in Architecture," John Wiley & Sons, Inc., New York, N. Y., 1950.

3 H. J. Sabine, "Absorption of Noise in Ventilating Ducts," *The Journal of the Acoustical Society of America*, vol. 12, July, 1940, p. 53.

4 Samuel Labate, "Porous Materials for Noise Control," *Noise Control*, vol. 2, January, 1956.

5 J. W. Mitchell, "Design Parameters for Subsonic Air-Air Ejectors," Technical Report No. 40, Department of Mechanical Engineering, Stanford University, Stanford, Calif., December 31, 1958.

6 W. J. Burch, "General Criteria for Ensuring Quiet Gas-Turbine Shipboard Installations," NavShips 250-645-3, available from Naval Supply Center, Norfolk, Va., and Oakland, Calif.

APPENDIX

Summary of Performance Data on Tests of Resilient Mounting 7E450

MOUNTING IDENTIFICATION

1 Type of mounting: 7E450

2 Mounting mfr: Rubber Laboratory, Mare Island Naval Shipyard

3 Mounting Dwg No.: (BUSHIPS) S2300-1445374[1]

4 Applicable specification: (Procurement) MIL-M-17508 (A)(Ships)

5 Standard Navy Stock No.: PN17-M-75623-8675

6 Rated load: 100 to 450 lb

7 Natural frequency:[2]

$$Z \text{ direction} = \frac{100 \text{ lb}}{9.3 \text{ cps}} \quad \frac{450 \text{ lb}}{6.5 \text{ cps}}$$

X and Y directions = not applicable

NOTES: [1] Since the issuance of this report, revised drawing of the 7E450 mountings have been made. The new BUSHIPS Dwg No. is 5000-S1112-F-1385778-C.

[2] These values of natural frequency were obtained shortly after the load had been applied. The design engineer should use the values given for the natural frequency after drift tests.

MOUNTING DETAILS

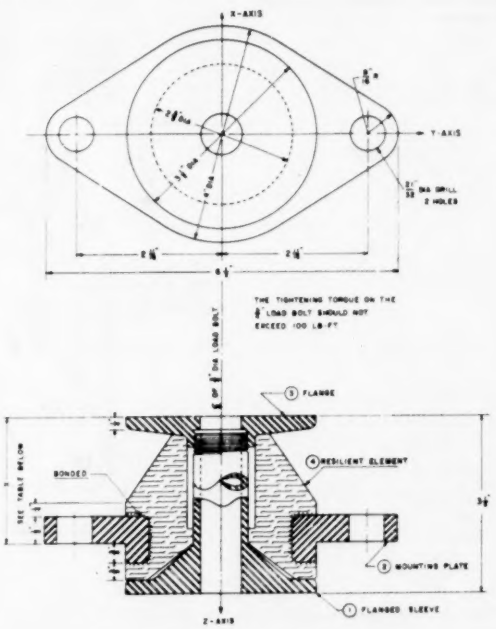

Load, lb	Dimension X, inches
0	$2^{5}/_{32} \pm {}^{1}/_{16}$
100	$2^{5}/_{64} \pm {}^{1}/_{16}$
120	$2^{3}/_{64} \pm {}^{1}/_{16}$
150	$2 \pm {}^{1}/_{16}$
200	$1^{15}/_{16} \pm {}^{1}/_{16}$
250	$1^{55}/_{64} \pm {}^{1}/_{16}$
300	$1^{13}/_{16} \pm {}^{1}/_{16}$
350	$1^{49}/_{64} \pm {}^{1}/_{16}$
400	$1^{23}/_{32} \pm {}^{1}/_{16}$
450	$1^{43}/_{64} \pm {}^{1}/_{16}$

NOTE: This table is for use by installing or design activities only for approximating heights X under various loads. It is not a procurement requirement.

Summary of Test Data for Mounting 7E450

1. Vibration:

Characteristics	Load on mtg: 450 lb Z	450 lb X	450 lb Y	Load on mtg: 250 lb Z	250 lb X	250 lb Y	Load on mtg: 100 lb Z	100 lb X	100 lb Y
Natural frequency, f_n (cps)	6.5	*	*	6.7	*	*	9.3	*	*
Critical damping, per cent	3.2	6.8	6.8	3.7	6.5	6.5	4.6	6.3	6.3
Maximum transmissibility	15.5	*	*	13.4	*	*	10.8	*	*
Spring constant, K_d (lb/in.)**	1940	785	785	1150	620	620	880	550	550

* Since the mountings are to be used with the load applied along the *Z*-axis only, these values are of little practical value.
** All spring constants are for axial loading.

2. Drift:

Direction	Load, lb	Temp, deg F	Defl after 1 hr, in.	Drift 1 hr to 200 hr, in.	Natural frequency, cps: Room temp before test	3 min after test	Room temp after test
Z	450	160	0.550[1]	0.034	6.5	...	7.4
	450	80	0.542	0.027[2]	...	...	...
	450	30	0.500[1]	0.054[3]	7.4	...	7.2

(1) Values are approximate.
(2) Extrapolated from drift curve up to 85 hours.
(3) Resilient element crystallized at about 67 hours.

3. Static Load Deflection:

Load, lb	Deflection, inch, *Z* direction: Normal	Inverted
100	0.08	0.02
450	0.47	0.06
1,000	0.72	0.11
2,000	0.92	0.17
4,000	1.11	0.22
8,000	1.22	0.25
13,000	1.25	0.26

4. Shock Deflection:

Direction	Load on 4 mountings, lb	Deflection, inch: Up	Down
Z	1,800	0.98	0.80
	400	0.45	0.90
X and *Y*	1,800	1.25	1.25
	400	0.95	0.95

5. Brief Remarks:

(*a*) Inspection: Mountings conformed to drawing details except for slight dimensional changes of rubber element probably caused by shrinkage. Mountings may be readily disassembled. Neoprene rubber, Mare Island Stock N-35-1 (E21-1383) used. Mountings manufactured in March, 1954. Tests completed June, 1954.

(*b*) Test specification: MIL-M-17185 (Ships).

(*c*) Transmissibility: No remarks.

(*d*) Uniformity: f_n varied less than 0.2 cps from the average value of four mountings tested.

(*e*) Static load deflection: No remarks.

(*f*) Noise isolation: Satisfactory.

(*g*) Shock damage: During radial tests, resilient element was punctured at two points 180° apart but no appreciable change in characteristics occurred. Slight distortion of metal parts (Specification MIL-S-20166, Grade M) occurred. No damage to either load bolts (3/4"-16NF-3 of Alloy No. 2), or foundation bolts (5/8"-11NC-2 of mild steel).

(*h*) Salt spray: No damage or significant change.

(*i*) Oil immersion: No damage or significant change.

(*j*) Drift: A 0.9 cps increase in f_n occurred as a result of drift at 160 F and a slight reduction occurred for the 30 F drift test.

(*k*) Cold storage: No tests made to date.

Summary of Test Data for Mounting 6E900

1. Vibration:

Characteristics	Load on mtg: 900 lb Z	900 lb X and Y	Load on mtg: 720 lb Z	720 lb X and Y	Load on mtg: 540 lb Z	540 lb X and Y	Load on mtg: 400 lb Z	400 lb X and Y
Natural frequency, f_n (cps)	6.6	*	6.5	*	5.7	*	6.3	*
Critical damping, per cent	4.1	5.2	3.6	5.3	3.8	4.9	3.5	5.0
Maximum transmissibility	12.2	*	13.8	*	13.2	*	14.1	*
Spring constant axially loaded K_d (lb/in.)	4010	1610	3110	1340	1790	1050	1620	1010

* Since the mountings are to be used with the load applied along the *Z*-axis only, these values are of little practical value.

2. Drift:

Direction	Load, lb	Temp, deg F	Defl after 1 hr, in.	Drift 1 hr to 200 hr, in.	Natural frequency, cps: Room temp before test	3 min after test	Room temp after test
Z	900	160	0.550*	0.035	6.4	...	6.9
	900	80	0.550*	0.040	6.4	...	6.9
	900	30	0.550*	0.036	6.9	...	6.9

* Values are approximate.

3. Static Load Deflection:

Load (lb)	Deflection, inch Z-direction Normal	Inverted
400	0.22	0.05
900	0.56	0.09
2,000	0.75	0.16
4,000	1.04	0.27
8,000	1.29	0.45
16,000	1.51	0.57
20,500	1.56	0.59

4. Shock Deflection:

Direction	Load on 4 mountings lb	Deflection, inch Up	Down
Z	3,600	1.19	1.08
	1,600	0.85	1.16
X and Y	3,600	1.40	1.40
	1,600	0.90	0.90

5. Brief Remarks:

(*a*) Inspection: Mounting conformed to drawing details. Neoprene rubber, Mare Island Stock N-29-1 used. Mountings manufactured in September, 1953. Tests completed September, 1954.

(*b*) Test specification: MIL-M-17185(SHIPS)

(*c*) Transmissibility: No remarks.

(*d*) Uniformity: f_n varied less than 0.2 cps from average value of 4 mountings tested.

(*e*) Static load deflection: No remarks.

(*f*) Noise isolation: Satisfactory.

(*g*) Shock damage: During radial tests, resilient element was punctured at 2 points 180° apart but no appreciable change in characteristics resulted. No damage to metal parts (Specification MIL-S-20166, Grade M) occurred. No damage to either load bolts (1″-14NF-3 of Alloy No. 2) or to foundation bolts (3/4″-16NF-3 of Alloy No. 2). Class B foundation bolts are also suitable.

(*h*) Salt spray: No damage or significant change.

(*i*) Oil immersion: No damage or significant change.

(*j*) Drift: 1/2 cps increase in f_n occurred as a result of 160° and 80° drift test.

(*k*) Cold storage: No change in f_n.

Summary of Performance Data on Tests of Resilient Mounting 6E900

MOUNTING IDENTIFICATION

1 Type of mounting: 6E900

2 Mounting mfr: Rubber Laboratory, Mare Island Naval Shipyard

3 Mounting Dwg No.: (BUSHIPS) S2300-1419292, Alt 3.(1)

4 Applicable specification: (Procurement) MIL-M-17508A (Ships)

5 Standard Navy Stock No.: P17-M-75849-1626

6 Rated load: 400 to 900 lb

7 Natural frequency:(2)

$$Z\text{-direction} = \frac{400 \text{ lb}}{6.3 \text{ cps}} \quad \frac{900 \text{ lb}}{6.6 \text{ cps}}$$

X and Y-directions = not applicable

NOTES: (1) Since the issuance of this report, revised drawings of the 6E900 mountings have been made. The new BUSHIPS Dwg No. is 5000-S1112-F-1385778-C.

(2) These values of natural frequency were obtained shortly after the load had been applied. The design engineer should use the values given for the natural frequency after drift tests.

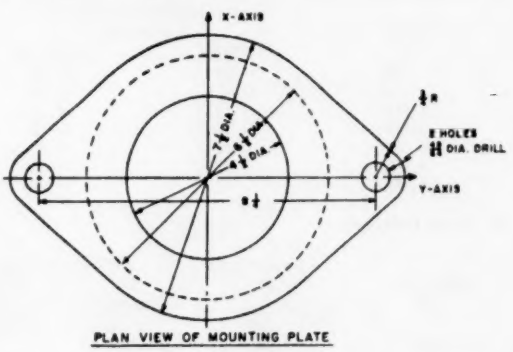

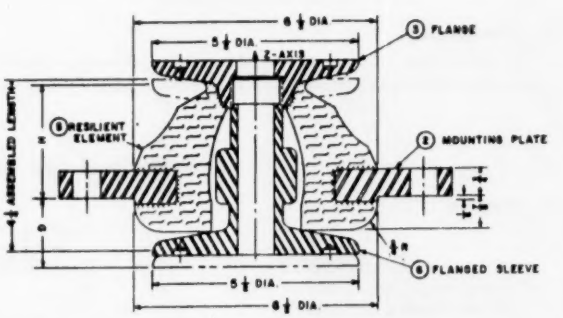

MOUNTING DETAILS

Load, lb	Dimension H, inches	Dimension D, inches
0	$3 \pm 1/16$	$1\,1/4 \pm 1/16$
400	$2\,25/32 \pm 1/16$	$1\,15/32 \pm 1/16$
500	$2\,49/64 \pm 1/16$	$1\,35/64 \pm 1/16$
600	$2\,39/64 \pm 1/16$	$1\,41/64 \pm 1/16$
700	$2\,35/64 \pm 1/16$	$1\,45/64 \pm 1/16$
800	$2\,31/64 \pm 1/16$	$1\,49/64 \pm 1/16$
900	$2\,29/64 \pm 1/16$	$1\,51/64 \pm 1/16$

NOTE: This table is for use by installing or design activities only for approximating dimensions H and D under various loads. It is not a procurement requirement.

Summary of Performance Data on Tests of Resilient Mounting 6E2000

MOUNTING IDENTIFICATION

1 Type of mounting: 6E2000
2 Mounting mfr: Rubber Laboratory, Mare Island Naval Shipyard
3 Mounting Dwg No.: (BUSHIPS) S2300-1419291, Alt 3(1)
4 Applicable specification: (Procurement) MIL-M-17508 (A)(Ships)
5 Standard Navy Stock No.: P17-M-75894-2085
6 Rated load: 700 to 2,000 lb
7 Natural frequency:(2)

$$Z\text{-direction} = \frac{2{,}000 \text{ lb}}{5.3 \text{ cps}} \quad \frac{700 \text{ lb}}{5.7 \text{ cps}}$$

X and Y-directions = not applicable

NOTES: (1) Since the issuance of this report, revised drawings of the 6E2000 mountings have been made. The new BUSHIPS Dwg No. is 5000-S1112-F-1385778-C.

(2) These values of natural frequency were obtained shortly after the load had been applied. The design engineer should use the values given for the natural frequency after drift tests.

MOUNTING DETAILS

Load, lb	Dimension H, inches	Dimension D, inches
0	$3^{5}/_{32} \pm {}^{1}/_{16}$	$1^{3}/_{8} \pm {}^{1}/_{16}$
700	$2^{59}/_{64} \pm {}^{1}/_{16}$	$1^{39}/_{64} \pm {}^{1}/_{16}$
900	$2^{15}/_{16} \pm {}^{1}/_{16}$	$1^{23}/_{32} \pm {}^{1}/_{16}$
1,150	$2^{45}/_{64} \pm {}^{1}/_{16}$	$1^{53}/_{64} \pm {}^{1}/_{16}$
1,600	$2^{37}/_{64} \pm {}^{1}/_{16}$	$1^{61}/_{64} \pm {}^{1}/_{16}$
2,000	$2^{31}/_{64} \pm {}^{1}/_{16}$	$2^{3}/_{64} \pm {}^{1}/_{16}$

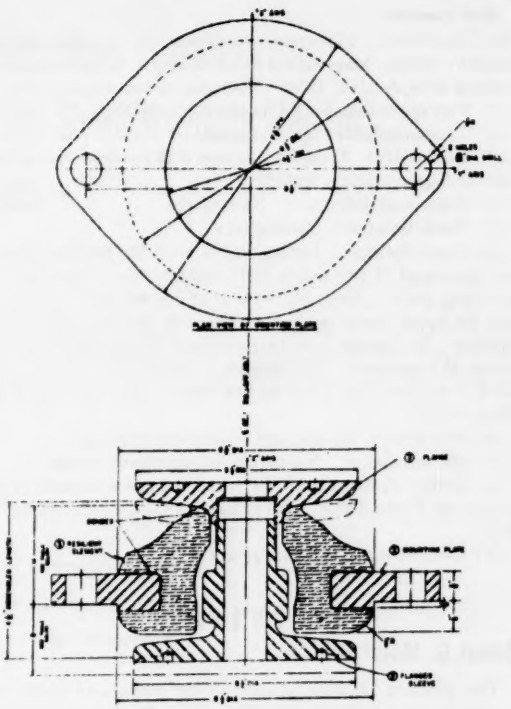

NOTE: This table is for use by installing or design activities only for approximating dimensions H and D under various loads. It is not a procurement requirement.

Summary of Test Data for Mounting 6E2000

1. Vibration:

Characteristics	Load on mtg: 2000 lb			Load on mtg: 1600 lb			Load on mtg: 1150 lb			Load on mtg: 700 lb		
	Z	X	Y	Z	X	Y	Z	X	Y	Z	X	Y
Natural frequency, f_n (cps)	5.3	*	*	5.5	*	*	5.5	*	*	5.7	*	*
Critical damping, per cent	3.7	5.7	5.7	3.2	5.5	5.5	3.7	5.4	5.4	4.0	5.2	5.2
Maximum transmissibility	14.0	*	*	15.6	*	*	13.7	*	*	12.4	*	*
Spring constant, axial loading K_d (lb/in.)	5750	2580	2580	4950	2340	2340	3560	2000	2000	2320	1425	1425

* Since the mountings are to be used with the load applied along the Z axis only, these values are of little practical value.

2. Drift:

Direction	Load, lb	Temp, deg F	Defl after 1 hr, in.	Drift 1 hr to 200 hr, in.	Natural frequency, cps: Room temp before test	Natural frequency, cps: 3 min after test	Natural frequency, cps: Room temp after test
Z	2,000	160	0.680	0.057	5.2	...	5.6
	2,000	80	0.680	0.075[1]	5.1	...	5.5
	2,000	30	0.680	0.058	5.6	...	5.6

(1) Extrapolated from curve.

3. Static Load Deflection:

Load, lb	Deflection, inch Z-direction: Normal	Deflection, inch Z-direction: Inverted
700	0.23	0.03
2,000	0.67	0.10
4,000	0.96	0.19
8,000	1.22	0.33
16,000	1.45	0.46
35,000	1.60	0.55

4. Shock Deflection:

Direction	Load on 4 mountings, lb	Deflection, inch: Up	Deflection, inch: Down
Z	8,000	1.3	0.9
	2,800	1.0	1.3
X and Y	8,000	1.2	1.2
	2,800	1.2	1.2

5. Brief Remarks:

(*a*) Inspection: Mountings conformed to drawing details. Neoprene rubber, Mare Island Stock N-29-1. Mountings manufactured in September, 1953. Tests completed August, 1954.

(*b*) Test specification: MIL-M-17185(SHIPS)

(*c*) Transmissibility: No remarks.

(*d*) Uniformity: f_n varied less than 0.13 cps from the average value of four mountings tested.

(*e*) Static load deflection: No remarks.

(*f*) Noise isolation: Satisfactory.

(*g*) Shock damage: During radial tests, the resilient element was punctured at two points 180° apart between the sleeve and mounting plate. Resilient element of one mounting separated near the upper flange but had no effect on the mounting characteristics. No damage to metal parts (Specification MIL-S-20166, Grade M) occurred. No damage to either load bolts (1-1/4"-12NF-3 of Alloy No. 2) or to foundation bolts (7/8"-14NF-3 of Alloy No. 2)

(*h*) Salt spray: No damage or significant change.

(*i*) Oil immersion: No damage or significant change.

(*j*) Drift: f_n increased 0.4 cps and 0.3 cps as a result of drift tests at 80 F and 160 F. No change in f_n as a result of drift at 30 F.

(*k*) Cold storage: No change in f_n.

DISCUSSION

Robert G. Mills[2]

The problem of noise aboard Navy boats and ships is of rapidly growing importance. The author is to be congratulated for his excellent coverage of this complex subject within the limited time and space available.

This paper has considered primarily the subject of the reduction of the airborne noise of gas turbines—the noise component that is of particular importance from a comfort and habitability viewpoint. Some ships' machinery noise also finds its way into the water, where it can be detected by hydrophone listening. With the increasing importance of anti-submarine warfare, this is frequently the paramount factor to be considered in the machinery installation.

The use of resilient mounts in a properly designed mounting system is highly effective in reducing direct hull excitation through the machinery foundations. As mentioned in the paper, accurate balancing, prevention of rattles, and use of damped housings will reduce the noise of the basic machine, and hence its waterborne noise. Such contributions to waterborne noise as may be transmitted through the air to the ship's structure may be reduced by the damping and absorption techniques described by the author.

Most of these measures require weight, space, and money—all of which are at a premium in ship construction. For this reason, use of a gas turbine prime mover frequently proves to be particularly advantageous. The gas turbine is light and can be compactly mounted on resilient mounts. The acoustic hood (if required) is small because the engine is small. Auxiliaries are generally engine mounted and do not require separate treatment. Finally, gas turbine noise is characteristically of high frequency, and is more easily and rapidly attenuated than the lower frequency radiations from slower prime movers. For these reasons, the gas turbine will have increasing use where noise characteristics are important. This gives added emphasis to the value of the work in noise reduction performed by Mr. Herrmann and his associates.

[2] Commander, Bureau of Ships, Navy Department, Washington, D. C.

A Torsional Vibration Problem as Associated With Synchronous Motor Driven Machines

R. N. BROWN
Compressor Department,
Allis-Chalmers Manufacturing
Company, Milwaukee, Wis.

Certain component failures in synchronous-driven high-inertia rotating equipment may be traced to a phenomenon peculiar to the starting characteristic of a salient-pole synchronous motor: A synchronous motor contributes a pulsating torque during the starting cycle. Though this fact is well known in itself, it has not been associated with the effect it may have on a high inertia load. The pulsating torque may excite a torsional resonance, which will in turn induce very high stresses in the driven train members.

CERTAIN component failures in synchronous-motor-driven high-inertia rotating equipment have been the source of great concern to rotating-equipment manufacturers. The following example of a compressor-shaft failure can be considered as typical of the type of failure indicated. Figs. 1 (*a* and *b*) show a three-inch compressor shaft which failed. This compressor is of the centrifugal type and is driven by a salient-pole synchronous motor through a speed increaser. An investigation revealed that this was a torsional fatigue failure.

This particular unit was operated for several years with from four to five starts per day. The shaft failure was detected when the compressor began to vibrate excessively.

A check by the metallurgy laboratory revealed that the material surpassed specifications. A recheck of the engineering calculation indicated that maximum design shear stress based on maximum full-load condition was less than half of the endurance limit for shear for this particular material. Because the apparent stress level seemed well within good design practice, it was reasoned that additional stress was induced. It seemed that one likely possibility was that this stress might be due to some unknown resonant condition.

The following phenomena were then brought out. These phenomena, though well known individually, had apparently never been considered together.

Salient-pole synchronous motors, when started without field excitation as induction machines, exhibit a pulsating torque. The torque pulsation frequency is equal to twice the slip frequency. The slip frequency varies from line frequency at zero speed to zero slip at synchronous speed. In most of the literature available on synchronous motor starting, the pulsating effect is ignored and only the average torque figures are given. This is misleading in that, when a synchronous motor driver is applied to high inertia loads, the potential problems caused by the pulsating component are not evident.

To illustrate this, consider the following equation giving the general starting torque for a salient-pole synchronous motor starting as an induction motor [1].[1]

$$T = 2\times\text{real part of } (I_f B_f + I_b B_b + I_b B_f e^{j2st} + I_f B_f e^{-j2st}) \quad (1)$$

$$s = \text{slip frequency} = f\left(\frac{N - N_{\text{Rotor}}}{N}\right) \quad (2)$$

N = synchronous speed

N_{Rotor} = rotor speed

f = line frequency

t = time

$I_f I_b B_f B_b$ are complex numbers and are functions of the a-c circuit as presented by the motor [1].

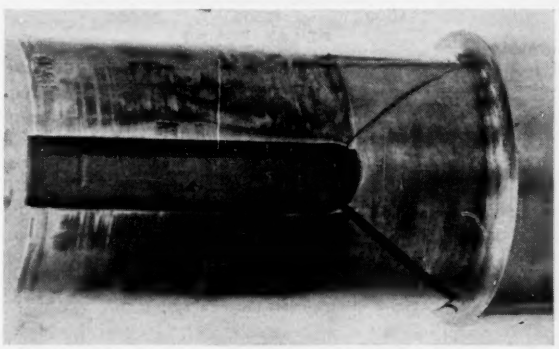

Fig. 1(a) Three-inch compressor shaft showing where failure occurred between coupling and journal

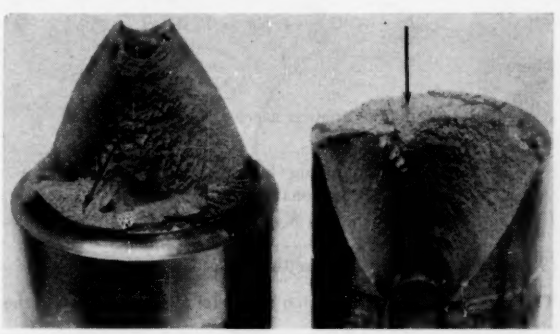

Fig. 1(b) The fractured surface indicated that the failure started in the corner at each side of the keyway and progressed by torsional fatigue. Arrows show the final portion of the failure which was made in the laboratory.

[1] Numbers in brackets designate References at end of paper.

Contributed by the Compressor Subcommittee of the Hydraulic Division and presented at the Annual Meeting, Atlantic City, N. J., November 29–December 4, 1959, of THE AMERICAN SOCIETY OF MECHANICAL ENGINEERS.

NOTE: Statements and opinions advanced in papers are to be understood as individual expressions of their authors and not those of the Society. Manuscript received at ASME Headquarters, July 13, 1959. Paper No. 59—A-141.

The first two terms give the average torque, whereas the last two terms contribute the pulsating components of torque. The last two terms are counter-rotating vectors, rotating at twice slip frequency. These alternately add positive, cancel, and add in the negative direction. The results, when plotted, are represented by the limits of torque, as shown by a plot of the speed-torque curve for the direct axis and a plot of the torque for the quadrature axis. Fig. 2 shows a typical motor curve. The net result is the torque pulsation between the direct axis curve and the quadrature axis curve.

A synchronous motor, when connected to a load, exhibits the characteristics of a multimass torsional spring. The following will review some of the fundamentals of a torsional system. The basic equation may be written for a single mass connected to a shaft (Fig. 3).

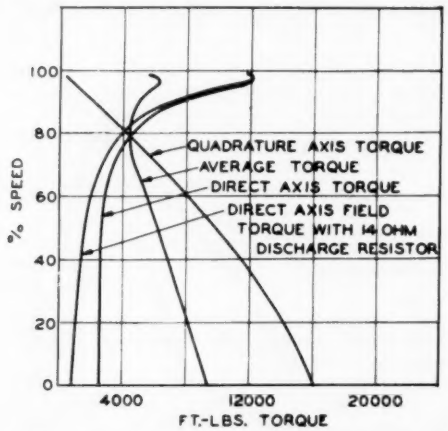

Fig. 2 Typical salient-pole synchronous motor starting characteristic speed torque curve

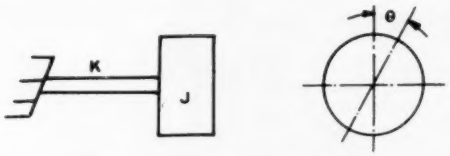

Fig. 3 Single-mass torsional spring

The general differential equation, found by summing up the torques is:

$$J\frac{d^2\theta}{dt^2} + C\frac{d\theta}{dt} + K\theta = T_0 \sin \omega t \qquad (3)$$

where

$J\dfrac{d^2\theta}{dt}$ = torque due to angular acceleration

$c\dfrac{d\theta}{dt}$ = torque due to damping (here assumed as viscous damping and proportional to angular velocity)

$K\theta$ = spring torque, with K being the spring constant of the shaft

$(T_0 \sin \omega t)$ = the external exciting torque

This equation may be rewritten in the following form, using the operator p to replace $\dfrac{d}{dt}$

$$(Jp^2 + cp + K)\theta = T_0 \sin \omega t \qquad (4)$$

One of the most common, and a single case to consider for an actual system, would be a synchronous motor driving a compressor through a gear. This system, when reduced to equivalent quantities, can be represented as a three-mass system (Fig. 4).

This system can be described by writing the following set of equations:

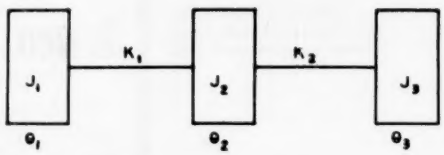

Fig. 4 Three-mass torsional system

$$J_1\frac{d^2\theta_1}{dt^2} + C_1\frac{d\theta_1}{dt} + K_1(\theta_1 - \theta_2) = T_0 \sin \omega t \qquad (5)$$

$$J_2\frac{d^2\theta_2}{dt^2} + C_2\frac{d\theta_2}{dt} + K_1(\theta_2 - \theta_1) + K_2(\theta_2 - \theta_3) = 0 \qquad (6)$$

$$J_3\frac{d^2\theta^2}{dt^2} + C_3\frac{d\theta_3}{dt} + K_2(\theta_3 - \theta_2) = 0 \qquad (7)$$

These equations may be rewritten into the following form if damping is to be neglected. Also, the operator p replacing d/dt will be used.

$$J_1p^2\theta_1 + K_1(\theta_1 - \theta_2) = T_0 \sin \omega t \qquad (8)$$

$$J_2p^2\theta_2 + K_1(\theta_2 - \theta_1) + K_2(\theta_2 - \theta_3) = 0 \qquad (9)$$

$$J_3p^2\theta_3 + K_2(\theta_3 - \theta_2) = 0 \qquad (10)$$

If this set of equations is to be used for obtaining the natural resonant frequency of the system, the equation may be written by substituting $j\omega$ for p. These, rewritten, will become:

$$-\left(\frac{J_1}{K_2}\right)\omega^2\theta_1 + \theta_1 - \theta_2 = 0 \qquad (11)$$

$$-\left(\frac{J_2}{K_2}\right)\omega^2\theta_2 + K_1/K_2(\theta_2 - \theta_1) + \theta_2 - \theta_3 = 0 \qquad (12)$$

$$-\left(\frac{J_3}{K_2}\right)\omega^2\theta_3 + \theta_2 - \theta_3 = 0 \qquad (13)$$

This form can be solved for ω^2 with simultaneous equations. It may also be solved with a digital computer by use of matrix algebra, substituting $T = 1$ in equation (1), and using a trial and error method. This three-mass system will give two modes of vibration. Resonance in the computer method is determined by one of the angles (θ) going to infinity. This method is not limited to the number of masses in the system.

A more rigorous solution would use the oscillating torque, as obtained from the synchronous-motor equation, as the torque in the forced-vibration equation and make an allowance for damping.

To this point, we have considered two basic phenomena individually. Earlier, it was stated that it is the combined effect that presents the problem. This problem becomes more apparent when we note that most synchronous-motor-driven compressors have at least one torsional natural frequency in the frequency range of excitation exhibited by the synchronous motor.

In Fig. 5, on which a typical compressor starting curve is superimposed on a typical motor starting-torque curve, the amount of torque available for acceleration can be observed. Also, the quantity of the torque which is oscillatory in nature, may be seen as part of the torque between the limits of direct-axis and quadrature-axis torque. This illustration alone indicates the possibility of rather large magnitude torsional vibration as the

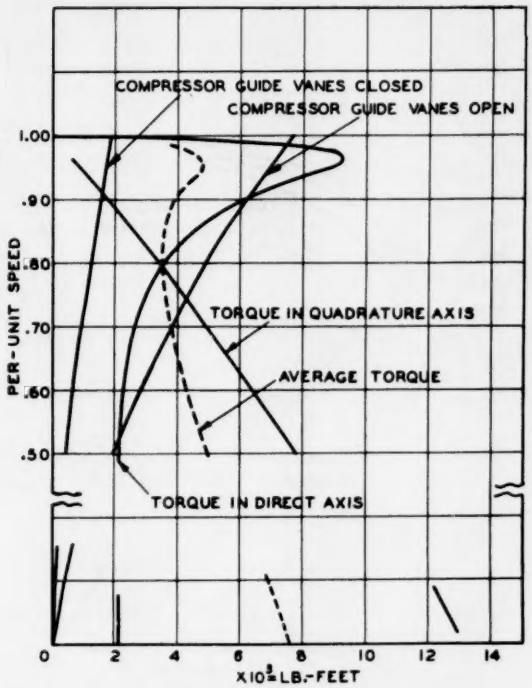

Fig. 5 Typical synchronous motor starting characteristic speed torque curve with a loaded and unloaded centrifugal compressor starting curve superimposed

system nears resonance. Since startup is transient in nature, the actual severity of the case is founded on the length of time the system will dwell at resonance. Here may be injected the fact that the situation is amplified by the number of startups to which the unit is subjected. To consider first what happens during the period of a single startup, consider the relationship required to compute time.

$$T = J\alpha \tag{14}$$

where

T = torque = $f(N)$ as described by the torque speed curve
α = angular acceleration = dN/dt

Substituting these quantities into equation (14) yields:

$$J\frac{dN}{dt} = f(N) \tag{15}$$

$$\frac{dN}{dt} = \frac{1}{J}f(N) \tag{16}$$

This equation can be arranged in the following form for integration:

$$\int_0^t dt = \int_0^N \frac{J}{f(N)}\,dN \tag{17}$$

If N is taken as synchronous speed, the equation will yield the total time to accelerate the load to speed. The integration can be performed graphically by using the form:

$$t = \sum_{N_1}^{N_n} \frac{\Delta N_n}{T_n/J} \tag{18}$$

Refer also to Fig. 6.

Using the graphical method outlined, the time required to accelerate through any desired portion of the starting-speed spectrum may be approximated.

To evaluate the possible severity of the torsional problem, the speed at which the torsional natural frequency occurs should be noted. At this point, two approaches can be taken. One is to arbitrarily pick a band width with the critical frequency as the center point and evaluate the time required to pass this band width. Knowing the time and the center frequency, the number of cycles which the system accumulates during this time can be computed. This will give some indication of the danger involved, in that, quantitatively speaking, the greater number of cycles accumulated at a high stress level such as resonance, the more the possibility of a fatigue failure of some member in the driven train. There will be many times, due to the many unknowns, when this will be the best that can be done toward an actual evaluation of the potential danger of a fatigue failure.

A more rigorous and more desirable approach is to actually plot the shape of the resonance curve for each mode of torsional resonance. This admittedly is difficult and is not always feasible. It will resolve itself into the evaluation of all the damping factors, such as damping contributed by material hysteresis, and resolving the angles of twist as computed from the vibration equation into a stress level.

By using the resonance curve, the dangerous band width can be read directly. This knowledge, combined with time-element calculation, results in the number of cycles at a certain stress level. The stress level in turn, can be plotted on a Goodman diagram of the material of which the various components are fabricated. An indication of the actual picture of stress is then obtained. This information then can be used to limit the number of starts, if such is possible, or can indicate the necessity of a design modification.

To return to the example originally cited, an analysis of the torsional natural frequency reveals the following: This system, consisting of a synchronous-motor driver, a gear, and a compressor, may be analyzed as a three-mass torsional system. Physical parameters are such that the first mode torsional natural frequency occurs at 860 cpm. This corresponds to a motor speed of 1058 rpm, which is 88.2 per cent of synchronous speed. By referring to the starting torque curve of the drive motor, Fig. 7, it is noted that at this point the torque variation from average is approximately ±45 per cent. The stress ratio at this point is approximately 0.38, nonreversing in magnitude. The ratio of maximum stress to endurance limit is 2 to 1.

These figures are based on a nonresonant condition. At reso-

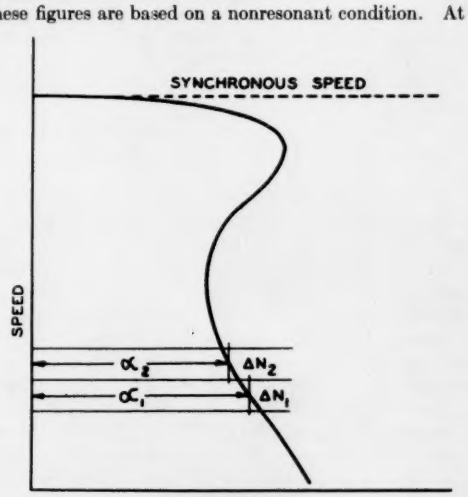

Fig. 6 Average synchronous motor starting speed torque curve

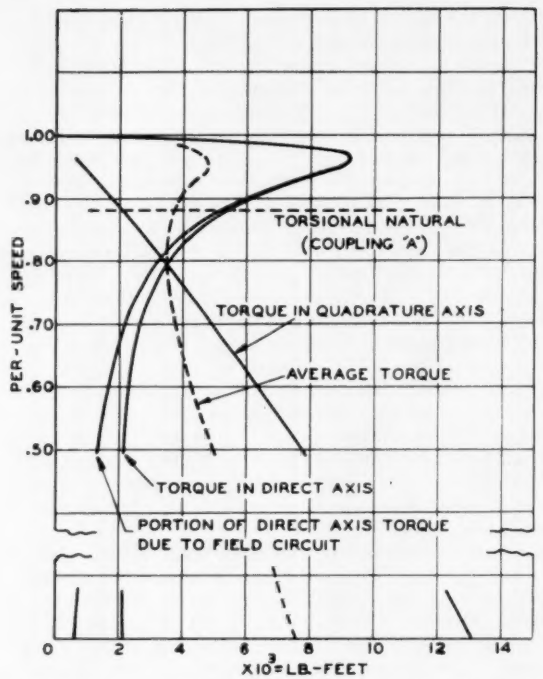

Fig. 7 Typical salient-pole synchronous-motor starting characteristic curve with a 14-ohm discharge resistor showing the location of a system torsional natural frequency

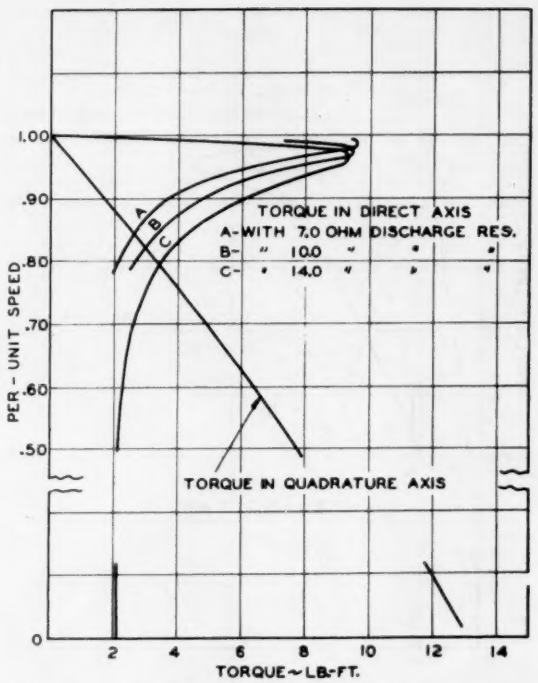

Fig. 8 Effect of varying the discharge resistor on the starting characteristic speed torque curve of a synchronous motor

nance, magnification factors of from 10 and up may be experienced. Taking this into account, it may readily be seen that a conservatively designed shaft based on nonresonant conditions is definitely not safe when subjected to such stress levels for relatively short duration but large cycle accumulation. For the example cited this was approximately 50,000 cycles. Another problem is that the torsional resonance phenomena cannot be easily detected, except for the possibility of noise in the gear, until a component failure causes a lateral vibration.

To remedy the torsional natural frequency problem, there are several alternatives, which the designer may pursue. The first thing to consider is where the resonance point occurs when superimposed on the motor starting curve. Once this has been determined, the system may be retuned to shift the resonant frequency should it become obvious that a problem might occur, or has occurred as in the case of a field installation. The relocation of resonance may be in such a direction so as to move to a more favorable point of accelerating torque to reduce the time in resonance.

The alternate to this is to move to the point where the direct axis torque curves cross the quadrature axis torque curve. At this point there is no excitation force for resonance and it is, therefore, an ideal point at which to locate the natural frequency. Means available for changing resonance, outside of redesign of the actual machine involved, are to change couplings to change overall shaft stiffness. This gives only a limited amount of latitude. Another alternative is to change the motor field discharge resistor to modify the motor curve, as shown in Fig. 8. This changes the point at which the direct axis and quadrature axis cross. This can be used alone, or with a coupling change, to reduce the excitation torque to a minimum. This method is probably the most useful in solving a field problem where major changes are impractical.

In the example cited, both the couplings between the gear,

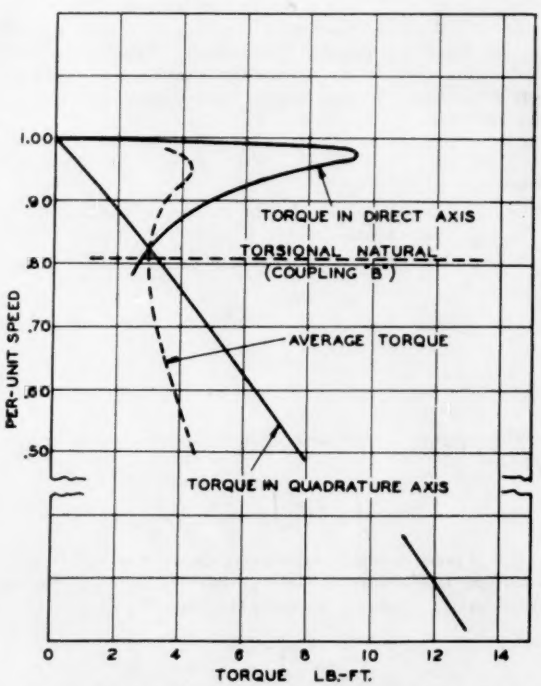

Fig. 9 Salient-pole synchronous motor starting characteristic curve with a 10-ohm discharge resistor showing the location of the system torsional natural frequency with Coupling B

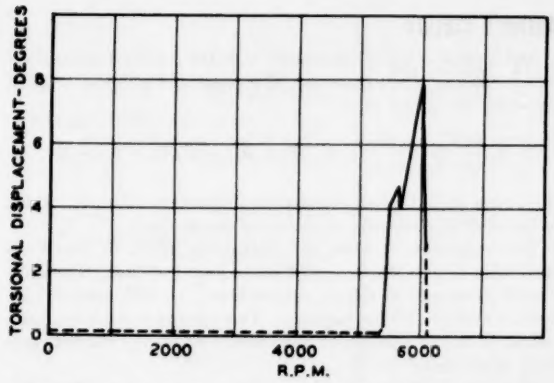

Fig. 10 Torsional vibration amplitude plotted against starting rpm—Coupling A

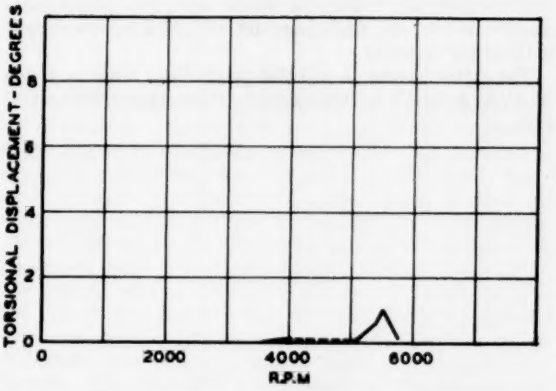

Fig. 11 Torsional vibration amplitude plotted against starting rpm—Coupling B

compressor, and motor, and the discharge resistor were changed (see Fig. 9). Plots of actual torsional vibration before and after are shown in Figs. 10 and 11.

From this discussion it may be seen that shaft stress problems are only one of the potential dangers which may be caused by torsional vibration problems in synchronous driven equipment. Couplings, gear teeth, and impeller rivets are just a few of other components which are in possible danger of damage. Unfortunately, these are somewhat more difficult to calculate.

Other alternatives which can best be applied during the design stage are to switch to another type driver or to use an auxiliary starting motor such as a wound-rotor motor. These also have disadvantages which are obvious.

The best remedy the engineer has is to recognize the problem and try to design away from it.

To summarize, the factors which the engineer must consider are:

1 Characteristics of the synchronous drive.
2 Number of potential starts which the unit will experience.
3 Resonant frequency and its related location on the motor curve.
4 The acceleration torque available at the resonant point or time the unit will dwell in the resonance region.

Once these four factors have been analyzed, the designer can make use of the following remedies, depending on his own particular case:

(*a*) Change natural frequency by:

1 Redesign of components
2 Change coupling

(*b*) Remove excitation:

1 Moving quadrature and direct axis intersection
2 Use of auxiliary starting
3 Use of different type driver

References

1 Charles Concordia, "Synchronous Machines, Theory and Performance," John Wiley & Sons, Inc., New York, N. Y., 1951.

2 "Synchronous Motors," Westinghouse Electric and Manufacturing Co., Course 14, The Industrial Relations Company, East Pittsburgh, Pa., 1942.

3 J. P. Den Hartog "Mechanical Vibrations," McGraw-Hill Book Company, Inc., New York, N. Y., fourth edition, 1956.

4 C. R. Freberg and E. N. Kemler, "Elements of Mechanical Vibration," John Wiley & Sons, Inc., New York, N. Y., 1943.

DISCUSSION

Leonardt F. Kreisle[2]

This paper is a warning to the designer not to neglect a transient dynamic analysis of his problem if such is applicable. Only too often he is satisfied to do a steady-state dynamic analysis or even a static analysis and to safely (he hopes) hide behind high factors of ignorance! The author has shown that by the simple expedient of changing the stiffness of the system (by use of a different coupling) or through the alternate possibility of making a simple change in the exciting force (by changing a discharge condenser in the electrical circuit), the maximum amplitudes of torsional vibration under transient conditions have been reduced by a factor of approximately eight to one, enabling the system to operate safely throughout the numerous transients that occur during the expected useful lifetime of the equipment.

Unfortunately, the author was careless in setting up his equations of motion for his equivalent three-mass torsional system since algebraic sign errors were made in equations (6) and (9). These correctly appear as follows:

$$J_2 \frac{d^2\theta_2}{dt^2} + C \frac{d\theta_2}{dt} - K_1(\theta_1 - \theta_2) + K_2(\theta_2 - \theta_3) = 0$$

(Corrected equation 6)

$$J_2 p^2\theta_2 - K_1(\theta_1 - \theta_2) + K_2(\theta_2 - \theta_3) = 0 \quad \text{(Corrected equation 9)}$$

It would have been better had the author indicated that in equations (5) through (7), the coefficients of viscous damping C probably differ for each equation; perhaps this best could be indicated by the use of C_1, C_2, and C_3 instead of a single C value.

Equations (11) through (13) correctly should have been written as follows:

$$-\frac{J_1\omega^2\theta_1}{K_1} + \theta_2 - \theta_2 = 0 \qquad \text{(Corrected equation 11)}$$

$$-\frac{J_2\omega^2\theta_2}{K_2} - \frac{K_1(\theta_1 - \theta_2)}{K_2} + \theta_2 - \theta_3 = 0$$

(Corrected equation 12)

$$-\frac{J_3\omega^2\theta_3}{K_2} + \theta_2 - \theta_3 = 0 \qquad \text{(Corrected equation 13)}$$

The author suggests that equations (11) through (13) may be solved simultaneously for the two nonzero undamped natural

[2] Associate Professor of Mechanical Engineering, The University of Texas, Austin, Texas. Mem. ASME.

circular frequencies, or by means of matrix algebra and a digital computer. An alternate and probably less difficult procedure would be by use of a Holzer analysis with or without damping. The solution with damping included would result in more nearly correct resonant frequencies than those obtained from the previously mentioned procedures.

The author states that the maximum design shear stress based upon maximum full-load conditions was less than one half the shearing endurance limit of the material used. It is to be hoped that the design shear stress included the effects of stress concentration and surface finish, however no mention is made of inclusion of either. Since the over-all stress concentration factor at the point of failure of the compressor shaft due to the keyway, the press fit of the coupling, and all other causes combined could be of the order of two or more, and since the actual shearing endurance limit of the material with its surface roughnesses may have been measurably less than that determined for the same material fabricated into a test specimen with highly polished surface finishes, it is possible that the actual maximum stress due to maximum full-load conditions (excluding overloads due to starting conditions) may have been close to or even exceeded the polished-specimen shearing endurance limit of the material. It is hoped that the author took these items into account in the establishment of his design shearing stress.

Author's Closure

The author is in full agreement with the equation corrections as set down in the discussion. The original intent was to have equation (6) appear as:

$$J_2 \frac{d^2\theta_2}{dt^2} + C_2 \frac{d\theta_2}{dt} + K_1 (\theta_2 - \theta_1) + K_2(\theta_2 - \theta_3) = 0$$

This form should follow in equation (9) and equation (12) which is the same algebraically as shown by the discusser.

The suggestion of using the designation of C_1, C_2, and C_3 is also valid in that this is needed in the practical case. The additional corrections as shown in equations (11), (12), (and 13) are correct as shown by the discusser. These points were all originally intended by the author and have been corrected in the text portion of the paper.

The use of Holzer or other means of calculating natural frequency is probably more a matter of personal preference on the part of the engineer making the calculation. The author agrees that the addition of damping would make the solution more exact—however, also much more difficult. This point is covered in the text of the paper.

The author hastens to add that design shear stress as stated does very definitely include a generous stress concentration allowance.

E. O. BRANSFORD
Manager, Engineering and Development, Beaman Engineering Corporation, Greensboro, N. C.

R. A. STEIN
Research Engineer, Battelle Memorial Institute, Columbus, Ohio
Assoc. Mem. ASME

Design Control of Overcompression in Rotary-Vane Compressors[1]

In its simplest terms, the design of a rotary-vane compressor of a given displacement consists of selecting a particular combination of rotor and cylinder radius, cylinder length, and number of vanes. A study of the rotary-vane compressor has shown that the choice is not entirely arbitrary since thermodynamic and mechanical losses occurring in the compressor are intimately associated with these basic dimensions. One of the more important of these geometrically dependent losses was found to be potentially severe overcompression during the discharge process. In this paper, an equation is developed that describes in generalized form the relation of overcompression to the dimensions of the compressor. This equation is used to evolve an energy-loss criterion for design control of this loss. An example of the application of the criterion to a refrigeration compressor is included.

Of the many possible designs of rotary compressors, one of the most successful is the rotary-vane type. Acceptance of the rotary-vane compressor is due largely to its mechanical reliability, compactness, and adaptability to moderately high-speed operation in virtually an unlimited range of sizes. A recent design analysis has been directed toward enhancing these inherent advantages by developing generalized methods for selecting the basic configuration of the rotary-vane compressor to give high mechanical, thermodynamic, and volumetric efficiencies. It was found that one of the potentially greatest losses which can occur in a rotary-vane compressor depends on the dimensions chosen for the discharge region of the compression chamber. This loss, which is thermodynamic in nature, arises as a result of overcompression during the discharge stroke.

Overcompression is a term describing the condition wherein the cylinder pressure rises well above the pressure in the discharge line, as the direct result of flow resistance in the discharge system. This rise in pressure is reflected in the performance of the compressor as an undesired increase in the work of compression. Normally, overcompression can be kept within reasonable limits by design control of the discharge-port area, valving, and line size. However, even if these components are designed adequately, severe overcompression can occur during the discharge stroke of the rotary-vane compressor as the result of an essentially "built-in" restriction which depends on the basic geometry chosen for the compressor. For example, tests of experimental rotary-vane compressors showed that, with unfavorable dimensions, the loss from overcompression can amount to as much as 25 per cent of the work of compression under certain operating conditions. Moreover, the higher cylinder pressures associated with overcompression produce undesirable secondary effects such as increased bearing loads, lubrication difficulties, and gas leakage. Although it is not possible to eliminate overcompression completely, the loss can be held to an acceptable value by a proper choice of dimensions. The following development of a design procedure provides a basis for this choice.

Description of the Rotary-Vane Compressor

Fig. 1 shows a plan view of a typical rotary-vane compressor having a circular rotor and cylinder. A two-vaned compressor is illustrated although any number of vanes may be used. Radial slots machined in the cylindrical rotor contain these vanes, which are held against the cylinder by either centrifugal force, oil

[1] The research on which this paper is based was part of a broad fundamental study of rotary-vane refrigeration compressors sponsored by the Whirlpool Corporation, Evansville Division, Evansville, Ind.

Contributed by the Compressor Subcommittee of the Hydraulic Division and presented at the Annual Meeting, Atlantic City, N. J., November 29–December 4, 1959, of The American Society of Mechanical Engineers.

Note: Statements and opinions advanced in papers are to be understood as individual expressions of their authors and not those of the Society. Manuscript received at ASME Headquarters, August 13, 1959. Paper No. 59—A-109.

Nomenclature

A_θ = area of compression chamber, sq in.
A_D = area of compression chamber at beginning of compression, sq in.
A_t = area of throat, sq in.
c = dimensionless constant defined in Equation (4)
d = throat width measured at discharge port, in.
$f(k) = (cR_c^2/A_D)^{1/3}$, dimensionless
$G = \frac{1}{\eta_d}\left(\frac{\omega^2 V_d}{2gKV_D}\right)^{1/3}$, ft^{-1}
k = radius ratio, R_r/R_c
$K = P_d/\rho_d$, ft-lb/lb
l = cylinder length, in.
P = pressure (P_d, discharge), psi
R_c = cylinder radius, in.
R_r = rotor radius, in.
t = time measured from beginning of discharge (t_d, time required for discharge), sec
v_t = velocity of gas in throat, fps
V_θ = volume of compression chamber (V_D, displacement; V_d, at beginning of discharge), cu in.
W_θ = weight of gas in compression chamber, lb
$x = \frac{c[V_D/(A_D/R_c^2)]\omega^2(t_d - t)}{\eta_d/2g\overline{K}A_t}$ (x_d = $x_{t=0} = Gf(k)V_D/A_t$), dimensionless
$y = P/P_d$; y_m = maximum P/P_d
α_p = discharge-port position measured clockwise from axial seal, deg
η_d = coefficient of discharge of throat
θ = angular vane position measured counterclockwise from axial seal, deg (θ_d = vane position at beginning of discharge)
ρ = specific weight, pcf
ω = angular velocity of rotor, radians per sec

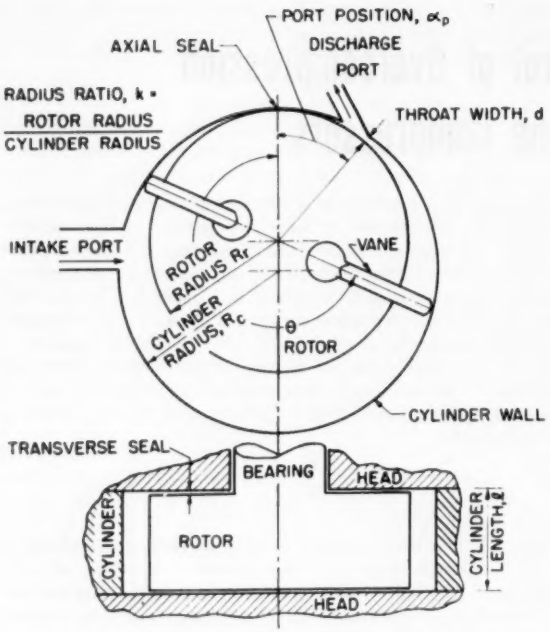

Fig. 1 Basic design dimensions of a rotary-vane compressor

pressure, springs, or a combination of these forces in order to seal the compressor compartmentally. Axial and transverse sealing between the high and low-pressure sides of the compressor usually is accomplished by maintaining small clearances at the interfaces of the cylinder and rotor surfaces. The eccentricity of the cylinder wall with respect to the rotor center causes the volume enclosed between any two vanes to vary from a maximum to a minimum value during each revolution of the rotor. Thus, with proper location of the intake and discharge ports, the rotor-vane-cylinder combination acts as a positive-displacement compressor. The intake ports are normally terminated at an angular vane position for which the volume enclosed between the vanes is a maximum. For the two-vaned compressor of Fig. 1, this maximum volume occurs at a vane position 90 deg from the axial seal. The compression process begins as a vane passes the intake port and continues until discharge pressure is reached at a vane position, $\theta = \theta_d$, which depends on the operating pressure ratio. The discharge valve, usually of the pressure-actuated type, then opens and the gas is displaced from the compression chamber. The discharge port angle α_p usually is made as small as possible so that the volume of gas trapped between the discharge port and axial seal is small. The trapped gas either must be forced through the axial seal into the intake side of the compressor, thereby reducing the volumetric efficiency, or it must re-expand past the vane into the following compression chamber with a resulting increase in the work of compression. In either event, the effect is undesirable.

Geometric Dependence of Overcompression

From the standpoint of efficient discharge of the gas, it would be preferred that the cross-sectional area of the compression chamber remain constant throughout the discharge period. This would permit the compressed gas to be displaced from the cylinder at a uniform velocity, hence, with little increase in pressure. Unfortunately, such a configuration is impractical from the standpoints of vane travel and sealing between the high and low-pressure sides of the compressor as well as from that of manufacturing economy. To achieve proper vane travel and sealing, a design with a circular cylinder wall such as that shown in Fig. 1 is required, and this necessitates a continually decreasing cross section of the compression chamber.

Owing to the convergence of the cylinder walls, the minimum cross section through which the gas must flow in the compression chamber occurs at the port position α_p. This cross section is referred to as the compressor throat and has an area equal to the product of the cylinder length l and the throat width d measured at α_p. Thus, in a practical design, the gas velocity at the throat must be greater than that prescribed for an ideal design in order to maintain a discharge flow consistent with the rate of decrease of volume of the compression chamber. This greater velocity can be obtained only at the expense of overcompression.

The magnitude of the overcompression and the attendant thermodynamic loss depend on the choice of cylinder length, rotor and cylinder radius, and port position since these dimensions determine the throat area. Also, overcompression is to some degree a function of the type of gas being compressed and of the compression ratio. In order to develop a design method for controlling this loss, it is necessary first to establish the interrelation of overcompression and these parameters.

Equation of State During Discharge. If it is assumed that discharge occurs at constant temperature and that perfect-gas laws are applicable, the discharge process may be represented by:

$$PV_\theta = W_\theta K, \tag{1}$$

where V_θ is the volume of the compression chamber at a particular time or vane position during discharge, and W_θ is the weight of gas remaining in this volume. W_θ, as well as V_θ, is a variable since gas is flowing from the compression chamber during discharge. The constant K is the product of the gas constant and the absolute discharge temperature. As shown later, by comparison with experimental results, Equation (1) describes with good approximation the discharge process and consequently permits a considerable simplification of the following derivation.

Relation of Pressure to Time During Discharge. Since V_θ and W_θ are functions of the common variable time or vane position, Equation (1) implicitly relates the pressure P at any instant during discharge to time or vane position. The variables V_θ and W_θ can be most conveniently expressed as a function of time.

The volume of the compression chamber of the rotary compressor at any vane position can be expressed as

$$V_\theta = lR_c^2(A_\theta/R_c^2), \tag{2}$$

where A_θ is the area of the compression chamber enclosed between two consecutive vanes or, for $\theta > 180$ deg, the vane and axial seal. Equation (2) is used to define the displacement as

$$V_D = lR_c^2(A_D/R_c^2), \tag{3}$$

where A_θ is replaced by A_D, the area of the compression chamber just at the beginning of the compression process. It is useful for generalizing the final results to retain the ratios A_D/R_c^2 and A_θ/R_c^2 in the derivation since they are constant for a given ratio of rotor radius to cylinder radius, k, and vane position. It has been found that A_θ/R_c^2 is approximately a parabolic function of time or vane position for $\theta > 180$ deg. Using this parabolic function together with Equations (2) and (3), the volume during discharge can be expressed:

$$V_\theta = c\,\frac{V_D}{A_D/R_c^2}\,\omega^2(t_d - t)^2 \qquad 180 \text{ deg} < \theta_d \leq 360 \text{ deg} \tag{4}$$

where c is constant for each k, t_d is the time interval from the beginning of discharge to $V = 0$, ω is the angular velocity, and t is time measured such that $t = 0$ at the beginning of discharge.

Fig. 2 shows exact values of the cyclic variation of the ratio

A_θ/R_c^2 at different radius ratios for a single-vaned compressor. These curves were plotted from computations made at Battelle with a digital computer. The approximation used in Equation (4) is indicated by the broken lines in Fig. 2. Knowing the intake-port position and the angular separation of the vanes, A_D/R_c^2 can be found from Fig. 2 for compressors having any number of vanes. Empirical values of the constant c in Equation (4) for the radius ratios shown in Fig. 2 are:

Radius ratio, k	Constant, c
0.75	0.112
0.80	0.088
0.85	0.063
0.90	0.041
0.95	0.020

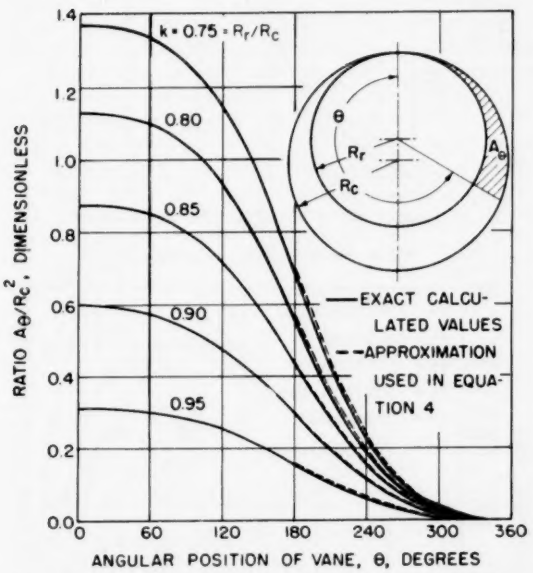

Fig. 2 Cyclic variation of A_θ/R_c^2 at various values of radius ratio

The small reduction in area due to vane thickness is not included in Fig. 2.

The weight of gas remaining in the compression chamber at any volume after the beginning of discharge is the total weight of gas delivered per stroke minus the amount of gas that has been discharged, or

$$W_\theta = W_i - \int_0^t \rho v_t A_t \, dt, \tag{5}$$

where W_i is the total weight of gas delivered per stroke, ρ is the specific weight of the gas in the compression chamber, v_t the gas velocity in the throat, and A_t the throat area. In Fig. 1 the throat section of the compression chamber is seen to be quite similar to a convergent nozzle. Thus, treating the flow as incompressible, the throat velocity at any instant during discharge can be approximated by

$$v_t = \eta_d \left[\frac{2g(P - P_d)}{\rho}\right]^{1/2}, \tag{6}$$

where η_d is the coefficient of discharge for the throat. Introducing Equations (4) through (6) into Equation (1) and replacing the specific weight ρ by P/K reduces the variables to P and t resulting in

$$c\,\frac{V_D}{A_D/R_c^2}\,\omega^2 P(t_d - t)^2 = K\left\{W_i - \frac{\eta_d\sqrt{2g}\,A_t}{\sqrt{K}}\int_0^t [P(P - P_d)]^{1/2} dt\right\} \tag{7}$$

Now, differentiating both sides of Equation (7) with respect to time and rearranging gives

$$\frac{dP}{dt} = \frac{2P}{(t_d - t)} - \frac{\eta_d(2gK)^{1/2}A_t[P(P - P_d)]^{1/2}}{c[V_D/(A_D/R_c^2)]\omega^2(t_d - t)^2} \tag{8}$$

The solution of this equation produces the desired relation of pressure to time; thus, it is possible to plot either P versus θ or P versus V for the discharge process.

Equation (8) is a nonlinear differential equation and, as yet, its general solution has not been found. However, a transformation of variables reduces the equation to a form such that a limited number of numerical solutions covers all possible combinations of k, A_t, and operating conditions. For this transformation, let

$$x = \frac{c[V_D/(A_D/R_c^2)]\omega^2(t_d - t)}{\eta_d(2gK)^{1/2}A_t} \quad \text{and} \quad y = P/P_d \tag{9}$$

Introducing the new variables x and y reduces Equation (8) to

$$\frac{dy}{dx} = \frac{[y(y - 1)]^{1/2}}{x^2} - \frac{2y}{x} \tag{10}$$

The minimum value of y is 1 and occurs at the beginning of discharge when $P = P_d$. The value of x at $y = 1$ is denoted by x_d and may take on any value greater than 0. The numerical solutions are made by assigning increasing values to x_d until the maximum value of y becomes excessive, say 2.5. A y-value of 2.5 represents a pressure rise due to throat restrictions of $2^1/_2$ times the discharge pressure.

Fig. 3 shows the numerical solutions of Equation (10) for values of x_d of 0.25, 0.388, 0.50, 0.75, and 1.0. An additional calculation for x_d of 1.5 was made and resulted in a maximum y

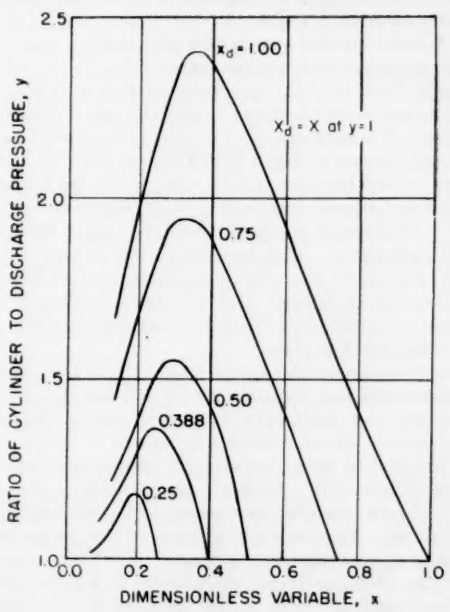

Fig. 3 Solution of $dy = \left\{\frac{[y(y-1)]^{1/2}}{x^2} - \frac{2y}{x^2}\right\} dx$

of 3.55. The solution results in a particular overcompression represented by the ratio y for each distinct value of x_d.

Fig. 4 shows the maximum value of y corresponding to each value of x_d as obtained from Fig. 3. Using Equation (4) and Equation (9), x_d can be written:

$$x_d = Gf(k)V_D/A_t, \tag{11}$$

where

$$G = \frac{1}{\eta_d}\left(\frac{\omega^2 V_d}{2gKV_D}\right)^{1/2}$$

is a constant for each operating condition and type of gas, and

$$f(k) = \left(\frac{cR_e^2}{A_D}\right)^{1/2}$$

Equation (11) links the result shown in Fig. 4 to the pertinent design parameters of the rotary compressor. However, before attempting a specific design application, it is of interest to compare the solution of Equation (10) with experimental measurements of overcompression.

Comparison of Theoretical and Experimental Discharge Processes. One of the widest areas of application for the rotary-vane compressor is for refrigeration. The rotary-vane compressor is ideally suited to meet the practical refrigeration requirements of low noise level and compactness. On the other hand, the operating conditions associated with refrigeration service generally lead to comparatively large values for G in Equation (11), indicating a potential for severe overcompression and, consequently, low efficiency. In order to determine the actual loss of overcompression in rotary compressors designed for use in both refrigeration and air conditioning, several experimental units were instrumented to permit a study of the discharge stroke. Refrigerant 12 was used in this work. The following results are for one of these compressors in the range of capacity of one to two tons of refrigeration which had a V_D/A_t ratio of 79 in. and a radius ratio of approximately 0.85. Data for typical air-conditioning evaporator and condenser temperatures of 45 and 115 F, respectively, are given in Fig. 5.

Fig. 5 shows the discharge portion of pressure-volume curves obtained experimentally, and the same result obtained from the solution of Equation (10), for several compressor speeds. The theoretical curves are based on a unity coefficient of discharge for the throat. The additional work due to overcompression for the experimental curves of Fig. 5 is 13.3 per cent at 1700 rpm and increases to 27.8 per cent at 3200 rpm. Since the mechanical efficiency of the rotary compressor is high, this overcompression results in numerically about the same percentage reduction in over-all performance. Thus, it is unlikely that a compressor with a V_D/A_t ratio of 79 in. would be satisfactory for application at these operating conditions. However, the wide range of overcompression covered by the data for this compressor is of value for checking Equation (10).

The comparatively close agreement in form and magnitude of the experimental and theoretical curves indicates that Equation (10) is of sufficient exactness for design application. The discrepancies which do appear between the two sets of curves can be traced in large part to the nature of the assumptions made in developing Equation (10). Certainly, the assumptions of constant K and isothermal discharge become less exact as the range of pressure increases. Thus, as would be expected, the curves become less similar as overcompression increases. Further, it is assumed tacitly that discharge begins instantaneously whereas actually there is a small increment of time required for the discharge valve to open and for full flow conditions to develop in the throat. This time lag possibly accounts for the calculated peak pressure

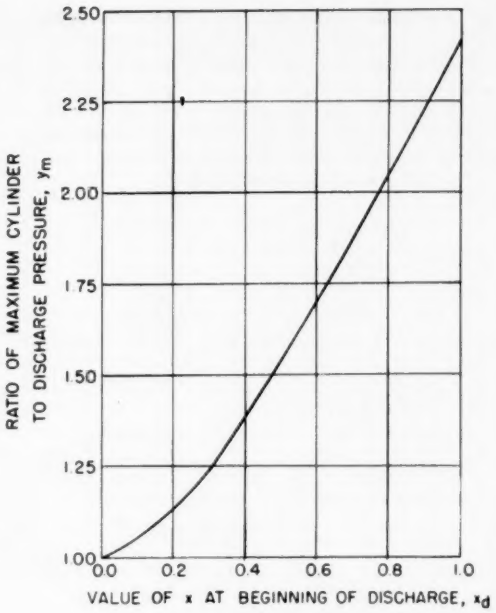

Fig. 4 Maximum value of y versus x_d

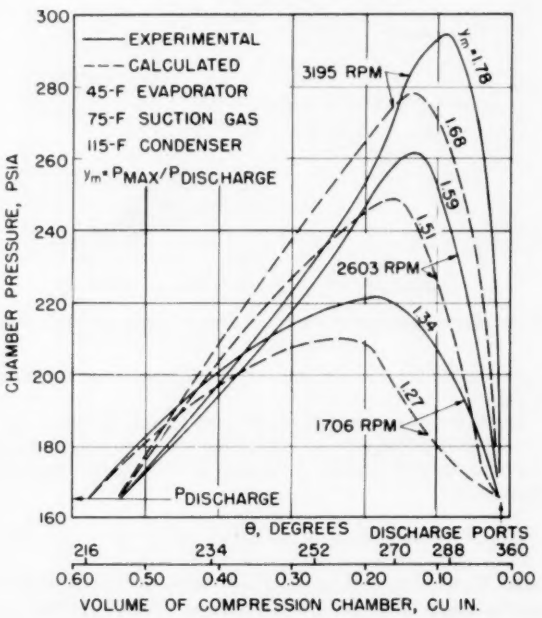

Fig. 5 Pressure during discharge for experimental compressor

occurring at an earlier angular position than the measured value. Taking an opposite point of view, experimental inaccuracy of the pressure-volume diagram also may be responsible for some part of the differences between the curves.

A number of compressors, each with different throat areas, have been studied over a range of operating conditions. The measured peak pressures were consistently higher than those calculated from Equation (10), indicating that a coefficient of discharge somewhat less than unity should be used for the throat. For example, using $\eta_d = 0.89$ rather than unity in the calculations

for Fig. 5 brings the experimental and calculated peak pressures into agreement. However, pressure losses resulting from restrictions in the discharge ports, valves, or the discharge line also contribute to the experimentally measured overcompression. Inasmuch as it was not possible to separate the pressure losses occurring in these components of the discharge system from those occurring in the throat, the coefficient of discharge for the throat section has not been determined. It would seem on this basis that a value somewhat higher than the value 0.89 indicated by Fig. 5 would be more realistic.

Design Application

The objective in the design application of the solution of Equation (12) is to determine a compressor geometry such that overcompression resulting from throat restrictions is reduced to a practical minimum. The procedure begins by choosing trial values of overcompression and radius ratio. These trial values together with the required displacement, speed, and operating conditions for the intended application are then used to calculate the throat area from Equation (11). The throat area is related to compressor geometry as follows.

Fig. 6 shows the radial dimension d between the rotor and cylinder wall expressed as a dimensionless ratio d/R_c for throat

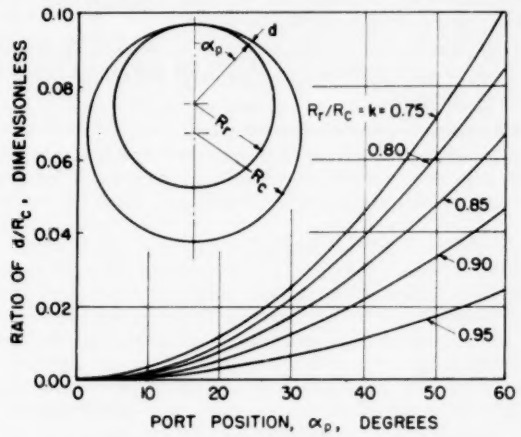

Fig. 6 Variation of ratio d/R_c with port position

positions from 0 to 60 deg. At each angular position, the throat area is the product of this ratio, the cylinder length, and the cylinder radius, or

$$A_t = lR_c(d/R_c) \tag{12}$$

The cylinder dimensions corresponding to a particular throat area and trial port position are found by solving Equation (12) simultaneously with Equation (3). Finally, the rotor radius is calculated by taking the product of the radius ratio and cylinder radius. If these dimensions are compatible with other design considerations, the basic design may be considered complete. If not, or if it appears that the loss due to overcompression can be reduced still further, new values can be selected for A_t, k, or α_p. It should be pointed out that, for practical geometries, the radius ratio k should in general be between 0.75 and 0.95. Small values of k lead to excessive vane extensions whereas large k-values require the cylinder to be disproportionately long. Also, as mentioned earlier, it is desirable to make α_p as small as possible in order to minimize the volume between the discharge ports and the axial seal.

Suppose that it is required to design a two-vane rotary compressor having a refrigeration capacity of one ton at a speed of 1750 rpm. Overcompression is to be limited to correspond to a y-value of 1.17. This is approximately one half of the overcompression represented by the y-value shown for the 1700-rpm experimental compressor in Fig. 6. At the same operating conditions used in the experiments, the refrigerant flow must be about 244 lb/hr or 1.145×10^{-3} lb/stroke to produce one ton of refrigeration. Assume that the gas enters the compression chamber with 30 deg F superheat and no pressure loss in the suction passage and that the discharge pressure is 4 psi above condenser pressure or 165 psia. For an estimated volumetric efficiency of 90 per cent, the displacement must be

$$V_D = \frac{1.145 \times 10^{-3}\ \text{lb/stk}}{1.292\ \text{lb/ft}^3} \times \frac{1728\ \text{in}^3/\text{ft}^3}{0.90} = 1.70\ \text{in}^3/\text{stroke}$$

where 1.292 lb/ft^3 is the density of Refrigerant 12 at the suction pressure (56 psia) and temperature (75 F).

Since heat transfer as a rule is low in the rotary compressor, the actual compression process up to the beginning of discharge is idealized to an isentropic process for this design example. For isentropic compression, the density at the beginning of discharge is 3.57 lb/ft^3 for these operating conditions. Then,

$$V_d/V_D = \frac{1.145 \times 10^{-3}\ \text{lb/stk} \times 1728\ \text{in}^3/\text{ft}^3}{1.70\ \text{in}^3/\text{stk} \times 3.57\ \text{lb/ft}^3} = 0.326$$

and

$$K = P_d/\rho_d = 165 \times 144\ \text{lb/ft}^2/3.57\ \text{lb/ft}^3 = 6650\ \text{ft}$$

from which the constant G in Equation (11) is

$$G = 183\ \text{rad/sec} \left(\frac{0.326}{2g \times 6650\ \text{ft}}\right)^{1/2} = 0.159\ \text{rad/ft}$$

For a trial $k = 0.85$, $f(k)$ is 0.304, and, from Fig. 4, x_d corresponding to $y = 1.17$ is 0.242. Substituting V_D, G, $f(k)$, and x_d into Equation (11), the required throat area is 0.0282 sq in. For a trial port position of $\alpha_p = 30$ deg, l and R_c are found to be 1.15 and 1.42 in., respectively, from Equations (12) and (3). The rotor radius is kR_c or 1.20 in. As suggested earlier, these dimensions can be adjusted to conform with other design requirements by selecting different trial values.

If a compressor built to the dimensions just found were doubled in capacity by operating it at 3500 rpm instead of 1750 rpm, x_d would approximately double giving a maximum cylinder pressure of 250 psia. Therefore, the dimensions should be altered to obtain a more acceptable throat area. If this is done using the same trial values for k, α_p, and overcompression loss as in the 1750 rpm example, the resulting cylinder length is 4.65 in. It has been found that leakage and friction losses in the rotary compressor increase rapidly with cylinder length so that the improved thermodynamic efficiency obtained with a 4.65-in. cylinder length may be offset by reductions in volumetric and mechanical efficiencies. However, the cylinder length may be reduced to obtain a more favorable over-all performance by increasing either or both the throat position and number of vanes. For example, using a throat position of 34 deg, and 3 vanes, gives a 3500-rpm design with the same R_r, R_c, l, and overcompression loss as the 1750-rpm unit

It is also of interest to consider the effect that compression ratio and the type of gas have on overcompression. At compression ratios of 6 or 7, encountered in refrigeration service, the loss of overcompression is only about half of that at air-conditioning operation for a given compressor. For example, at refrigeration loads, overcompression is 1.09 as opposed to 1.17 for the one-ton air-conditioning compressor designed earlier. Similarly, if this compressor was used to compress air instead of Refrigerant 12 over the same pressure range used in the air-conditioning example,

the maximum cylinder pressure would then be only 1.05 times the discharge pressure. Therefore, in either of these cases, the loss of overcompression would probably be of less importance to the over-all design than for an air-conditioning application.

Conclusion

The full advantage of the inherently high volumetric efficiency, balanced design, and compactness of the rotary compressor is best realized in applications involving low compression ratios and high rotational speeds. As shown by Equation (11) and the preceding examples, these are precisely the conditions which can lead to severe losses due to overcompression. This analysis provides an effective technique for quantitatively defining and controlling this loss through the proper selection of compressor dimensions.

Acknowledgment

The authors are particularly indebted to J. A. Eibling of Battelle Memorial Institute for his interest and assistance. Appreciation is extended to H. G. Semler and H. E. Lehmkuhl of the Whirlpool Corporation for their comments and valuable suggestions throughout the work.

DISCUSSION

C. E. Boettcher[2]

The paper provides an interesting approach for the designer. As has been demonstrated through years of service a very efficient and reliable compressor can be designed, and, of course, low overcompression is one of the factors which should not be overlooked. Several factors supplementary to the paper should be kept in mind when the engineer considers overcompression.

Basic dimensions of rotor head and cylinder which result in minimum losses due to overcompression are also favorable to other important criteria of design such as mechanical losses, bearing loading, and transverse sealing. In addition, experience has shown some latitude is available in the selection of discharge port angles, described as α_p. Although this should be small in order to minimize the volume between discharge ports and axial seal, as stated by the authors, the angle may be made to favor less overcompression without an appreciable loss in performance of the compressor.

H. F. Lehmkuhl[3]

In practice, it is found that the analysis presented here can be used to predict optimum compressor dimensions provided, however, that other equally important criteria are satisfied at the same time.

The preferred choice of dimensions is more appropriately defined when the "throat area criterion" is used in conjunction with the concepts for minimum friction; allowable rotor and shaft deflections; requirements for internal hydrodynamic film sealing; and bearing design requirements.

Compressors where the design is based on effective application of these concepts perform very dependably and exhibit excellent over-all efficiency.

[2] Whirlpool Corporation, Evansville, Ind.

[3] Whirlpool Corporation, Evansville, Ind.

Operation of Steam Turbines to Minimize Shell Cracking[1]

S. B. COULTER
R. L. JACKSON
Large Steam Turbine-Generator Department, General Electric Company, Schenectady, N. Y. Mem. ASME

Some methods for reducing the tendencies toward cracking in steam-turbine shells are described. Involved are improved operating procedures, application of accessories, and improved mechanical design, all of which aid in properly controlling shell thermal distribution.

An earlier paper [1][2] discussed the relations between temperature changes, temperature difference, and thermal stresses in large-steam-turbine shells, and the changes in temperatures measured during start-ups. The objective was to correlate all these factors with the cracking of turbine shells.

Analysis of the inspection records of over 800 turbines shipped by the authors' company in the last 20 years shows that there is a definite relationship between the type of service operation and shell cracking. The highest incidence of cracking occurs where frequent starting and loading cycles are encountered without development of proper procedures to minimize thermal stresses. There also is evidence that turbines with higher steam conditions are more susceptible to cracking due to their heavier metal sections. With the trend toward more frequent starting and loading cycles and higher pressure and temperature turbines being delegated to this type of cyclical service, the development of procedures and devices to minimize cracking has become imperative.

Procedures for reducing turbine-shell cracking to be described include those for turbines yet to be built and those for units already in service. Generally, the only means available for the latter are improved operating procedures and the application of accessories to control shell-temperature differentials.

Although cracking is caused by the thermal cycling of the unit, the prevalence of cracking is most closely related to the unit operating temperature. Very little cracking has occurred for units rated 600 F and below; a progressively higher incidence of cracking has been occurring at operating temperatures above 600 F.

There does not appear to be any very definite difference in the resistance to cracking of any of the various ferritic-shell materials used to date. Differences in mechanical design have been of less importance than the type of operation and control of steam temperature. However, records do indicate that 360-deg admission, and provisions for flexibility to accommodate differential expansions, are definitely beneficial. One very successful design, used up to the present time on the smaller rated turbines and now being extended to the larger rated units, has the cast-nozzle port passages so arranged as to be free of the main bulk of the horizontal joint.

Crack Locations

The most serious cracking generally occurs in the high-temperature, asymmetrical portion of the turbine inlet (thick flange or wall sections attached to thin sections), primarily in the bridges separating the various control-valve passages, and also in the first-stage nozzle fit, including cracks into a main-flange-bolt hole, Figs. 1, 2, and 3. The great majority of serious cracks occur in the two locations. Some infrequent cracking has occurred in nearly every portion of the shell, usually associated with casting defects. Because the severe cracking occurs in or ahead of the first-stage shell area, and is somewhat greater around the No. 1 control-valve passage, it seems quite certain that the major cause of the cracking is due to the rapid and nonuniform thermal changes to which the shells have been subjected. The severity of

Fig. 1 Crack in bridge separating first-stage bowl passages in turbine high-pressure shell

[1] When this paper was written, the authors included information and expressed opinions believed to be correct and reliable. Because of the constant advance of technical knowledge, the widely differing conditions of possible specific application, and the possibility of misapplication, any application of the contents of this paper must be at the sole discretion and responsibility of the user.

[2] Numbers in brackets designate References at end of paper.

Contributed by the Power Division of The American Society of Mechanical Engineers and presented at the AIEE-ASME National Power Conference, Kansas City, Mo., September 27–30, 1959.

Note: Statements and opinions advanced in papers are to be understood as individual expressions of their authors and not those of the Society. Manuscript received at ASME Headquarters, September 11, 1959. Paper No. 59—Pwr-10.

Fig. 2 Cracks in first-stage nozzle fit including that through flange into bolt hole in turbine high-pressure shell

cracking varies widely, being largely dependent upon the rated temperature of the unit and the operating conditions to which it is subjected.

Shell-Temperature Distribution

An intensive investigation by the authors' company of operating-shell temperatures, particularly the temperature distribution occurring during the transient conditions of starting and loading cycles, has required the development of reliable and precise means of temperature measurement for inner-metal surfaces of turbine high-pressure shells. Some data have been published and the importance of obtaining desirable steam-temperature control has been described [1]. Two curves depicting these data are reproduced from that reference, Figs. 4 and 5, which show typical conditions occurring during the starting of a warm turbine after an overnight, or about 8-hr, shutdown, and also during the starting of a cool turbine after about a 4-day shutdown.

Fig. 4 shows that a large temperature difference results between the inner and outer surfaces of the No. 1 valve bowl, as well as between the inner surfaces of both the No. 1 and No. 2 valve bowls during the rolling period. This occurred during a cooling cycle which was subsequently followed by a rather rapid heating cycle after synchronizing. During the heating cycle somewhat smaller, but rapid, temperature changes occurred in the opposite direction. The data of Fig. 4 have now been revised to show the temperature of the No. 2 valve bowl.

Different conditions prevailed for the starting cycle illustrated by Fig. 5. Little thermal change occurred during the rolling period, but later during loading an extremely large temperature difference resulted between the inner surfaces of both the No. 1 and No. 2 valve bowls. The data of Fig. 5, previously published, were obtained on a 50,000-kw 3600-rpm, 1250-psig, 950-F unit, but it exhibits a striking similarity to that obtained on a unit of quite different design, Fig. 6.

Fig. 6 shows data for an 80,000-kw, 1800-rpm, 850-psig, 900-F machine, operated from a main-steam header, after a 30-hr shutdown. For both Figs. 5 and 6 a cool turbine was started with hot steam; for Fig. 4 a warm turbine was started with cool steam. These two types of starting and loading cycles have been found to be representative of a great many installations, although the exact characteristics are modified from one to another. Simply defined, the major thermal problem resolves into:

1 Avoidance of quenching during the rolling period followed by rapid heating when starting a hot machine.

2 Avoidance of very rapid heating after synchronizing when starting a cold unit.

In each case, obtaining sufficiently gradual and uniform heating or cooling during the rolling period would be a major benefit.

Thermal Stress and Mechanism of Cracking

Careful investigations of the material in typical cases of shell cracks reveal that, in general, these cracks are due to a form of high-temperature-rupture failure from the accumulation of creep strain over one or more starting and loading cycles. This strain can come either from rapid heating of a cold turbine or from quenching of the bowl passages when starting a hot turbine with relatively cold steam. In starting a cold turbine, the surface of the metal exposed to steam flow may be heated rapidly going into compression beyond the elastic limit. Later, when the main body of metal comes up to temperature, there is a residual-tensile stress which is then gradually reduced by creep. When the total amount of this strain becomes sufficient, a crack results. This depends on both the strain per cycles and number of cycles.

In the case of starting a hot turbine, the quenching action causes the reverse of the above and leaves a compressive prestress to aggravate further the subsequent heating cycle.

Laboratory tests have now been made on low-cycle, strain-fatigue, elevated-temperature apparatus which produced the predominantly integranular cracking of the type found in one of the first shells to be replaced due to cracking.

By determining the type of temperature distribution most prevalent in shell walls, and knowing the operating-temperature range and material properties, a limit of temperature difference may be selected. The examination of temperature data obtained by measurements during typical starting and loading cycles, including those of Figs. 4, 5, and 6, demonstrates that very large temperature differences—as great as 410 F between the inner surfaces of the No. 1 and No. 2 valve bowls, Fig. 6—may occur unless specific means are employed for their prevention. Such very large thermal differences will produce plastic strain, and they are an index of the high stresses which can occur across various shell walls separating the bowl passages, or which join together various portions of the shell. For this type of turbine the authors' company has selected 150 F as being a desirable limit for temperature differences.

Methods for Reducing Cracking

The control of temperature differences, and thereby thermal stress, can be accomplished by the perfection of operating procedures, or by the use of new or modified equipment, or both. In any case, good operating practices are indispensable. It is evident that efforts must be made to match steam and turbine-metal temperatures to the greatest degree possible. Some equipment modifications are of appreciable aid.

New Units. For new machines, the authors' company employs insert-steam-chest or nozzle-box designs in many cases. The

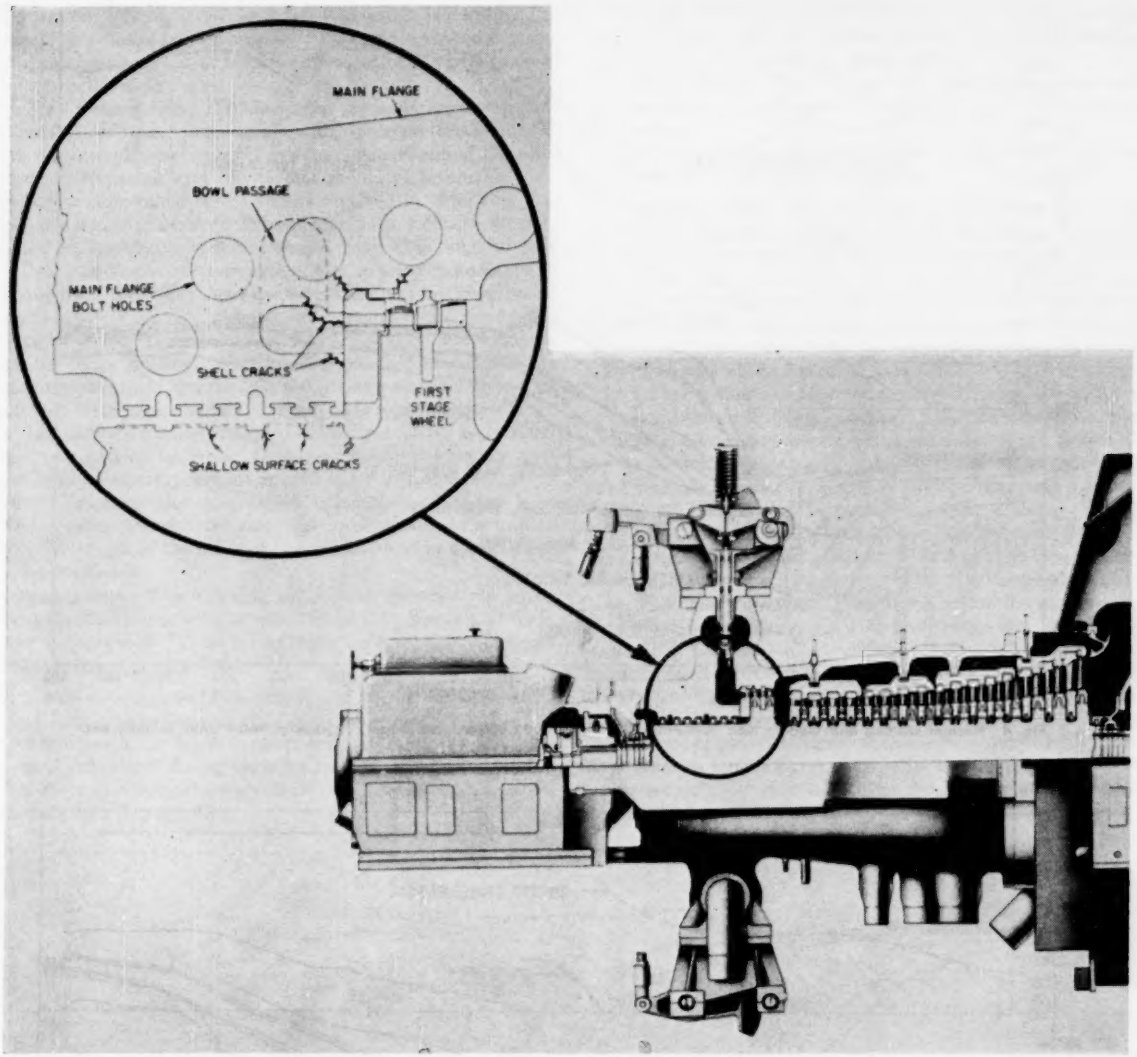

Fig. 3 Inlet region of high-pressure turbine most subject to cracking

salient features of this construction, with respect to the inlet-passage shell components, are:

1 Freedom for thermal expansion in three directions.

2 Use of relatively thin walls which prevent large thermal differences across the walls, and which also provide desirable flexibility and allow necessary deflection.

3 Use of simplified castings for the inlet components, as well as for the inner shell itself, which minimize rapid transitions in wall thickness or contour and reduce stress concentrations.

Each of these features helps minimize excessive thermal stress. The design is made possible by inserting the inlet-passage component into the inner shell and supporting it at its outer end only. The first-stage pressure and temperature completely surround the inserted portion producing small operating-pressure and temperature drops across the component walls.

In the future, all new machines will have a turbine stop-valve bypass which allows starting, synchronizing, and loading to about 20 per cent load with all the control valves wide open but with the mainstop valve closed. The speed and load are controlled by a motor-positioned, oil-operated pilot valve which passes steam through the stop valve. When reaching 20 per cent load all the turbine control valves are closed, except No. 1, which is then nearly wide open. At this time, the main stop valve can be opened and additional load applied in the normal manner. By reaching 20 per cent load on the bypass, it is possible to avoid the large throttling steam-temperature decrease across the No. 1 control valve which otherwise could occur under normal operation while this valve is only partially open. This condition normally would occur while reaching speed, during synchronizing, and at light load.

Further, the unit may be brought to near rated temperature on the bypass as the main steam temperature is increased. The bypass is beneficial because rapid throttling temperature changes are eliminated across the turbine control valves. Flow passes uniformly through all inlet passages, lower average steam velocities and lower rates of heat transfer occur, and a larger mass flow for any given speed and load results. Thus, the bypass equipment allows both gradual and uniform heating of the entire inlet region. Of interest is the belief that use of the stop-valve

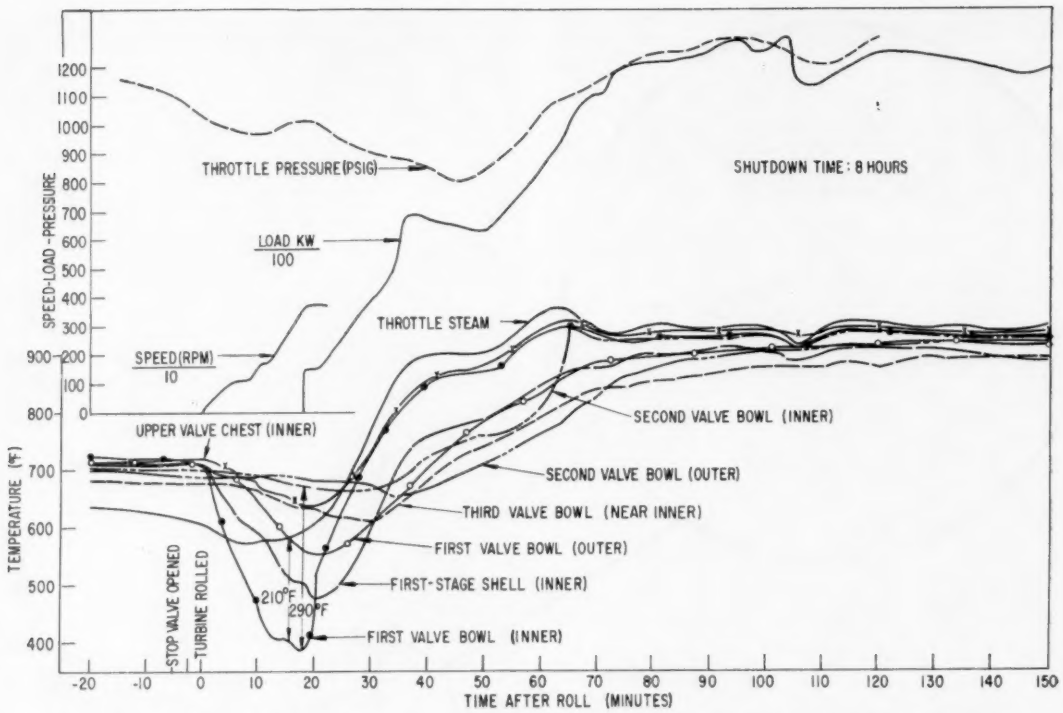

Fig. 4 Normal starting and loading test; September 27, 1954. 132,000-kw, 3600-rpm, 1250-psig, 960-F unit; initially hot.

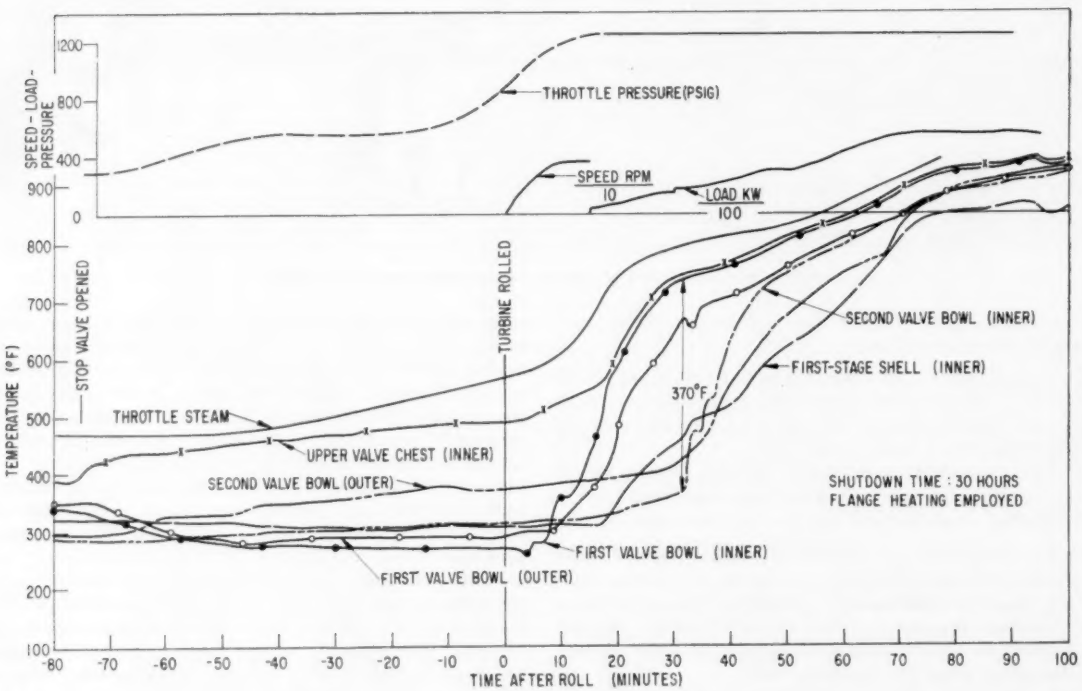

Fig. 5 Normal starting and loading test; November 7, 1955. Flange heating employed. 50,000-kw, 3600-rpm, 1250-psig, 950-F unit; initially cold.

bypass, by lowering velocities in the light-load range, will tend to minimize nozzle-partition erosion. The bypass method of starting and loading is one of the most effective for the prevention of excessive thermal stresses.

Shell materials and manufacturing processes are being continually improved. For example, a high-pressure turbine shell of 12 per cent chrome material has been manufactured recently. Experience gained with this turbine should be invaluable for a better understanding of the factors involved in improving material cracking resistance. Present knowledge indicates that the most crack-resistant materials should have both high rupture ductility and more creep strength. Also, in the recent past, more shells have been fully heat-treated during the latter stages of manufacture in order to obtain better material properties by further removing residual stresses or heat-affected zones due to machining or welding. Greatly expanded furnace facilities are under construction in order that this practice may be followed on all high-temperature shells.

The author's company has also endeavored for the last several years to develop improved turbine-operation procedures, particularly for starting and loading, in order to minimize thermal stress, cracking, and other allied difficulties. This has been accomplished through the co-operation of many steam-turbine owners. Some of the methods will be described in approximate order of efficacy.

Existing Units. The following methods of operation are applicable to machines now in service. Some have been adapted for new units as well. These six methods are first enumerated and then explained in more detail.

1 Stop-valve bypass (Figs. 7, 8, 9, and 10)—all control valves open during the rolling and initial-loading period.

2 Start with low boiler pressure (Figs. 11 and 12)—multiple control valves open during the initial loading period.

3 Start on existing stop-valve pilot (Fig. 13)—all control valves initially open during rolling.

4 Special valve cams for simultaneous control valve opening, (Fig. 14)—No. 1 and No. 2 valves initially open during loading and, under certain conditions, during rolling.

5 Flange heating (Figs. 15 and 16)—flow through passages interconnecting main-flange-bolt holes prior to and during rolling and loading.

6 Drilled holes through shell bridges—small flow through an inactive bowl during rolling and loading.

1 Stop-Valve Bypass. The existing emergency-stop valves for most steam turbines now in service can be modified so that units can be started and loaded to about 20 per cent load with all control valves wide open—similar to the method previously described. This method appears to be the most effective for application to existing units to obtain good temperature control and thereby minimize thermal stress. Data obtained on a small-capacity bypass will be described.

Figs. 7 and 8 illustrate a hot and a cold start, respectively, for a turbine fed from a unit-system boiler. The data were taken on a 60,000-kw, 3600-rpm, 850-psig, 900-F machine. Figs. 9 and 10 are for hot and cold starts, for a 35,000-kw, 3600-rpm, 800-psig, 850-F machine supplied from a header system operating continuously at approximately rated pressure and temperature. For all four tests, the turbine inlet, including the control-valve passages was gradually and uniformly heated. The maximum temperature difference between the inner surfaces of the No. 1 and No. 2 valve bowls for all four tests did not exceed 150 F. For the two tests on the header system this temperature difference did not exceed about 75 F. These thermal differences can be compared to those of Figs. 4, 5, or 6, depicting typical data without improved temperature control, where the corresponding bowl-temperature differences were, respectively, 290, 370, and 410 F.

A measure of the effectiveness of the turbine stop-valve bypass for controlling temperatures of the critical turbine-inlet area is easily seen. It should be noted that the capacity of the bypass flow for the four, Figs. 7, 8, 9, and 10, was limited by the size of

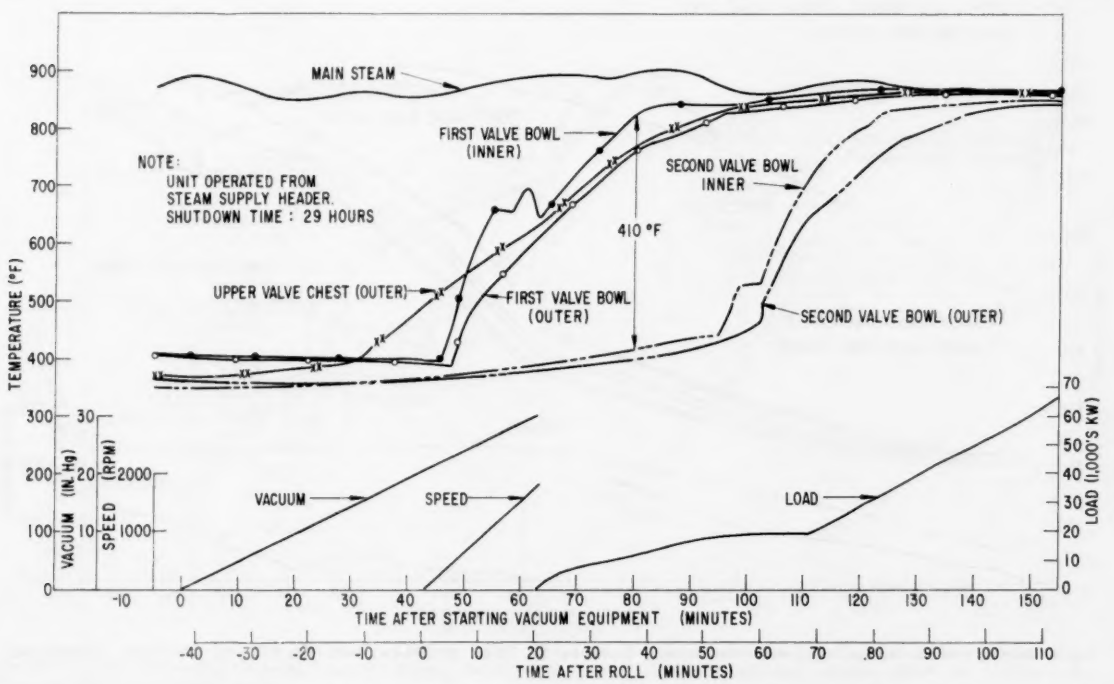

Fig. 6 Normal starting and loading test; March 4, 1957. 80,000-kw, 1800-rpm, 850-psig, 900-F unit; initially cold. Operated from main-steam header.

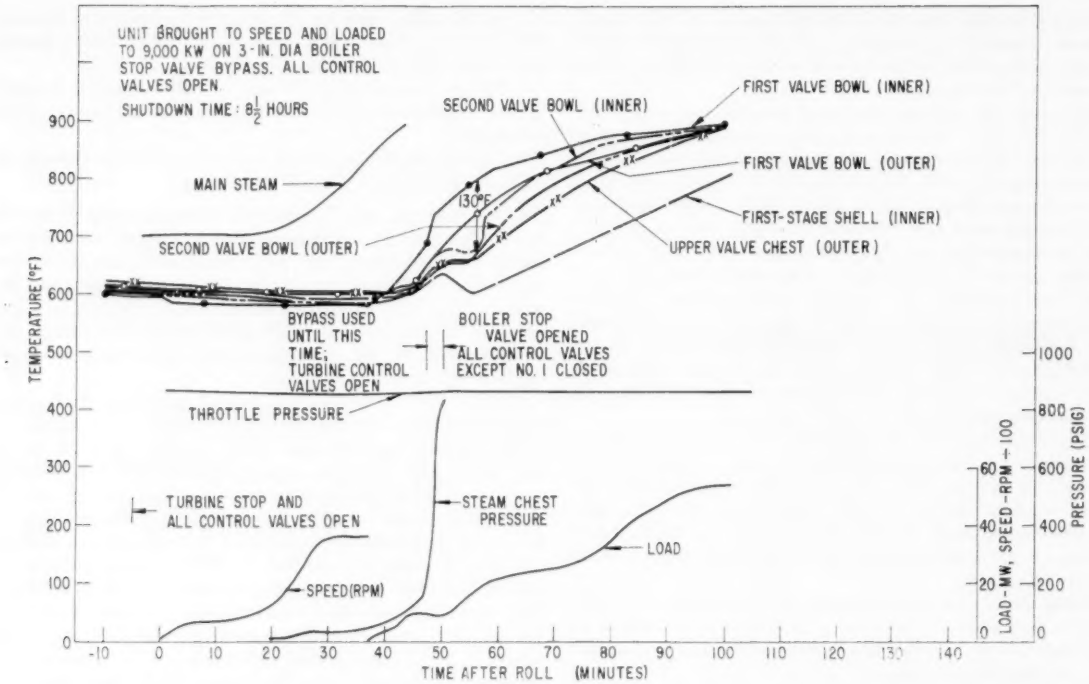
UNIT BROUGHT TO SPEED AND LOADED TO 9,000 KW ON 3-IN. DIA BOILER STOP VALVE BYPASS. ALL CONTROL VALVES OPEN
SHUTDOWN TIME: 8½ HOURS
SECOND VALVE BOWL (INNER)
FIRST VALVE BOWL (INNER)
FIRST VALVE BOWL (OUTER)
MAIN STEAM
130°F
FIRST-STAGE SHELL (INNER)
SECOND VALVE BOWL (OUTER)
UPPER VALVE CHEST (OUTER)
BYPASS USED UNTIL THIS TIME; TURBINE CONTROL VALVES OPEN
BOILER STOP VALVE OPENED ALL CONTROL VALVES EXCEPT NO. 1 CLOSED
THROTTLE PRESSURE
TURBINE STOP AND ALL CONTROL VALVES OPEN
STEAM CHEST PRESSURE
LOAD
SPEED(RPM)
TEMPERATURE (°F)
LOAD - MW, SPEED - RPM ÷ 100
PRESSURE (PSIG)
TIME AFTER ROLL (MINUTES)

Fig. 7 Starting and loading test using stop-valve bypass; May 1, 1957. 60,000-kw, 3600-rpm, 850-psig, 900-F unit; initially hot.

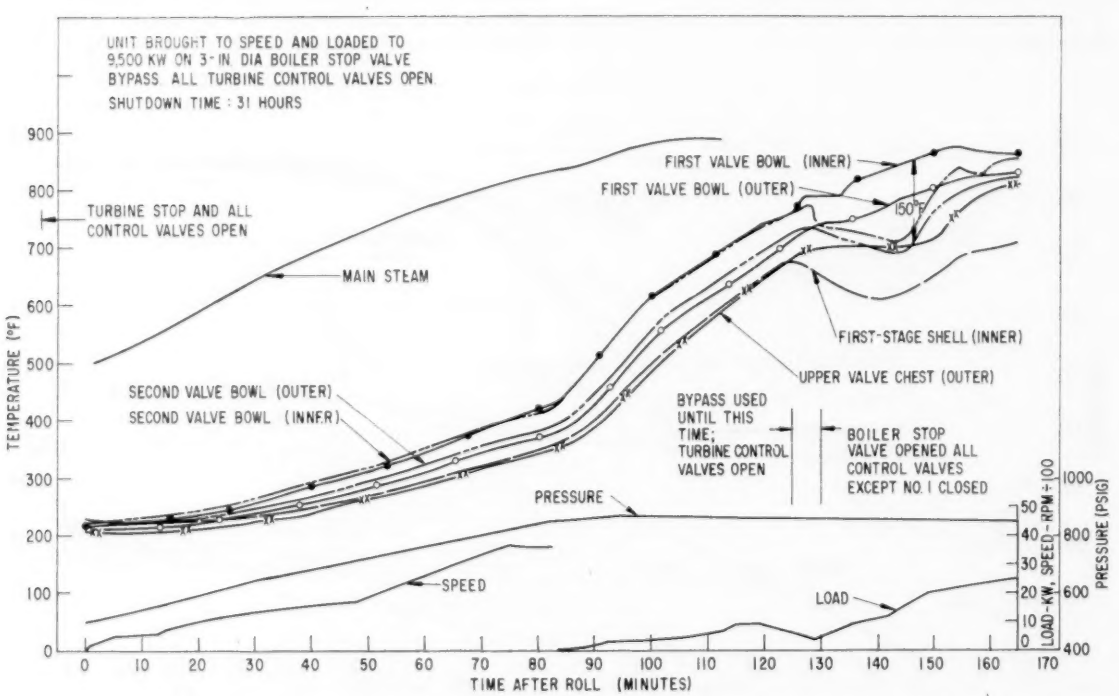
UNIT BROUGHT TO SPEED AND LOADED TO 9,500 KW ON 3-IN. DIA BOILER STOP VALVE BYPASS. ALL TURBINE CONTROL VALVES OPEN
SHUTDOWN TIME: 31 HOURS
FIRST VALVE BOWL (INNER)
FIRST VALVE BOWL (OUTER)
TURBINE STOP AND ALL CONTROL VALVES OPEN
150°F
MAIN STEAM
FIRST-STAGE SHELL (INNER)
UPPER VALVE CHEST (OUTER)
SECOND VALVE BOWL (OUTER)
SECOND VALVE BOWL (INNER)
BYPASS USED UNTIL THIS TIME; TURBINE CONTROL VALVES OPEN
BOILER STOP VALVE OPENED ALL CONTROL VALVES EXCEPT NO. 1 CLOSED
PRESSURE
SPEED
LOAD
TEMPERATURE (°F)
LOAD - KW, SPEED - RPM ÷ 100
PRESSURE (PSIG)
TIME AFTER ROLL (MINUTES)

Fig. 8 Starting and loading test using stop-valve bypass; September 24, 1956. 60,000-kw, 3600-rpm, 850-psig, 900-F unit; initially cold.

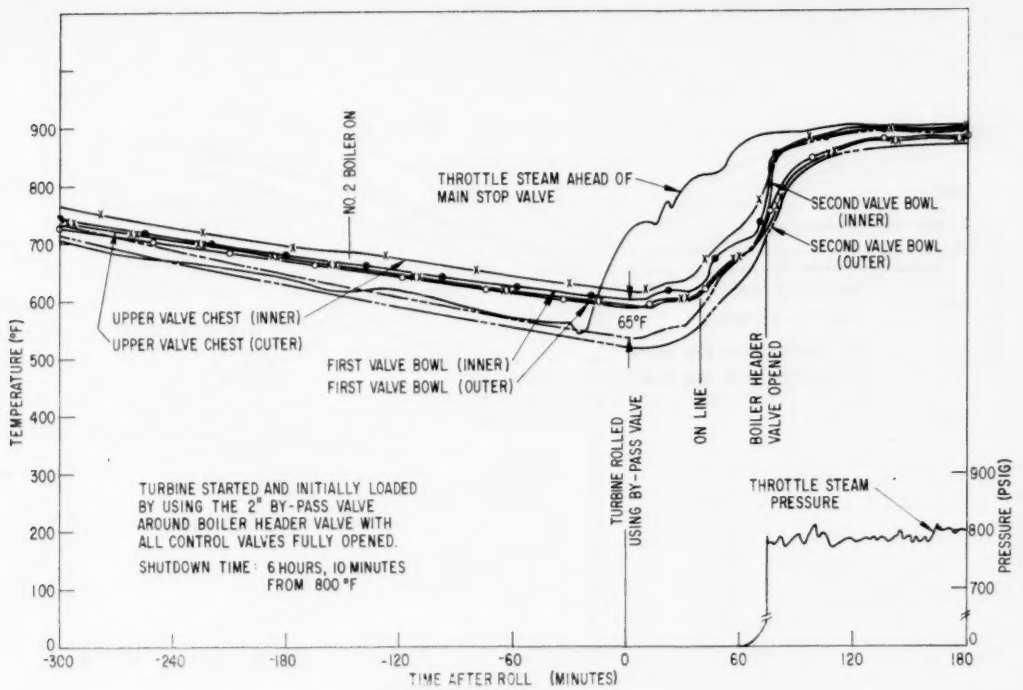
NO. 2 BOILER ON
THROTTLE STEAM AHEAD OF MAIN STOP VALVE
SECOND VALVE BOWL (INNER)
SECOND VALVE BOWL (OUTER)
UPPER VALVE CHEST (INNER)
UPPER VALVE CHEST (OUTER)
65°F
FIRST VALVE BOWL (INNER)
FIRST VALVE BOWL (OUTER)
TURBINE ROLLED USING BY-PASS VALVE
ON LINE
BOILER HEADER VALVE OPENED
THROTTLE STEAM PRESSURE
TURBINE STARTED AND INITIALLY LOADED BY USING THE 2" BY-PASS VALVE AROUND BOILER HEADER VALVE WITH ALL CONTROL VALVES FULLY OPENED.
SHUTDOWN TIME: 6 HOURS, 10 MINUTES FROM 800 °F
TEMPERATURE (°F)
PRESSURE (PSIG)
TIME AFTER ROLL (MINUTES)

Fig. 9 Starting and loading test using stop-valve bypass; December 5, 1957. 35,000-kw, 3600-rpm, 800-psig, 850-F unit; initially hot. Operated from a main-steam header.

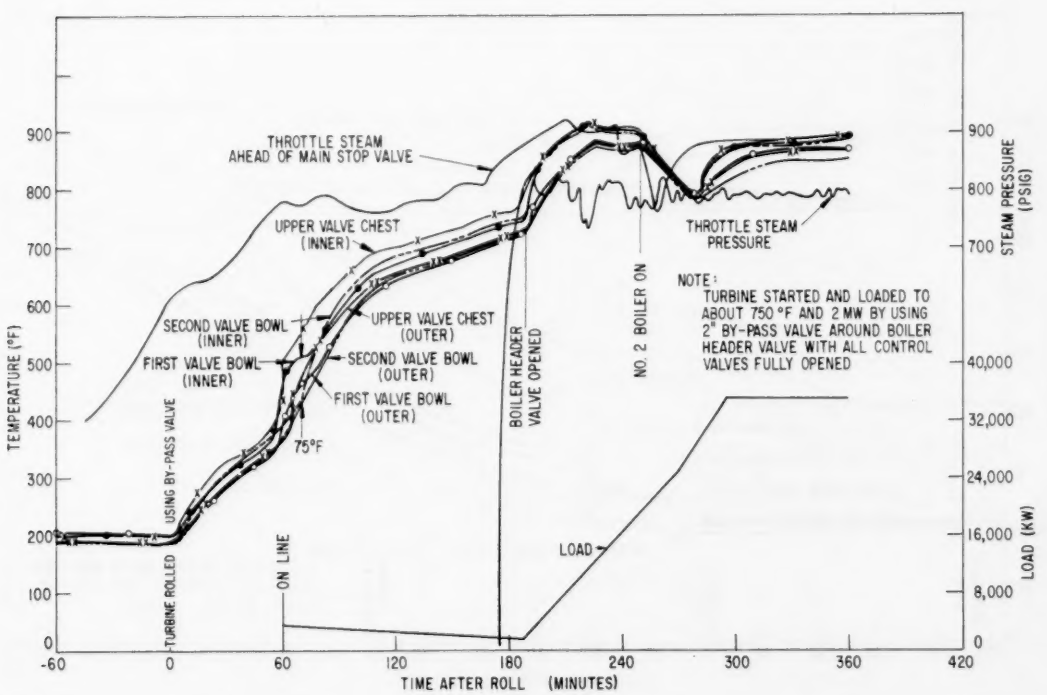
THROTTLE STEAM AHEAD OF MAIN STOP VALVE
UPPER VALVE CHEST (INNER)
THROTTLE STEAM PRESSURE
NOTE: TURBINE STARTED AND LOADED TO ABOUT 750 °F AND 2 MW BY USING 2" BY-PASS VALVE AROUND BOILER HEADER VALVE WITH ALL CONTROL VALVES FULLY OPENED
SECOND VALVE BOWL (INNER)
UPPER VALVE CHEST (OUTER)
FIRST VALVE BOWL (INNER)
SECOND VALVE BOWL (OUTER)
FIRST VALVE BOWL (OUTER)
75°F
NO. 2 BOILER ON
BOILER HEADER VALVE OPENED
TURBINE ROLLED USING BY-PASS VALVE
ON LINE
LOAD
TEMPERATURE (°F)
STEAM PRESSURE (PSIG)
LOAD (KW)
TIME AFTER ROLL (MINUTES)

Fig. 10 Starting and loading test using stop-valve bypass; December 16, 1957. 35,000-kw, 3600-rpm, 800-psig, 850-F unit; initially cold. Operated from a main-steam header.

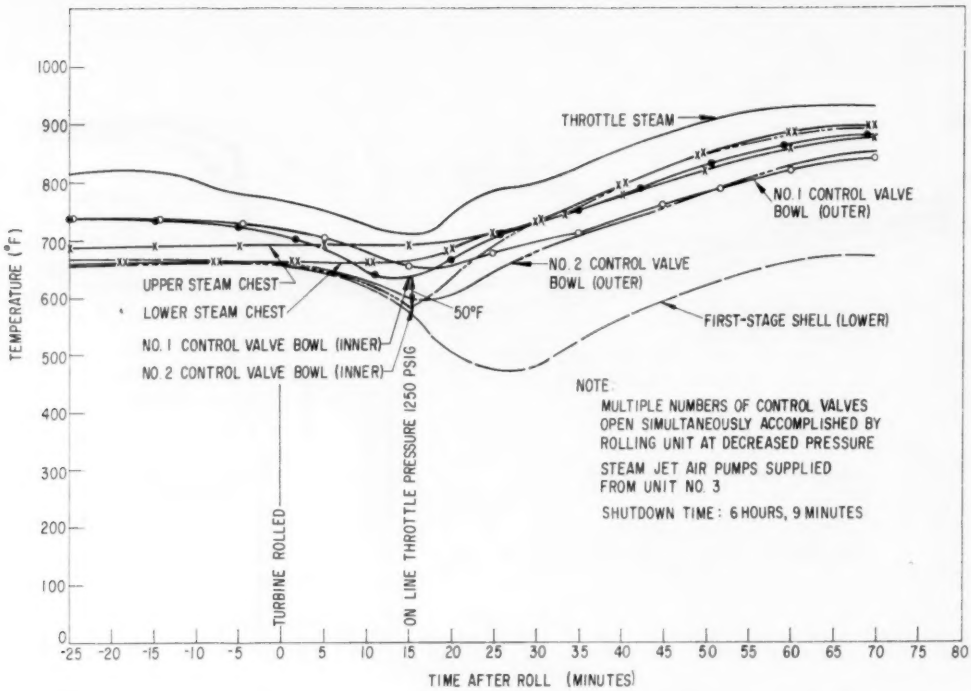
TEMPERATURE (°F)
TIME AFTER ROLL (MINUTES)
THROTTLE STEAM
NO. 1 CONTROL VALVE BOWL (OUTER)
NO. 2 CONTROL VALVE BOWL (OUTER)
UPPER STEAM CHEST
LOWER STEAM CHEST
NO. 1 CONTROL VALVE BOWL (INNER)
NO. 2 CONTROL VALVE BOWL (INNER)
50°F
FIRST-STAGE SHELL (LOWER)
TURBINE ROLLED
ON LINE THROTTLE PRESSURE 1250 PSIG
NOTE:
MULTIPLE NUMBERS OF CONTROL VALVES OPEN SIMULTANEOUSLY ACCOMPLISHED BY ROLLING UNIT AT DECREASED PRESSURE
STEAM JET AIR PUMPS SUPPLIED FROM UNIT NO. 3
SHUTDOWN TIME: 6 HOURS, 9 MINUTES

Fig. 11 Starting and loading test at low boiler pressure; April 3, 1957. 60,000-kw, 3600-rpm, 1250-psig, 950-F unit; initially hot.

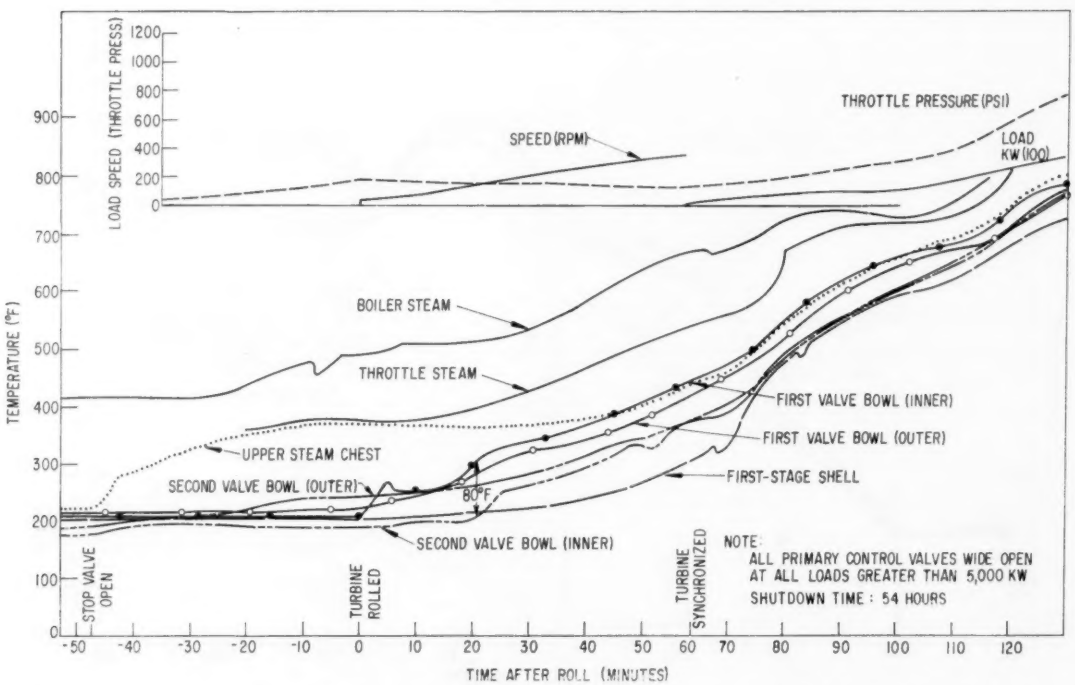

Fig. 12 Starting and loading test at low boiler pressure; March 26, 1957. 60,000-kw, 3600-rpm, 1250-psig, 950-F unit; initially cold.

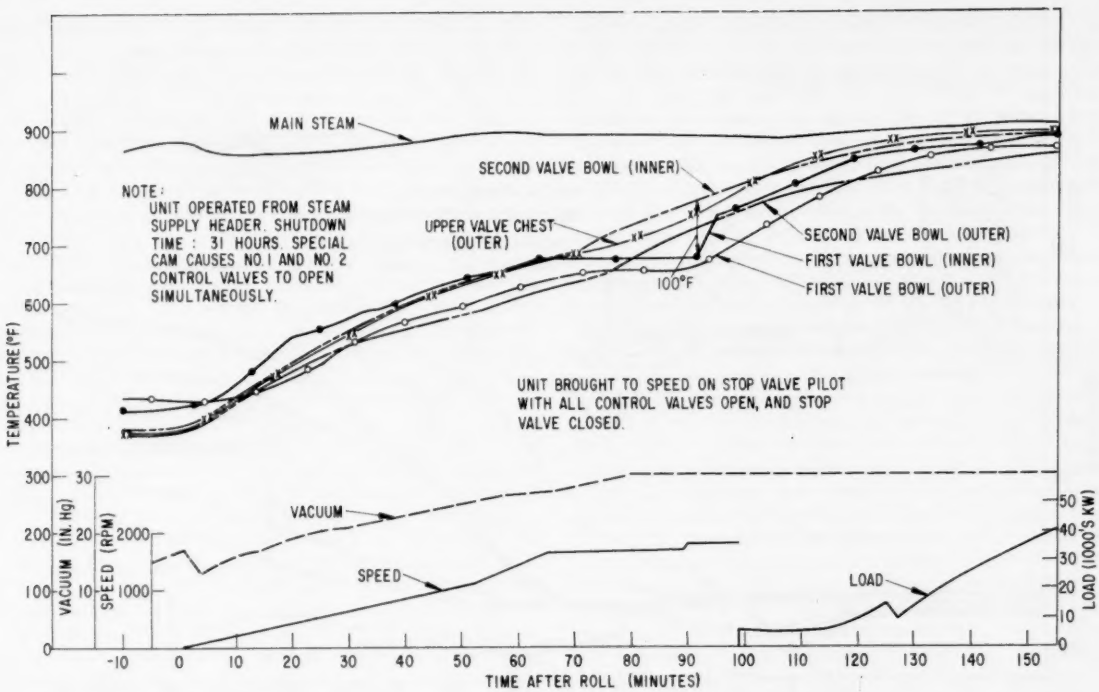
MAIN STEAM
SECOND VALVE BOWL (INNER)
NOTE:
UNIT OPERATED FROM STEAM SUPPLY HEADER. SHUTDOWN TIME : 31 HOURS. SPECIAL CAM CAUSES NO. 1 AND NO. 2 CONTROL VALVES TO OPEN SIMULTANEOUSLY.
UPPER VALVE CHEST (OUTER)
SECOND VALVE BOWL (OUTER)
FIRST VALVE BOWL (INNER)
100°F
FIRST VALVE BOWL (OUTER)
UNIT BROUGHT TO SPEED ON STOP VALVE PILOT WITH ALL CONTROL VALVES OPEN, AND STOP VALVE CLOSED.
TEMPERATURE (°F)
VACUUM
SPEED
LOAD
VACUUM (IN. Hg)
SPEED (RPM)
LOAD (1000'S KW)
TIME AFTER ROLL (MINUTES)

Fig. 13 Starting and loading test on stop-valve pilot; June 30, 1958. 80,000-kw, 1800-rpm, 850-psig, 900-F unit; initially cold. Operated from main-steam header.

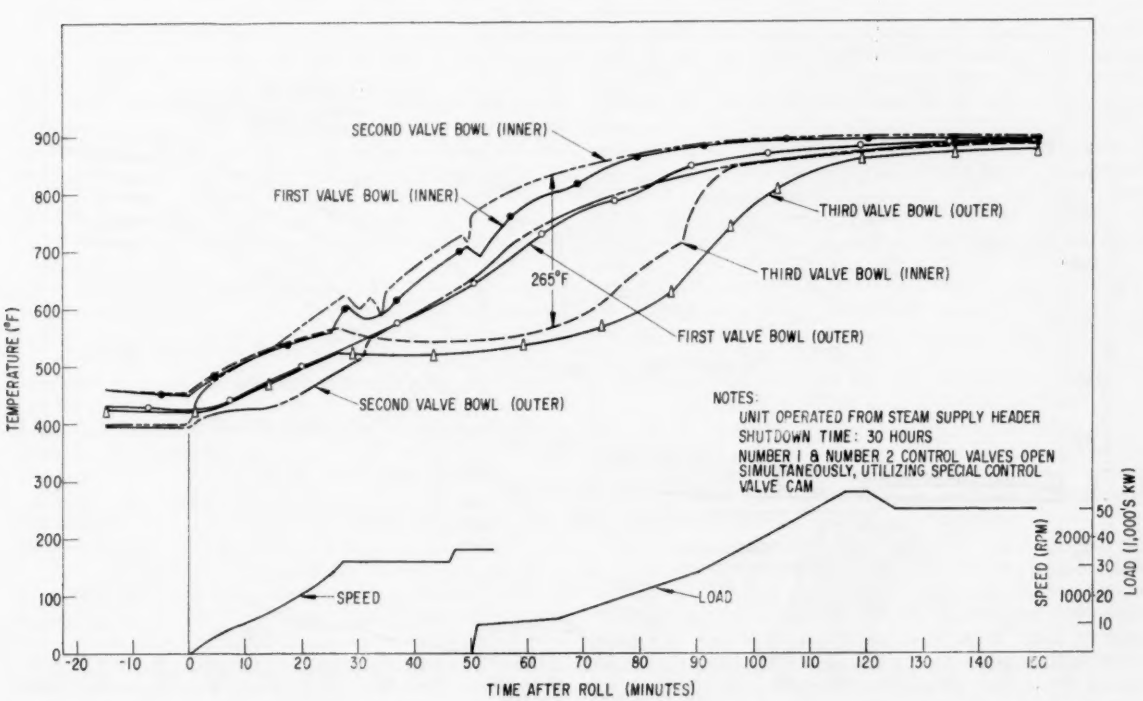

Fig. 14 Starting and loading test using special control-valve cam; October 27, 1953. 80,000-kw, 1800-rpm, 850-psig, 900-F unit; initially cold. Operated from main-steam header.

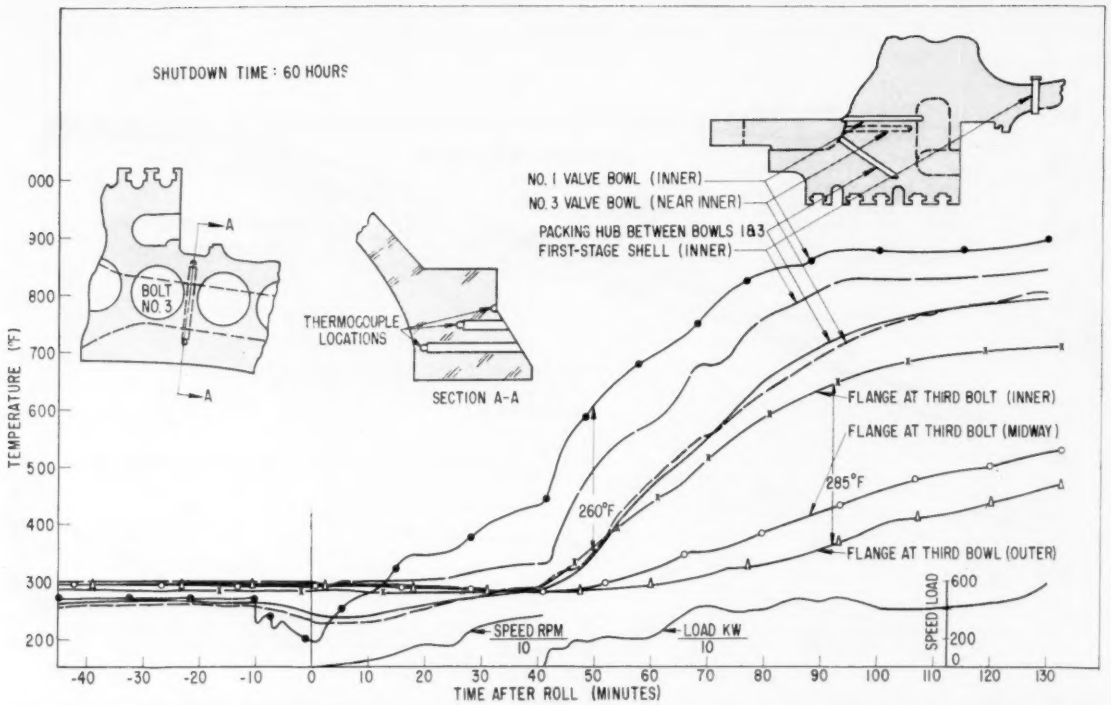

Fig. 15 Normal starting and loading test; September 23, 1954. Flange temperatures depicted. 132,500-kw, 3600-rpm, 1250-psig, 950-F unit; initially cold.

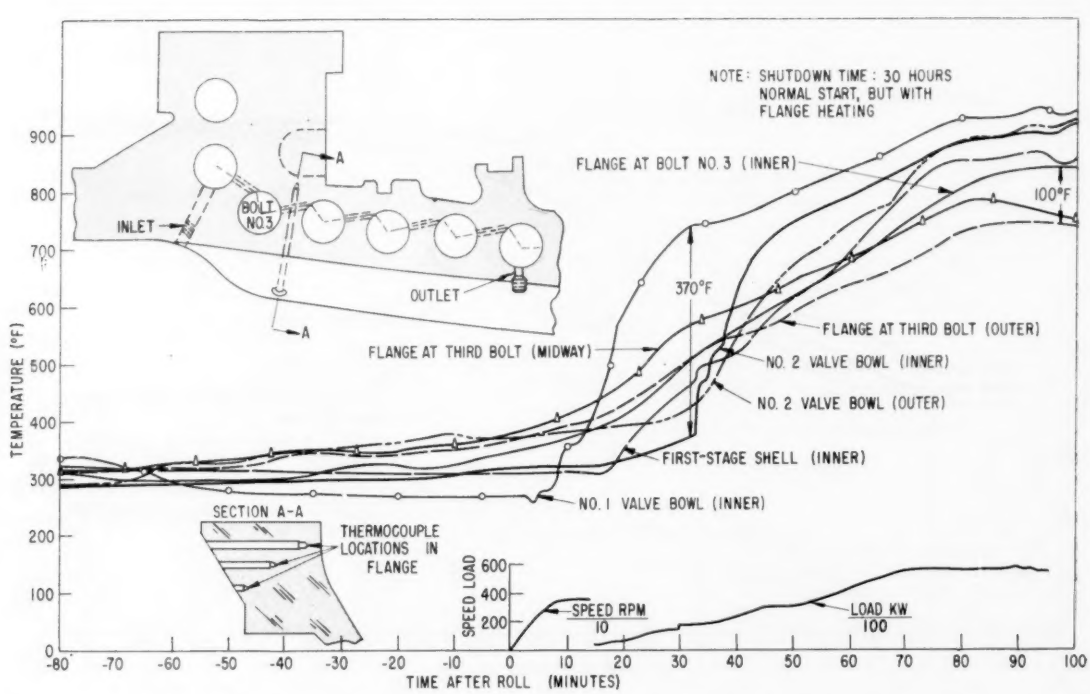

Fig. 16 Normal starting and loading test; November 7, 1955. Flange heating employed, flange temperatures depicted. 50,000-kw, 3600-rpm, 1250-psig, 950-F unit; initially cold.

the bypass line, it being either 2-in. or 3-in. diameter. The largest temperature differences occurred while closing the No. 1 control valve prior to transferring control from the bypass to the normal system. With the application of a turbine stop-valve modification, which could pass about 20 per cent flow, the turbine-shell thermal distribution should be further improved and easily controlled. It is also important to observe that, even with the relatively small 2-in. bypass-line tests on the header system, the turbine-bowl metal was uniformly heated to within about 100 F of the machine rated temperature while all bowls were being heated and all control valves wide open.

2 Start With Low Boiler Pressure. Figs. 11 and 12 show starting and loading tests, for a hot and cold start while operating with greatly reduced boiler pressure. For both tests a multiple number of control valves were open immediately after synchronizing and the entire rolling period and initial-loading period occurred while at reduced steam pressure. This produced relatively low rates of heat transfer and temperature change and minimized turbine-metal wall thermal differences. For instance, for the cold start, the unit was started with less than 50-psig and the pressure did not rise above 400 psig until the turbine metal has reached about 700 F and the load was about 20,000 kw. For neither test did the maximum temperature difference between the inner surfaces of the No. 1 and No. 2 control valves exceed about 80 F. This method of control is definitely quite effective but it may not be widely applicable because of the necessity for obtaining very low steam pressure (10 per cent of rated). The time required for a complete loading cycle is also generally greater than for a stop-valve-bypass system.

3 Start on Existing Stop-Valve Pilot. In addition to utilizing a stop-valve bypass or operating with low boiler pressure, there is a third method for starting and loading with all control valves wide open—through the use of the normal emergency-stop-valve pilot. This pilot normally is employed to equalize the pressure across the stop-valve main disk prior to opening the valve. Although not so intended when designed, the pilot-valve opening for certain units is of such size that the turbine may be brought to rated speed with the pilot open, the stop valve closed, and all the control valves wide open. The control of speed is obtained by regulating the rate at which the turbine-exhaust pressure is improved. Data taken under these conditions are shown in Fig. 13 which covers an 80,000-kw, 1800-rpm, 850-psig, 900-F unit operated from a header. This unit is similar to that shown in Fig. 6. Other data obtained on a unit-system machine show similar information.

For this turbine, the greatest temperature difference between the inner surfaces of the No. 1 and No. 2 valves is only about 100 F and it occurs after reaching speed at the time the turbine-control valves are being closed. At this time, all control valves except one are closed and this one is only slightly open in preparation for switching the control to the normal procedure. Although this method is also quite effective, it is probably not as beneficial or as generally applicable as the methods previously discussed.

4 Special Valve Cams for Simultaneous Control-Valve Opening. Fig. 14 illustrates data for a unit similar to that of Fig. 13, but for this test special valve cams were utilized in order to open both No. 1 and No. 2 control valves as nearly simultaneously as possible. As shown, the No. 2 valve-bowl temperatures were generally slightly higher than those for the No. 1 bowl which indicates the No. 2 valve actually opened slightly ahead of the No. 1 valve.

Special cams originally were employed to obtain equal heating of the two steam chests and the upper and lower shells during starting or under steady-state operation at light load. By this means steam is passed through both steam chests for machines where the No. 1 and No. 2 valves are in opposite chests.

It is claimed that approximately simultaneous opening of the first two valves is an effective method of thermal control. This is undoubtedly true for minimizing the temperature differences between the No. 1 and No. 2 valve bowls or steam chests. However, for any unit where the first two valves lift together, it should be very important to compare these bowl temperatures to that of another idle bowl, for instance, the No. 3 valve bowl. This is shown in Fig. 14, which shows that the maximum difference of 265 F occurs between the No. 2 and No. 3 bowl-metal inner surfaces during the early portion of the loading period. This is rather excessive and indicates that the simultaneous valve opening of only two valves, in comparison to a greater multiple number of valves, does not generally provide sufficient temperature control, nor does it adequately reduce thermal stress.

5 Flange Heating. Main horizontal-joint flange heating was developed to control differential expansion, prevent overstress of flange or bolting, and to prevent flange leakage on certain units. Flange-heating data, as well as much other excellent information relative to starting and loading, have been published previously [2, 3]. Flange heating has been found very effective. But, in general, adequate provisions are made in design for the control of differential expansion, bolt stress, or flange leakage during transient conditions without the use of extensive heating methods.

For many years the authors' company has utilized steam flow through flange-drilled passages for temperature control primarily under steady-state conditions. In particular, inner-shell bolting is cooled to control creep rate, and some outer shell flanges utilize a cooling scheme to eliminate the tendency for flange leakage near a sharp steady-state thermal gradient at a major internal fit.

It is reasonable to conclude that the control of the main steam temperature and the temperatures of the inlet passages of the high-pressure shell including the valve bowls, is the most effective method of controlling the gradual and uniform heating of all other high-temperature parts of the turbine including the flanges, shaft-packing hub, and rotor. However, it is known that large temperature differences do exist between the inner and outer surfaces of the main flanges during certain starting and loading operations, and flange heating is being further studied as a means of preventing shell cracking. Large flange thermal differences occur particularly for single-shell units at the location of the first-stage region when started from the cold condition. The data of Figs. 15 and 16 show flange first-stage and bowl temperatures for the two units depicted in Figs. 4 and 5. Figs. 15 and 16 both are for a cold start. In both cases, the unit was started normally, except for Fig. 16, where flange heating was used in addition.

In Fig. 15 a relatively large thermal difference of about 285 F occurred across the flange. The flange inner-surface temperature followed the trend of the bowl and first-stage temperatures and its level was slightly below the No. 3 bowl inner-surface temperature. This indicates that the flange temperature is affected directly by the rate and magnitude of the bowl and inlet-area temperature changes. It is important to note that the temperature difference between the inner surfaces of the No. 1 and No. 3 bowls for this test was as great as 260 F which is excessive. This difference may likely be of most importance. Its adequate control should also improve the thermal distribution of the flange.

Fig. 16 shows that with flange heating the maximum difference across the flange was less than 100 F which is quite nominal, and that the general trend of the flange temperature followed that of the first-stage temperature. Also, the mean temperature of the flange was close to the first-stage temperature. Both of these conditions should minimize thermal stress. However, as shown in Figs. 5 and 16, there occurred simultaneously the extreme thermal difference between the inner surfaces of the No. 1 and No. 2 valve bowls of 370 F. Therefore, whenever flange heating is employed it should always be done in connection with good bowl-metal temperature control and never be considered as a substi-

tute for throttle steam or turbine-inlet temperature control.

Because flange heating is very effective for changing flange temperature, and has been utilized in some instances for regulating the turbine-shell-to-rotor differential expansion, it should be employed with caution. Improper flange-temperature control could cause rubbing, overstress of main bolting, or flange leakage.

6 Nozzle-Bridge Cross Drilling. A few units have had holes drilled through the bridges separating the shell-bowl passages in order to interconnect the various bowl passages circumferentially. The purpose is to gradually heat an inactive bowl adjacent to an active bowl by the leakage of steam through the bridge, into the idle bowl, and then through the idle nozzle arc. This cross drilling should tend to produce more gradual and uniform heating than would otherwise occur without it, but the magnitude of its benefit is not definitely known. Most units with drilled bridges employ other methods of temperature control as well. The drilling would not appear to afford any reduction in the rate of temperature change in the passage of the first control valve to open. The drilled holes produce a slight deleterious effect in turbine efficiency but usually this is less than 0.2 of 1 per cent at low load diminishing to zero at full load.

The drilling of holes through the control valves, suggested for idle-bowl heating, does not appear generally feasible because of speed control or overspeed protection; a large throttling-temperature change could still occur as the leakage steam passed through the holes.

Piping an external steam supply to all idle bowls, controlled by one or more valves in the individual lines supplying various bowls, does not seem to offer any advantage in comparison to utilizing a turbine stop-valve bypass.

Conclusions

Most evidence indicates that the great majority of turbine-shell cracks are due to transient thermal stresses. Careful study of individual installations, development of procedures, and application of devices can go far toward elimination of these cracks. No one method, item of equipment, nor any specific instrumentation alone will prevent cracking. Combinations of all must be used. The stop-valve-bypass method of starting combined with adequate instrumentation and steam-temperature control now seems to be the most effective step, using automatic recording of essential temperatures as a basis for procedure development.

The cracking problem is believed to be a common problem among boiler manufacturers, turbine manufacturers, consulting engineers, and operating companies. In addition to the means described for minimizing thermal stress to reduce cracking, further effort should be made to integrate the steam-supply characteristics of the steam generator to those desirable for admission to the turbine and its components.

Acknowledgment

The authors wish to acknowledge the contributions of the many power companies whose co-operation has made this paper possible.

References

1 R. L. Jackson, S. B. Coulter, and R. Sheppard, "Importance of Matching Steam Temperatures With Metal Temperatures During Starting of Large Steam Turbines," TRANS. ASME, vol. 79, 1957, pp. 1669–1678.

2 W. C. Beattie, J. M. Driscoll, and M. Salvage, "Accelerated Loading of Large High-Pressure, High-Temperature Turbine-Generators," ASME Paper No. 55—SA-63.

3 F. W. Kuehn, "Controlled Starting and Loading of Modern Central Power Stations," TRANS. ASME, vol. 80, 1958, pp. 1183–1209.

4 S. Neal and V. S. Renton, "Operating Characteristics of the 100,000-Kw Essex Turbine Generator," TRANS. ASME, vol. 72, 1950, pp. 267–284.

5 Robert L. Reynolds, "Controlled Starting of Steam Turbines," *Westinghouse Engineer*, September, 1951, pp. 159–164.

6 Jefferson C. Falkner, "Quick-Starting of Large High-Pressure, High-Temperature Boilers," TRANS. ASME, vol. 75, 1953, pp. 1407–1460.

7 C. W. Elston, "Factors Involved in the Starting and Subsequent Loading of Modern Steam Turbines," ASME Paper No. 52—A-150.

8 E. M. Kratz and R. C. Wiley, "Turbine Starting and Loading Tests at Dunkirk Station," ASME Paper No. 53—F-33.

9 E. J. Rosecky, "Requirements for Quick Starting Steam Turbines," presented at the Missouri Valley Electric Association Conference, April 8, 1953.

10 J. S. Hall, "The Starting Rates of Steam Turbines," *The Metropolitan-Vickers Gazette*, vol. 25, October, 1954, pp. 387–399.

11 H. Haas and W. Trasel, "Starting of Steam Turbines," *Siemens Zeitschrift*, No. 9, September, 1958, pp. 665–673 and No. 10, October, 1958, pp. 735–742 (German).

12 A. G. Prokopenko, G. E. Krushel, and V. A. Kryzhanovsky, "Starting Experiences With a 150-MW Unit Installation," *Combustion*, October, 1958, pp. 38–45 translated from issue No. 2, 1958, Russian Publication *Teploenergetika*, pp. 8–18.

13 "Starting and Loading Instructions," General Electric Company publications GEI-69660A, GEI-75342A, GEI-75344, and GEI-75345.

DISCUSSION

J. J. Fleischmann[3] and E. J. Rosecky[3]

We concur in the need for controlling inlet steam temperatures in relation to the metal temperatures existing in the turbine at start-up. However, the reasons for requiring such control and the selection of metal temperature points to be controlled are somewhat different from those of the authors. This can best be explained by reviewing Allis-Chalmers high-pressure cylinder design which has been effective in avoiding thermal stress cracking.

All Allis-Chalmers units with inlet temperatures of 950 F or higher have used nozzle chests which are entirely separate from the main cylinder casting. Fig. 17 is typical of this single wall cylinder construction which has been used successfully for over

[3] Allis-Chalmers Manufacturing Company, Milwaukee, Wis.

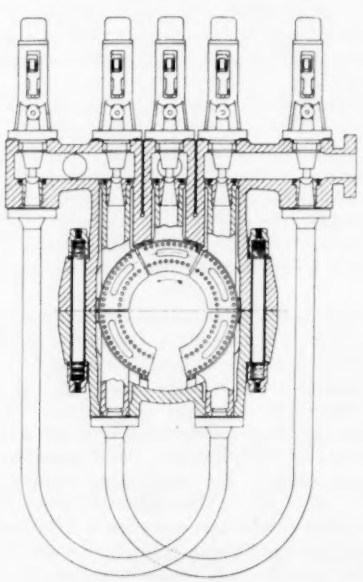

Fig. 17 Single cylinder with separate nozzle chests

20 years. Since the nozzle chests are separated from the cylinder, they are free to expand independently of the heavier cylinder parts. Thus their temperature conditions are not a critical consideration in establishing a starting time or loading rate.

For higher pressures and temperatures, where double-cylinder construction (Fig. 18) is desirable, separate steam chests containing the inlet valves are used, as well as nozzle chests which are separated from the inner cylinder. In this way, the inlet steam temperature only contacts the nozzle chest and the inlet pipes. The more massive cylinder parts are never heated to full inlet steam temperature, in fact they remain at least 100 F cooler than they would be on an integral steam-chest design. Because the stresses are proportional to total temperature changes obtained at a fast rate, the isolation of steam chests and nozzle chests materially reduces the temperature range through which the cylinders operate and thus the thermal stresses.

Since cold starts are infrequent, holding reduced inlet and reheat steam temperatures for a relatively short period of time, until metal temperatures have stabilized, offers further opportunity to reduce thermal stresses.

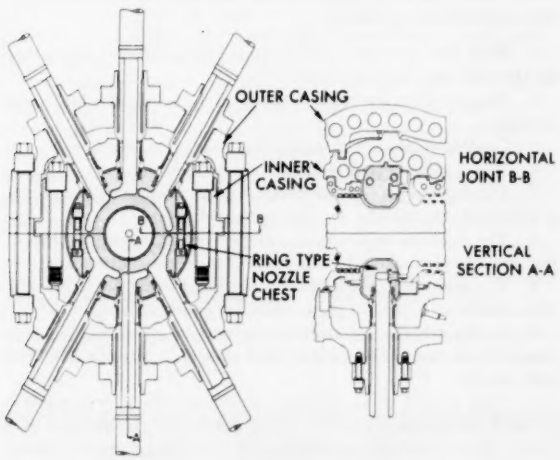

Fig. 18 Double cylinder with ring type nozzle chest

Although thermal stress cracking has not been a problem with separate nozzle chest designs, lower value thermal stresses, caused by improper temperature control, can produce plastic flow and permanent distortion of the cylinder with attendant leakage losses. Our experience has shown that the region of the turbine to watch for temperature control on these units is the 360 deg arc of admission at reaction and reheat inlet belts. For this purpose thermocouple provisions are made at these belts to check the following:

1 Total temperature and differential across the cylinder flanges.
2 Cylinder wall to flange temperature differential.
3 Differential between cylinder wall at top and bottom.

Proper control of these temperatures, the rate of change of these temperatures, and the differential between them, which is a function of inlet steam temperature and loading rate, is highly recommended. The number of these readings is quite large for an operator to correlate. For this reason, differential recorders, which measure temperature differences between two locations, have been installed on a number of our recent units.

On units with separate steam chests further control of the inlet system temperatures is achieved by the use of an external warm-up system on inlet pipes as shown in Fig. 19. For start-ups, the orifice valves at the low point of these pipes can be opened wide for draining the pipes. Then, to equalize temperatures, the header drain valve is closed and the steam circulates between the inlet pipes. After temperatures have stabilized at some light load, the orifice valves can be closed to a point where the flow is just sufficient to keep the inlet pipe and various nozzle groups close to operating temperature at all times.

The use of low boiler pressure for starting is of value in so far as the larger steam flow allows better control of the steam inlet temperatures for cold starts.

The complications of the stop-valve bypass system proposed by the authors seems unwarranted with the turbine construction we have described.

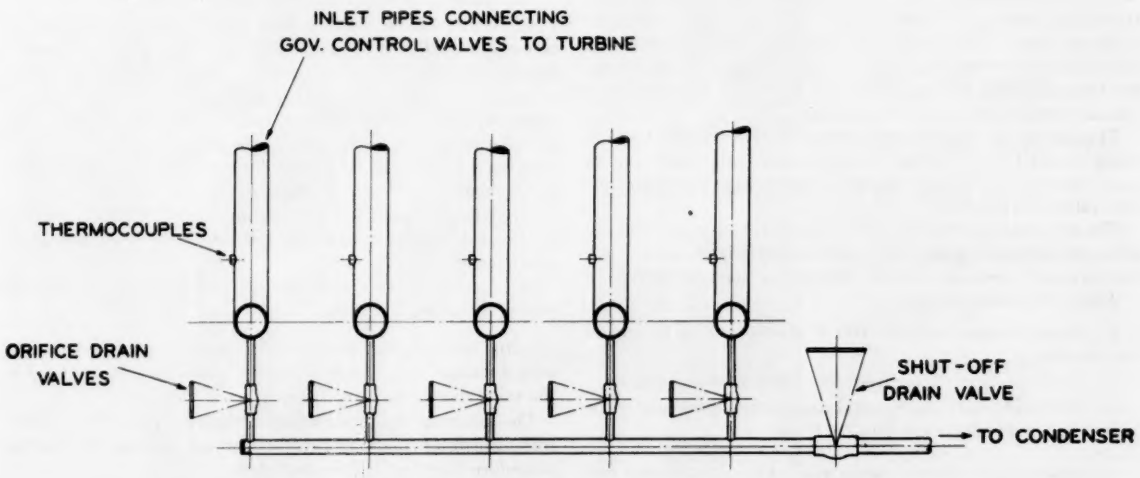

Fig. 19 Schematic arrangement for heating inlet pipes between valves and steam turbine

Paul Murphy, Jr.,[4] Fred G. Campau,[5] and Homer W. Diebler[6]

The authors of this paper are to be congratulated for the information and opinions they have collected and presented here today.

Severe cracking of valve chests and bowls has been experienced throughout the industry on partial-admission turbines. This problem has been receiving considerable attention in the last several years by many operating groups. Temperature investigations have shown that this cracking is due to severe thermal shock during start-up and loading.

The Detroit Edison Company has fifteen partial-admission turbines representing 1200 mw of capacity. During the past six years, considerable testing has been done to improve the start-up and loading of these units. Since these units are now experiencing daily off-and-on service and week-end shutdowns, an early solution to the shell cracking problem has become imperative. Within the last two months, a satisfactory start-up, heating, and loading procedure has been accomplished, which does not require large steam flows through an enlarged bypass arrangement as recommended by the authors.

Our developments have been greatly assisted by publications and direct help in response to inquiries, especially from Consolidated Edison Company of New York, Cleveland Electric Illuminating Company, Duquesne Light Company, and Union Electric Company.

The three most important developments that resulted in this start-up, heating, and loading procedure are:

1 Redesign of the No. 1 and 2 control valve cams.

2 The vacuum start-up with all control valves in the wide open position.

3 Heating of head end of turbine with steam 500–600 F higher than metal temperature.

The first major step forward resulted from the efforts at the Marysville Plant to overcome the severe Monday morning heating of the upper valve chest of a 75 mw turbine which had been operated with no-flow during previous light-load operation. A new cam design was requested from the turbine manufacturer to open the No. 1 and No. 2 valves simultaneously. These were installed and improved the light load operating conditions by maintaining flow through both valve chests.

The present start-up, heating, and loading procedure was first tried on an 1800-rpm, 75,000-kw unit with inlet steam conditions of 850 psi, 900 F, at the Delray Power Plant. This procedure was developed after witnessing a turbine start-up at The Union Electric Company, which brought a turbine up to speed by increasing vacuum with control valves wide open.

The further development introduced at Delray has been to bring a cold turbine quickly to speed and initial load, and to carry out most of the warm-up on a synchronized unit with control valves wide open.

The new start-up, heating, and loading procedure was initially accomplished in August, 1959, and has many advantages over that originally recommended by the turbine manufacturer.

These advantages include:

A Steam temperature 500–600 F above that of the metal can be used.

B Prewarm-up of the control valve chests is eliminated.

C The inside and outside metal temperature difference of the valve chest and bowls is less than 150 F.

D The time required to bring the turbine to synchronous speed and initial loading is reduced to about 20 minutes.

E The start-up time and attention required by the operators is reduced considerably.

F The start-up, heating, and initial loading is accomplished with all control valves in the wide open position, thus obtaining full peripheral heating.

G The safety features of the turbine such as governor control, overspeed trip, and throttle valve trip remain in active service at all times.

H The turbine speed is controlled to permit synchronizing by regulation of the condenser back pressure.

I The unit is carrying 2 mw of load during the heating period.

J The newly designed cams for the No. 1 and 2 control valves maintain steam flow through both upper and lower valve chest during light-load periods.

K The adoption of this procedure on similarly designed turbines requires very little modification and expense.

The following is the detailed procedure used in starting, heating, and loading this unit:

1 With unit primed, the vacuum is held at 10 in. by bleeding air through the vacuum breaker.

2 The governor limit switch is placed in the all raised full load position.

3 Control valves are placed in the wide open position.

4 Water sprays are turned on in exhaust casing.

5 The turbine stop valve internal pilot is opened, and steam is admitted through the wide open control valves.

6 The vacuum breaker valve is then closed, to stop air bleeding, and speed is allowed to increase with increase of vacuum.

7 The generator field breaker is put on at usual speed, and the disconnects are closed in preparation for synchronizing.

8 As the turbine approaches synchronous speed, air bleeding should be started (1750 rpm) to level off speed and approach 1800 rpm slowly.

9 Fine control of air bleeding is accomplished by regulation of the $^1/_2$ and 1-in. valves installed in the vacuum breaker line.

10 When synchronous speed is reached, the generator breaker is closed.

11 Air bleeding is stopped and vacuum allowed to reach maximum obtainable.

12 Water sprays are shut off in exhaust casing.

13 Initial load of the unit with control valves wide open is carried by steam passing through internal pilot. (Approximately 2 mw.)

This is the principal part of the heating cycle and the length of operation under this condition will be determined by temperature of valve chest and bowls. Since the unit is synchronized and carrying a small load (2 mw) very little operating care and attention is required during the heating period.

14 When the head end temperatures reach 700 F, the turbine is unloaded, the valve chests are pressurized, and the emergency stop opens.

15 Loading is then accomplished by regulation of control valves in the usual manner.

Initial loading after opening of the stop valve should be done in such a manner that temperature limitations are not exceeded in the valve chests, bowls, and first stage.

The following modifications were required on a Delray 75-mw turbo-generator to accomplish the start-up, heating, and loading procedure described in this discussion.

1 The No. 1 and No. 2 control valve cams were redesigned to open simultaneously.

2 Water sprays were installed in the exhaust casing to control casing temperature during the rolling period.

[4] Assistant Superintendent, Delray Power Plant, The Detroit Edison Company, Detroit, Mich.

[5] Technical Engineer, Delray Power Plant, The Detroit Edison Company, Detroit, Mich.

[6] Assistant Operations Engineer, Delray Power Plant, The Detroit Edison Company, Detroit, Mich.

3 Small auxiliary valves were installed in the vacuum breaker line to permit fine control of speed for synchronizing.

For units with stop valve internal pilots that are either open or closed, adjustments may be necessary to obtain desired steam flow to accomplish maximum allowable head end heating.

This start-up procedure has demonstrated that a turbine can be supplied with steam 500–600 F above that of metal temperatures. Inner and outer metal temperature differences, which conservatively should not exceed 150 F, reach a maximum of 120 F. Steam flow through the stop valve internal pilot of the 75-mw unit at Delray is sufficient for heating even a cold turbine in a reasonable time ($1^1/_2$ hours). This start-up, heating, and loading procedure can be accomplished with very little expense and modification to existing equipment.

W. Sinton[7] and W. R. Berry[8]

The subject paper presents an interesting account of certain constructive measures for dealing with the industry-wide problem of cracking of turbine cylinders of the type that have the steam chest and control stage nozzle chambers cast as an integral part of the cylinder proper, and which are subjected to frequent starting, stopping, and load changing cycles.

Westinghouse experience indicates that this type of cylinder cracking has been limited to integral chest-chamber units operating with inlet steam temperatures in the range of 850 F minimum up to 950 F. We wish to emphasize that Westinghouse turbine designs for 1000 F and higher inlet temperatures have always incorporated a high degree of flexibility in critical areas by means of completely separating the chambers for each nozzle group, and by detaching the steam chest from the cylinder. These units have been free of cylinder cracking caused by cylic operation and are expected to perform favorably even when subjected to more frequent shutdowns in the future (Figs. 20 and 21).

We are certainly in agreement with the start-up practice the authors have recommended, namely, bringing the turbine from rest to speed with all governor valves wide open, while throttling on the inner element of the throttle-stop valve. This has always been the standard method of starting Westinghouse units and

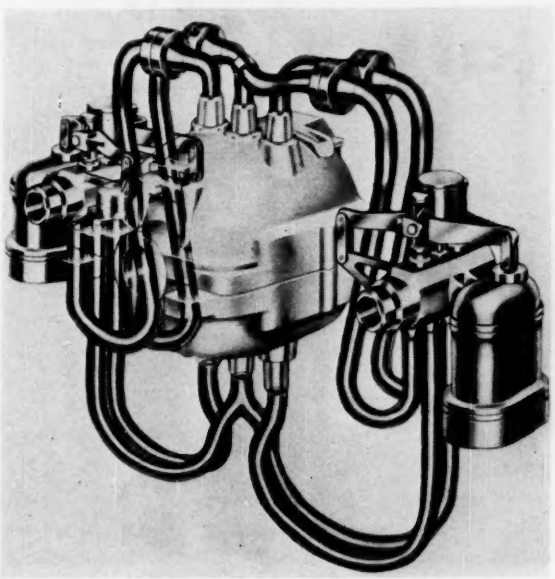

Fig. 20 Separate steam chests with flexible inlet piping

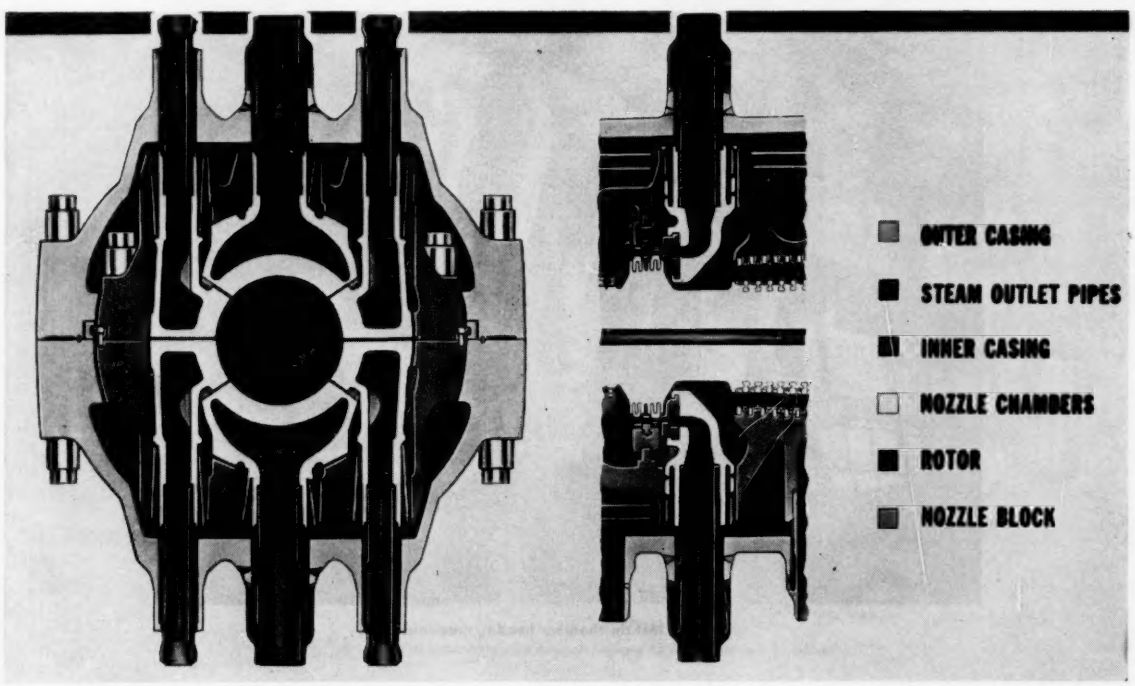

Fig. 21 Higher temperature inlet features

[7] Manager Medium Turbine Apparatus Engineering Section, Westinghouse Electric Corporation, Steam Division, Lester, Pa. Mem. ASME.

[8] Large Turbine Mechanical Section, Westinghouse Electric Corporation, Steam Division, Lester, Pa. Mem. ASME.

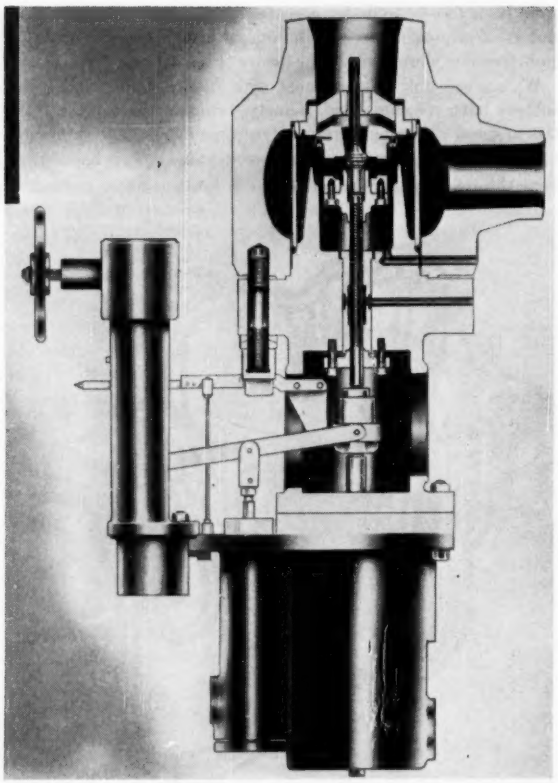

Fig. 22 Auto stop throttle valve and servo motor

results in uniform heating of all nozzle chambers. Maximum effectiveness in controlling start-ups can best be achieved by application of strategically located metal temperature recording devices with a review of the records obtained to determine optimum starting procedures (Fig. 22).

We determined as early as 1956, from temperatures measured in the field, that the addition of a nozzle chamber interconnection arrangement had a substantial effect in moderating temperature differentials between various nozzle chambers during the loading period. Steam from the primary valve chamber is fed by a pipe manifold into the adjacent inactive valve chambers at a point physically above the nozzle chamber outlet so as to heat the walls of these chambers (Fig. 23).

On a typical installation, using a total heating flow of approximately 4 per cent of maximum throttle flow temperature differentials in the circumferential direction between adjacent chambers is held to 115 deg or less. As a result of these experiences some recent machines of this type have been shipped with heating manifolds attached. Furthermore, our Service Department has applied this arrangement to numerous machines in the field.

Westinghouse turbines currently being designed for inlet steam temperatures of 850 to 950 F embody a construction directed toward elimination of the cracking problem by permitting substantially more freedom for independent thermal expansion of the nozzle chambers, together with provision for uniform heating of groups of chambers by nozzle chamber interconnections. This is illustrated in Figs. 24 and 25.

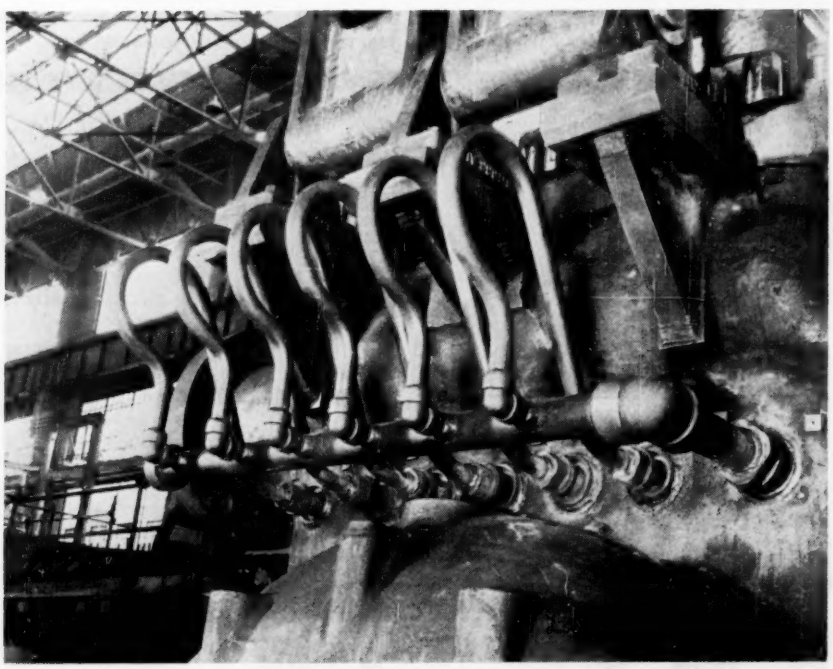

Fig. 23 Nozzle chamber heating manifold

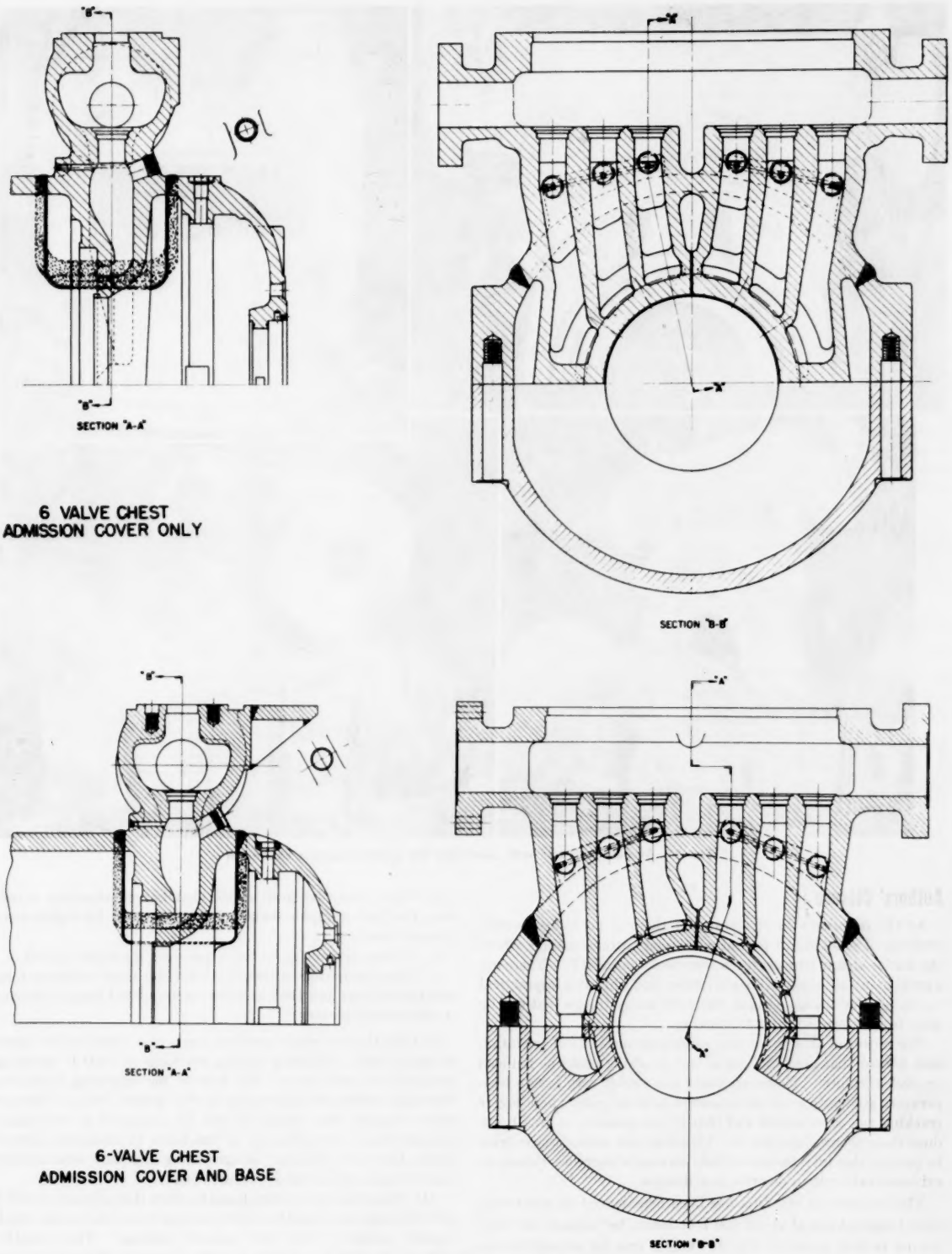

Fig. 24 Steps in assembly of steam chest and nozzle chamber in cylinder

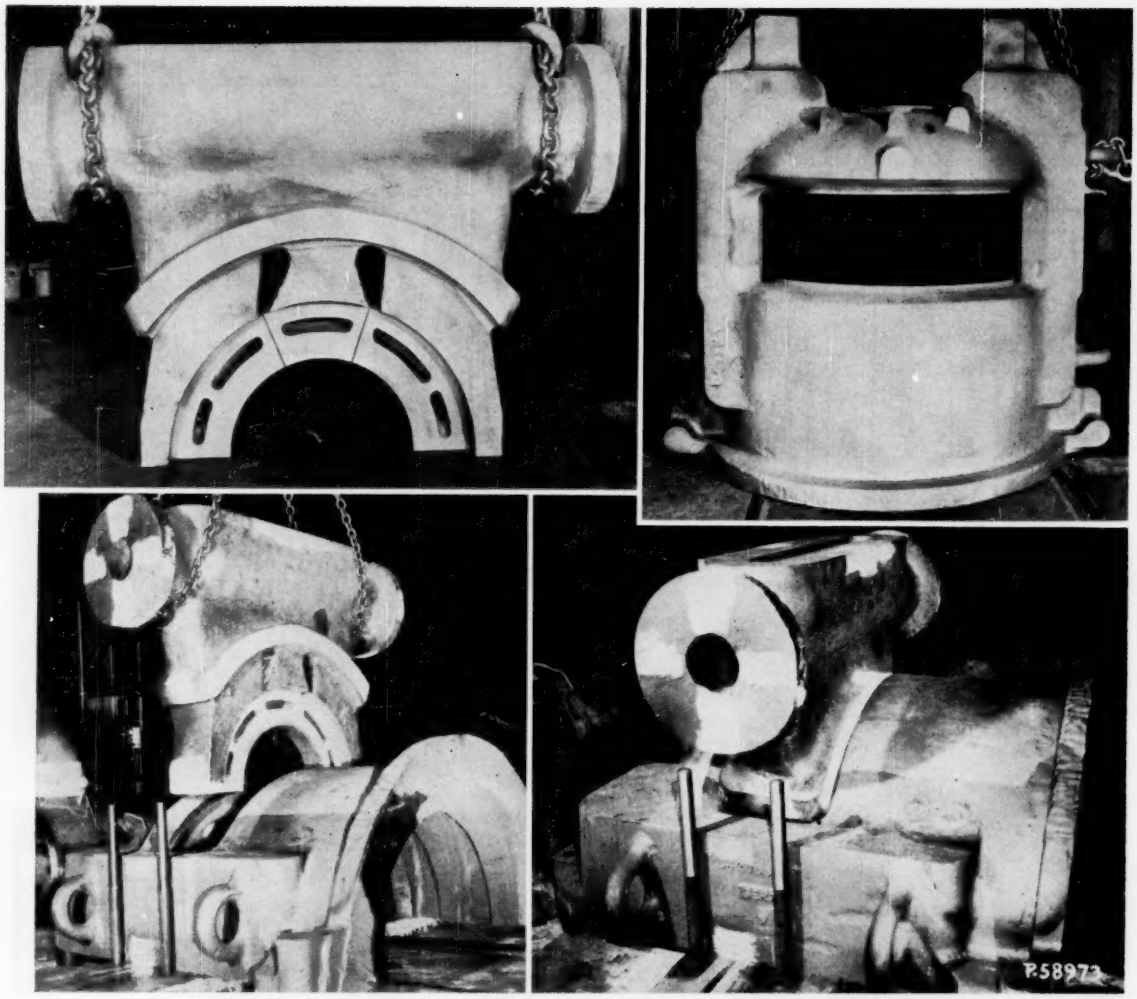

Fig. 25 Turbine cylinders with provisions for nozzle chamber expansion

Authors' Closure

As the discussers have mentioned there is an industry-wide problem of cracking of partial admission turbine casings where the initial steam temperatures were less than 950 F. There are a great many of these turbines in service and while it is impractical to change the casings designs, there are many things that can be done to minimize additional cracking.

The object of this paper was to present methods of operation and devices that are practical so that cracking could be reduced on such turbines. Thorough study has shown very severe temperature gradients could be measured in those cases where severe cracking was experienced and that it was possible to greatly reduce these thermal gradients. Therefore the authors have tried to present this information to help owners of turbines already in existence rather than describe new designs.

The majority of cracking has been experienced on units with inlet temperatures of about 950 F or lower, for instance on those similar to that shown in Fig. 3. This is true for several reasons including:

1 There are more of these units in service than those at higher temperature ratings.

2 Many have integral nozzle chamber construction rather than the more complex designs found necessary for higher temperature service.

3 A large percentage of these units are thermally cycled.

4 The average age of these units is older than for higher temperature ratings and their material accumulated fatigue damage is presumably greater.

But the thermal stress problem exists to a considerable degree on many units, including modern machines of 1000 F operating temperature and above. We believe the following comments forcefully reflect the necessities of the present state of the art which require that special means be employed in the nozzle passage region for all kinds of machines to minimize thermal stress, the more elaborate designs being generally economically justified on units of 950 F rating or higher.

Mr. Fleischmann and Mr. Rosecky state that all units of 950 F or higher manufactured by their company have used nozzle chests entirely separate from the cylinder casting. They mention cylinder distortion and leakage difficulties through improper temperature control on 360-deg arc admission units. They note that turbine thermocouple measurements should be made and good temperature control obtained. The authors agreed; and

their company has been providing casing thermocouples for several years. The warm-up system, described in Fig. 19, is undoubtedly beneficial, but the data obtained by the authors' company on similar systems does not seem to indicate a significant improvement in comparison to other means such as a stop valve bypass system. The authors greatly appreciate Mr. Fleischmann's and Mr. Rosecky's comments.

Mr. Sinton and Mr. Berry state that their company's designs for 1000 F and higher have always employed means of completely separating the chambers of each nozzle group. They mention the industry-wide problem of cylinder cracking on integral chest chamber units and the experience on their company's 850 to 950 F machines. They point out the desirability of coming to speed with all control valves wide open but it has been the authors' experience that the maximum thermal shock comes at speed and immediately after synchronizing and to be really effective all control valves should remain open until approximately 20 per cent flow has been established, rather than having the governor take control on one valve prior to reaching synchronous speed. The nozzle chamber manifold is certainly a step in the right direction but, in the authors' experience, is much less effective than the stop valve bypass and, in addition, causes an efficiency loss at all except full load. The authors wish to thank Mr. Sinton and Mr. Berry for their fine discussion.

Mr. Murphy, Mr. Campau, and Mr. Diebler presented very interesting information describing an improved starting and loading procedure to minimize thermal cracking. They and their company are to be congratulated in taking a significant step forward through the development of the excellent control procedure.

The authors believe that the procedure employed was applied to machines operated from a header system, since it is usually not possible to get steam temperatures this much over metal except on them. It was stated that the three most important developments of the procedure were:

1 Use of redesigned cams for the simultaneous opening of the No. 1 and No. 2 control valves.

2 Vacuum startup with all control valves wide open.

3 Starting with steam 500–600 F higher than the turbine metal.

The authors believe the procedure to be a good one because it uses the methods they have described as Method No. 3 and Method No. 4 in this paper. The procedure appears only second in general order to effectiveness to all procedures the authors have enumerated because Method No. 2 of the paper, starting with low boiler pressure, is not normally applicable to a header system installation.

The method used should be very similar to that described in Fig. 13. For this figure, note that the unit was started with steam about 500 F above the initial turbine metal temperature and the unit was brought to speed by increasing the vacuum while all control valves remained wide open. For this test, the first two control valves also opened simultaneously, but this, of course, has no influence throughout the rolling period while all valves are wide open. Although the control method of Fig. 13 is excellent, there is little doubt the stop valve bypass method described in Fig. 10, for a unit operated from a steam header, shows additional improvement in thermal control. For the test of Fig. 10 no special valve cams were employed nor would they have been of benefit. The rather small 2-in. bypass around the header valve for the test of Fig. 10 safely permitted a 2000-kw load before transferring to normal operation.

Note that load was not applied while on the stop valve pilot in the test of Fig. 13. The authors believe it important to state that the internal pilot valves for the emergency stop valves manufactured by their company are not designed to pass flows as large as no load flow at rated pressure and temperature conditions. An enlarged pilot, allowing even some small load such as 2000 kw, does not appear adequately safe unless it has fully automatic trip protection. If, during an emergency while operating with an enlarged pilot, the control valves were not to close satisfactorily and the stop valve internal pilot was reopened, the unit could overspeed.

Journal of ENGINEERING FOR POWER

Information for Authors

• Manuscripts should be submitted in final form to the Editor. Each manuscript must be accompanied by a statement that it has not been published elsewhere nor has it been submitted for publication elsewhere. A paper which would occupy more than 8 pages of the Journal may be returned to the author for abridgment.

• The author should state his business connection, the title of his position, and his mailing address. A short abstract (50 to 100 words) should be included on the first page immediately preceding the introductory paragraph of the paper.

Three copies of the manuscript are required. One of these must be a carefully prepared printer's copy, typed in double spacing, on one side of the page only, with wide margins, on $8^1/_2$ by 11-in. opaque white paper. Mimeographed manuscripts, if prepared with exceptional care, can be accepted provided they are completely edited.

• As far as possible, all mathematical expressions should be typewritten. Greek letters and other symbols not available on the typewriter should be carefully inserted in ink. Care should be taken to distinguish between capital and lowercase letter, between zero (0) and the letter (*O*), between the numeral (1) and the letter (*l*), etc. A letter representing a vector cannot be printed with an arrow above or below it. The letter should be underscored with a single wavy line, wherever it appears in the text, to designate boldface type.

• A list of symbols carefully marked for the use of the editor (thus: κ, Greek l.c. kappa), if it has not been included in the body of the paper, should accompany the manuscript on a separate page.

• Before preparing a manuscript the author should study printed articles in the Journal, with special attention to the form and style of mathematical expressions, tables, footnotes, references, and abstract. Numbers that identify mathematical expressions should be enclosed in parentheses. Numbers that identify references at the end of the paper should be enclosed in brackets. Care should be taken to arrange all tables and mathematical expressions in such a way that they will fit into a single column when set in type. Equations that might extend beyond the width of one column (fractions that should not be broken or long expressions enclosed in parentheses) should be rephrased to go on two or more lines within column width. Fractional powers are preferred to root signs and should always be used in more elaborate formulas. The solidus should be used instead of the horizontal line for fractions wherever possible.

• A normal paper should not exceed 8 pages in the Journal. It is about 8000 words or 20 double-spaced typewritten pages exclusive of drawings. A Technical Brief should not exceed 750 words or about one page in the Journal inclusive of drawings.

• Originals and two copies of figures must accompany the manuscript. Line drawings should not be larger than $8^1/_2 \times 11$ in. and should be planned for reduction to column width. Lettering should be large enough to be clearly legible when the illustration is reduced. The originals of line drawings must be in India ink on white or pale blue tracing paper or tracing cloth. Photographs of equipment or test specimens must be glossy prints and should be used sparingly. Captions for figures should be typed double-spaced and included as the last page of the manuscript. The figure number and author's name should be written in the margin or on the back of each illustration.

• Titles of papers should be brief.

• Authors can obtain copies of the ASME Manual MS-4, "An ASME Paper," from the Editor and are urged to do so before drafting their papers in final form.

• Papers published in Journals of the Transactions of the ASME must be presented at a Meeting, either in person or by title.

• An author is entitled to 25 preprints free of charge (in the case of two authors, 15 each; three or more authors, 10 each). Larger quantities of preprints or reprints can be ordered from Editorial Department, The American Society of Mechanical Engineers, 29 West 39th Street, New York 18, N. Y. Quotations will be sent on request.

ASME Publications Committee

Please address all communications to:

Editor, ASME,

29 West 39th Street,

New York 18, N. Y.